



HAL
open science

High-resolution numerical analysis of land-river-floodplains-atmosphere interaction in La Plata Basin

Anthony Schrapffer

► **To cite this version:**

Anthony Schrapffer. High-resolution numerical analysis of land-river-floodplains-atmosphere interaction in La Plata Basin. *Climatology*. Institut Polytechnique de Paris; Universidad de Buenos Aires, 2022. English. NNT: 2022IPPAX022 . tel-03683965

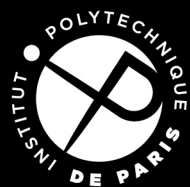
HAL Id: tel-03683965

<https://theses.hal.science/tel-03683965>

Submitted on 1 Jun 2022

HAL is a multi-disciplinary open access archive for the deposit and dissemination of scientific research documents, whether they are published or not. The documents may come from teaching and research institutions in France or abroad, or from public or private research centers.

L'archive ouverte pluridisciplinaire **HAL**, est destinée au dépôt et à la diffusion de documents scientifiques de niveau recherche, publiés ou non, émanant des établissements d'enseignement et de recherche français ou étrangers, des laboratoires publics ou privés.



INSTITUT
POLYTECHNIQUE
DE PARIS

NNT : 2022IPPAX022

Thèse de doctorat



High resolution numerical analysis of the land-river-floodplains-atmosphere interaction in the La Plata Basin

Thèse de doctorat de l'Institut Polytechnique de Paris
en cotutelle avec l'Université de Buenos Aires
préparée au

Centro de Investigaciones del Mar y de la Atmósfera
(CIMA/CONICET-UBA)

et au Laboratoire de Météorologie Dynamique (École polytechnique)

École doctorale n°626 École doctorale de l'Institut Polytechnique de
Paris (EDIPP)

Spécialité de doctorat: Physique

Thèse présentée et soutenue à Palaiseau, le 26 Avril 2022, par

M. ANTHONY SCHRAPFFER

Composition du Jury :

Dr. Hervé Le Treut Professor, Sorbonne Université.	Président du Jury
Dr. Angel Nicolás Menéndez Associate professor (Faculty of Engineering, UBA), Chief of the Hydraulic Computational Program (INA, Instituto Nacional del Agua).	Rapporteur
Dr. Isabelle Braud Research Director, INRAE (RiverLy).	Rapporteur
Dr. Simon Dadson Professor in Physical Geography, University of Oxford, Fellow, Christ Church University.	Examineur
Dr. Moira Evelina Doyle Associate Researcher, CONICET (Departamento de Ciencias de la Atmósfera y los Océanos, UBA).	Examineur
Dr. Jan Polcher Research Director, CNRS (Laboratoire de Météorologie Dynamique).	Directeur de thèse
Dr. Anna Amelia Sorensson Associate Researcher, CONICET (CIMA).	Co-Directeur de thèse
Dr. Lluís Fita Borrell Associate Researcher, CONICET (CIMA).	Directeur adjoint de thèse

Résumé

Analyse numérique à haute résolution de l'interaction surface-rivière-plaines d'inondation-atmosphère dans le bassin de La Plata Basin

Les plaines d'inondation tropicales sont des régions inondées temporairement ou en permanence dû au débordement des rivières sur des zones de faible relief. Les plaines d'inondation liées au débordement de grands fleuves peuvent avoir un régime annuel d'inondation prévisible ce qui en fait d'importants écosystèmes avec une riche biodiversité qui fournissent de nombreux services écologiques. De plus, étant des surfaces d'eau libre, leur présence a un fort impact sur les interactions entre la surface et l'atmosphère notamment dans le cas où ces plaines d'inondation sont situées dans des régions tropicales. Le Pantanal, l'une des plus grandes plaines d'inondation tropicales au monde, est la région d'étude de cette thèse qui a pour objectif de développer un schéma de plaines d'inondation pour le modèle de surface ORCHIDEE compatible avec des modèles atmosphériques à haute résolution. Ce schéma a pour finalité : (1) d'améliorer la représentation de l'impact des plaines d'inondation sur les cycles de l'eau et de l'énergie dans ORCHIDEE, (2) d'étudier la dynamique des plaines d'inondation du Pantanal et (3) d'évaluer l'impact des plaines d'inondation sur les interactions sol-atmosphère dans cette région.

Dans un premier temps, la version originale à basse résolution des plaines d'inondation dans ORCHIDEE a été utilisée pour montrer l'importance d'inclure les plaines d'inondation dans les modèles de surface parce que cela améliore la représentation du cycle de l'eau et permet de représenter des flux plus réalistes entre la surface et l'atmosphère. Ces simulations ont permis de compléter les rares observations dans la région pour estimer l'évapotranspiration sur le Pantanal et quantifier la sous-estimation de l'évaporation par les modèles de surface ne prenant pas en compte les plaines d'inondation.

Dans le but de mieux évaluer la représentation des surfaces inondées dans le modèle et de comprendre les incertitudes de l'estimation des surfaces inondées par satellite, diverses méthodes utilisant des données de satellite optique ont été explorées.

Le schéma de plaines d'inondation à haute résolution développé au cours de cette thèse est basé sur la construction d'un graphe de routage des rivières sur une grille atmosphérique utilisant des modèles numériques de terrain conditionnés hydrologiquement à haute résolution via le concept d'Unité de Transfert Hydrologique (HTUs). Un outil de pré-traitement flexible et parallélisé a été développé pour faciliter et améliorer la construction du graphe de routage des rivières sur différents types de grilles atmosphériques ce qui facilite l'intégration de données additionnelles qui sont requises pour la représentation des plaines d'inondation. Ce schéma doit faire face à de nouvelles problématiques liées à la résolution telles que la possibilité pour un HTU d'inonder ses voisins. Ce schéma a été validé en comparaison avec des observations et en comparaison avec la version précédente des plaines d'inondation dans ORCHIDEE.

La comparaison des simulations avec et sans plaines d'inondation forcées par des forçages atmosphériques à différentes résolutions a permis d'évaluer : (1) l'impact des plaines

d'inondation sur les variables de la surface terrestre et (2) comment la résolution affecte la simulation de la dynamique des plaines d'inondation. Le débit en sortie du Pantanal est considérablement amélioré, notamment la corrélation avec les observations et le débit moyen. En revanche, la variabilité annuelle est surestimée. Les surfaces inondées sont aussi correctement représentées bien que certaines zones soient absentes dû à la présence d'autres procédés non pris en compte comme les flux divergents.

La présence de plaines d'inondation augmente l'humidité du sol dû à l'infiltration et favorise le développement de la végétation. La température en surface diminue notamment à cause de la diminution des flux de chaleur sensible au profit des flux de chaleur latente.

Le schéma des plaines d'inondation à haute résolution a été intégré dans une simulation du modèle RegIPSL (modèle couplé entre ORCHIDEE et WRF) pour étudier comment celui-ci modifie les interactions surface-atmosphère dans la région du Pantanal et comment il impacte la précipitation local et régional ainsi que la circulation régional du Bassin de La Plata. Le couplage est essentiel pour ne pas surestimer les flux évaporatifs dû à l'absence de couplage. En présence de plaines d'inondations, la précipitation diminue sur les zones les plus inondées et augmente au voisinage de celles-ci. L'intégration du Pantanal dans les simulations couplées impacte tout l'Ouest du bassin de La Plata à travers l'influence des plaines d'inondation sur le courant jet de basse altitude sud-américain et via un apport supplémentaire d'humidité dû à l'évaporation depuis les plaines d'inondation. L'inclusion des plaines d'inondation, et notamment dans la région du Pantanal, mène à des changements significatifs de la couche limite localement et de la circulation régionale.

Mot clés: Modélisation, Plaines d'Inondation, Pantanal, Hydrologie, Interaction Sol Atmosphère

Abstract

High resolution numerical analysis of the land-river-floodplains-atmosphere interaction in the La Plata Basin

Tropical floodplains are regions which are temporarily or permanently flooded due to the overflow of rivers over a lowland area. Floodplains over large rivers may have a predictable annual flood regime which is why they are important ecological places with a rich biodiversity providing important ecological services. The Pantanal which is one of the world's largest tropical floodplains is the region of study for this thesis. The aim is to develop a floodplains scheme for the ORCHIDEE Land Surface Model (LSM) compatible with high resolution atmospheric models for the following reasons : (1) improve the representation of the impact of floodplains on the water and energy cycle in ORCHIDEE, (2) study the dynamic of the Pantanal floodplains and (3) evaluate the impact of floodplains on the land-atmosphere interactions over this region. Initially, the original low resolution version of the floodplains in ORCHIDEE has been used to show the importance of including floodplains in a Land Surface Models as it improves the representation of the water cycle and allows to represent more realistic land-atmosphere fluxes.

The high resolution floodplains scheme developed here is based on the construction of the river routing graph on an atmospheric grid using high resolution Hydrologically-conditioned DEM via the Hydrological Transfer Units (HTUs) concept. A parallelized flexible pre-processing tool has been developed in order to facilitate and improve the construction of the river routing graph on different types of atmospheric grids which facilitates the integration of additional hydrological data required for the representation of floodplains. This scheme had to handle new issues related to the resolution such as the possibility of an HTU to flood its neighbours. This scheme has been validated in comparison to observations and to its previous version in ORCHIDEE.

The comparison of simulations with and without floodplains forced by atmospheric forcings with different resolutions allowed us to evaluate : (1) the impact of floodplains on land surface variables and (2) how the resolution affects the simulation of the floodplain dynamics.

The high resolution floodplains scheme has been used in a simulation of the RegIPSL model (coupled ORCHIDEE-WRF model) to study how it modifies land-atmosphere interactions over the Pantanal region and the local and remote impact on the climate of South America.

Keywords: Modelling, Floodplains, Pantanal, Hydrology, Land-Atmosphere Interaction

Resumen

Análisis numérico a alta resolución de la interacción suelo - río- planicie de inundación - atmósfera de la Cuenca de la Plata

Las llanuras de inundación tropicales son regiones temporalmente o permanentemente inundadas debido al desbordamiento de los ríos en zonas de llanura. Las llanuras de inundación ubicadas sobre importantes ríos pueden tener un régimen anual de inundación predecible lo que explica que sean importantes lugares ecológicos con una gran biodiversidad proporcionando importantes servicios ecológicos. El Pantanal, una de las más extensas llanuras de inundación tropical del mundo, es la región de estudio de esta tesis. El objetivo es de desarrollar un esquema de llanuras de inundación para el modelo de superficie ORCHIDEE que sea compatible con modelos atmosféricos de alta resolución para las razones siguientes : (1) mejorar la representación del impacto de las llanuras de inundación sobre los ciclos del agua y de la energía en ORCHIDEE, (2) estudiar la dinámica del Pantanal y (3) evaluar los impactos de las llanuras de inundación sobre las interacciones suelo-atmósfera en esta región.

En un primer tiempo, la versión original a baja resolución de las llanuras de inundación en ORCHIDEE fue utilizada para mostrar la importancia de incluir las llanuras de inundación en los modelos de superficie para mejorar la representación del ciclo del agua y permitir una representación más realista de los flujos suelo-atmósfera.

El esquema de llanuras de inundación desarrollado está basado en la construcción del grafo rutaje de los ríos en una retícula atmosférica usando modelos de elevación digital a alta resolución vía el concepto de Unidades de Transferencia Hidrológica (HTU). Una herramienta de pre-procesamiento flexible y paralelizada fue desarrollada para facilitar y mejorar la construcción de los grafos de rutaje de los ríos en distintas retículas atmosféricas para facilitar la integración de datos hidrológicos suplementarios para la representación de las llanuras de inundación. Este esquema tiene que enfrentarse a nuevos problemas relacionados con la resolución como la posibilidad para un HTU de inundar a sus vecinos. Este esquema fue validado en comparación con observaciones y con su versión previa en ORCHIDEE.

La comparación de simulaciones con y sin el esquema de inundación activado, forzadas por forzantes atmosférica a distintas resoluciones nos permitió evaluar (1) el impacto de las llanuras de inundación en las variables de superficie y (2) como la resolución afecta la simulación de la dinámica de las llanuras de inundación.

El esquema de llanuras de inundación fue utilizado en una simulación del modelo RegIPSL (modelo acoplado ORCHIDEE-WRF) para estudiar cómo modifica las interacciones suelo-atmósfera sobre la región del Pantanal y cuales son los impactos locales y remotos sobre el clima de Sur America.

Palabras Claves: Modelado Numérico, Llanuras de inundación, Pantanal, Hidrología, Interacciones Suelo-Atmsféra

Remerciements

Cette thèse est le résultat d'un long chemin rempli d'obstacles, qu'ils soient scientifiques ou pandémiques. Au cours de ce long parcours je n'ai cessé d'apprendre et de grandir, comme on dit "*l'important ce n'est pas la destination c'est le voyage*". Néanmoins, je suis heureux d'être arrivé au bout et j'ai hâte de reprendre la route. Ce chemin ne s'est pas fait seul et pour cette raison je tiens à saluer et remercier toutes les personnes qui ont pu m'aider, que cela soit sur le plan professionnel ou personnel.

Je tiens tout d'abord à remercier mes directeurs, Anna, Jan et Lluís. Merci Jan pour ton accompagnement, pour m'avoir guidé dans la démarche scientifique que représente une thèse de doctorat, merci d'avoir partagé avec moi ton enthousiasme pour la science et de m'avoir aidé à faire face aux méandres de la modélisation climatique. Gracias Anna por haber hecho posible esta tesis, por haber facilitado mi integración en la comunidad científica Argentina, por haberme guiado a lo largo de los diferentes temas de investigación que surgieron y por ayudarme a aprehender el ámbito científico y sus códigos. Gracias también a Lluís por tu acompañamiento a lo largo de la tesis.

Agradezco también a las personas que fueron mis profesores en el CIMA / DCAO, sus enseñanzas fueron esenciales para que pueda capacitarme para afrontar esta tesis. Gracias a todas las personas con las cuales tuve la oportunidad de trabajar y compartir proyectos apasionantes y, en particular, el grupo ILLAPA. Merci au Laboratoire de Météorologie Dynamique de m'avoir reçu et de m'avoir donné les moyens, entre autres numériques, de réaliser cette thèse.

Sur le plan personnel, je dédie cette thèse à ma famille qui m'a toujours soutenu et encouragé. Une pensée particulière pour mes parents avec qui j'ai beaucoup partagé que cela soit dans la plaine des Vosges ou dans les montagnes de Salta, à Quentin et Mélanie ainsi que Sylvie, Francis, Manon et Juliette. Um abraço grande para os meus avós, obrigado por estes bons momentos compartilhados que fazem bem à cabeça e ao estômago. A ma grand-mère qui n'aura pas pu voir l'aboutissement de cette thèse, je pense à toi.

Une dédicace à mes amis néocastriens, pour tous ces instants volés entre les allers-retours Buenos Aires/Neufchâteau et pour tous ces bons souvenirs qui aident à aller de l'avant en souriant au passé. Dédicace à Johan et Charline, Lucas et Morgane, Charles et Sophie, Maëlle, Jimmy, Mathieu, Quentin. La liste est encore longue mais une grosse pensée à tous les autres et spécialement aux petits nouveaux, Gabriel et Georges. Spéciale dédicace à mes camarades de la Tanière et un grand salut aux anciens de Nancy que j'ai pu revoir et avec qui j'ai pu partager quelques aventures parisiennes au cours des dernières années.

Un saludo grande a todos mis compañeros becarios de la facu. Gracias por convertirme en un argento más, por ayudarme a lo largo de la tesis y salvarme de los meandros

burocráticos de la universidad. Un recuerdo especial a todos los buenos momentos, los asados, las charlas de almuerzo y discusiones de pasillo. Un saludo en particular para Inés, siempre presente cuando necesite ayuda, Sol, mi maestra financiera y cumbiera, Pablo por todas estas charlas de pasillo en las cuales se nos iba el tiempo, Felix siempre con buenos planes, para todos los ocupantes del box (Julian, Tanea y Guillermo), para Noelia, Vicky, Celeste, Leandro, Lucia, Romina, Natalia, Nadia, Hernán y todos los demás. Un grand salut aussi aux doctorants et post-docs du LMD pour m'avoir toujours intégré durant mes passages à Palaiseau, un salut en particulier à Antoine, Aissa, Doug, Julie et Lucia.

Finalmente, dedico esta tesis a la persona que me acompañó a lo largo de este viaje, en las buenas y en las malas. Agustina, gracias por tu amor y por los bailes de cuarteto. Gracias por todo amorcito.

VI

*Desde o começo do mundo água e chão se amam
e se entram amorosamente
e se fecundam.
Nascem peixes para habitar os rios
E nascem pássaros para habitar as árvores.
As águas ainda ajudam na formação dos caracóis e das
suas lesmas.
As águas são a epifania da criação.*

*Agora eu penso nas águas do Pantanal.
Penso nos rios infantis que ainda procuram declives
para escorrer.
Porque as águas deste lugar ainda são espriadas
para alegria das garças.*

Menino do Mato
Manoel de Barros

Contents

1	Introduction	1
1.1	Scientific Context	1
1.2	Literature Review	5
1.2.1	Tropical floodplains in the world and in South America	5
1.2.2	The Pantanal	7
1.2.3	Hydrological modelling of the floodplains	11
1.2.4	Interaction with the atmosphere	17
1.2.5	Ecology and Hydrology	20
1.2.6	Carbon cycle	22
1.2.7	Human impact on Pantanal	23
1.3	Motivation	26
1.4	Document Structure	26
1.5	Acronyms	28
2	Benefits of representing foodplains in a Land Surface Model: Pantanal simulated with ORCHIDEE CMIP6 version	31
2.1	Introduction	31
2.2	Pantanal simulated with ORCHIDEE CMIP6 version	32
2.3	Acronyms	59
3	Estimation of the flooded area over the Pantanal, a South American floodplains, using MODIS data	63
3.1	Introduction	63
3.2	Remote sensing of floodplains	64
3.3	Acronyms	81
4	RoutingPP: Parallelized construction of a flexible river routing graph for Earth System Models	83
4.1	Introduction	83
4.2	General Methodology	86
4.2.1	General Objectives and Issues	87
4.2.2	Global methodology	88
4.2.3	Partitioning of the atmospheric grid	89
4.2.4	Overlap of the atmospheric and hydrologic grids	90
4.2.5	Routing construction	91
4.2.6	Truncate	95
4.2.7	Calculation of the upstream area	97

4.2.8	Localization of the fluviometric stations	97
4.3	Validation	98
4.3.1	Hydrological Inputs	98
4.3.2	Methodology	100
4.3.3	Influence of the hydrological input	100
4.4	Discussion and Conclusion	102
4.5	Access to RoutingPP	103
4.6	Acronyms	104
5	Development of a high resolution floodplains scheme	105
5.1	Introduction	106
5.2	Floodplains scheme description	106
5.2.1	Representing the water flow on a graph	106
5.2.2	Water Continuity Equation: stream reservoir	108
5.2.3	Water Continuity Equation: floodplain reservoir	110
5.2.4	Floodplains geometry	112
5.2.5	Ancillary data	114
5.2.6	Workflow of the Module	116
5.3	Methodology and Dataset	116
5.3.1	Model Description: ORCHIDEE	116
5.3.2	Methodology of Validation	117
5.3.3	Discharge	118
5.3.4	Statistical indexes	119
5.3.5	Flooded area	120
5.3.6	Water Storage	121
5.4	Results	122
5.4.1	Comparison with the previous version	122
5.4.2	Assessment of the floodplains at different resolutions	126
5.5	Discussion and Conclusion	134
5.6	Acronyms	137
6	Evaluation of the impact of the high resolution floodplains scheme on the surface variables in ORCHIDEE	141
6.1	Introduction	141
6.2	Methodology	142
6.2.1	Simulations	142
6.2.2	Overview	143
6.2.3	Water Cycle and Vegetation	143
6.2.4	Land atmosphere fluxes	144
6.2.5	Evapotranspiration and Budyko Diagram	145
6.3	Results	146
6.3.1	Impact on the surface variables	146
6.3.2	Changes in Surface Energy Budget	153
6.3.3	Evapotranspiration	155
6.3.4	Budyko Diagram	157
6.4	Conclusion	159
6.5	Acronyms	163
7	Feedback between the floodplains and the atmosphere	165
7.1	Introduction	165
7.2	Model description and Methodology	170
7.2.1	RegIPSL : Model description	170
7.2.2	Subdivision of the Pantanal region	172
7.2.3	Methodology	172

7.3	Results	174
7.3.1	Impact of the coupling	174
7.3.2	Impact of the floodplains on the coupled simulations	175
7.3.3	Changes in Precipitation over the Pantanal	183
7.3.4	Impact on the regional circulation	188
7.4	Discussion and Conclusion	192
7.5	Acronyms	195
8	Discussion, conclusion and perspectives	197
8.1	Synthesis	197
8.1.1	What brings the necessity to represent the tropical floodplains in a LSM?	198
8.1.2	Highlight the difficulties of flooded area detection / representation	198
8.1.3	Importance to facilitate the development and integration of new processes in LSM	199
8.1.4	Implementation of a high resolution floodplains scheme	200
8.1.5	Assess the impact of the tropical floodplains on the surface conditions	200
8.1.6	Evaluate the impact of the tropical floodplains on the atmosphere	201
8.1.7	Analyze the impact of the Pantanal on the regional climate	201
8.2	Perspectives	202
8.2.1	Improve the floodplains representation	202
8.2.2	Going further on the floodplains study	203
8.2.3	Include more wetland type	203
8.2.4	Going further in the River Modelling	205
8.2.5	Toward more Coupled simulation with RegIPSL	205
8.3	Acronyms	206
	Appendices	207
	A Acronyms	208
	B List of Variables	215

List of Figures

1.1	Illustration of the floodplains in normal conditions (a) and in flood conditions (c). Illustration of the different precipitation processes that may cause a flood: remote precipitation over a area upstream of the floodplains in a large catchment (b) and local precipitation (d).	4
1.2	World's most important tropical floodplains.	6
1.3	(a) Topography of South America from MERIT HydroDEM (Yamazaki et al, 2019) and (b) Mean annual precipitation between 1981 and 2019 from the precipitation product of the Global Precipitation Climatology Centre (GPCC).	7
1.4	Global Lakes and Wetland Dataset (GLWD , WWF, 2004) of floodplains, flooded forest and flooded swamps categories, as well as the location of the major tropical South American Floodplains and Flooded Forest.	8
1.5	Description of the main sub-catchment of the La Plata Basin.	9
1.6	Description of the Upper Paraguay River Basin (UPRB) with the localization of the Pantanal, the Cerrados mountain and the Gran Chaco Plains.	10
1.7	(a) Mean austral summer precipitation (wet season over Amazon and UPRB) and (b) mean austral winter precipitation (dry season over Amazon and UPRB) between 1981 and 2019 from GPCC.	11
1.8	Illustration of the hydrological processes of land and atmosphere of the Upper Paraguay River Basin from Bergier (2013).	12
1.9	Scheme of the austral summer large scale circulation over South America with the fluxes of moist air from the Northeast trade winds that cross the Amazon to the Southeastern South America (SESA) and the localization of the South American Low-Level Jet (SALLJ).	13
1.10	River network over the Upper Paraguay River Basin (extracted from Silva et al, 2017). The main Paraguay river has been underlined.	14
1.11	Landsat 8 images extracted from Google Earth Engine from (a) the Mekong Delta in Vietnam (b) The Paraná Delta in Argentina (c) the Lena Delta in Russia and (d) the Yukon river in the USA.	14
1.12	Description of the different types of unit-catchment in CaMa-Flood: (a) vector-based unit catchment, (b) river network and regular atmospheric grid, (c) grid-based unit catchment and (d) hybrid-based unit catchment.	15
1.13	Illustration of the representation of the floodplains in the ORCHIDEE floodplains scheme (D'Orgeval, 2006; Guimberteau et al, 2013; Schrapffer et al, 2020).	16

1.14	Illustration of how the CAMA-FLOOD model (Yamazaki et al, 2009, 2011, 2013) simulates the river channel and floodplains reservoir for each hydrological unit (Figure from Yamazaki et al, 2011).	17
1.15	Illustration of how the different component of the MGB model interacts (Figure from Fleischmann et al.,2017).	18
1.16	Main heat fluxes over (a) non-flooded and (b) flooded regions is the net radiation, H the sensible flux, LE the latent heat flux related to evaporation and LT to transpiration.	19
1.17	Resume of the different impact of a westward MCS on the atmosphere when passing over a dry (a) and a moist (b) surface (extracted from Adler et al, 2011).	21
1.18	Schematic diagram showing the major components of the carbon cycle (extracted from Kayranli et al, 2010).	23
1.19	Human-related changes to the Pantanal hydrology (extracted from Bergier, 2013).	25
2.1	Location and description of the Pantanal topography, including Porto Murtinho and Ladário river gauging stations	34
2.2	Description of ORCHIDEE routing scheme, the floodplain module and their interactions with the atmospheric forcing and soil hydrology module	38
2.3	Mean annual precipitation (a) and piechart of mean annual precipitation covered by three classes: < 800, between 800 and 1200 mm and > 1200 mm (b) upstream of the Porto Murtinho station.	41
2.4	Mean annual precipitation over Porto Murtinho upstream area between 1961 and 2000 for the different forcing	42
2.5	(a) to (f) represent the mean annual cycle of discharge at Porto Murtinho station between 1961 and 2000 for each forcing with FP in green, NOFP in orange and observations in black, mean discharge is also displayed by a line left of each annual cycle. Concentration degrees and concentration period vectors for Porto Murtinho discharge between 1961 and 2000 are represented for original forcing and CLARIS-lpb corrected forcing respectively in (g) and (h), with FP (solid lines) and NOFP simulations(dashed lines) and Observations (black line).	44
2.6	Standardized Taylor diagram comparing simulated monthly river discharge with observation for Porto Murtinho station between 1961 and 2000. CRUNCEPv7, WFD and GSWP3 forcings and their CLARIS correction are represented respectively by red, blue and green elements. Circles and stars are for original forcings while squares and crosses represent CLARIS corrected forcings. Circles and squares indicate simulations with an activated floodplain module (FP) module whereas stars and crosses indicate NOFP simulations.	46
2.7	Distribution of (a) the concentration degree and (b) the concentration period of each one of the 40 years of simulation for the discharge in Porto Murtinho for the FP and NOFP simulations forced by CRUNCEPv7, WFD and GSWP3. The distribution of the concentration degree uses 6 evenly spaced bins between 0 and 0.6. The distribution of the concentration period uses 5 bins, one for each month between January and May.	47
2.8	Annual cycle of flooded area upstream of Ladário for ORCHIDEE's simulations and Hamilton (2002) averaged over the 1961-2000 period and for Padovani (2010) averaged over the 2000-2009 period.	48
2.9	Geomorphic description of floodplains from GFPLAIN250m dataset (a) upscaled to 0.5° (b) and mean flooded fraction in ORCHIDEE averaged over the 1961-2000 period for each grid point and all 6 forcing (b-d and f-h).	50

2.10	Distribution of mean monthly flooded fraction upstream of Porto Murtinho (x-axis) in relation with the mean difference of evapotranspiration between the FP and the NOFP simulations ($\Delta E = E_{FP} - E_{NOFP}$, y-axis) among the grid points with mean flooded fraction up to 10 %	51
2.11	Mean difference between precipitation and evapotranspiration (P-E) for all 6 forcings with the FP and the NOFP configurations between 1961 and 2000.	52
2.12	Mean annual cycle of monthly P-E flux between 1961 and 2000 for the 6 different forcings with the FP simulation (solid blue line) and the NOFP simulation (dashed red line) among the grid points with mean flooded fraction up to 10 %. The mean value is also displayed by a line left of each annual cycle.	53
3.1	Localization and description of the Pantanal wetlands inside the Upper Paraguay River Basin. The blue layer corresponds to the flood extent from WaterMap (Pekel et al. 2016; Source: EC JRC/Google).	68
3.2	Number of monthly available data for this MODIS product and number of dates available without clouds between 2002 and 2004.	69
3.3	Results of the spectral indexes for two different dates: one during the dry period and one during the wet period.	71
3.4	Distribution of the mNDWI / NDMI / NDVI values of the pixels.	72
3.5	Illustration of k-means model output for $k = 6$ for (a) the wet and (b) the dry reference images and (c) distribution of the cluster in the (mNDWI / NDMI space).	73
3.6	Values for the second dimension of the PCA for the wet reference image.	73
3.7	Time series of Padovani (2010), the river height at Ladário and of the results from the threshold-based methods using (a) mNDWI, (b) NDMI and (c) NDMI-NDVI.	75
3.8	Time series of Padovani (2010), the river height at Ladário and of the results from the threshold-based methods using (a) the Principal Component Analysis (PCA) method and (b) the k-means algorithm with $k = 6$	76
3.9	Flood frequency between 2002 and 2009 obtained from the different methods presented: 3 threshold-based methods using the (a) mNDWI, (b) NDMI and (d) NDMI-NDVI index and 2 unsupervised classification methods: (e) Principal Component Analysis and (f) k-means. Occurrence of flood from (c) Padovani (2010) and (g) WaterMAP (Pekel et al, 2016; Source: EC JRC/Google) between 1984 and 2015 and floodplains delimitation from GFPLAIN250m (Nardi et al, 2019).	78
3.10	NDVI (a,b,c) and flood estimate (d,e,f) and for t_0 (21/03/2004; a and d), t_1 (22/03/2007; b and e) and t_2 (06/03/2021; c and f).	79
4.1	(a) Overlap of the Hydrological grid and the Model grid, (b) construction of the HTUs, (c) HTUs after truncate.	87
4.2	Environment of the RoutingPP program.	88
4.3	Representation of how the optimal recut of a subdomain is done.	90
4.4	Representation of the steps to recut a domain from 3 subdomains to 12 subdomains.	90
4.5	Representation of a subdomain with its core domain and halo	91
4.6	Illustration of the fraction of hydrological pixels overlapping with an atmospheric grid point.	91
4.7	Resume of the steps of the construction of the high resolution river routing graph.	92
4.8	Illustration of the decomposition steps of the area driven subdivision of the HTUs.	93
4.9	Illustration of the decomposition steps of the area driven subdivision of the HTUs.	94

4.10	Illustration of the the construction of the HTU over the Rhone basin near Valence in France with the map of the region (a), the flow accumulation (b) and orography (c) in MERIT-Hydro and the construction of the HTUs over this grid point (d). In (d), the HTU corresponding to the main river is in yellow and the mainstream river, i.e. the Rhone river, is represented in dark yellow.	96
4.11	Illustration of the calculation of the upstream area within the parallelized structure.	97
4.12	Localization of stations in the routing graph using MERIT compared to Fekete-Vorosmarty (a) and using MERIT compared to HydroSHEDS for Western Europe over a 0.5° atmospheric grid.	99
4.13	Map of the Western Europe with the representation of the 8 basins considered and their respective key stations emplacement. The annual cycle of the observed and discharge of the 3 simulations with different routing graph (Fekete-Vorosmarty, MERIT and HydroSHEDS) are represented using the reference at their emplacement on the map.	101
4.14	Normalized Taylor Diagram for the discharge at the key stations over Western Europe for the simulation forced by WFDEI_GPCC with the routing scheme based on MERIT during the 1990-2010 period.	102
5.1	A sample graph to illustrate the indexing convention and the placement of fluxes out the vertices (F) as well as the overflow fluxes (O).	107
5.2	Scheme resuming the movement between the different reservoirs for a HTU which has floodplains and its upstream HTUs depending if (a) the upstream HTU has floodplains or if (b) the upstream HTU doesn't have floodplains.	109
5.3	Schematic representation of the definition of the water involved in the overflow.	112
5.4	(a) Figure 4.9 from Tristan d'Orgeval's thesis representing the parameterization of the floodplains shape, (b) relationship between the floodplains area and floodplains height depending on β parameter with $h_0 = 2m$ and $f_{max} = 1$ and (c) relationship between the volume in the floodplains reservoir and the height of the floodplains depending on the value of the β parameters for $h_0 = 2m$	113
5.5	Workflow of the floodplains processes over a time step.	117
5.6	Annual cycle of the variables in the atmospheric forcings WFDEI_GPCC and AmSud_GPCC between 1990 and 2013 over the Upper Paraguay River Basin (UPRB).	119
5.7	Mean duration in months of the floods over the Pantanal in the monthly GIEMS-D15 product over the 1993-2004 period (extracted from Fluet-Chouinard et al, 2015).	121
5.8	Normalized Taylor Diagram for the discharge at Porto Murtinho between 1961 and 2000 for the pair of simulation (with -FP- and without -NOFP- floodplains) forced by the GSWP3 and CRUNCEPv7 with the previous floodplains scheme (LR) and the high resolution floodplains scheme (HR).	123
5.9	(a) Cp /Cd diagram for the discharge at Porto Murtinho between 1961 and 2000 for the pair of simulation (with and without floodplains) forced by the GSWP3 and CRUNCEPv7 with the previous floodplains scheme (LR) and the high resolution floodplains scheme (HR). Annual cycle for the discharge at Porto Murtinho for the simulations forced by GSWP3 (b and c) and CRUNCEPv7 (d and e) for the dry period from 1961 to 1975 (b and d) and for the wet period from 1980 to 2000 (c and e).	124
5.10	Annual cycle of the flooded area over the Pantanal for the different FP simulations (GSWP_HR, GSWP_LR, CRUNCEPv7_HR and CRUNCEPv7_LR) and the flooded area estimated by Hamilton (2002) for the dry period from 1961 to 1975 (a) and for the wet period from 1980 to 2000 (b).	126

5.11	Map of the flooded area forced by GSWP3 (a-h) and CRUNCEPv7 (i-p) with the high resolution version of the floodplains (a-d; i-l) and with the previous version of the floodplains (e-h; m-p). The mean flooded area is presented for the period 1961-1975 (a,e,i,m), for the period 1981-2000 (b,f,j,n), the anomaly for the dry season - SON - between 1961 and 2000 (c,g,k,o) and the anomaly for the flood season - MAM - between 1961 and 2000 (d,h,l,p).	127
5.12	Taylor Diagram between 1990 and 2013 for the discharge at Porto Murtinho for the pair of simulations with (FP) and without floodplains (NOFP) forced by WFDEI_GPCC and AmSud_GPCC with high resolution floodplains scheme (HR).	128
5.13	(a) Taylor Diagram and (b) annual cycle of the discharge at Porto Murtinho between 1990 and 2013 simulated by each pair of simulations (with -FP- and without floodplains -NOFP-) forced by WFDEI_GPCC and AmSud_GPCC with the high resolution floodplains scheme (HR).	129
5.14	Annual cycle of the content of water in the different reservoir: slow (a-b), stream (c-d), fast (e-f), flood (g-h), integrated Soil Moisture (i,j) for the pair of simulations FP and NOFP forced by WFDEI_GPCC (a,c,d,e,g,i) and AmSud_GPCC (b,d,f,h,j). (k) shows the annual mean value of the water storage in the different reservoirs, a logarithmic scale is used to facilitate the comparison.	131
5.15	Time serie of the flooded area in the simulations with the high resolution floodplains scheme (HR) forced by WFDEI_GPCC and AmSud_GPCC for the 1990's (a), 2000's (b) and 2010's (c) in comparison to the different satellite estimate available over the region: Hamilton (2002) until 2000, Padovani (2010) between 2000 and 2010, GIEMS-2 (Prigent et al, 2020) for the period 1992-2015 and the flood estimate based on MODIS MOD09A1 using the mNDWI spectral index (cf. Chapter 3).	133
5.16	Evaluation of the spatial representation of the floodplains in ORCHIDEE in the simulation forced by WFDEI_GPCC (a-c), by AmSud_GPCC (d-e) and estimated by GIEMS-2 (g-i) for the full 1992-2013 period (a,d,g) and over two specific seasons over the same period: the dry season - SON - over the same period (b,e,h) and the flood season - MAM - (c,f,i).	135
6.1	Description of the potential vegetation cover ($max_{vegetfrac}$) for all the vegetation types (PFT) existing over the Pantanal in the simulations. The PFT are constructed from the ESA-CCI database (European Space Agency-Climate Change Initiative; ESA, 2017).	144
6.2	Illustration of the Budyko diagram.	146
6.3	Mean of the soil moisture over the upper level (below 0.5m depth) during the 1990-2013 period considering the full year (a,d,g,j) the dry season - SON (b,e,h,k) and the flood season - MAM (c,f,i,l) for the WFDEI_GPCC_FP simulation (a,b,c) and the AmSud_GPCC_FP (d,e,f) as well as the difference between the FP and NOFP simulations for WFDEI_GPCC (g,h,i) and AmSud_GPCC (j,k,l).	147
6.4	Average Surface Temperature in the NOFP simulation forced by WFDEI_GPCC (a,b,c) and AmSud_GPCC (d,e,f) and the difference between the FP and NOFP simulation for WFDEI_GPCC (g,h,i) and AmSud_GPCC (j,k,l) between 1990-2013 period considering the full period (a,d,g,j), the dry season (b,e,h,k) and the flood season (c,f,i,l).	149
6.5	Representation of the distribution of the average daily temperature over the most flooded part of the Pantanal for the pair of simulation with and without floodplains forced by WFDEI_GPCC and AmSud_GPCC during the period 1990-2013. The extremas, the median as well as the percentile 10, 25, 75 and 90 are represented.	150

6.6	Bar plot of the percentage of the maximum vegetation cover in the model for the FP (blue) and NOFP (orange) simulations during the dry season - SON (no hatch) and during the flood season - MAM (hatched) for the simulations forced by WFDEI_GPCC (a) and AmSud_GPCC (b).	151
6.7	Fraction of each grid point covered by vegetation ($\sum_{j \in PFT} \text{vegetfrac}_j$ without considering the bare soil fraction) in WFDEI_GPCC_FP (a,b,c) and AmSud_GPCC_FP (d,e,f) and the relative difference between FP and NOFP for WFDEI_GPCC (g,h,i) and AmSud_GPCC (j,k,l) for the period 1990-2013 considering the full year (a,d,g,j), the dry season - SON (b,e,h,k) and the flood season - MAM (c,f,i,l).	152
6.8	Mean Evaporative fraction for each grid point in WFDEI_GPCC_NOFP (a,b,c) and AmSud_GPCC_NOFP (d,e,f), the WFDEI_GPCC_FP (g,h,i) and the AmSud_GPCC_FP (j,k,l) for the period 1990-2013 considering the full year (a,d,g,j), the dry season - SON (b,e,h,k) and the flood season - MAM (c,f,i,l).	154
6.9	Average value over the Pantanal of the different terms of the equation 6.1 between 1990 and 2013.	155
6.10	Annual cycle of the Evapotranspiration variables for WFDEI_GPCC: (a) Total evapotranspiration, (b) Bare soil evaporation, (c) Transpiration, (d) Potential Evaporation, (e) Evaporation from floodplains and (f) Interception loss.	156
6.11	Evapotranspiration over each grid point in WFDEI_GPCC_FP (a,b,c) and AmSud_GPCC_FP (d,e,f) and the relative difference between FP and NOFP for WFDEI_GPCC (g,h,i) and AmSud_GPCC (j,k,l) for the period 1990-2013 considering the full year (a,d,g,j), the dry season - SON (b,e,h,k) and the flood season - MAM (c,f,i,l).	158
6.12	Budyko diagram for the FP and NOFP simulations forced by AmSud_GPCC and WFDEI_GPCC between 1990 and 2013. Each points represent the mean of the different variable over the Upper Paraguay River Basin (UPRB) averaged over a year of simulation. The stars represents the mean value over the 24 years of simulation.	159
6.13	Budyko Inspired diagram for the evolution for the different season and the mean state of the most flooded grid points, i.e. with a mean flooded fraction higher than 5% for the different pair of simulations. The results for WFDEI_GPCC are shown in a) and for AmSud_GPCC in b).	160
6.14	Summary of the different impact of the floodplains over the land surface variables in a Land Surface Model.	162
7.1	Floodplains in the river routing file for the AmSud domain.	169
7.2	Scheme of RegIPSL coupled model.	170
7.3	CORDEX-SA domain used for the simulations.	172
7.4	Regions considered to subdivide the Pantanal and its surroundings.	173
7.5	(a) shows the annual cycle between 1998 and 2019 of the precipitation over the Upper Paraguay River Basin for both coupled simulations, (b) and (c) represents respectively the mean flooded area in AmSud_Flood and AmSud_offline_FP while (e) represents the annual cycle of the flooded area for these two simulations. (d) shows the discharge at Porto Murtinho in the three simulations.	175
7.6	Changes of (a) Evapotranspiration, (b) bare soil evaporation, (c) transpiration, (d) Potential evapotranspiration, (e) Evaporation from floodplains and (f) Interception loss over the Pantanal between AmSud_Flood, AmSud_NoFlood AmSudNOF_offline_FP.	176
7.7	Annual cycle of the precipitation for AmSud_Flood, AmSud_NoFlood and the GPCC dataset over the five subregions defined between 1998 and 2019.	177

- 7.8 Presentation of the mean value of Precipitation minus Evapotranspiration for AmSud_NoFlood (a-d), AmSud_Flood (e-h) and the difference between both (i-l) average over the different season : DJF (a,e,i), MAM (b,f,j), JJA (c,g,k), SON (d,h,l). The differences between AmSud_Flood and AmSud_NoFlood, which have a significance level higher than 95% using a Student's t-test are hatched. 178
- 7.9 Mean vertical profile of actual temperature between 25°S and 12.5°S for AmSud_NoFlood (a-d) and the difference between AmSud_Flood and AmSud_NoFlood (e-h) for the different season: DJF (a,e), MAM (b,f), JJA (c,g) and SON (d,h). The differences between AmSud_Flood and AmSud_NoFlood, which have a significance level higher than 95% using a Student's t-test are hatched. The average of the difference of near-surface temperature between AmSud_Flood and AmSud_NoFlood as well as the average of the flooded fraction in AmSud_Flood between 25°S and 12.5°S is shown for DJF (i), MAM (j), JJA (k) and SON (l). 179
- 7.10 Mean vertical profile of specific humidity between 25°S and 12.5°S for AmSud_NoFlood (a-d) and the relative difference between AmSud_Flood and AmSud_NoFlood (e-h) for the different season: DJF (a,e), MAM (b,f), JJA (c,g) and SON (d,h). The differences between AmSud_Flood and AmSud_NoFlood, which have a significance level higher than 95% using a Student's t-test are hatched. The average of the difference of near-surface specific humidity and evapotranspiration between AmSud_Flood and AmSud_NoFlood between 25°S and 12.5°S is shown for DJF (i), MAM (j), JJA (k) and SON (l). 180
- 7.11 Mean value of the Planetary Boundary Layer height for AmSud_NoFlood (a-d), AmSud_Flood (e-h) and the relative difference between both (i-l) average over the different season : DJF (a,e,i), MAM (b,f,j), JJA (c,g,k), SON (d,h,l). The differences between AmSud_Flood and AmSud_NoFlood, which have a significance level higher than 95% using a Student's t-test are hatched. 181
- 7.12 Mean vertical profile of equivalent potential temperature between 25°S and 12.5°S for AmSud_NoFlood (a-d) and the relative difference between AmSud_Flood and AmSud_NoFlood (e-h) for the different season: DJF (a,e), MAM (b,f), JJA (c,g) and SON (d,h). The differences between AmSud_Flood and AmSud_NoFlood, which have a significance level higher than 95% using a Student's t-test are hatched. The average of the difference of near-surface equivalent potential temperature and precipitation between AmSud_Flood and AmSud_NoFlood between 25°S and 12.5°S is shown for DJF (i), MAM (j), JJA (k) and SON (l). 182
- 7.13 Annual cycle between 1998 and 2019 of the cloud cover fraction (clt, a-e), the low (cll, f-j), medium (clm, h-o) and high (clho-t) cloud cover over the different subregions: P (a,f,l,p), NNE (b,g,k,q), W (c,h,m,r), S (d,i,n,s) and F (e,j,o,t). 183
- 7.14 Annual cycle between 1998 and 2019 of the different radiative fluxes at the surface: downward (a-e) and upward (f-j) longwave radiation, downward (h-o) and upward (o-t) shortwave radiation over the different subregions: P (a,f,l,p), NNE (b,g,k,q), W (c,h,m,r), S (d,i,n,s) and F (e,j,o,t). 184
- 7.15 Non-convective (pr_{NOC} , a-d) and convective (pr_C , i-l) precipitation for AmSud_NoFlood and the respective difference between AmSud_Flood and AmSud_NoFlood (d-h for pr_{NOC} and m-p for pr_C). The results are averages between 1998 and 2019 over the different seasons: DJF (a,e,i,m), MAM (b,f,j,n), JJA (c,g,k,o) and SON (d,h,l,p). The differences between AmSud_Flood and AmSud_NoFlood, which have a significance level higher than 95% using a Student's t-test are hatched. 185
- 7.16 Frequency of rainless days ($PP < 1\text{mm}$) over the different regions: the Pantanal (P), North/East (NNE), South (S), West (W) and the most flooded area (F) between 1998 and 2019 for AmSud_Flood, AmSud_NoFlood and GPCC for the different seasons: DJF (a), MAM (b), JJA (c) and SON (d). 186

7.17	Boxplot of the distribution of the precipitation considering the rainy days ($PP > 1\text{mm}$) over the 5 subregions (P,NNE,W,S,F) for AmSud_Flood, AmSud_NoFlood and GPCC for the different seasons: DJF (a), MAM (b), JJA (c) and SON (d) during the 1998-2019 period.	187
7.18	Average diurnal cycle of precipitation for AmSud_NoFlood (a-d), AmSud_Flood (e,h) and the difference between AmSud_Flood and AmSud_NoFlood (i-l) for the different 6 hours interval of a day considered in the local time (UTC-3): 0h-6h (a,e,i), 6h-12h (b,f,j), 12h-18h (c,g,k) and 18h-24h (d,h,l) averaged between 1998 and 2019. The differences between AmSud_Flood and AmSud_NoFlood, which have a significance level higher than 95% using a Student's t-test are hatched.	188
7.19	Wind at 850 hPa for AmSud_NoFlood (a-d), AmSud_Flood (e-h) and the difference between both between 1998 and 2019. The average for the different season is shown: DJF (a,e,i), MAM (b,f,j), JJA (c,g,k) and SON (d,h,l). The filled contour on the subplots indicates the windspeed.	189
7.20	Vertically integrated moisture transport from the surface to 300 hPa for AmSud_NoFlood (a-d), AmSud_Flood (e-h) and the difference between both between 1998 and 2019. The average for the different season is shown: DJF (a,e,i), MAM (b,f,j), JJA (c,g,k) and SON (d,h,l). The filled contours on the subplots indicates the norm of the flux the AmSud_NoFlood (a-d) and AmSud_Flood (e-h) and the difference of precipitation between AmSud_Flood and AmSud_NoFlood in (i-l). The differences between v _{imt} in AmSud_Flood and AmSud_NoFlood, which have a significance level higher than 90% using a Student's t-test are hatched.	190
7.21	Specific humidity at 850 hPa for AmSud_NoFlood (a-d), AmSud_Flood (e-h) and the difference between both between 1998 and 2019. The average for the different season is shown: DJF (a,e,i), MAM (b,f,j), JJA (c,g,k) and SON (d,h,l). The differences between v _{imt} in AmSud_Flood and AmSud_NoFlood, which have a significance level higher than 95% using a Student's t-test are hatched.	191
7.22	Summary of the local impacts of the floodplains (a) on the atmosphere, (b) on the local precipitation, (c) on the regional precipitation and (d) on the regional circulation as demonstrated with the comparison of a coupled simulation integrating the floodplains with a coupled simulations without floodplains.	194

List of Tables

2.1	Assessment of the monthly river discharge simulated by the ORCHIDEE model at Porto Murtinho station between 1961 and 2000 by two hydrological indexes. NSE is the Nash–Sutcliffe efficiency and PBIAS is the Percentage Bias of the volume.	45
2.2	Correlation between monthly simulated flooded area upstream of Ladário and Hamilton (2002) monthly flooded area for the 1961-2000 period, all correlations have a confidence level higher than 99%	49
2.3	Water closure budget with CRUNCEPv7_FP and CRUNCEPv7_NOFP simulations to perform a residual estimation of evapotranspiration over Pantanal region upstream of Porto Murtinho and downstream of the different inflows. The error of P is the standard deviation of the 4 observational datasets used in the forcings (CRU TS3.24, CRU TS2.10, GPCC and CLARIS-lpb).	56
3.1	Spectral indexes considered in this study with some reference papers and the specificity of these indexes.	70
3.2	Methods and their corresponding threshold values.	74
3.3	Resume of the statistics (Percentage bias - PBIAS, Root-Mean Square Error - RMSE, Correlation) comparing Padovani (2010) estimate with the different methods: threshold-based applied to mNDWI, NDMI and NDMI-NDVI, Principal Component Analysis (PCA) method and k-means with k = 6. The correlations are significant with a significance level of 99 %.	77
5.1	Parameterization of the floodplains scheme depending on the resolution of the atmospheric grid.	116
5.2	Comparison of the simulation between the high resolution floodplains scheme and the previous version of the floodplains scheme using statistical index (NSE, PBIAS, RMSE, Corr). The asterisk is used next to the value of the correlation if the confidence of the correlation is higher than 99%.	125
5.3	Evaluation of the discharge at the outflow of the Pantanal for the simulations with the high resolution routing scheme with and without the floodplains scheme activated forced by two atmospheric forcings with a different resolution (WFDEI.GPCC and AmSud.GPCC) using statistical index (NSE, PBIAS, RMSE, Corr).	129

5.4	Correlation between the anomaly of total water storage from GRACE and the volume of water in the different reservoir over the Pantanal region between 2003 and 2013 normalized by the mean and standard value between 2004 and 2010. The asterisk signals that the correlation has a level of significance higher than 99%.	130
7.1	Parameterization of the WRF simulations.	171
7.2	Description of the simulations.	173

CHAPTER 1

Introduction

Contents

1.1	Scientific Context	1
1.2	Literature Review	5
1.2.1	Tropical floodplains in the world and in South America	5
1.2.2	The Pantanal	7
1.2.3	Hydrological modelling of the floodplains	11
1.2.4	Interaction with the atmosphere	17
1.2.5	Ecology and Hydrology	20
1.2.6	Carbon cycle	22
1.2.7	Human impact on Pantanal	23
1.3	Motivation	26
1.4	Document Structure	26
1.5	Acronyms	28

1.1 Scientific Context

Water is a key element of the Earth System climate which affects the energy fluxes and is part of large-scale circulations processes regulating the climate ([Sorooshian et al, 2005](#) - GEWEX). The water cycle affects all the climate components: the atmosphere, the ocean, the land and the cryosphere. Although water fluxes over land are smaller compared to the oceanic and atmospheric fluxes ([Rodell et al, 2015a](#)), they have an important impact on land processes and, as it usually concerns freshwater, they are of vital interest for the human system and the ecosystem we live in ([IPCC, 2019](#); [Sorooshian et al, 2005](#); [Vörösmarty et al, 2000](#); [Oki and Kanae, 2006](#)).

The land surface is a lower boundary for the atmosphere through which land and atmosphere can exchange energy, water and carbon (Seneviratne and Stöckli, 2008). Precipitation drives locally the terrestrial hydrological cycle whereas soil moisture and evapotranspiration processes impacts the repartition between latent and sensible heat fluxes between the land and the atmosphere (Dirmeyer, 2011; Seneviratne et al, 2010a). Therefore, depending on the region and season, there may exist a strong coupling between the land surface and the atmosphere (Knist et al, 2017). Many modelling studies show that this coupling may affect the atmosphere at larger time scales (Charney et al, 1975; Shukla and Mintz, 1982; Delworth and Manabe, 1989; Dirmeyer, 2003). This coupling is said to be more important in transitional climate zones (Koster et al, 2004, 2006; Dirmeyer et al, 2009; Dirmeyer, 2013; Knist et al, 2017) such as the Southeastern South America (SESA) and the South Atlantic Convergence Zone (SACZ) (Sörensson and Menéndez, 2011; Wei and Dirmeyer, 2012; Ruscica et al, 2015; Spennemann and Saulo, 2015; Spennemann et al, 2017). These strong coupling areas may evolve with the future climate changes and, for example, the SESA and the SACZ are projected to extend northward in the Pantanal region in Mato Grosso (Ruscica et al, 2016). Strong surface contrasts in temperature and surface heat fluxes, such as floodplains or wetlands in a dry region, may also play an important role on the land-atmosphere coupling (Taylor, 2010; Taylor et al, 2018).

The terrestrial hydrological cycle is at the heart of the land-atmosphere interaction loop as it drives the availability of water. The terrestrial hydrological cycle is interacting with the atmosphere in different ways and the atmosphere is sensitive to changes in land hydrological conditions (Seneviratne et al, 2010b; Subin et al, 2012; Taylor, 2010). It also has a vital importance for the human system and the human activities which are very dependent on land hydrology such as agriculture, whether it is rainfed (Bradford et al, 2017) or irrigated (Schlenker et al, 2007; Yin et al, 2020; Wada et al, 2013), hydroelectricity production (Xie et al, 2019; Getirana et al, 2020), industry and human consumption (Wakode et al, 2018; Sutanudjaja et al, 2018). Thus, the knowledge of the terrestrial hydrological cycle is imperative for various strategic reasons: assessment of the water availability to organize and facilitate sustainable uses (Douveille and Chauvin, 2000; Baik et al, 2019; Peng et al, 2019; Ahmad and Hossain, 2020), prediction and adaptation to the extreme hydrological events such as droughts and floods, protection of the natural ecosystem and valorization of their systemic services (Alfieri et al, 2012; Hao et al, 2017; Hamilton, 1999; Davis et al, 2015; Brauman et al, 2007). Understanding the terrestrial hydrological cycle is a first step to solve adaptation issues related to climate change (IPCC, 2019; Sorooshian et al, 2005 - GEWEX).

Wetlands are regions which are temporarily or permanently flooded. These areas are places of rich ecological diversity with intense interactions with the carbon cycle (Ramsar, Iran, 1971; Mitsch et al, 2013). The floodplains are a specific type of wetland which can be defined by the following definition from Junk et al (1989):

"floodplains are areas that are periodically inundated by the lateral overflow of rivers or lakes, and/or by direct precipitation or groundwater, changing the physicochemical environment such that the biota respond by morphological, anatomical,

physiological, phenological and/or ethological adaptations, and produce characteristic community structures.”

In other terms, floodplains are wetlands which flood is related to the overflow of lakes/ivers or to groundwater rise. The overflow may have different origins: the precipitation, the river flow or the tidal water. Figure 1.1.a and 1.1.c illustrate the flood process over the floodplains. Meanwhile the tidal water occurs over the coastal area, the precipitation-related floodplains are usually located over low-order streams and are a response to local intense rainfall and soil moisture conditions (cf. Figure 1.1.b). The floodplains related to river flow occur over large rivers and are the results of the precipitation over remote regions in the upstream area (cf. Figure 1.1.d). There is an important interest for the river-flow-related floodplains because they are an area of rich biodiversity as the water of the river producing the floods brings nutrients from the upstream regions and also because they modulate the discharge of important rivers (Junk and Furch, 1993). Their floods are more predictable as they are principally caused by remote precipitation over large areas and, thus, are related to climate characteristics. It is the case of the Pantanal and Amazon which annual floods are related to the monsoon precipitation (Junk and Furch, 1993). The precipitation-related floodplains are affected by non-periodic floods driven by the interaction of different flood processes related to the precipitation and/or to the groundwater such as it occurs in the Pampa (Kuppel et al, 2015). In conclusion, this type of floodplains is a very particular place for both the terrestrial hydrological cycle and the ecosystem. In general, water flowing in the river system has a limited impact on the land-atmosphere interaction as it mainly remains in the river channel but in large floodplains, the river system has a direct impact on the land-atmosphere fluxes due to the extensive open-water surface which can impact the heat and water fluxes at the surface.

La Plata Basin is located in Central South America. It is the world's fifth largest basin (Barros et al, 2006) and is located in a transitional zone and contains a large variety of climate from the tropical savanna in the North of the Basin, the semiarid climate in the West and the Humid Subtropical climate in the South. The largest part of the La Plata Basin is recognized for being a high coupling strength (hotspots) between land and atmosphere (Sörensson and Menéndez, 2011; Ruscica et al, 2014) and is also impacted by the South American Low Level Jet (SALLJ) which brings moisture from the Amazon (Salio et al, 2007). The La Plata Basin is composed of the Paraná river and the Uruguay river. The Paraguay basin which is the major tributary of the Paraná river hosts the world's largest floodplains: the Pantanal. UNESCO considers this floodplains, as extensive as five time Belgium, as a World Heritage Site since 2000. It is located in a tropical region between the Amazon and Southeastern South America (SESA). Beside the local land-atmosphere interactions, such a large extension of open water in a tropical region may also affect the regional atmospheric circulation as the SALLJ, which transports moisture from the Amazon to the SESA region, flows over the Pantanal region (Thielen et al, 2020; Araujo et al, 2018). The Pantanal is a region sparsely populated and with scarce meteorological observations. This is limiting the possibility to properly study and understand the local dynamic of its hydrological cycle. This is why satellite data and modelling are required to further investigate this type of region at a larger scale.

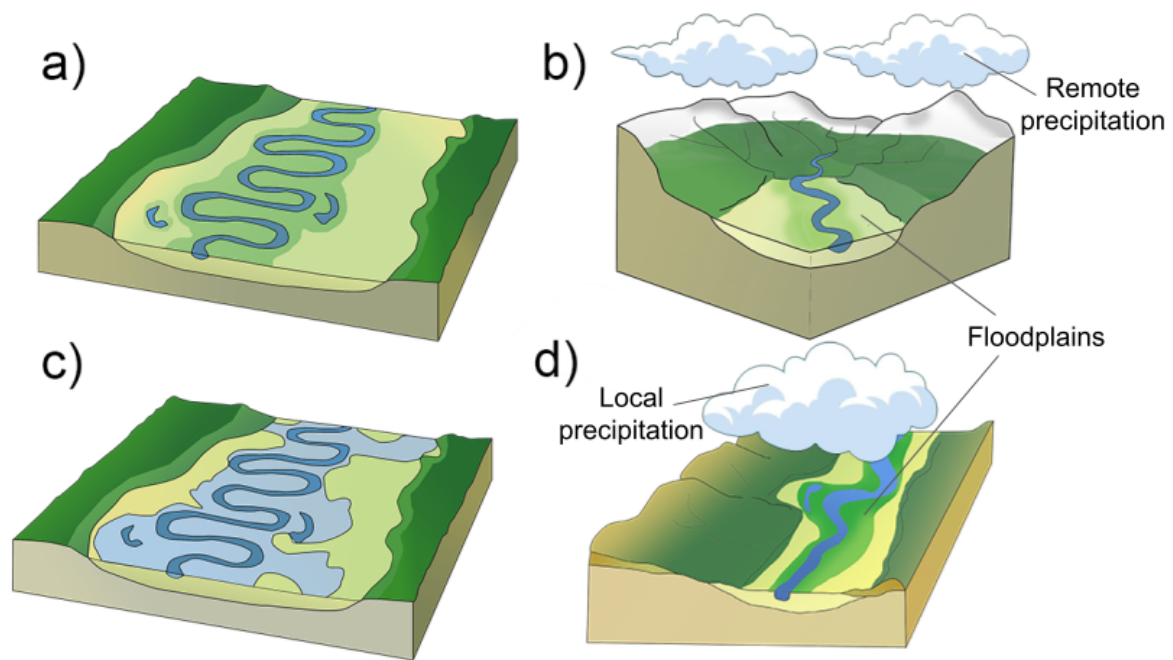


Figure 1.1. *Illustration of the floodplains in normal conditions (a) and in flood conditions (c). Illustration of the different precipitation processes that may cause a flood: remote precipitation over a area upstream of the floodplains in a large catchment (b) and local precipitation (d).*

Apart from the Pantanal, the other large tropical floodplains are also considered as biodiversity hotspots with a complex hydrology. Although they may share some common characteristics, each one has its specificities and is located in a different climatological context. The Amazon and the Congo basins are extensive and contains many floodplains (Junk and Piedade, 2005; Lee et al, 2011). The study of these regions is a challenging task for hydrologist whether is concerns their hydrological simulation of the use of remote sensing in particular for their extensive surface, the diversity and the density of the vegetation and the presence of other flood type such as flooded forest or swamps (Junk et al, 2011; Jung et al, 2010; Fatras et al, 2021; Fassoni-Andrade et al, 2021). The Sudd over the Nile basin has a complex divergent flow which is difficult to study considering the relative absence of river gauge (Sutcliffe and Brown, 2018). The Niger Inner delta has been largely studied and in particular the important land-atmosphere interactions occuring there (Taylor, 2010), for its hydrology (D'Orgeval et al, 2008; Fleischmann et al, 2018) and the challenge to identify the flood through remote sensing (Ogilvie et al, 2015a).

Numerical modelling of the Earth System is a powerful tool for studying numerous processes and how they interact with each other. It also helps to overcome the scarcity of data when trying to understand poorly quantified processes. It is also essential to perform forecasts and future projections such as meteorological forecasts or climate change projections. The modelling of land processes and of the terrestrial water cycle is performed through Land Surface Models (LSMs) which can be coupled to an atmospheric model within the framework of a regional model to study, among other subjects, the land-atmosphere interactions. To represent the river hydrology, LSMs either include a river routing scheme (Dadson et al, 2011; Guimberteau et al,

2012a; Sheng et al, 2017) or can be coupled to an hydrological model (Vincendon et al, 2010). Some LSMs already represents the floodplains processes in their river routing scheme such as ORCHIDEE (D'Orgeval et al, 2008; Guimberteau et al, 2012a) and JULES (Dadson et al, 2010). Recent advancement in LSMs tend toward higher resolution river routing schemes (Nguyen-Quang et al, 2018a; Lin et al, 2019). The higher resolution of the routing scheme may bring a more detailed representation of the river network but the change in resolution requires re-designing some of the processes already implemented, such as the floodplains or the irrigation.

This present thesis is at the crossroad between the study of the floodplains, their interaction with the atmosphere and the model development needed to adapt the floodplains scheme at higher resolution. For this reason, this thesis has three main objectives: (1) to show the benefits of representing floodplains in LSMs to improve the representation of hydrology and land-atmosphere interactions, (2) to develop a high resolution floodplains scheme to represent the floodplains and the corresponding pre-processing tools to do so and (3) to better understand the floodplains hydrology and their interactions with the atmosphere using the floodplains scheme developed in a LSM and to possibility to couple this LSM to an atmospheric model. In order to complete the present objectives, this thesis focus on the Pantanal in South America, one of the world's largest floodplains, using the ORCHIDEE LSM.

This chapter will present the scientific context and litterature review of the floodplains modelling by giving more details on the large tropical floodplains with a particular interest for the major South American floodplains and, in particular, for the Pantanal which is at the heart of this thesis. This chapter will also underline the importance of the tropical floodplains in different domains such as modelling, land-atmosphere interaction, hydrology and ecology as well as their strong interaction with the carbon cycle. It will also make a particular focus on how the human activity threats floodplains.

1.2 Literature Review

1.2.1 Tropical floodplains in the world and in South America

The different types of ecosystemic services provided by the floodplains and their interaction with the other key components of the earth system become more important as the area of the floodplains is larger. This is why large tropical floodplains are of great significance as their relation with the hydrology, the ecosystem and the atmosphere are much larger than medium-sized floodplains on higher latitude.

Among the workd's largest tropical floodplains we can cite the Amazon basin (Junk and Piedade, 2005), the Congo river basin (Lee et al, 2011), the Pantanal in the Paraguay river basin (Alho, 2005), the Sudd in the Nile river basin (Sutcliffe and Brown, 2018), the Lake Chad basin (Mitsch, William J, Gosselink, 2015; Fraser and Keddy, 2005), the Inner Niger Delta (D'Orgeval et al, 2008; Ogilvie et al, 2015b; Taylor, 2010). We may also cite an important subtropical floodplains: the Mississippi river basin (Shaffer et al, 2005) whose floods in spring/summer can be driven by different processes such as snowmelting (van der Wiel et al, 2018). Please

see Figure 1.2 for more details.



Figure 1.2. *World's most important tropical floodplains.*

The large tropical floodplains are all part of some of the largest basins in the world. They are generated by rivers from hydrologically important catchment flowing into poorly drained regions. Each large tropical floodplains has its specificity because their interaction with the rest of the Earth System relies on the regional climate, on their configuration relative to the local topography, on the local river network, on their seasonality and the type of soil and vegetation cover.

Most of the tropical part of South America on the eastern side of the Andes has a moist climate with high values of annual precipitation except in Northeastern Brazil where precipitation only reaches between 250 and 500 annual mm (cf. Figure 1.3). As a consequence of the high level of incoming water, Tropical South America has a dense river network with some of the world's largest basins which have among the world's largest streamflow (Neiff, 1996). The two largest basins are the Amazon and the Paraná basin. The precipitation in this region has a strong seasonal variability with a dry and a wet period which means that the incoming water will be concentrated on a certain period of the year. The peak of the discharge over large rivers will overflow the surrounding area when reaching poorly drained regions. Thus, due to this dense river network, the high quantity of water it transports and the relative flatness of the region, most of the wetlands in Tropical South America are actually floodplains (Neiff J., 1999). The main tropical floodplains in tropical South America are shown in Figure 1.4.

Most of the Amazon can be considered as potential floodplains but the most active region is the Amazon mainstream (Alsdorf et al, 2010) which transport very large volumes and flood the river banks. There are other floodplains in the Amazon such as the Llanos de Moxos in the Madeira basin (Hamilton et al, 2004) and the Roraima floodplains along the Rio Negro basin (Hamilton et al, 2002). We may also cite the Llanos del Orinoco (Hamilton et al, 2004) and the Bananal (Borma et al, 2009). The Pantanal is another very remarkable tropical South American floodplains as it's the world's largest continuous floodplains.

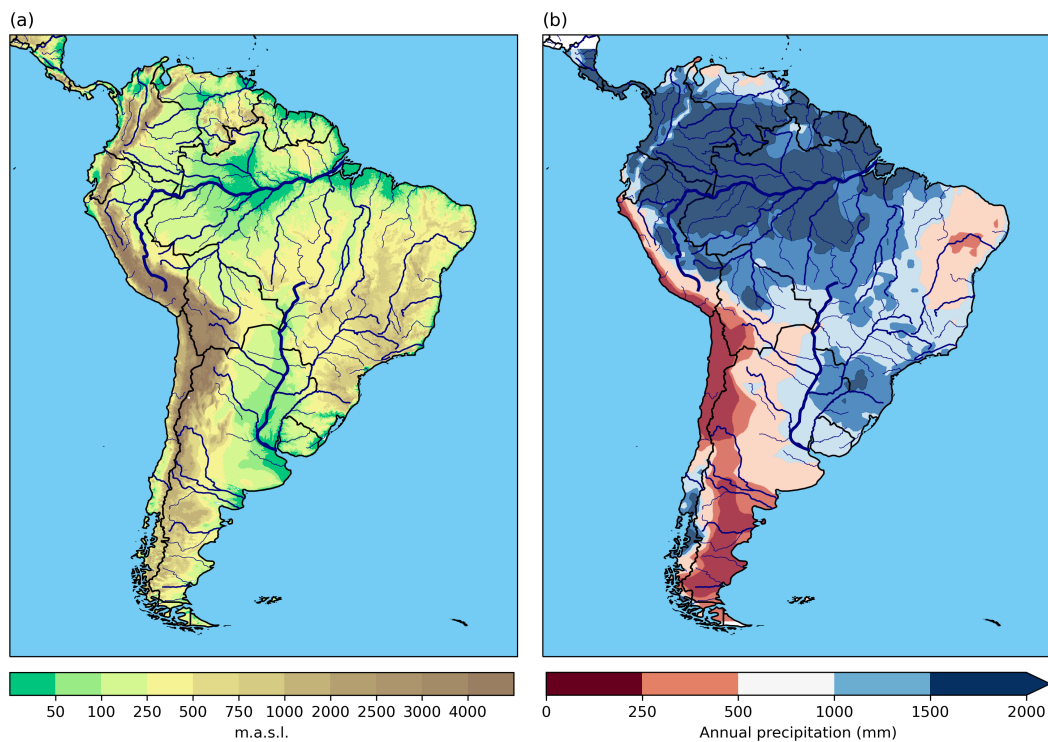


Figure 1.3. (a) Topography of South America from MERIT HydroDEM (Yamazaki et al, 2019) and (b) Mean annual precipitation between 1981 and 2019 from the precipitation product of the Global Precipitation Climatology Centre (GPCC).

1.2.2 The Pantanal

The La Plata Basin is the fifth largest basin in the world with an extension of 3,100,000 km² (Barros et al, 2006) and is represented in Figure 1.5. It mainly flows in a North-South direction bringing water from the tropical latitude to the subtropical latitude and thus connecting both areas. This fluvial corridor contributes to the richness of the sediments along the rivers in the subtropical part of the basin (Neiff et al, 2005; Minotti, 2018). It is composed of two main rivers: the Paraná and the Uruguay rivers which flow into the La Plata Estuary (Berbery and Barros, 2002; Barros et al, 2005; Gonçalves et al, 2011). The major tributary of the Paraná river is the Paraguay river which flows from the Central North of the basin. It has its source in South West Brazil then flows along the border between Brazil and Bolivia, flows across the Paraguay and then joins the Paraná in the North of Argentina, near Corrientes (cf. Figure 1.5). The upper part of the Paraguay Basin is referred as the Upper Paraguay River Basin (UPRB) and contains the world's largest floodplains: the Pantanal (Alho et al, 1988; Penatti et al, 2015; Bravo et al, 2012; de Almeida et al, 2015).

The UPRB is composed of three different regions: the Cerrado, the Gran Chaco plains and the Pantanal. The Gran Chaco Plains are located at the west of the UPRB meanwhile the Cerrado highlands at the north / east of the basins which are also referred to as Planalto. Both of these regions flow into the Pantanal located at the Central south of the UPRB. The Pantanal is a very flat region of 150 000 km², with between 80 and 150 m.a.s.l of altitude (Hamilton et al, 1996; Alho, 2005; Gonçalves et al, 2011), meanwhile the Cerrado highlands altitude ranges between

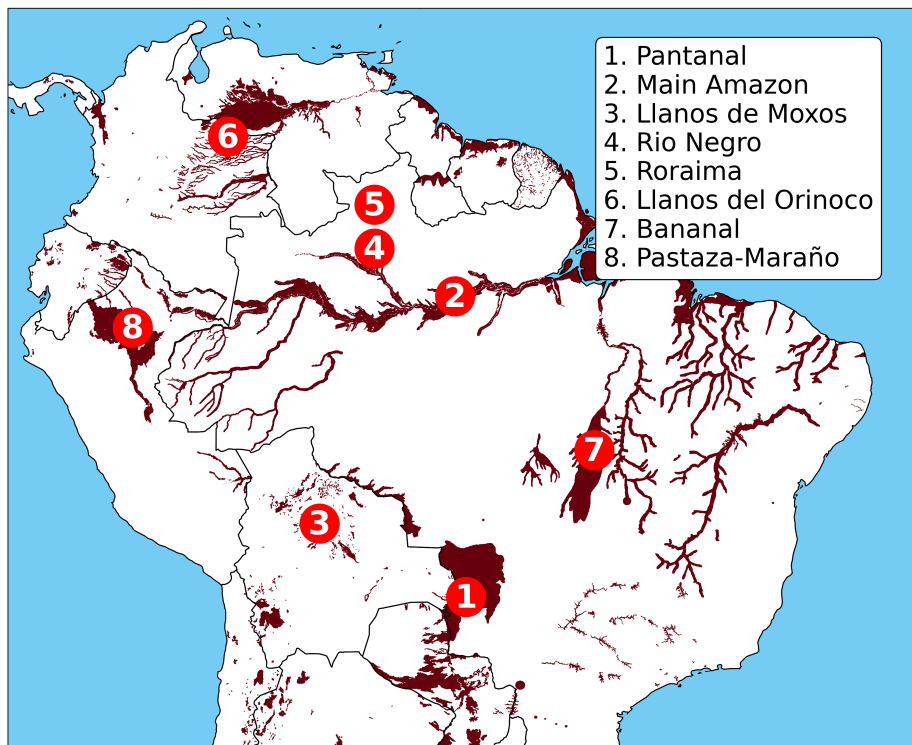


Figure 1.4. *Global Lakes and Wetland Dataset (GLWD , WWF, 2004) of floodplains, flooded forest and flooded swamps categories, as well as the location of the major tropical South American Floodplains and Flooded Forest.*

200 and 1400 m.a.s.l (Alho, 2005; Gonçalves et al, 2011).

During the austral summer, the trade winds gets stronger due to the warming of the continent and the contrast between land-sea temperature. They are deflected to the south due to the Andes Cordillera. This moist and warm air is responsible for higher precipitation over the region during the austral summer meanwhile the austral winter is much drier (cf. Figure 1.7). This phenomenon is referred to as the South American Monsoon System (SAMS - Zhou et al, 1998; Barros et al, 2006). The monsoon system is located over the Amazon and extends to the Southeast of the basins in what is called the South Atlantic Convergence Zone (SACZ). The UPRB is composed of lowlands surrounded by the Cerrado mountain range and is located at the limits of the SAMS and SACZ. The combination of the moist and warm mass of air from the SACZ and the topography generate higher precipitation on the Cerrado due to an orographic effect (cf. Figure 1.8; Bergier, 2013).

Tropical South America at the East of the Andes (except Northeastern Brazil) has a wet season from October to March and a dry season from April to September. The climate in this tropical region also affects directly higher latitude climate due to the South American Low Level Jet (SALLJ - Carvalho et al, 2004; Montini et al, 2019) which flows from the Amazon to the La Plata basin and brings the moist air from the Amazon to the higher latitudes (cf. Figure 1.9). The SALLJ increases the humidity in the La Plata Basin and, in particular, in the SouthEastern South America (SESA). It also enhances the development of Mesoscale Convective Systems in the region (Salio et al, 2007). The SALLJ may flow over the Pantanal region and, therefore,

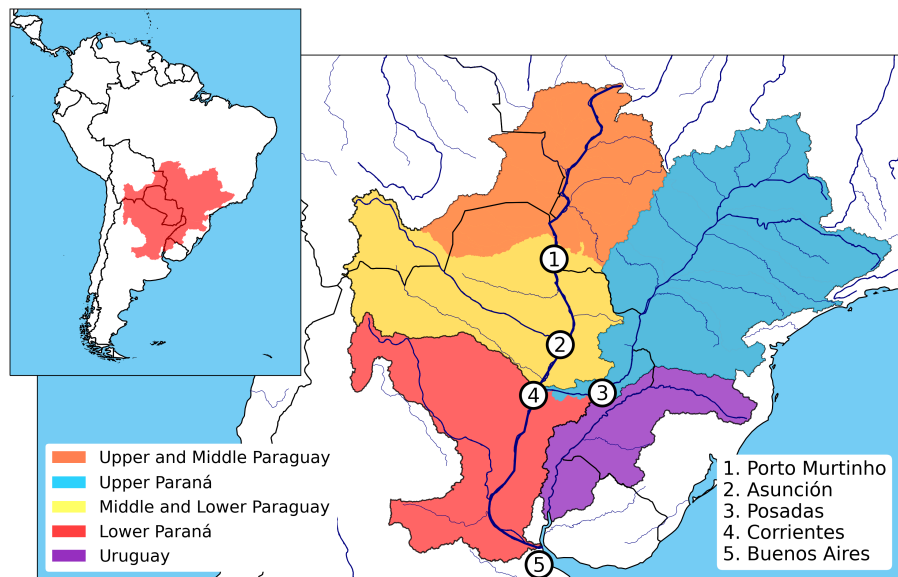


Figure 1.5. Description of the main sub-catchment of the La Plata Basin.

may affect the local precipitation (Martins et al, 2013). However, the SALLJ may also be affected by the Pantanal surface conditions (Martins et al, 2013) which is how the Pantanal may affect the climate at higher latitude in the SESA regions such as what happens with the low-level jets in the Great Plains (Campbell et al, 2019; Arcand et al, 2019; Yang et al, 2020). This interaction between the Pantanal and the SALLJ is not well documented.

All these major circulation patterns are themselves affected by the global teleconnections and the Sea Surface Temperature (SST) patterns such as the South Atlantic High, the Madden-Julian Oscillation, or by La Niña, El Niño conditions in the Pacific ocean (Haylock et al, 2006). The influence of the different teleconnections patterns over the Pantanal region have been studied in different publications (Thielen et al, 2020; Silva et al, 2017; Bergier, 2010; Clarke, 2005).

The UPRB follows the same precipitation pattern as the SAMS with a wet and a dry season. Although, the subbasin is a climate transition zone between the SAMS and the higher latitude climate that we may decompose between 3 regions: (1) the Cerrado mountain range at the North / Northeast of the basin which has a wet tropical climate with intense precipitation during the wet season from October to March due to the SAMS, (2) the Gran Chaco at the west of the subbasin which have a semi arid climate and (3) the Pantanal which is between the two last-mentioned regions and is a transitional climate zone between the wet and the semi-arid climate (Gonçalves et al, 2011). Bravo et al (2012) estimate that the Cerrado provides around 80% of the UPRB outflow.

The local river network is described in Figure 1.10. The main river in the Pantanal is the Paraguay river which comes to the North / Northwest of the Pantanal in the Cerrado mountain and crosses the Pantanal along its Western delimitation. Its main tributaries are the São Lourenço river which drains the water from the Cuiaba river and from the Itiquira-Piquiri river. Then, in the middle of the Pantanal, the Paraguay river receives the water from the Taquari

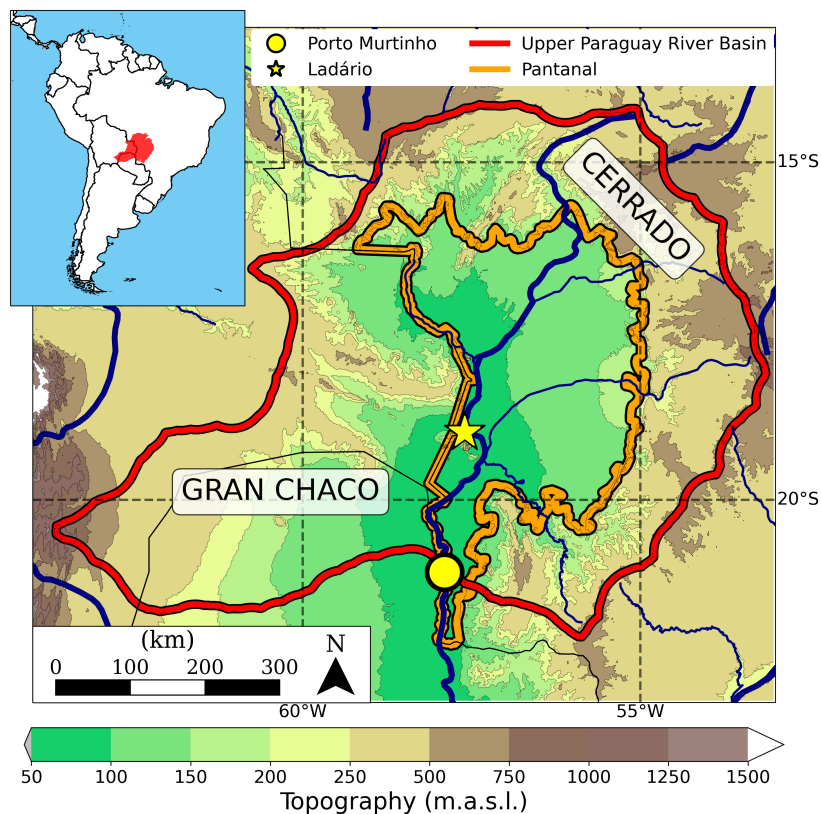


Figure 1.6. Description of the Upper Paraguay River Basin (UPRB) with the localization of the Pantanal, the Cerrados mountain and the Gran Chaco Plains.

river and a few dozen kilometers from there it receives the water from the basins of the Southern Pantanal through the Miranda river which also drains the Aquidauana basin. Due to the low slope, the rivers in the Pantanal usually contain many meanders (Barros et al, 2005). As the local orography reduces the velocity of the flow, the Pantanal delay the river flow coming from the austral summer precipitation over the basin between 3 and 5 months at the outflow of the basin (Barros et al, 2005; Hamilton et al, 1996; Padovani, 2010; Gonçalves et al, 2011). It converts the region into an important natural reservoir of water which generates extensive floods following a regular and predictable annual cycle (i.e. it has a large annual flood pulse).

The flood pulse in the Pantanal has its origin from the precipitation in its North-Northeast upstream area during the austral summer (December-February). The floods over the Pantanal are influenced by the variability of the precipitation, the complexity of the river network and of the memory of the floodplains - the impact of the previous year flooding on the actual year (Clarke, 2005). Despite this, the Pantanal presents a high seasonality of flooded areas with a maximum in April and a minimum in October (Penatti et al, 2015). The flooding diminishes and delays the discharge peak compared to the one of rainfall (Hamilton et al, 1996) acting as a low-pass filter for the river discharge and the catchment hydrology. This delayed discharge effect is crucial to understand the hydrology of the Paraguay river hydrology which contributes to the Middle Paraná stream (Barros et al, 2005) and may prevent the floods downstream of the Pantanal (Hamilton, 1999).

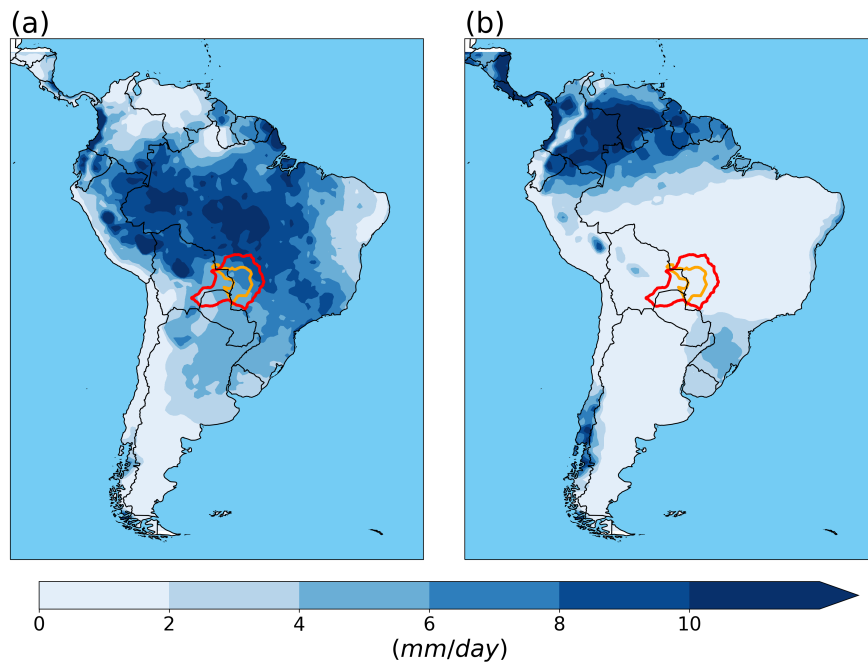


Figure 1.7. (a) Mean austral summer precipitation (wet season over Amazon and UPRB) and (b) mean austral winter precipitation (dry season over Amazon and UPRB) between 1981 and 2019 from GPCP.

1.2.3 Hydrological modelling of the floodplains

Types of models available to simulate floodplains

Different approaches can be taken to model floodplains. Two main trends can be distinguished: (1) the approach of the Land Surface Models and (2) the approach of the Regional / Global Hydrological Models. In the first case, the main objective is to correctly simulate the land processes over the floodplains and thus, the impact of the floodplains on the land surface conditions. This is crucial in the case of a land-atmosphere coupled simulation. The second approach aims principally to correctly simulate the river discharge with the flooded area as a diagnostic of the correct simulation of the water in the floodplains.

The LSMs are generally based on an atmospheric grid because they are either forced by an offline forcing or coupled to an atmospheric model. The atmospheric grid does not correspond to the characteristics of the natural river system which poses a major difficulty improving the modelling of the rivers and the floodplains in this type of model. On the contrary, the recent hydrological models are generally using a vector-based routing system which respects the actual shape of the sub-catchment. They simulate the river discharge through the river height and the parameterization of the channel (shape and characteristics). These models may be forced by the river height or discharge. They can also be coupled to a Land Surface Model forced by an offline forcing to provide runoff and drainage inputs. The election of the type of model to use depends on the finality of the study. As LSMs focuses on the representation of the land surface processes, they are perfectly adapted to study the land-atmosphere interactions. Hydrological models focuses on the simulation of the river dynamic but, in the case of being used to study land-atmosphere interactions, they need to be coupled to a LSM and may

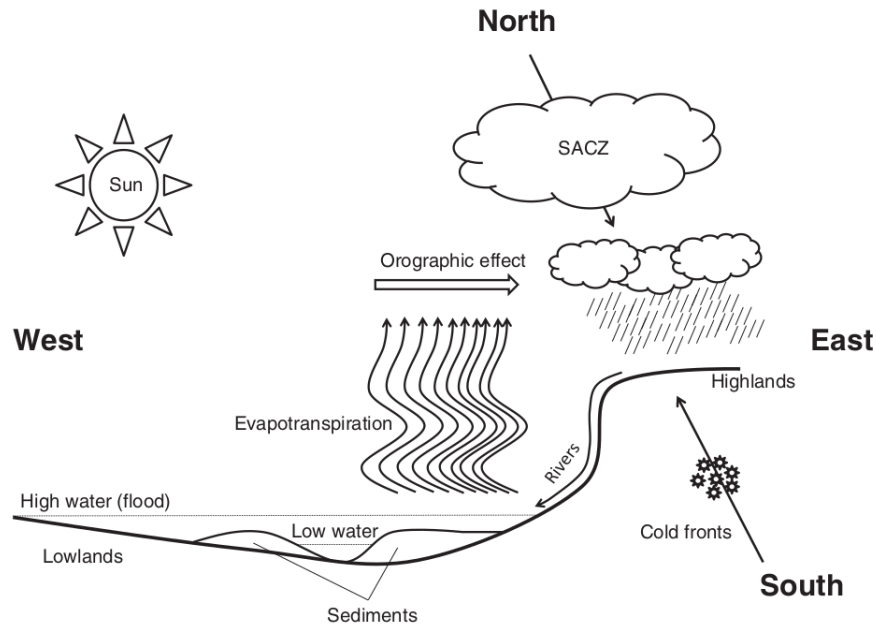


Figure 1.8. Illustration of the hydrological processes of land and atmosphere of the Upper Paraguay River Basin from [Bergier \(2013\)](#).

require an extra-interpolation which would bring an information loss. Hydrological models don't usually calculate the heat fluxes so they may require an extra-layer to do the energy balance. It brings more complexity while the LSMs already integrate the calculation of the land surface variables. Both approaches have additional limits because the dynamic of the floodplains is determined by the local topography at different scale and this variable brings some uncertainty over lowland region. Some complex high resolution processes (< 1 km) may also be difficult to model such as alluvial fans, deltas or other types of divergent flows (cf. [Figure 1.11](#)). Moreover, the rivers over the floodplains also evolve dynamically and their course can change over time.

Representation of the Hydrological network

Different types of river network maps exist in LSMs and Global Hydrological Models (GHMs). All these river network maps are based on basic hydrological units which may have different definitions depending on the model. Each hydrological unit has its own hydrological characteristics and is connected to other hydrological units. It is possible to classify the river network maps in three categories: grid-based, vector-based and hybrid unit-catchment ([Yamazaki et al, 2013](#)), see [Figure 1.12](#). The grid-based unit catchment is the most common river network map in LSMs; it divides the river network in a regular grid in which the river is defined for each cell (flow direction, upstream area etc.). The vector based-description ([Figure 1.12.a](#)) uses hydrological units corresponding to the sub-catchment. These units are constructed based on Geographic information systems data (GIS) without considering an atmospheric grid issue. Although the actual gridded description of the river network benefits from a high resolutions (90-m for MERIT Hydro; [Yamazaki et al, 2019](#)), the recent large-scale hydrological models tend to prefer the vector-based approach due to its lower computational cost, a reduction of the model uncertainty and other advantages for the hydrological studies ([Fan et al, 2021](#)).

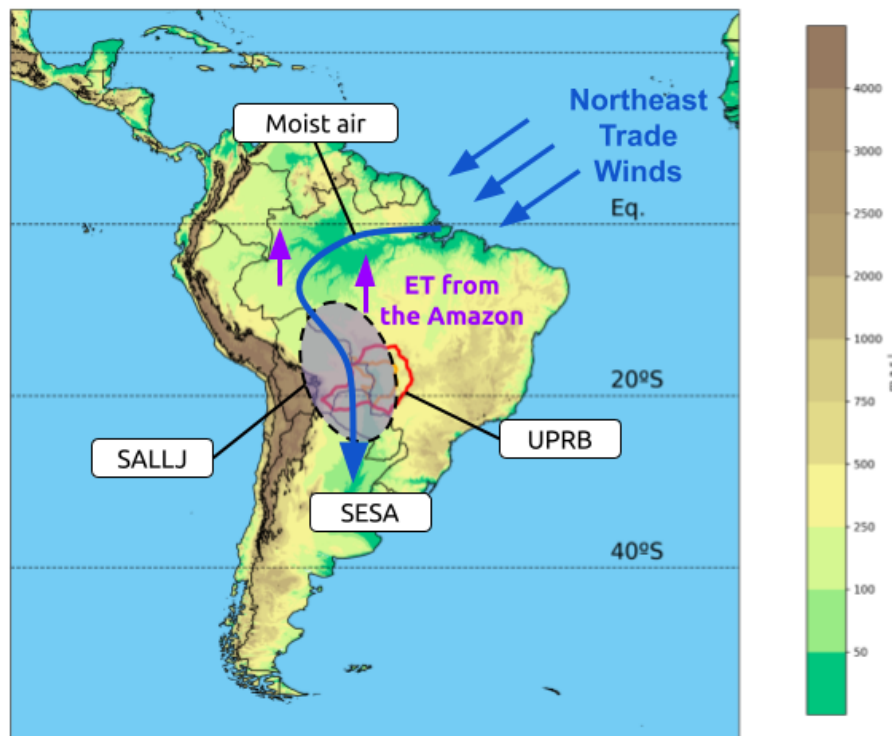


Figure 1.9. Scheme of the austral summer large scale circulation over South America with the fluxes of moist air from the Northeast trade winds that cross the Amazon to the Southeastern South America (SESA) and the localization of the South American Low-Level Jet (SALLJ).

The LSMs usually respects the atmospheric grid as their original purpose is to provide realistic land surface conditions for atmospheric models (cf. Figure 1.12.b). However, although their river routing scheme generally uses a grid-based description of the river network (cf. Figure 1.12.c), the grid used by the routing scheme of the LSM do not necessarily correspond to the grid used by the LSM. If the grids are different, the river routing may: (1) be used only as a diagnostic or (2) be interpolated to give a feedback to the LSM. In the last years, different efforts have been made to combine the vector-based unit catchment respecting the atmospheric grid such as with the Hydrological Response Units (HRUs - Chaney et al, 2016) or the Hydrological Transfer Units (HTUs - Nguyen-Quang et al, 2018b). Thus, the river routing in LSM tends toward a subgrid parameterization based on unit-catchment. These approaches are called hybrid unit-catchment (cf. Figure 1.12.d). Nowadays, the two way coupling between the river routing and the Land Surface Model is a particular struggle (Getirana et al, 2021) due to the interest in land-atmosphere feedbacks and the coupled simulations that can be performed to study them. To fulfill this objective, the challenge for hydrological modeling is to improve the coupling with the LSMs while the challenge for the river routing integrated into the Land Surface Models is to improve their representation of the river network while respecting the atmospheric grid constraints.

The recent GHMs aim to study principally the river dynamic, thus most of them base their model on vector-based river networks. The GHMs using vector-based river networks are usu-

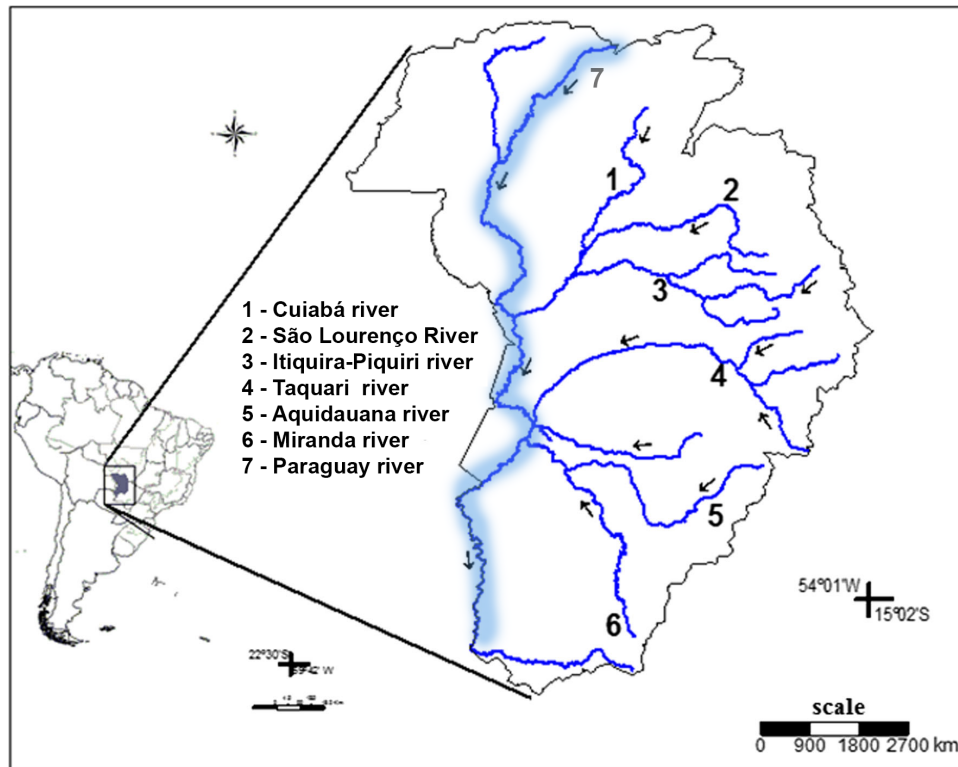


Figure 1.10. River network over the Upper Paraguay River Basin (extracted from [Silva et al, 2017](#)). The main Paraguay river has been underlined.

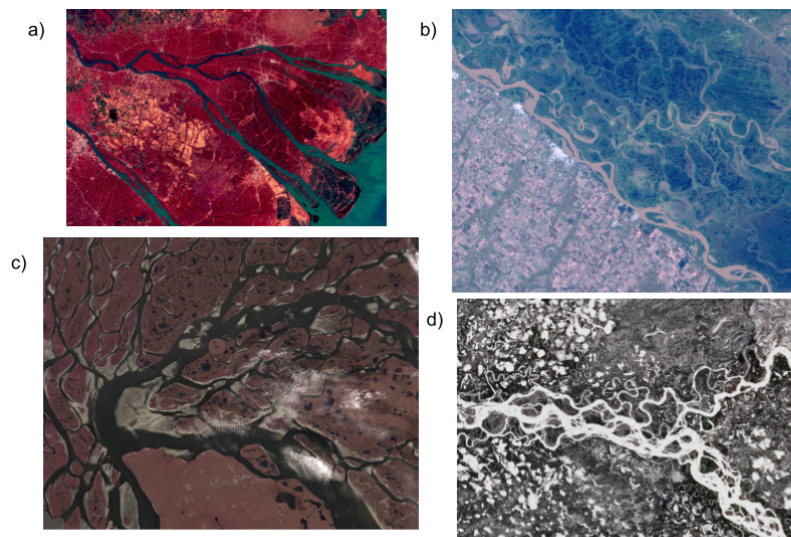


Figure 1.11. Landsat 8 images extracted from Google Earth Engine from (a) the Mekong Delta in Vietnam (b) The Paraná Delta in Argentina (c) the Lena Delta in Russia and (d) the Yukon river in the USA.

ally forced by the runoff or by an interpolated atmospheric forcing (Yamazaki et al. 2013; Pontes et al. 2017). These models obtain good results simulating the complexity of the basins ([Lin et al, 2019](#)). However, they are not adapted to global scale ([Lin et al, 2019](#)) and are hardly compatible with ESMs because they use different grids. The hybrid unit-catchment concept

which is used in this thesis is mixing both approaches by dividing the atmospheric grid into subgrid units which would be like vector-based unit catchment within the grid. In other words, each atmospheric grid cell contains various inter-connected hydrological units. This allows to represent the river network at higher resolution while keeping a structure coherent with the atmospheric grid.

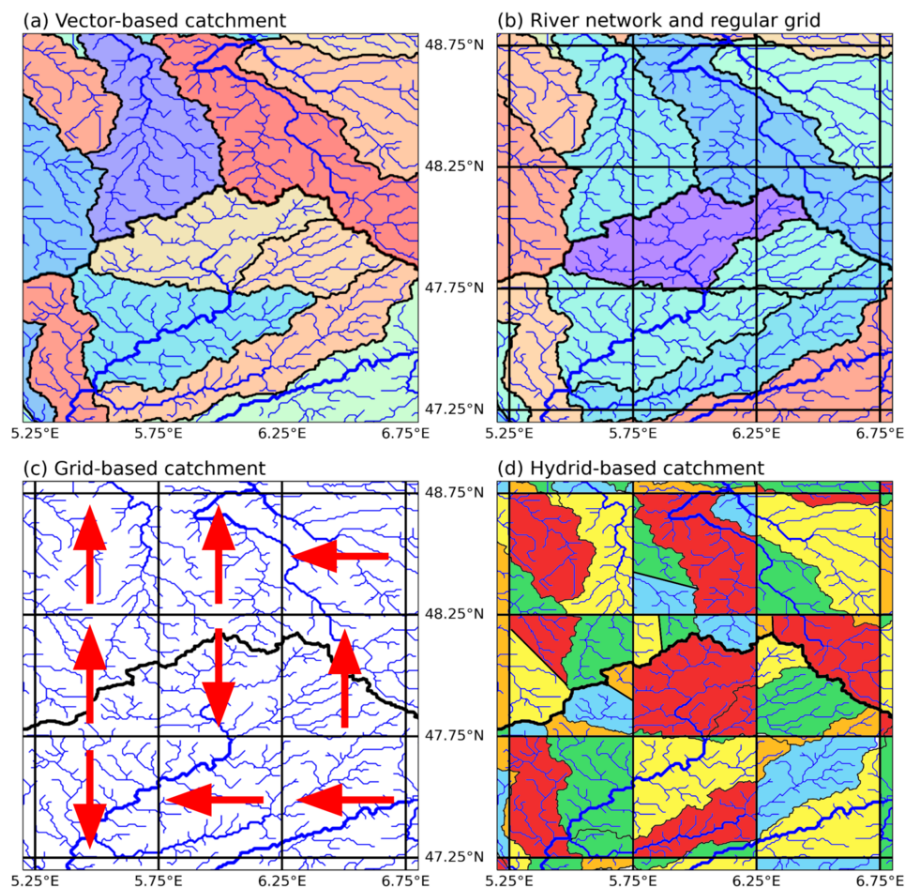


Figure 1.12. Description of the different types of unit-catchment in CaMa-Flood: (a) vector-based unit catchment, (b) river network and regular atmospheric grid, (c) grid-based unit catchment and (d) hybrid-based unit catchment.

Floodplains modelling

The modelling of the floodplains should be adapted to the resolution of the model and to the atmospheric input that are used. Thus, the floodplains processes must be simplified and adapted in order to fit the LSM resolution. From the LSMs that included the floodplains, we may cite JULES (Dadson et al, 2011), ORCHIDEE (D'Orgeval et al, 2008; Guimberteau et al, 2013; cf. Figure 1.13) and ISBA-CTRIP (Decharme et al, 2008, 2019). Their approaches are using a grid-based description of the river network. The floodplains can be represented through the water in the hydrological unit and the flooded surface will be evaluated from the quantity of water in this reservoir. For example, the JULES model considers the subgrid topographic properties in the floodplains area using the mean and standard deviation of the logarithm of elevation. The occurrence of a flood will convert the change of the preexisting surface types

into open water land cover type proportionally to the importance of the flood. The open surface water will be able to evaporate and change the heat fluxes. In ORCHIDEE and ISBA-CTRIP, the floodplains are considered through the use of an additional floodplains reservoir that permits delaying the discharge. The volume of water is also used to estimate the flooded surface which is used to calculate the quantity of evapotranspiration, precipitation, interception and soil re-infiltration from the floodplains. The low resolution of these models allows them to represent the floodplains locally without exchanging the water from the floodplains with other hydrological units.

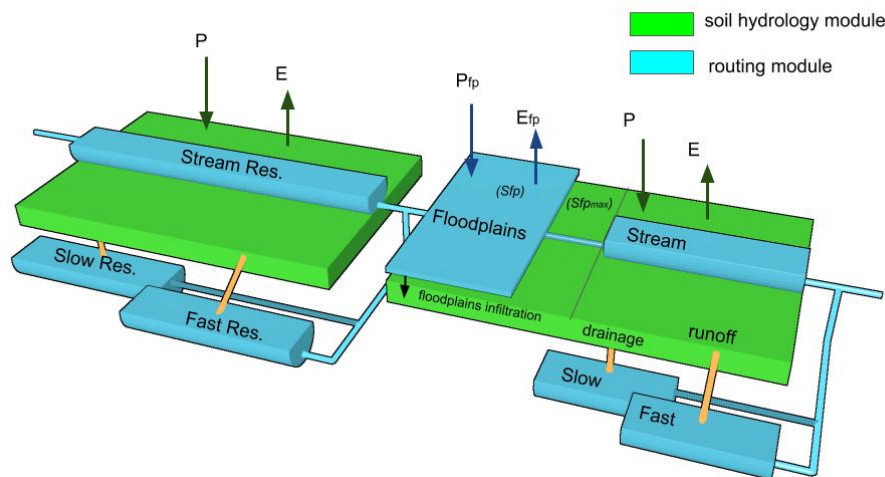


Figure 1.13. Illustration of the representation of the floodplains in the ORCHIDEE floodplains scheme (D'Orgeval, 2006; Guimberteau et al, 2013; Schrapffer et al, 2020).

A first approach of the hydrological modelling community to simulate large floodplains concerns the coupling of large-scale hydrological models to some hydrodynamic models allowing to simulate with more details the floodplains. For example, Bravo et al (2012) coupled the large scale model MGB-IPH to the hydrodynamic model HEC-RAS 1D and da Paz et al (2011) used a coupled model system called SIRIPLAN. These coupled models are difficult to implement and to calibrate and, moreover, the real sub-catchment doesn't respect the shape of grid boxes. This is why the recent evolution of Hydrological Models is going toward the use of catchment-based units (Yamazaki et al, 2013). These models can simulate the rivers with more details and are generally based on the river height, meanwhile LSM usually only consider the water volume. CAMA-FLOOD (Yamazaki et al, 2009, 2011, 2013) is a reference for the simulation of the large floodplains. It uses the catchment-based unit and the sub-grid floodplain topography to estimate the flooded area depending on the river height (cf. Figure 1.14). MGB-IPH (Collischonn et al, 2007; Paiva et al, 2011; Pontes et al, 2017), a Brazilian model, is following the same approach (cf. Figure 1.15). This method allows the floodplains to be slowed down because flooding will make the river height rise less than if considering only the river channel. These models are based on converging river networks but, in some specific cases, they attempt to integrate divergence. For example, CAMA-FLOOD integrate the divergence to simulate the Mekong Delta (Yamazaki et al, 2014). Nevertheless the main objective of these models is to

simulate as well as possible the river discharge, they require high calibration as the river height dynamic requires many parameters to be adjusted for each hydrological unit and it is difficult to adjust them for a global simulation. The major difficulty is also to estimate the sub-grid floodplain topography which may be difficult due to the DEM error over flat areas (Yamazaki et al, 2017).

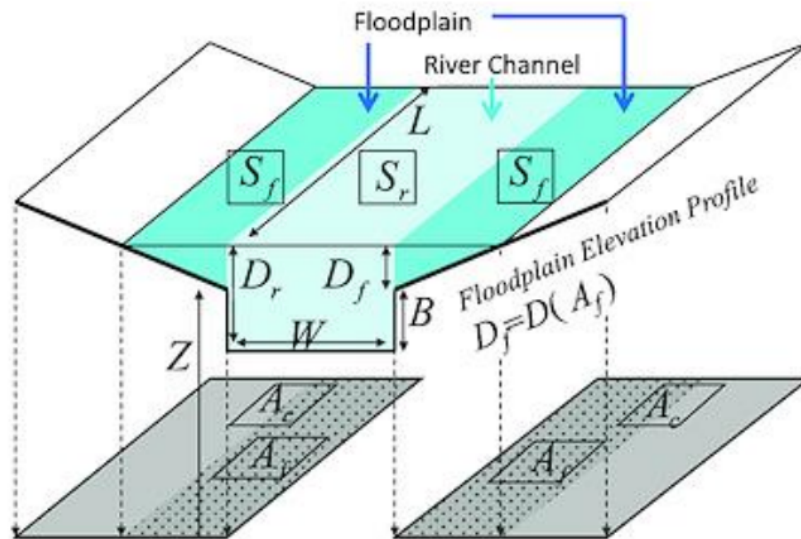


Figure 1.14. Illustration of how the CAMA-FLOOD model (Yamazaki et al, 2009, 2011, 2013) simulates the river channel and floodplains reservoir for each hydrological unit (Figure from Yamazaki et al, 2011).

1.2.4 Interaction with the atmosphere

Some flooded areas over the floodplains can be considered as open-water surfaces while others area well covered by vegetation because the low vegetation may have adapted to the recurrent floods and because of the flooded forests. Thus, over these flooded areas we may have a very strong evapotranspiration due to the fact that (1) the evaporation over the open-water surfaces can reach its potential rate and (2) the infiltration increases the soil moisture and, thus, favorize the development of the vegetation in the area surrounding the floodplains which increases the transpiration.

The terrestrial surface energy balance is driven by the longwave and shortwave radiations which can be resumed by the net radiation at the surface (R_n). This energy is then redistributed in different fluxes: the latent heat, related to the evapotranspiration, and the sensible heat (H), related to an increase of the surface temperature. There is also a flux concerning the exchange of energy with the ground (G). The latent heat fluxes can be divided into 2 different fluxes: the latent heat from the evaporation (LE) and the latent heat from the transpiration (LT). The transfer of energy with the ground can be neglected considering a period long enough to neglect the multi-decadal variability. Then, the terrestrial surface energy balance

MGB MODEL

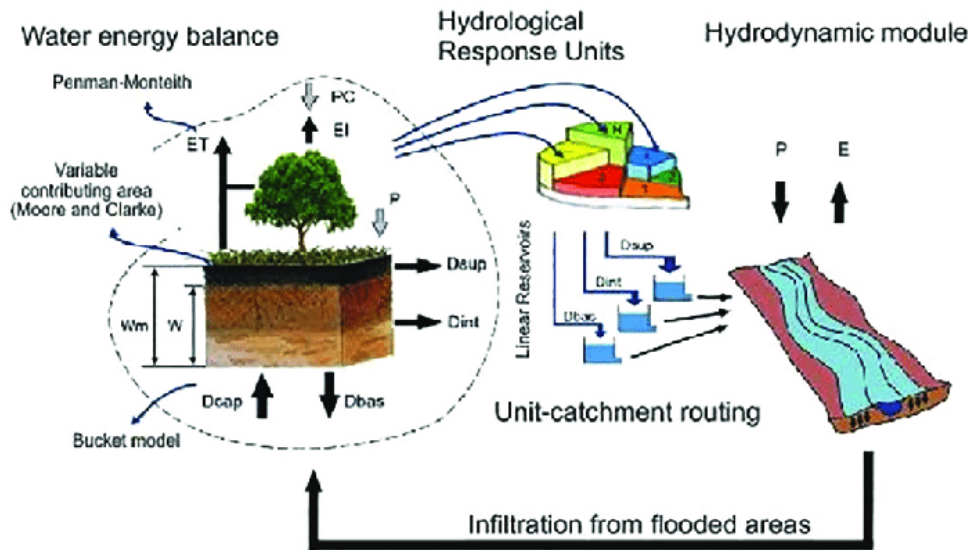


Figure 1.15. Illustration of how the different component of the MGB model interacts (Figure from Fleischmann et al., 2017).

can be represented by the equation 1.1.

$$R_n = H + LE + LT \quad (1.1)$$

The land surface properties (land cover, vegetation, soil moisture and soil composition) influence the energy balance in two different ways: (1) the surface conditions influence on the albedo which influences on the net radiation and (2) it define the distribution of the net radiation between the different fluxes (H, LE and LT). Figure 1.16 illustrates the differences between a flooded surface and a non-flooded terrestrial surface. Over a flooded area, the evaporation may be higher because of the water availability. The water has a lower albedo which may increase net radiation. On the contrary it has a higher specific heat capacity than non-flooded ground and, thus, may have a lower increase of temperature for the same amount of energy absorbed than non-flooded ground (Vanderkelen et al, 2020). Compared to the non-flooded case, the availability of water will also result in a different distribution of the fluxes with less sensible heat fluxes and more latent heat fluxes related to the increased evaporation (Bonan, 1995). This increased evaporation will have two different consequences: (1) it may result in a lower surface temperature (Bonan, 1995) and (2) the different repartition of the land-atmosphere heat fluxes may affect the atmospheric boundary layer (Koster et al, 2004; Krinner, 2003).

Following the Köppen climate classification (Peel et al, 2007), the tropical savanna are warm regions with marked wet and dry seasons. In the savannas, the water tends to be the limiting factor regulating the surface fluxes (Gentine et al, 2019). Therefore, the consideration of tropical floodplains in tropical savanna regions, such as the Pantanal, is particularly relevant. Apart from their impact on the local surface energy balance, the flooded surfaces will also create a horizontal contrast with neighbouring non-flooded surfaces through surface temperature

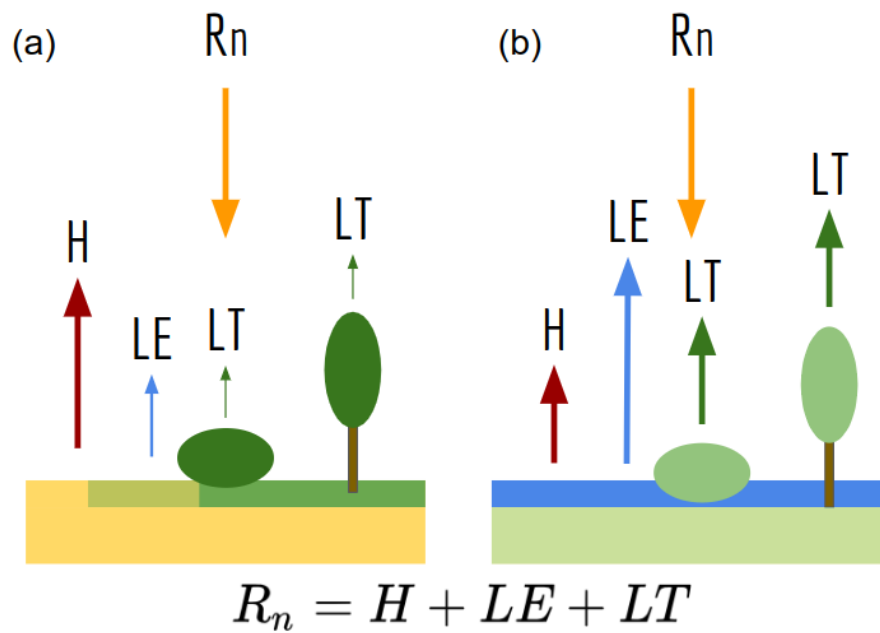


Figure 1.16. Main heat fluxes over (a) non-flooded and (b) flooded regions is the net radiation, H the sensible flux, LE the latent heat flux related to evaporation and LT to transpiration.

discontinuities and heat fluxes discontinuities (Taylor, 2010; Taylor et al, 2018).

There have been several studies confirming that, in some conditions, there may exist a strong feedback between the land and the atmosphere related to soil moisture conditions (Seneviratne et al, 2010b; Dirmeyer, 2011). The tropical floodplains can be considered as regions with high soil moisture and strong regional soil moisture contrast with the neighbouring non-flooded areas (Taylor et al, 2018). In such conditions, the soil moisture may influence the atmosphere by different mechanisms. First, it may impact the vertical profile of the PBL as it has been found that higher soil moisture conditions will result in higher values of equivalent potential temperature and of Convective Available Potential Energy (CAPE) (Kohler et al, 2010; Adler et al, 2011). The second impact is related to the spatial discontinuities in surface conditions and fluxes. These spatial discontinuities may have an impact on the mesoscale circulation and may also particularly affect and trigger the Mesoscale Convective Systems (MCSs) through wind shear and PBL instabilities (Taylor, 2010; Johnson and Mapes, 2001).

The strong large-scale gradient discontinuities may also affect the local and regional precipitation pattern (Taylor, 2010). This phenomenon has been largely studied and confirmed in West Africa within the African Monsoon Multi-disciplinary Analysis (AMMA) Project (Redelsperger et al, 2006). These studies confirmed the strong dependence between the surface condition (in particular the soil wetness) and the precipitation during the African Monsoon and its impact on an interannual scale (Lebel et al, 2009). The processes of initiation and development of the storms have also been studied through observations and coupled models confirming that the storms are triggered in the early afternoon at the interface between the dry and the wet soil issued from the previous days precipitation. These storms then develop themselves over the dry soil (Taylor, 2010; Adler et al, 2011). Taylor et al (2018) extended the previous analysis with a

focus on the influence of the Sub-Saharan Wetlands in regions where precipitation is predominantly driven by MCSs (similar to the Pantanal). His findings were consistent with the results of the AMMA project with MCSs more probable to initiate near the wetlands and floodplains meanwhile the precipitation will occur mostly over the drier area close to floodplains. The Figure 1.17.a (1.17.b) shows the impact of a dry (wet) soil moisture anomaly on the atmospheric variables with respect to a westward MSCs.

The cloud cover is an atmospheric condition which may strongly be related to the local surface conditions and thus can be affected by the flooded area. In tropical regions, the surface conditions are strongly coupled with the boundary layer and the clouds (Betts and Silva Dias, 2010; Ek and Holtlag, 2004). The surface discontinuities related to the flooded area will enhance the local shallow convection (Gentine et al, 2019) which will increase the cloud cover that will affect at its turn the radiative balance and thus the surface conditions.

The UPRB and the Pantanal are located at the transition between a tropical savanna climate (Cerrado) and a semi-arid Climate (Gran Chaco) where the precipitation is related to the South American Monsoon System and is partly related to MCSs (Salio et al, 2007). There is also a strong low-level jet that crosses the region from North to South. We may say that we have a similar configuration to the West African region studied during the AMMA project and thus that there might exist a strong land-atmosphere feedback related to the Pantanal floodplains but with a North-South orientation of the Low Level Jet. Therefore, the Pantanal may have an impact on the temporal and spatial patterns of the regional precipitation. The regional changes in precipitation may impact the temporal and spatial flood patterns in the Pantanal through: (1) the precipitation over the upstream area of the floodplains which will impact the inflow of water and (2) the local precipitation. If the land conditions have an important influence on the precipitation patterns, we may expect that changes of the Pantanal conditions can have an impact over the regional climate. Therefore, there may exist a strong land-atmosphere coupling over the tropical floodplains.

1.2.5 Ecology and Hydrology

Large tropical watersheds usually have one large river discharge pulse per year. It is the case, for example, for the Paraguay and the Amazon basins. The large floodplains existing over this type of watersheds have a low flood frequency which make the floods more predictable and durable. This allows the periodical adaptation of the biota, whether it concerns fish population, vegetation or animals. These large floodplains are rich biodiversity regions as they are transient aquatic ecosystems. From this starting point, Junk et al (1989) made the observation that the classical river ecology concepts are limited to represent the large river floodplains which are important habitats for the biota. They proposed a concept called "Flood Pulse Concept" to explain these ecosystems. It is based on the hypothesis that the river discharge is the major force driving the biota in the river-floodplains system.

It decomposes the large floodplains in two different units: the main river channel and the "Aquatic/terrestrial transition zone (ATTZ)". The main river channel is responsible for the floods due to the precipitation in the upstream region and the ATTZ is the transition zone that is

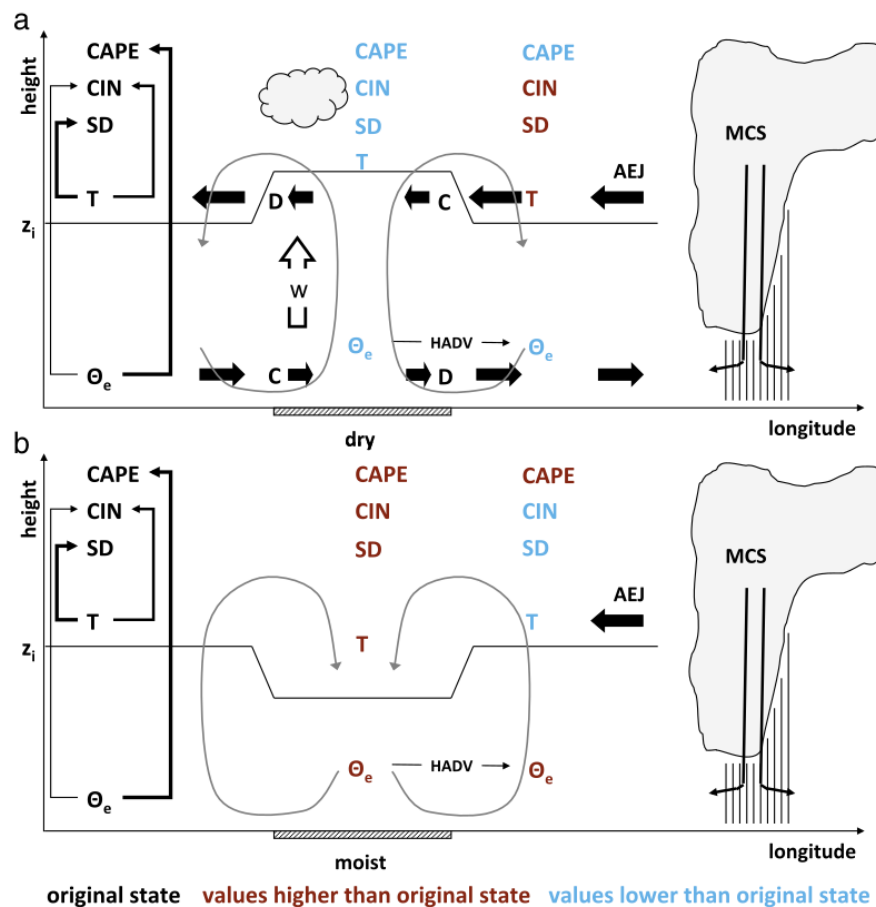


Figure 1.17. Resume of the different impact of a westward MCS on the atmosphere when passing over a dry (a) and a moist (b) surface (extracted from [Adler et al, 2011](#)).

evolving along the year depending on the floods. When the flooded area decreases, the local climate becomes the main hydrological driver over the non-flooded areas. Some parts of the floodplains may be disconnected from the main channel during months when the floods are receding. Predictable flood pulses, such as the monomodal one of the Pantanal, allows the flora and fauna to develop around this phenomena. Organisms within the floodplains have adapted strategies to survive the alternance of drought and flood periods. The stress periods are very selective processes for the biota in the floodplains.

Another of [Junk et al \(1989\)](#) hypotheses is that, although it is driven by the flood pulse and the hydrological exchange between the main channel and the floodplains, the biota doesn't depend on the nutrients from the river flow but mostly on the local nutrient recycling within floodplains. Nevertheless, the water flowing through some floodplains such as the Pantanal is black water (water with a high content of dissolved organic matter). In the case of Pantanal, the water may also contain some biological content from the Amazon basin coming from exchanges between the headwaters of the Paraguay and Amazon river basins due to the instability of the watershed ([Neiff, 1996](#); [Bonetto, 1975](#)). In the particular case of the Pantanal, the high nutrient content in the water benefits the downstream region and, due to the North-South flow direction of the Paraguay, is a transfer of biota and nutrients from tropical to subtropical latitude ([Minotti, 2018](#)).

Beyond these scientific and technical aspects, Neiff (1996) insists on the ecological complexity of the floodplains and believes that considering floodplains only as a transition zone would be a conceptual mistake as it would minimize the uniqueness of these highly dynamical and complex systems.

1.2.6 Carbon cycle

Such as the wetlands in general, floodplains are strongly interacting with the carbon cycle because they are very productive ecosystems compared to other regions with the same climate (Melton et al, 2013) and have the specificity to be flooded temporarily or permanently. Apart from the hydrological cycle, these regions are very important in Earth System modelling as they have a strong interaction with the carbon cycle.

In absence of flood, the organic matter is in contact with the atmosphere (aerobic conditions), this promotes the emission of carbon dioxide (CO₂) and the sequestration of methane (CH₄) (Kayranli et al, 2010). In the flooded area, the organic matter is not in contact with the atmosphere (anaerobic conditions) (Kayranli et al, 2010; cf. Figure 1.18). The backside effect of the anaerobic condition is that it increases the emission of CH₄ which is a greenhouse gas that, although it has a lower life duration than CO₂, has a more powerful greenhouse potential to contribute to the human-induced greenhouse effect than CO₂ and is also involved in the atmospheric ozone chemistry (Schlesinger and Bernhardt, 2013; Zhuang et al, 2009). The wetlands are considered the first natural emitter of methane (Ringeval et al, 2010; Kirschke et al, 2013). The anaerobic condition also promotes the denitrification (the removal of the excess of nitrogen in the water). Although this process has a positive impact on the water quality considering the excess of nitrogen related to the human activities such as agriculture, the denitrification is also a source of nitrous oxide for the atmosphere (Martínez-Espinosa et al, 2021).

The primary production is related to the production of biomass. Through primary production, the wetlands are capturing carbon from the atmosphere in the local vegetation (Le Quéré et al, 2014). On the one hand, the rate of decomposition is slower in the presence of water because this decomposition is done in anaerobic conditions in the saturated soil of the wetlands. The carbonic matter in the wetlands has a slow decomposition rate due to the floods. This produces the accumulation of carbon into the soil (Melton et al, 2013). On the other hand, the plants in the wetlands are normally more dependent on the recycling of the internal nutrients than to the nutrients inputs. The efficient nutrient recycling and the slow decomposition rate will lead to high content of nutrients accumulating in the wetlands and, then, to an enhanced carbon sequestration.

The floodplains are wetlands that are connected to other areas through the river network system. As they are a very productive area and due to the anaerobic conditions which only partially decompose the organic matter, the water in the floodplains contains important quantities of dissolved organic matter (DOM) that they are able to export to the downstream regions (Schlesinger and Bernhardt, 2013; Harrison et al, 2005).

The balance between the CO₂ and the CH₄ fluxes is complex and depends on many factors such as the flood extent, the temperature and the vegetation with numerous feedbacks be-

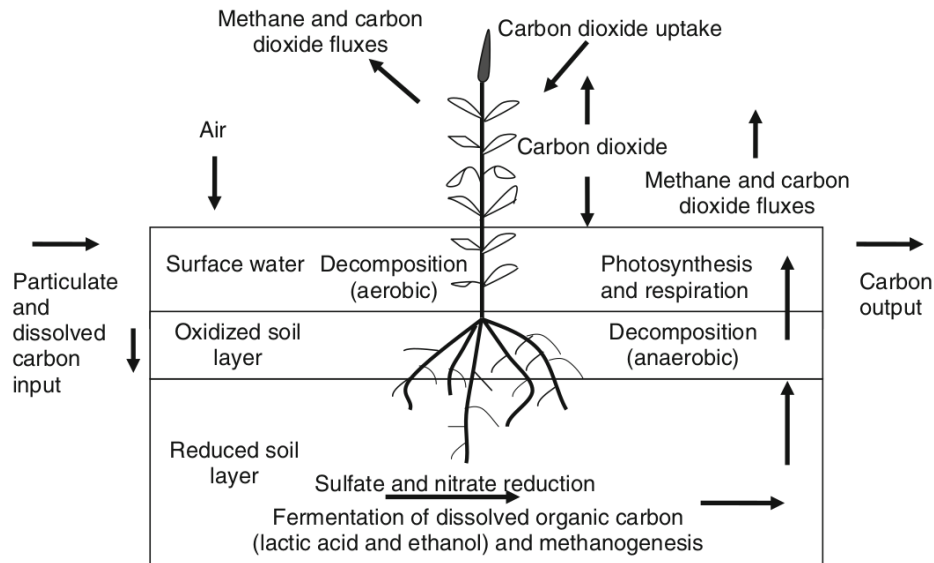


Figure 1.18. Schematic diagram showing the major components of the carbon cycle (extracted from [Kayranli et al, 2010](#)).

tween both fluxes. Some wetlands may be a source of carbon as others can be a carbon sink depending on the ratio between carbon sequestration and methane emission ([Kayranli et al, 2010](#)). In the case of floodplains, it should also be considered that some areas may not be flooded during the whole year and, thus, the oxidation of atmospheric methane can occur if the soils are not saturated ([Kayranli et al, 2010](#)).

These processes deserve further studies to be better understood to establish the role of wetlands in the carbon cycle and in relation to global warming ([Melton et al, 2013](#); [Mitsch et al, 2010, 2013](#); [Schlesinger and Bernhardt, 2013](#)). These studies may re-value the role of the wetlands in relation with their rich ecosystems, their contribution to other ecosystems through the DOM and their strong coupling with the carbon cycle. It is also useful to better understand the underlying processes in natural wetlands to improve the installation of artificial wetlands.

Carbon cycle modelling is a key to do so but there still are great discrepancies between models. For this reason, it is important to better understand the different interactions between the wetlands and the carbon cycle and in particular of the large tropical floodplains to estimate their participation in the carbon cycle ([Mitsch et al, 2010](#)).

1.2.7 Human impact on Pantanal

The floodplains are usually very important for the local population due to the ecosystem services they provide, whereas it concerns the local human activity or the populations living downstream of the floodplains. The human population living within the tropical floodplains have adapted their activities according to the hydrology of the rivers and to the flood seasons. The agricultural sector may, for example, adapt where it develops its activities depending on the lands which are usually flooded on a given year during the wet season ([Bravo et al, 2014](#)). In some cases, such as in the Niger Inner Delta or the Sudd, the floodplains are located in a

semi-arid area and the floodplains are essential for the local population to survive thanks to grazing or cropping related to the floodplains but also to freshwater fisheries. For these particular regions, human development would have been particularly difficult without the floodplains. Nevertheless, the natural equilibrium of the floodplains ecosystems is fragile and human activities may perturb their natural regulation and functioning. Thus, it may threaten their equilibrium and conservation (Junk et al, 2006; Bergier, 2013). The Pantanal is attractive for the development of different type of activities and, therefore, is also threatened by human development (Alho and Sabino, 2011). As a floodplains, the Pantanal depends not only on what is happening locally but also on the changes occurring over the upstream areas and, in particular, in the Cerrado savanna.

Land use changes and, in particular, deforestation may have an important impact on the floodplains hydrology (Woodward et al, 2014). In the Pantanal, the latter are principally related to farming and cattle raising. As the floodplains are fertile regions with space for extensive agriculture, the crops and grasses for cattling replaces the natural savanna vegetation in the Pantanal and the Cerrado at a concerning rate (Bergier, 2013). The land use changes may have an impact on the hydrology as they will increase the runoff and the discharge (Vorosmarty and Sahagian, 2000) and promote larger floods over the Pantanal. The local farmers start fires during the dry season in order to clear the vegetation over their ranch which enhance larger land cover changes. Due to the local dry conditions, these fires may expand and achieve the destruction of the natural vegetation over a larger area (Alho and Sabino, 2011).

On the other hand, these basins are regions rich in large rivers. The dams over the UPRB are principally small scale dams as the construction of large dams over the UPRB have been banned (Bergier, 2013) but nevertheless the presence of dams have different impacts over the catchment hydrology: (1) they generate the presence of permanent flooded areas and thus damage the local flora and (2) they reduce the variability of the discharge. Concerning the ecosystem, they also have an important impact because (1) they reduce the transport of sediment and rich nutrients downstream and (2) they limit the displacement of the local fishes population (Alho and Sabino, 2011).

The Paraná-Paraguay rivers are important ways of navigation for the transport of merchandises from the Mato Grosso, Bolivia, Paraguay and Argentina as they provide an easy access from the center of the continent to the Atlantic ocean. The Paraná-Paraguay Hidrovia project involves the channelization of the river network to facilitate the navigation of large ships (Junk et al, 2006). It was projected to make some channel operation on the Paraguay river over the Pantanal but this project has been abandoned largely because of the evaluation of the environmental impacts (Gottgens et al, 2001). It is estimated that this would have had an important impact on the Pantanal hydrology by decreasing the river levels which would have result, even for a decrease of a few decimeters, in an important reduction of the flooded area and have a negative impact on the floodplains ecosystem (Hamilton, 1999). Changes of the extent of the flooded area may have an important impact on the carbon fluxes seen in the former section. Larger than usual extent of floodplains are responsible for increased methane emissions while a drying wetlands will emit more carbon to the atmosphere through the oxidation of the organic matter and through the higher probability of wildfire (Mitsch et al, 2010).

As for many other ecosystems, climate change represents a threat for the Pantanal in particular because the floodplains are very sensitive to the temperature, the precipitation, the inflow of water from the upstream area and the concentration of CO₂ in the air. Although the climate projections are still quite uncertain for the precipitation over this region (IPCC AR6 WGI, 2021; Marengo et al, 2016; Bravo et al, 2014), it is estimated that the precipitation over the Pantanal region will decrease during both dry and wet seasons combined with higher temperatures (Marengo et al, 2016). A warmer and drier climate may provoke the dryness of the Pantanal.

Finally, some other aspects of human activities may also have a negative impact on the Pantanal ecosystem such as the unsustainable tourism in the Pantanal which affect the fauna by hunting and fishing activities and may also generate contamination. Some illegal activities may also pollute the water such as unregulated mine golding producing mercury contamination in the Pantanal waters (Leady and Gottgens, 2001; Alho and Vieira, 1997).

The different impacts of the land use changes toward traditional agriculture on the Pantanal hydrological cycle are resumed in Figure 1.19 extracted from Bergier (2013) as well as the different consequences these threats may have.

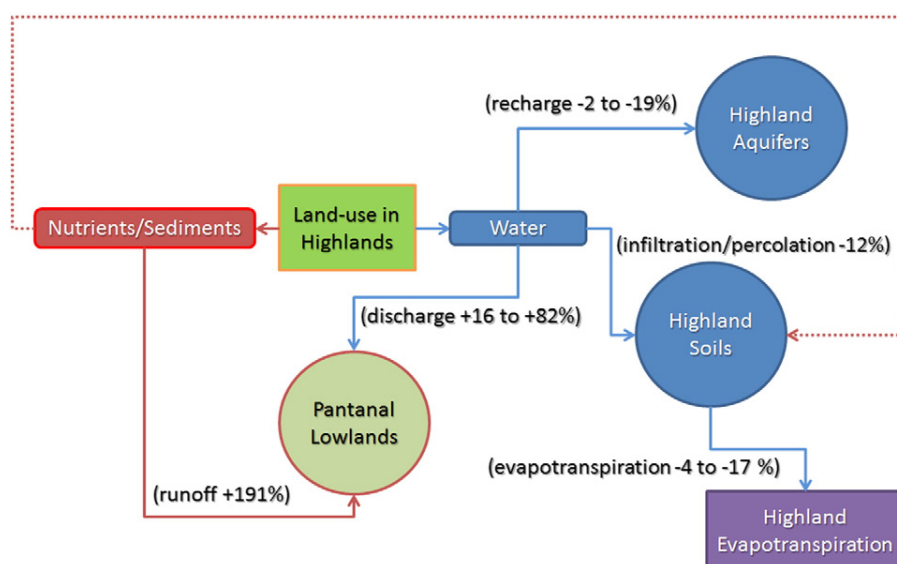


Figure 1.19. Human-related changes to the Pantanal hydrology (extracted from Bergier, 2013).

Although the large wetlands such as the Pantanal are included in different conservation plans such as the RAMSAR convention, the Pantanal habitat has to be considered as a whole by including its upstream areas in this sustainable conservation (Bergier, 2013). Different efforts have to be made on the land use changes with reforestation of the native forest and using more ecological agriculture practices such as agroforestry management (Watanabe and Ortega, 2014). Responsible tourism should be incentivated in order to avoid the negative consequences of unsustainable tourism (Alho and Sabino, 2011). All these efforts must come along with a better comprehension and a more rigorous monitoring of the Pantanal hydrology.

1.3 Motivation

This thesis has a double objective:

- improve the representation of the high resolution river routing of the ORCHIDEE Land Surface Model and, in particular, by the development of an adapted floodplains module;
- understand the complex water cycle of the Pantanal with a special focus on Land-Atmosphere fluxes.

The development of the high resolution floodplains scheme has required the development of a complete pre-processing tool in order to generate a flexible river routing description for all type of atmospheric grid. This development is an important step forward for the future implementations of hydrological processes in the ORCHIDEE model (irrigation, dams, swamps).

The representation of the river network at high resolution in a Land Surface Model is an opportunity as it allows to increase the heterogeneity of the different sub-unit represented but it is also a challenge as the different processes interacting between ORCHIDEE's hydrological scheme and its river scheme will need to be adapted to this new configuration. The Pantanal is a region with a complex hydrology and is a suitable region to develop a floodplains scheme. The modelling of the floodplains in ORCHIDEE will allow us to understand the different processes related to the water cycle over the Pantanal at a regional scale.

The possibility to have a working floodplains scheme in ORCHIDEE will also prepare the ground for future studies to better understand the impact of human activities on the floodplains, to study the transport of Dissolved Organic Matter in the river and to estimate the impact of the climate change over these fragile ecosystems.

1.4 Document Structure

This thesis is composed by 7 chapter:

Chapter 1: Introduction (this chapter)

This chapter presents the subject of the thesis and gives a scientific context and a wider introduction to the Pantanal floodplains. It also contains the motivation and the objectives of the present thesis.

Chapter 2: Benefits of the floodplains scheme

This chapter contains the study of the Pantanal using floodplains module of the previous version of the routing at a 0.5° resolution which has previously been developed by [D'Orgeval \(2006\)](#). The objective of this chapter is to compare the simulations with and without floodplains using different atmospheric forcings to include the uncertainty related to the precipitation in the atmospheric forcings. The publication which corresponds with this part of the thesis ([Schrapffer et al, 2020](#)) has been included.

Chapter 3: Estimation of the flooded area over the Pantanal, a South American floodplains, using MODIS data

This chapter contains the description and evaluation of different methods to estimate the flooded area over the Pantanal using spectral indexes calculated with MODIS data. Based on the evaluation of these methods, the difficulties of estimating the flooded area based on satellite products are discussed. This chapter contains the corresponding publication which is under review.

Chapter 4: Parallelized construction of a flexible river routing graph for Earth System Models (RoutingPP)

This chapter describes the pre-processing tool developed to generate the river routing for ORCHIDEE on a specific atmospheric grid. The development of this tool has been an indispensable step previous to the development of the high resolution floodplains scheme. The advantages of generating the river routing previously to the simulation are presented as well as the functioning of the high resolution river routing. In addition, some evaluation tests have been included to show the performance of the routing generated in ORCHIDEE.

Chapter 5: Development of a high resolution floodplains scheme

The high resolution floodplains scheme developed as a part of the thesis work is described in this chapter. It contains the theoretical explanation and also the details of the implementation. The evaluation is performed over the different variables of the water cycle simulated by the river routing scheme and affected by the floodplains such as the discharge, the volume of water in the reservoirs and the flooded area. This evaluation is performed: (1) by comparing the high resolution floodplains scheme with its previous version and (2) by comparing different resolutions of atmospheric grids.

Chapter 6: Evaluation of the impact of the high resolution floodplains scheme on the surface variables in ORCHIDEE

This chapter evaluates the differences between a simulation of ORCHIDEE without floodplains and with the floodplains scheme activated. It aims to show the different aspects that are missed when not considering floodplains at a regional scale and to understand the hydrological cycle of the Pantanal. These aspects include the surface variables (soil moisture, temperature and vegetation), the surface energy budget and the evapotranspiration.

Chapter 7: Land-atmosphere interactions

This chapter contains the evaluation of the impact of considering or not the floodplains in a coupled simulation using the Regional Earth System Model of the Institut Pierre Simon Laplace (RegIPSL, <https://gitlab.in2p3.fr/ipsl/lmd/intro/regipsl/regipsl/wikis/home>) and in particular the impact on the atmospheric conditions.

Chapter 8: Discussion, Conclusion and Perspective

This chapter summarized the different results obtained along the development of this thesis. Moreover, future perspective of work around the study of the floodplains and their interactions with the atmosphere and the hydrological cycle are discussed as well as potential future improvement of the floodplains scheme in the ORCHIDEE model.

1.5 Acronyms

AMMA	African Monsoon Multidisciplinary Analysis
ATTZ	Aquatic-Terrestrial Transition Zone
CAMA-FLOOD	Catchment-based Macro-scale Floodplain model
CH₄	Methane
CO₂	Carbon Dioxide
DEM	Digital Elevation Model
DOM	Dissolved organic Matter
ESM	Earth System Model
GEWEX	Global Energy and Water Exchanges
GLWD	Global Lake and Wetlands Dataset
GPCC	Global Precipitation Climatology Centre
HEC-RAS 1D	Hydrologic Engineering Center's River Analysis System
HRU	Hydrological Response Unit
HTU	Hydrological Transfer Unit
HydroDEM	Hydrologically coherent Digital Elevation Model
IPCC	Intergovernmental Panel on Climate Change
IPSL	Institut Pierre Simon Laplace
ISBA-CTRIP	Interaction Sol-Biosphère-Atmosphère CNRM's Total Runoff and Integrating Pathways
JULES	Joint UK Land Environment Simulator

LPB	La Plata Basin
LSM	Land Surface Model
MERIT Hydro	Multi-Error-Removed Improved-Terrain Hydrologically coherent Digital Elevation Model
MGB-IPH	Modelo de Grandes Bacias do Instituto de Pesquisas Hidráulicas
MODIS	Moderate Resolution Imaging Spectroradiometer
ORCHIDEE	ORganizing Carbon and Hydrology in Dynamic EcosystEms
PBL	Planetary Boundary Layer
RAMSAR	Ramsar Convention on Wetlands of International Importance Especially as Waterfowl Habitat
RegIPSL	Institut Pierre Simon Laplace's Regional Earth System Model
RoutingPP	Pre-Processor of the routing input for ORCHIDEE high resolution routing scheme
SACZ	South Atlantic Convergence Zone
SALLJ	South American Low Level Jet
SAMS	South American Monsoon System
SAR	Synthetic Aperture Radar sensor
SESA	Southeastern South America
SST	Sea Surface Temperature
UPRB	Upper Paraguay River Basin

Benefits of representing floodplains in a Land Surface Model: Pantanal simulated with ORCHIDEE CMIP6 version

Contents

2.1 Introduction	31
2.2 Pantanal simulated with ORCHIDEE CMIP6 version	32
2.3 Acronyms	59

2.1 Introduction

This chapter was developed as the initial step of this thesis and demonstrates the benefits of integrating a floodplains module in a Land Surface Model by using a floodplains scheme that has already been developed at a 0.5° resolution by [D'Orgeval et al \(2008\)](#). This demonstration is performed by comparing different pairs of simulations, one with the floodplains scheme activated and one deactivated. The model used to perform these simulations is the version 2.0 of ORCHIDEE. This version is the Land Surface Component of the Institut Pierre Simon Laplace Earth System model for the CMIP6 simulations. It uses the version of ORCHIDEE's routing at 0.5° previous to this thesis and its corresponding floodplains scheme. This study has been performed over the world's largest floodplains in South America, the Pantanal. This work has been published in the journal *Climate Dynamic* (Springer).

Large tropical floodplains have an impact on the different variables of the water cycle and may be places of strong interaction between the land and the atmosphere. Thus, their integration in Land Surface Models may allow to improve the representation of the regional hydrological cycle and lead to more realistic local land-atmosphere fluxes.

The hydrology of the Pantanal is mainly driven by the precipitation that occurs in its upstream areas during the wet period from November to March. The low slope within the Pantanal slows

the flow of the water and, in consequences, produces floods over the region. These floods remains even until the dry period and take on great importance for the vegetation and the land-atmosphere fluxes.

The floodplains modelling is an interesting tool to understand the functioning of the floodplains and their impact on the rest of the Earth System. Although some previous studies tried to represent the Pantanal with the coupling of a one-dimensional large-scale hydrological model and an inundation model (Bravo et al, 2012; da Paz et al, 2011), most of the studies representing the floodplains in a Land Surface Model principally focused on other large floodplains such as the Amazon river (Guimberteau et al, 2012a); the Inner Niger Delta (D'Orgeval, 2006; Dadson et al, 2010).

Along with floodplain modelling, remote sensing is another possibility to try to understand the hydrology of the Pantanal. Penatti et al (2015) studied the different variables related to the water cycle over the Pantanal and tried to close the hydrological cycle of the Pantanal using the variety of remote sensing products available. Although the remote sensing products used allow to understand the hydrology of the region, there still remains large uncertainties that don't allow to close properly the water budget with this type of data. However as the Land Surface Models keeps the coherence between the variables involved, it is an interesting tool to perform this type of water budget. The simulations used in this study have also been used for such a purpose.

The paper published in the Climate Dynamic Journal is presented in the following section. It presents the simulations over the Pantanal forced by six different atmospheric forcings in order to evaluate the uncertainty of the precipitation over the region. For each pair of forcing, the representation of the different variables of the hydrological cycle have been evaluated (discharge, flooded area, evapotranspiration, surface heat fluxes). The model-guided water budget close performed over the Pantanal using the simulations is also contained in this publication.

2.2 Benefits of representing floodplains in a Land Surface Model: Pantanal simulated with ORCHIDEE CMIP6 version

Anthony Schrapffer^{1,2,3}, Anna Sörensson^{1,2,3}, Jan Polcher⁴, Lluís Fita^{1,2,3}

(1) *Universidad de Buenos Aires, Facultad de Ciencias Exactas y Naturales. Buenos Aires, Argentina.*

(2) *CONICET – Universidad de Buenos Aires. Centro de Investigaciones del Mar y la Atmósfera (CIMA). Buenos Aires, Argentina.*

(3) *CNRS – IRD – CONICET – UBA. Instituto Franco-Argentino para el Estudio del Clima y sus Impactos (UMI 3351 IFAECI). Buenos Aires, Argentina*

(4) *Laboratoire de Météorologie Dynamique (LMD), IPSL, CNRS, École Polytechnique, Palaiseau, France*

Abstract

Tropical floodplains have a significant impact on the regional water cycle and on land-atmosphere interaction but are not always considered in Land Surface Models (LSMs) or in Earth system models. This study evaluates the importance of representing tropical floodplains in an LSM to provide realistic river discharges, evapotranspiration fluxes and other variables crucial for land's interaction with the ocean and atmosphere.

Off-line simulations of the world's largest tropical wetland, the Pantanal are conducted with ORCHIDEE, the LSM of IPSL's regional and global Earth system model. We analyse the period 1961-2000, which includes both dry and wet decades. Atmospheric uncertainty is considered through the utilization of 3 forcing data sets, each one in two versions: the original dataset and a regionally bias adjusted version.

The activation of the floodplain module leads to a systematic improvement of intra-annual variability and extremes of river discharge. Temporal evolution and spatial distribution of flooded area are coherent with satellite estimations, although the model, due to the coarse resolution of the topography, underestimates the extent of the area. Considering floodplains in ORCHIDEE enhance the evapotranspiration since it permits the water from the upstream region to evaporate in the plains. This has strong consequences on the water balance and on the spatial pattern of surface fluxes. The simulations allow us to perform a model-guided residual estimation of evapotranspiration through a water balance obtaining an annual evapotranspiration over Pantanal of 1220 mm while precipitation is estimated to be 1250 mm with an uncertainty of 180 mm.

Keywords: Land Surface models, floodplains, land-atmosphere interaction, South America.

1. Introduction

Tropical Floodplains have a large impact on the regional water cycle and the land-atmosphere interactions (Adam et al, 2010; Taylor, 2010; Sutcliffe and Brown, 2018; Alsdorf et al, 2010; Lee et al, 2011). Despite their importance, they are not systematically integrated in Land Surface Models (LSM) (Bierkens, 2015; Mishra et al, 2010; D'Orgeval et al, 2008) which are a key component of Earth system models (ESM).

Floodplains are wetlands located in alluvial plains adjacent to rivers which can be temporarily or permanently flooded. Some of the major tropical floodplains are located in the Congo basin (Lee et al, 2011), in the Amazon basin (Alsdorf et al, 2010), in the Nile basin (Sutcliffe and Brown, 2018) and in the inner Niger Delta (D'Orgeval et al, 2008). The La Plata Basin, a very extensive basin of 3 200 000 km² in Southeastern South America (Berbery and Barros, 2002; Barros et al, 2005; Gonçalves et al, 2011), contains the world's largest tropical floodplain, the Pantanal (Alho et al, 1988; Penatti et al, 2015; Bravo et al, 2012; de Almeida et al, 2015). This region is located in Southeastern Brazil, mainly in the Mato Grosso region and has an extension of around 140,000 km² (Hamilton et al, 1996; Alho, 2005; Gonçalves et al, 2011; da Paz et al, 2014). It is part of the Upper area of Paraguay Basin, an important tributary of the Paraná. The Paraguay river comes from South-West Brazil and then runs through Bolivia, Paraguay and finally Argentina to its confluence with the Paraná river. The Pantanal is a very flat area,

with between 80 and 150 m.a.s.l of altitude (Hamilton et al, 1996; Alho, 2005; Gonçalves et al, 2011), and receives the runoff from the Cerrado highlands at its north and northeast end which altitude ranges between 200 and 1400 m.a.s.l (Alho, 2005; Gonçalves et al, 2011) and from the Gran Chaco plains on its western border (Figure 2.1).

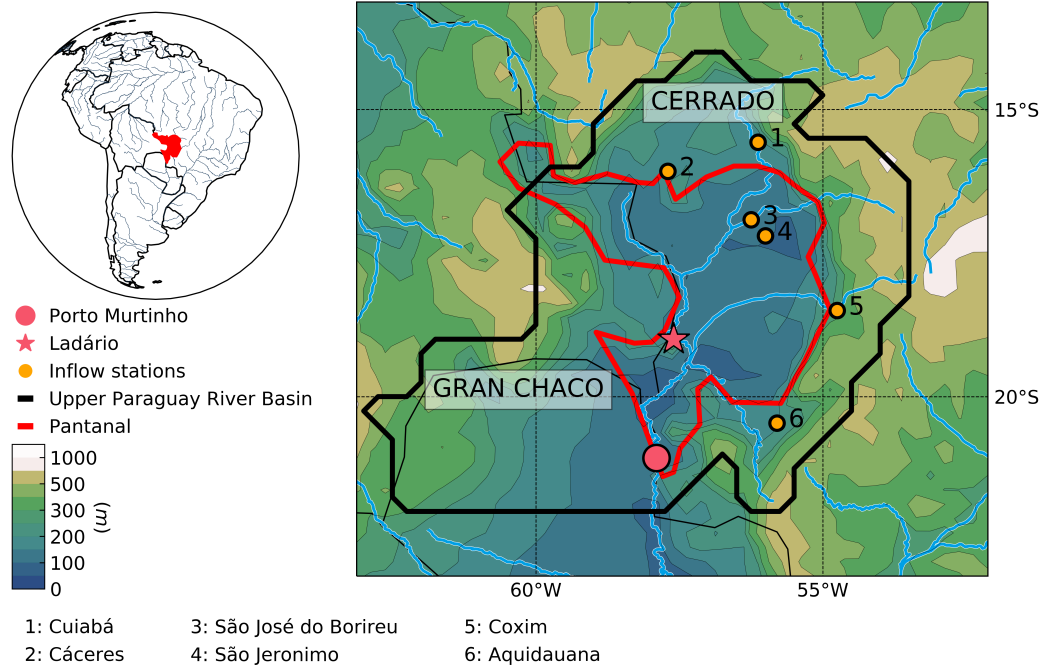


Figure 2.1. Location and description of the Pantanal topography, including Porto Murtinho and Ladário river gauging stations

The Pantanal is a transition climate zone between a wet tropical climate to the north-northeast and the Gran Chaco semi arid climate to the west (Gonçalves et al, 2011). The highlands upstream of the Pantanal (Cerrado mountain range) have very intense precipitation during the South American Monsoon System (SAMS) season (October to March) (Penatti et al, 2015; Barros et al, 2006; Gonçalves et al, 2011; Zhou et al, 1998) and low precipitation for the rest of the year. The seasonal cycles of precipitation over Pantanal and the Gran Chaco are also governed by the SAMS, although with a smaller total annual precipitation than the Cerrado mountain range (Barros et al, 2006; Hamilton et al, 1996; Gonçalves et al, 2011). For this reason, the main part of the inflow to Pantanal comes from the Cerrado highlands. The Pantanal contains many meanders (Barros et al, 2005) and constitutes a voluminous natural reservoir acting as a buffer zone that can delay the river flow between 3 and 5 months (Barros et al, 2005; Hamilton et al, 1996; Padovani, 2010; Gonçalves et al, 2011). The Pantanal presents a high seasonality of flooded area with a maximum in April and a minimum in October (Penatti et al, 2015). The flooding diminishes and delays the discharge peak compared to the one of rainfall (Hamilton et al, 1996). This delayed discharge effect is crucial to understand the hydrology of the Paraguay river hydrology which contributes to the Middle Paraná stream (Barros et al, 2005).

After the rainy austral summer, the Pantanal is flooded producing a large area of surface water exposed to the atmosphere. Then, the Pantanal faces a dry austral winter which, at these

tropical latitudes, means high values of incoming radiation. This results in an increased evapotranspiration and thus in a reduction of sensible heat fluxes at the expense of latent heat fluxes.

[Taylor \(2010\)](#) and [Taylor et al \(2018\)](#) suggest that tropical wetlands such as the Pantanal may affect local and regional rainfall by favouring the triggering of Mesoscale Convective Systems (MCS) through the contrast of sensible heat between the wetland and the surrounding dry areas. The boundary layer over the wetlands is cooler and wetter due to the lower Bowen ratio at the surface, which can imply two different consequences: (1) the frontal updraft of MCS characterized by a propagating cold pool may be debilitated when meeting the cold air over the wetland; (2) when reaching the proximity of wetlands, MCS gain more convective available potential energy (CAPE) which may enhance the triggering of MCS generating higher precipitation amounts. This should be relevant for the Pantanal knowing that in the La Plata Basin the MCS play an important role in the precipitation regime ([Salio et al, 2007](#)). The Pantanal may also be affected by the South American Low Level Jet (SALLJ) which transports moist air from the Amazon and passes over the Pantanal ([Vera et al, 2006](#); [Montini et al, 2019](#)), generating wind-shear which may favour the initiation of convection ([Lauwaet et al, 2012](#)).

The above suggests that the representation of the water cycle and the interaction with the atmosphere in an ESM may be improved by including floodplains dynamics. Most of the LSMs include river routing schemes which are numerical representations of lateral water flows in the basins ([Sheng et al, 2017](#)). On that basis, and according to [Bierkens \(2015\)](#), floodplains representation is an essential step forward for ESMs and their LSMs river routing improvements.

The LSM considered for this study is the latest version of ORCHIDEE -Organising Carbon and Hydrology In Dynamic Ecosystems- ([Krinner et al, 2005](#)) LSM model used in CMIP6 exercise as the land component of the IPSL GCM. This model includes a floodplain representation in the river routing scheme ([D'Orgeval, 2006](#)). This module has already been used and studied over the Niger Delta ([D'Orgeval, 2006](#); [D'Orgeval et al, 2008](#)) and over the Amazon basin ([Guimberteau et al, 2012b, 2013](#)).

The dynamics of the Pantanal's hydrology and vegetation has been studied in previous works such as [Hamilton et al \(1996\)](#) who evaluated the temporal evolution of flooded area along the 20th century to discuss the inundation patterns. [Padovani \(2010\)](#) quantified the flooded area between 2000 and 2009 based on the vegetation indices from MODIS (MODIS13Q1) meanwhile [de Almeida et al \(2015\)](#) applied a Principal Component Analysis to MODIS Enhanced Vegetation Index (MODIS EVI2) images to analyze the variability of the vegetation cover. A more complete analysis on the Pantanal hydrodynamics has been performed by [Pennatti et al \(2015\)](#) who studied the different components of water cycle via satellital estimations and showed difficulties to close the water budget due to the underestimation of evapotranspiration from MOD16, to the uncertainty of the other inputs and to the scarcity of field measurement to assess satellital data.

Modelling the Pantanal hydrodynamic has been a challenge for the hydrological modelling community. [Bravo et al \(2012\)](#) coupled a simplified large-scale hydrological model to a hydrodynamic model. The first one, MGB-IPH, simulates the main drainage network of the basin from meteorological inputs. The second one, HEC-RAS 1D ([Brunner, 2010](#)) adapted by [da Paz](#)

et al (2010) over the Pantanal, simulates with more details the main drainage networks and the floodplains over Pantanal from the discharge provided by the first model. This model is able to reproduce the river dynamic, the rainfall-runoff processes and the river complexity despite the lack of data. It shows the importance of representing floodplains processes to improve the hydrological simulation of the Pantanal. *da Paz et al (2011)* went further by simulating the complex dynamics of the Pantanal by forcing a modelling system (SIRIPLAN) directly with precipitation, evapotranspiration and water inflow from the upstream area. This modelling system couples a one-dimensional hydrodynamic model to simulate the transport of water within the rivers, an inundation model to simulate the Pantanal inundations and a module handling the precipitation and potential evapotranspiration inputs to simulate the actual evapotranspiration and the infiltration processes. *da Paz et al (2014)* continued this work by evaluating the sensitivity of the model to changes in potential evapotranspiration over Pantanal and pointed out that the sensitivity of the model to these processes is crucial to represent the hydrological dynamic of the floodplains. Despite a good representation of the hydrographs and a reasonable consistency of floodplains map, there are still large uncertainties related to evapotranspiration (*da Paz et al, 2014*) and to lacking observations in the western basins in Bolivia (*da Paz et al, 2010; Bravo et al, 2012*).

The present study is motivated by the evaluation of the impacts of the floodplains on the water cycle and in particular land-atmosphere fluxes with the ORCHIDEE model. As a starting point, the simulation of the discharge at the outflow of the Pantanal is assessed in order to evaluate the impact of the floodplain scheme on the water cycle of the Pantanal. Thereafter the processes driving the exchange of water between the floodplains and the atmosphere in the floodplain module are evaluated: the water available for evapotranspiration through representation of open water surface over Pantanal as well as the representation of evapotranspiration and its consequences on the energy fluxes. Finally, a model-guided residual estimation of evapotranspiration is realized through a water balance over the region in order to quantify the role of the Pantanal in the regional water cycle.

The methodology, the model and the observational datasets employed are described in Section 2. Section 3 presents the evaluation of the sensitivity of the Pantanal water cycle to the floodplain scheme through a pair of simulations for each forcing, in one of them the scheme is activated and in the other not. The results of the study are discussed along with the estimation of evapotranspiration over the floodplains in Section 4 and conclusions are given in Section 5.

2. Methodology

The period considered in this study is 1961-2000. It is a long period for which several atmospheric forcings for land surface models exist as well as a regional daily rainfall observation dataset used to generate a bias-corrected version of these forcings (CLARIS-lpb). These forcings are based on meteorological re-analysis products in which precipitation is bias-corrected by daily rainfall observations (CRUNCEPv7, WFD and GSWP3). This period also presents the advantage of including a decade of dry conditions: the 1960-1972 (*Alho and Silva, 2012*) and another of wet conditions: 1980-1990 (*Padovani, 2010*), thus these 40 year allows to sample a large range of climatic conditions in the Pantanal.

A pair of simulations have been realized for each one of the 3 forcings and then with an alternative version in which rainfall is bias-corrected with CLARIS-lpb. In one simulation, the floodplain module of ORCHIDEE is activated (FP) and in the other it is not activated (NOFP). Therefore this study will consider a total of 12 simulations. In order to make sure that all the routing reservoirs and the soil variables are in equilibrium the model is previously run for a sufficiently large period, this process is known as spin-up. For each simulation, a 30-years spin-up (1961-1990) is performed using the same atmospheric forcing and the same configuration.

2.1 Model Description: ORCHIDEE

2.1.1 General

The IPSL Earth System Model includes ORCHIDEE as its land component. The experiments presented in this study are performed with the version of ORCHIDEE used in the Coupled Model Intercomparison Project Phase 6 (CMIP6). Simulations are made with ORCHIDEE in an offline configuration. Under this set-up, the model is forced with external atmospheric data (precipitation, 2-m air temperature and specific humidity, wind speed, snowfall, rainfall and downward long and short wave radiation) without atmospheric feedback.

Additionally ORCHIDEE requires two additional ancillary datasets providing the vegetation cover and soil description. For each grid cell, vegetation is represented through its composition in proportion of bare soil and 12 plant functional types (PFT) while soil description is represented through a combination of 3 soil textures (coarse, medium and fine). In this study we used the Olson's global classification of 94 PFT at 5 km resolution (Olson et al, 1985) for vegetation (interpolated by the model at 0.5° and grouped to the final 12 PFTs) and the USDA soil description (Reynolds et al, 2000) for soil description.

ORCHIDEE's soil hydrology module is a 11-layer scheme (De Rosnay et al, 2000; de Rosnay et al, 2002; Campoy et al, 2013) that represents the vertical transfer processes of water and heat such as diffusion and retention.

2.2.2 Lateral Water Transfer Scheme

The ORCHIDEE routing module is based on a global basin map at 0.5x0.5° resolution (Vörösmarty et al, 2000) in which each grid point is assigned to a basin with information on its flow direction, topography and channel length. The lateral transfer of the water drained into river is managed throughout the Hydrological Transfer Unit (HTU) (Nguyen-Quang et al, 2018c).

Each HTU contains 3 water reservoirs (Polcher, 2003) from which the water is transferred to the downstream HTU (Figure 2.2). Each reservoir is characterized by a different flow timescale: (1) the "stream" reservoir receives the inflow discharge from the upstream cells and has the lower time constant while the (2) "fast" and (3) "slow" reservoirs are respectively collecting water from surface runoff and drainage and have higher time constant. The flux of water (Q) out of each reservoir is a linear function of the water content (V) and the time constant (T). For the reservoir i (i standing for stream, fast or slow reservoir):

$$Q_i = \frac{V_i(t)}{T_i} \quad (2.1)$$

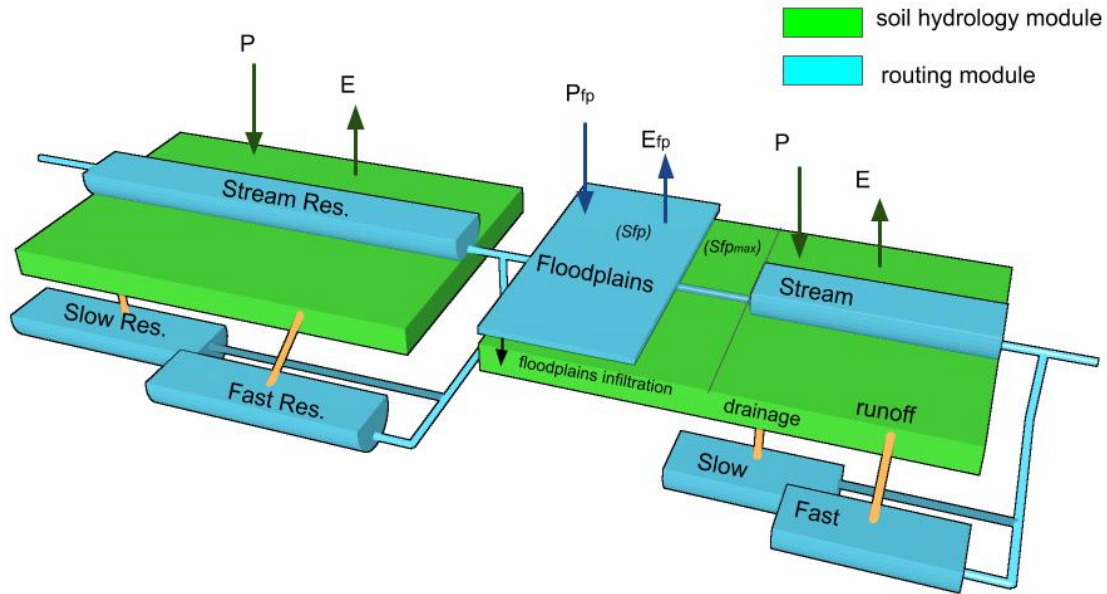


Figure 2.2. Description of ORCHIDEE routing scheme, the floodplain module and their interactions with the atmospheric forcing and soil hydrology module

The outflow from all three reservoirs goes to the "stream" reservoir of the downstream HTU. Total discharge (Q) is the sum of the transferred water from the reservoirs:

$$Q = Q_{stream} + Q_{fast} + Q_{slow} \quad (2.2)$$

This time constant is estimated via a simplification of the Manning formula (Ducharne et al, 2003):

$$T_i = \tau_i * \lambda \quad (2.3)$$

with λ , the topographical water retention index defined for each HTU to represent the effect of the topography and τ_i , a time constant specific for each reservoir that has been calibrated and validated over the world's major basins (Ngo-Duc et al, 2007). λ depends on d , the river length within the HTU and on Δz , the difference of height in kilometers between the HTU considered and the downstream HTU ($\lambda = \sqrt{d^3 / \Delta z \cdot 10^6}$).

2.1.3 Floodplains

The floodplain module was introduced and described by D'Orgeval et al (2008). Floodplains are described by the maximal potential fraction of flooded area of each grid point - $S_{fp,max}$ - based on the Global Lakes and Wetlands Database -GLWD- (WWF, 2004). Floodplains are considered as an additional reservoir which is, unlike the others, able to evaporate and infiltrate into the soil moisture (Figure 2.2). If floodplains are present in the grid cell ($S_{fp,max} > 0$), all incoming water goes to the floodplain reservoir (V_{fp}) first, from where it can flow back to the stream reservoir, evaporate to the atmosphere or re-infiltrate to the soil hydrology. In the floodplains scheme, two parameters describe the shape of the bottom of the floodplains: (1)

β characterize the convexity of the shape (here $\beta = 2$) and h_0 represent the water height at which all the basin is flooded (here $h_0 = 2$ m). This assumption of the shape of the bottom of the floodplains allows to estimate the effective flooded surface (S_{fp}) using V_{fp} .

Precipitation over the grid cell is split in two fractions: one for the flooded area ($S_{fp}/S_{gridcell}$) which goes to the floodplains reservoir and the other which goes to the soil hydrology.

2.2 Observations used for validation

2.2.1 Daily rainfall

The CLARIS-lpb gridded precipitation data set (Jones et al, 2013) is available at a 0.5° resolution for the period 1961–2000. It was produced under the scope of the CLARIS-lpb project by combining 3945 daily precipitation series from rain gauge stations in southeastern South America and following the gridding approach proposed by Haylock et al (2008). It is the only regional gridded daily precipitation datasets which covers the studied area.

2.2.2 Discharge

Monthly observed discharge are obtained from the National Hydro-meteorological Network managed by the Brazilian National Water Agency (Agência Nacional de Águas - ANA). The Porto Murtinho station (see in Figure 2.1) is considered the reference outflow station for the Pantanal (Penatti et al, 2015) and it has a continuous data record for the full study period (1961-2000). Additional available stations at the inflow into the Pantanal were also considered in order to perform a water budget in section 4, these stations are: Cáceres, Cuiabá, São José do Borireu, São Jeronimo, Coxim and Aquidauana (see Figure 2.1).

2.2.3 Flooded area

Temporal variability of the Pantanal flooded area is compared to two sources: Hamilton (2002) and Padovani (2010). Hamilton et al (1996) estimated the flooded area between 1979 and 1987 from satellite data by comparing the vertical and horizontal polarized brightness temperature from passive microwave sensor systems. The flooded area was then correlated with the river gauge at Ladário to establish a relationship between the two variables. In Hamilton (2002), this relationship is used to evaluate the flooded area between 1900 and 2000 from the available river gauge data. Padovani (2010) evaluated the Pantanal flooded area applying a Linear Model of Spectral Mixture to the MODIS vegetation index images between 2000 and 2009.

These studies are very useful to assess the representation of flooded area in ORCHIDEE, however they also have their limitations. The relationship used in Hamilton (2002) is based on a short and wet period but has been extended to a very large period which includes dryer years. This relation between flooded area and river height may differ under different climatic conditions and may have evolved over the century due to changes of river morphology. This estimation of the flooded area has another limitation associated with the infrequent revisit of satellite (data every 6-days) and the coarse spatial resolution (27 km). The method of Padovani (2010) faces other limitations: (1) the noise in the MODIS vegetation indices explains why it needs to be filtered (Padovani, 2010; Jönsson and Eklundh, 2004) and (2) the 2-weeks delay between two consecutive observations. As a consequence, the estimation of flooded area

from satellite observations can not be considered a direct measurement and is associated to non-negligible uncertainties.

Nevertheless, the flooded area simulated by ORCHIDEE will be compared to [Hamilton \(2002\)](#) which includes the period studied here (1961-2000) while [Padovani \(2010\)](#) will give an alternative estimate of the climatological annual cycle of flooded area, since the period of MODIS does not overlap with our study.

To assess the spatial representation of the flooded area, the simulations are compared with the floodplains delineation mask from GFPLAIN250m ([Nardi et al, 2019](#)). This dataset gives a geomorphic description of floodplains at a 8.33 arcsecond resolution. Shuttle Radar Topography Mission (SRTM) digital terrain model are used to perform a terrain analysis to evaluate the drainage network, the drainage area and the flow direction. This leads to a geomorphic floodplain delineation which should correspond to the 200 years flood prone zoning estimated from hydrodynamic models. In order to be comparable to ORCHIDEE, GFPLAIN250m is upscaled to 0.5°.

2.2.4 Atmospheric forcing

When evaluating the simulated water cycle of the Pantanal by ORCHIDEE, the atmospheric forcing uncertainty must be considered ([Bhuiyan et al, 2019](#); [Bierkens, 2015](#)). Therefore, three atmospheric forcings are used in this study. The first forcing is CRU-NCEP version 7 ([Viovy, 2018](#)). It is based on a 6-hourly reanalysis from the National Center for Environmental Prediction National Center for Atmospheric Research (NCEP-NCAR) interpolated to 0.5° where precipitation has been corrected using the CRU (Climatic Research Unit) TS3.24 monthly data at 0.5° resolution ([Harris et al, 2014](#)). The second forcing is the WATCH forcing data (Water and Global Change - [Harding et al \(2011\)](#), [Weedon et al \(2014\)](#)) and is based on ERA-40 3-hourly re-analysis interpolated to 0.5° where precipitation has been bias-corrected by CRU TS2.10 monthly data at 0.5° resolution ([New et al, 1999, 2000](#); [Mitchell and Jones, 2005](#)). Then, the last forcing is produced for GSWP3 v1, the third phase of GSWP ([Kim, 2017](#)). It is a 3-hourly global product based on the second version of 20th Century Reanalysis (20CR) from the NCEP land-atmosphere model ([Compo et al, 2011](#)) at 2° resolution and dynamically downscaled to 0.5° resolution using a spectral nudging technique. The precipitation is bias-corrected with the GPCP v6 monthly data.

These three forcings will respectively be referred to as CRUNCEPv7, WFD and GSWP3. It should be noted that none of these forcings is based on atmospheric re-analysis which includes floodplains. In other words, near surface relative humidity and incoming longwave radiation are not impacted by the higher evapotranspiration which characterized this region. This is a limitation of any off-line approach, although our objective is precisely to demonstrate the importance of simulating floodplains to correctly estimate evapotranspiration over these areas and demonstrate why atmospheric models should be used to capture this feedback.

The precipitation in each original forcing is bias corrected by global monthly observational dataset. A regional dataset of precipitation based on rain gauge stations may improve the representation of precipitation as it is based on a larger amount of local stations. The UPRB is a sparsely sampled region ([Jones et al, 2013](#); [Carril et al, 2012](#)), thus a denser network of rain gauges can improve the distribution of precipitation ([Schamm et al, 2014](#); [Schneider et al,](#)

2017). The data is also processed with a more detailed quality control assessment which is an important issue in the region (Jones et al, 2013; Liebmann and Allured, 2005). A simulation using a regional precipitation dataset may improve the representation of the hydrological cycle in ORCHIDEE. Whether it improves the hydrological cycle or not, it allows in any case to better assess the uncertainty of precipitation over the region. For this purpose, the daily precipitation of CLARIS-lpb dataset has been used to generate new forcings. The principal purpose of these forcings is not to correct the precipitation of the original datasets, but to explore how different estimates of precipitation in this under monitored basin can affect the water cycle.

Three CLARIS-lpb forcings have been constructed. Each one of these forcings combine the daily precipitation of CLARIS-lpb with the other variables that ORCHIDEE needs as input from one of the three forcings already presented. This results in the construction of three atmospheric forcings which will be referred to as CRUNCEPv7_CLARIS, WFD_CLARIS and GSWP3_CLARIS. They use the sub-daily distribution of the precipitation from the original forcing in order to maintain the coherence between precipitation and the other atmospheric variables. Special attention has been taken when the forcing presents a rainless day while CLARIS-lpb does not. In these cases, the precipitation has been allocated to the nocturnal time steps of the forcing so the coherence, with the other forcing variables such as short wave radiation, is kept. For the few grid points of the basin for which no data is available in the CLARIS-lpb dataset, the same precipitation as the original forcing is maintained. Generating 3 new forcings from the available data allows: (1) to assess the influence of the other atmospheric variables by comparing forcings with a similar precipitation, i.e. by comparing the CLARIS corrected forcings between them; (2) to assess the impact of precipitation when 2 forcings have the same atmospheric component except precipitation, i.e. by comparing the original forcings with their CLARIS-lpb corrected version; (3) to study a wider range of precipitation uncertainty by using the daily precipitation from a regional observational dataset.

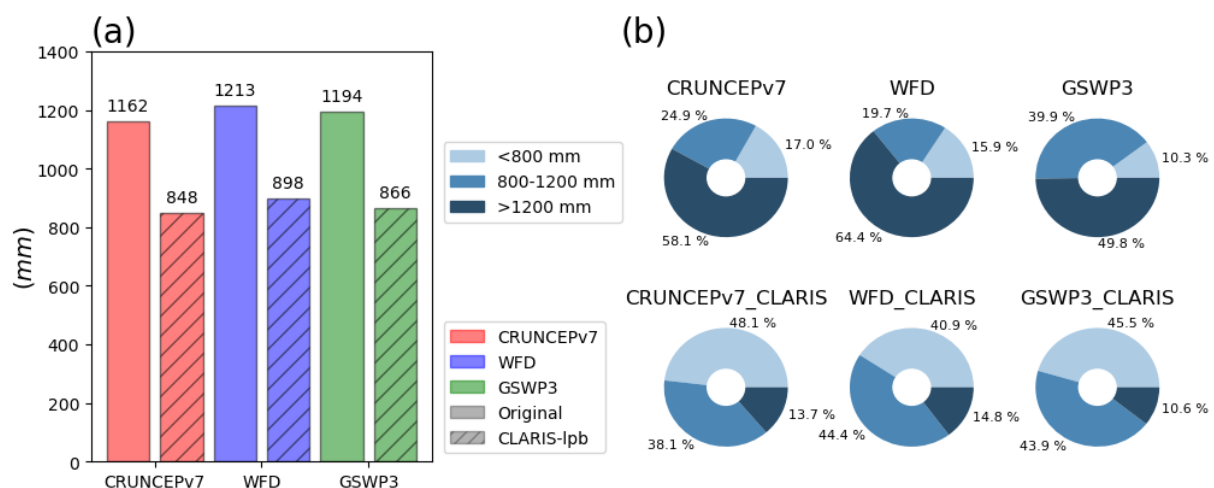


Figure 2.3. Mean annual precipitation (a) and piechart of mean annual precipitation covered by three classes: < 800, between 800 and 1200 mm and > 1200 mm (b) upstream of the Porto Murtinho station.

Figure 2.3.a compares the mean annual precipitation of the six forcing datasets over the whole Upper Paraguay river basin. The corrected forcings have lower annual precipitation than the

original forcing (800-900 mm instead of 1100-1200 mm) which also affects the spatial distribution of mean annual precipitation (Figure 2.3.b). Actually more than 50% of the grid points have a mean annual precipitation above 1200 mm in the original forcings while this proportion never goes beyond 15% in the corrected forcings.

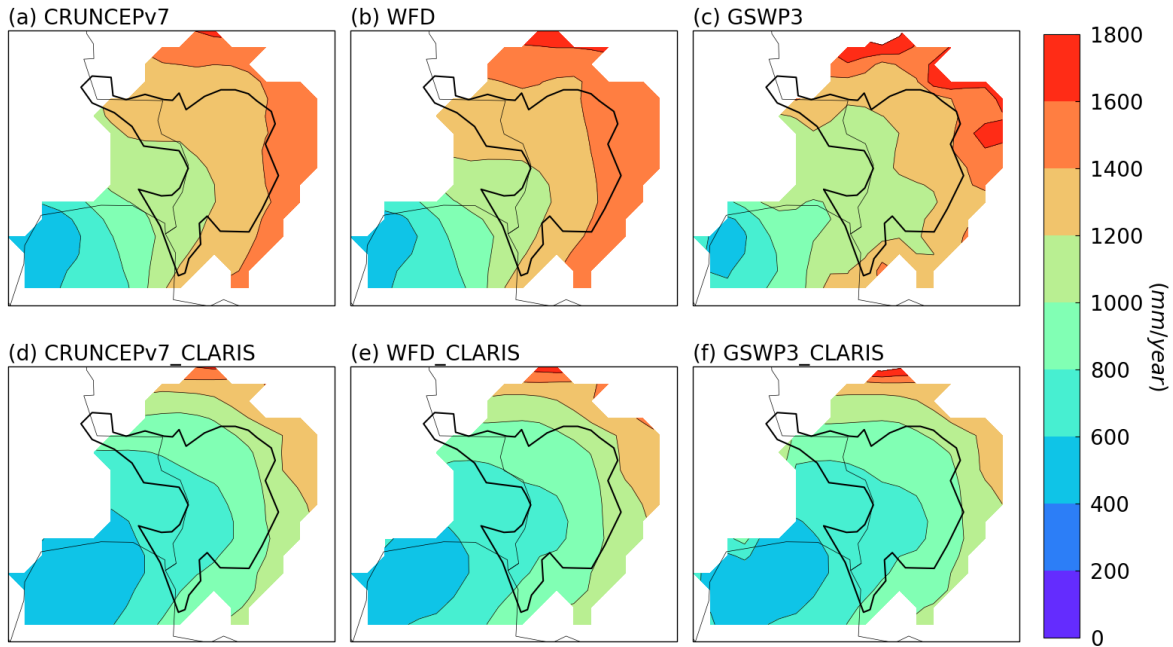


Figure 2.4. Mean annual precipitation over Porto Murtinho upstream area between 1961 and 2000 for the different forcing

The spatial distribution of the mean annual precipitation over the Upper Paraguay river basin between 1961 and 2000 is shown in the Figure 2.4 for each forcing. The mean annual precipitation gradually reduces from the North-Northeastern part of the basin where it reaches 1400 to 1500 mm to the southwestern region where it reaches a minimum between 400 and 600 mm. The difference between the original forcing and their bias-corrected version over Pantanal and the North-Northeastern region of the basin is around 400 annual mm. These differences over the north-northeastern region may lead to significant differences in the simulations because this region has the most important contribution to the water cycle of the Pantanal.

2.2.5 Analysis of river discharge

The annual cycle of river discharge is characterized through the concentration period (C_p) and concentration degree (C_d) (Li et al, 2008, 2011) which is based on a polar representation of monthly discharge values. In the polar representation, the discharge for the month i (Q_i) is associated with angle θ_i . Each month can then be projected onto the x-axis and the y-axis. The sum of the projections of monthly discharge onto the x-axis (Q_x) and the y-axis (Q_y) can be calculated as:

$$Q_x = \sum Q_i * \cos(\theta_i); Q_y = \sum Q_i * \sin(\theta_i) \quad (2.4)$$

These vectors are then used to calculate the concentration period and concentration degree:

$$C_p = \frac{\arctan(Q_y/Q_x)}{2 * \pi/12} \quad (2.5)$$

$$C_d = \sqrt{Q_x^2 + Q_y^2} / \sum_{i=1}^{12} Q_i \quad (2.6)$$

In the polar representation of annual cycle described previously, the distribution of the mean annual cycle of monthly discharge can be synthesized by a vector which time value and magnitude are respectively the C_p angle and the C_d . The concentration period is the centroid of the discharge over the annual cycle time axis and indicates when the highest discharges occur. The concentration degree provides information about the shape of the annual cycle of the discharge. The more the discharge is unequally distributed over the year, the higher is C_d . It reaches $C_d = 0$, its lower value, when the discharge is equally distributed over the year and reaches $C_d = 1$ if the discharge is only non-null for a single month.

In order to summarize the results of the simulations we use the Taylor diagram (Taylor, 2001). This diagram is a representation in a single graph of the Root Mean Square Error (RMSE) and the correlation between the simulations and the observations and of their respective standard deviation. For the normalized Taylor Diagram the standard deviation of each point is normalized by the observed value.

Two additional hydrological indexes are used to assess the representation of the monthly mean discharge: the Nash-Sutcliffe efficiency (NSE) index and the Percentage Bias (PBIAS) of the volume (Moriasi et al, 2007). The NSE index is a value between $-\infty$ and 1. It compares the simulated discharge to the mean value of the observations. If $NSE > 0$, the simulation simulates better the monthly discharge than the mean observed discharge and if $NSE < 0$, the opposite is occurring. The Percentage Bias (PBIAS) of the volume is the bias between the simulated discharge and the observations expressed as a percentage. A positive (negative) value means that the simulation is overestimated (underestimated) the discharge.

3. Results

3.1 Outflow

The impact of the floodplain module on the outflow of the Pantanal is first evaluated with the mean discharge, the annual cycle and its extremes (Figure 2.5.a to 2.5.f) at the Porto Murtinho station. The Table 2.1 presents the NSE index and PBIAS of each simulation.

The NOFP simulations of the original forcings overestimate the mean annual discharge while the NOFP simulations of the corrected forcings underestimate it. The activation of the floodplain module in the FP simulations reduces the mean annual discharge for all simulations with respect to the simulation without floodplains. This also applies to the monthly timescale as each FP simulation has a lower PBIAS than its respective NOFP simulation. This degrades the simulated volume for the forcings with an already negative PBIAS in their NOFP simulation

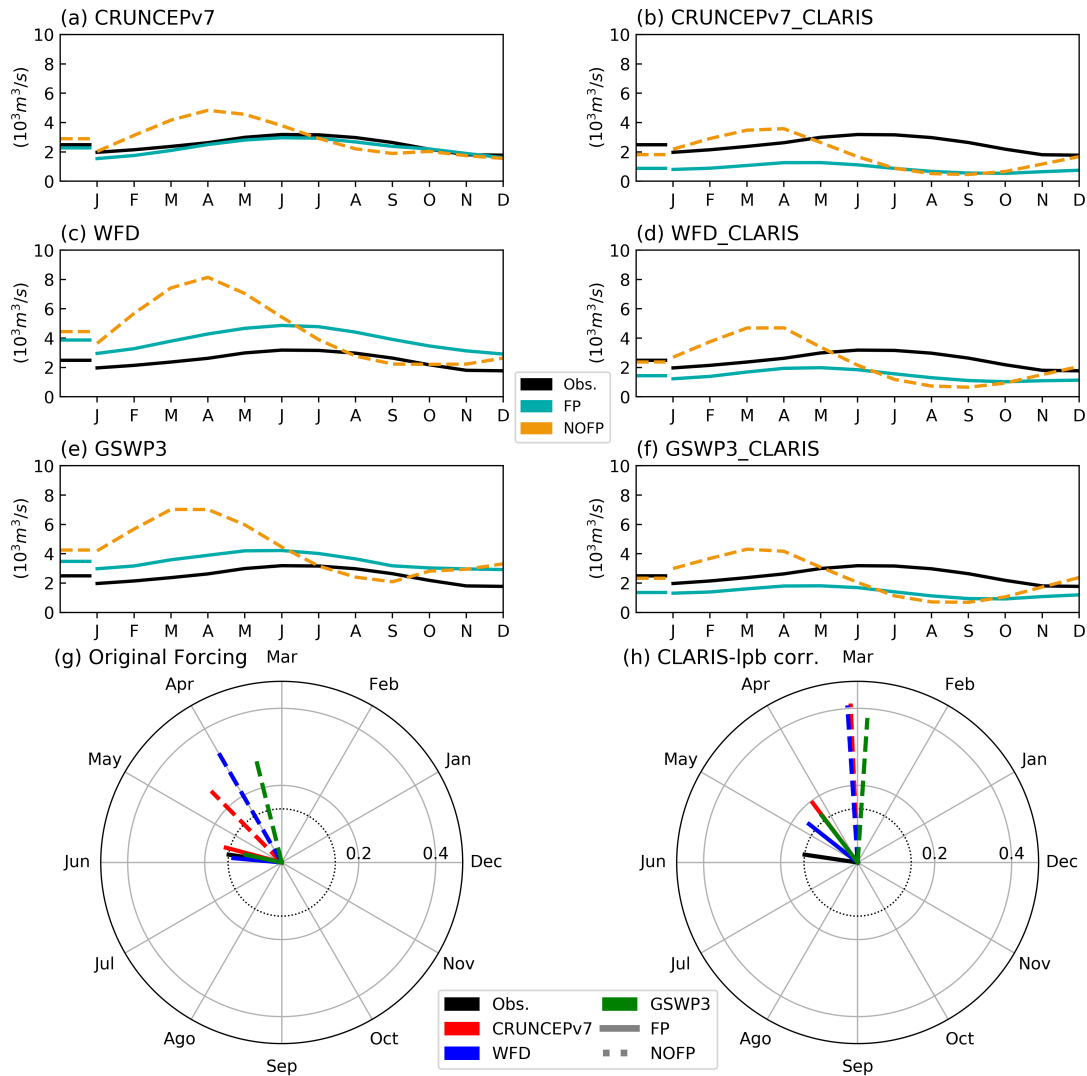


Figure 2.5. (a) to (f) represent the mean annual cycle of discharge at Porto Murtinho station between 1961 and 2000 for each forcing with FP in green, NOFP in orange and observations in black, mean discharge is also displayed by a line left of each annual cycle. Concentration degrees and concentration period vectors for Porto Murtinho discharge between 1961 and 2000 are represented for original forcing and CLARIS-lpb corrected forcing respectively in (g) and (h), with FP (solid lines) and NOFP simulations (dashed lines) and Observations (black line).

and improves the simulations for the forcings with a positive PBIAS in their NOFP simulation. For these reasons, the mean annual discharge and its monthly representation are improved by the activation of the floodplain module for the original forcings and degraded for the corrected forcings.

The activation of the floodplains module improves the NSE index for all the simulations except for the CRUNCEPv7_CLARIS forcing. The degradation of the NSE index of the CRUNCEPv7_CLARIS forcing, may be due to the fact that its FP simulation is strongly underestimating the monthly discharge with a PBIAS below -60%. CRUNCEPv7_FP is the best performing simulation at representing the river discharge at Porto Murtinho with a NSE index of 0.5 while the other simulations have negative NSE index. These negative NSE values means that the mean value of the observations is a better estimate of the monthly mean discharge than the

Table 2.1. Assessment of the monthly river discharge simulated by the ORCHIDEE model at Porto Murtinho station between 1961 and 2000 by two hydrological indexes. NSE is the Nash–Sutcliffe efficiency and PBIAS is the Percentage Bias of the volume.

	NSE		PBIAS	
	FP	NOFP	FP	NOFP
CRUNCEPv7	0.5	-0.83	-8.32	16.84
CRUNCEPv7_CLARIS	-1.52	-1.23	-65.01	-26.81
WFD	-1.07	-6.46	55.79	78.94
WFD_CLARIS	-0.28	-1.57	-41.91	-4.54
GSWP3	-0.16	-5.34	40.15	71.26
GSWP3_CLARIS	-0.54	-1.38	-45.43	-6.25

monthly mean discharge in the simulation. The observed river discharge at Porto Murtinho has a small variability, and thus even a small overestimation or underestimation of the simulated discharge may lead to a negative NSE value.

The annual cycle is improved in the FP simulations since it reduces both delay and bias between the simulated and the observed peak discharge. For example in Figure 5.a, the annual cycle for the FP simulation is in phase with the observation with a peak around June while the peak arrives two months earlier in the NOFP simulation. The phasing of the discharge reduces the bias except for CRUNCEPv7_CLARIS in which an excessive underestimation of discharge worsen the bias of the FP simulation compared to the NOFP simulation. At the same time, with the activation of floodplain module, the intra-annual variability is reduced as well as the inter-annual variability of the monthly discharge. This diminishes high and unrealistic extreme discharge (not shown).

Concentration period and concentration degrees for each simulation are represented in Figure 2.5.g and 2.5.h. For each forcing, the NOFP simulation has a much higher concentration degree and an earlier concentration period while the concentration degree of the FP simulation is closer to the observations and its concentration period is more in phase with observations. This means that the distribution of discharge over the year is better represented when the floodplain module is activated. Moreover, the standard deviation of the concentration degree is lower in the FP simulations than in the NOFP simulations. This indicates that the floodplains reduce the impact of precipitation uncertainty on the distribution of the discharge.

The mean annual discharge, the seasonal cycle and the high flows are important parts of the river discharge representation, but to fully assess the river flow, it is useful to also consider the inter-annual variability. For this purpose, a more complete analysis of monthly mean discharge in Porto Murtinho between 1961 and 2000 is presented in a Taylor diagram (Figure 2.6).

Correlations of monthly discharge of the NOFP simulations with the observations range between 0.2 and 0.6 while for the FP simulations it reaches values between 0.6 to almost 0.85 for this diagnostic. The same occurs with the RMSE, for which all NOFP simulations range from 1.2 to more than 2 whilst the FP simulations present results ranging between 0.6 and 1. The

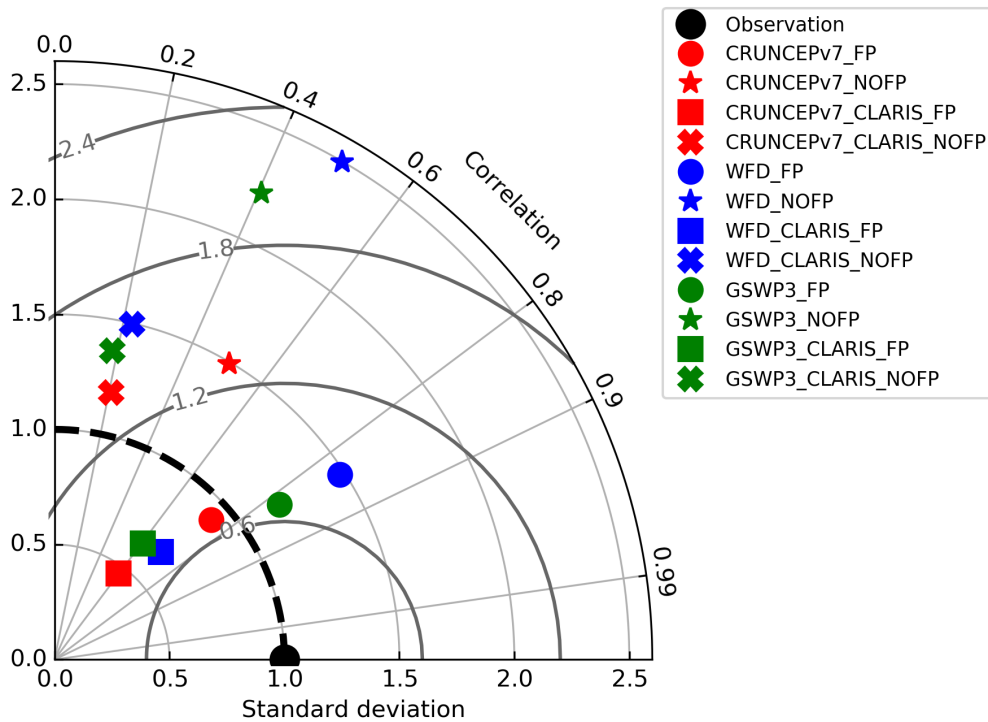


Figure 2.6. Standardized Taylor diagram comparing simulated monthly river discharge with observation for Porto Murtinho station between 1961 and 2000. CRUNCEPv7, WFD and GSWP3 forcings and their CLARIS correction are represented respectively by red, blue and green elements. Circles and stars are for original forcings while squares and crosses represent CLARIS corrected forcings. Circles and squares indicate simulations with an activated floodplain module (FP) module whereas stars and crosses indicate NOFP simulations.

FP simulations have a lower internal variability (standard deviation of monthly discharge) which is closer to the observed variability for all forcings. Moreover, the observed standard deviation is within the distribution of standard deviation for the FP simulations and out of the distribution for the NOFP simulations. The standard deviation of the FP simulations follows the pattern of the mean annual discharge, the forcings overestimating the mean discharge also overestimate the standard deviation while the opposite occurs with simulations which underestimate the mean discharge. A lower mean discharge usually results in a lower variance. In order to consider this effect, the representation of variability can be assessed with the relative variance. The FP simulations have a relative variance closer to the observed value than their respective NOFP simulations. This means that there is an effective improvement of the variability in the FP simulations which is not only related to the reduction of the mean discharge. Considering the full time series of monthly discharge leads to the same conclusion as the one for seasonal variability. The floodplain module improves all the evaluated metrics: correlation, magnitude of the error and variability.

To assess the impact of the activation of the floodplain module on the inter-annual variability of the discharge at the outflow of the Pantanal, the concentration degree and concentration period are calculated for the 40 simulated years. Their distribution is shown for the original version of

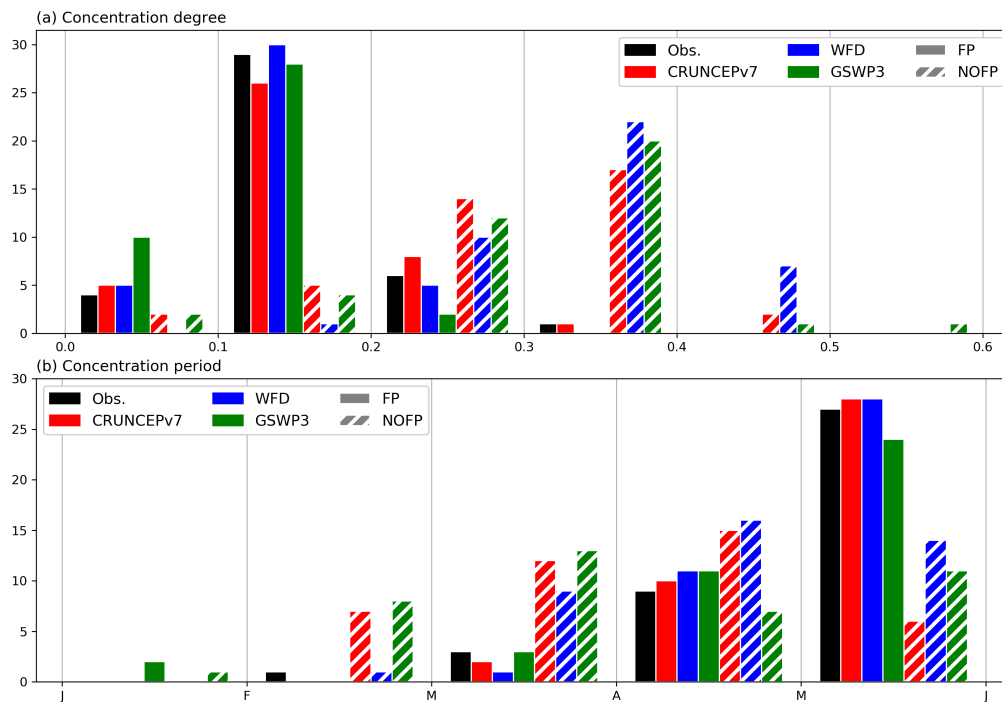


Figure 2.7. Distribution of (a) the concentration degree and (b) the concentration period of each one of the 40 years of simulation for the discharge in Porto Murtinho for the FP and NOFP simulations forced by CRUNCEPv7, WFD and GSWP3. The distribution of the concentration degree uses 6 evenly spaced bins between 0 and 0.6. The distribution of the concentration period uses 5 bins, one for each month between January and May.

the forcings in Figure 2.7 using 6 evenly spaced bins between 0 and 0.6 for the distribution of the concentration degree (Figure 2.7.a) and 5 bins, one for each month between January and May, for the distribution of the concentration period (Figure 2.7.b). For the forcings corrected by CLARIS-lpb, the results are similar and therefore are not shown. The distribution of the concentration degree (Figure 2.7.a) shows that the FP simulations are closer to the observed distribution of the annual concentration degree than the NOFP simulations. For the FP simulations, the distribution is centered on a value of 0.2 and ranges between 0 and 0.3 while, for the NOFP simulations, it is centered on a value of 0.3 and ranges between 0 and 0.5. It indicates that the floodplains tends to display a lower concentration degree and thus a lower intra-annual variability of the discharge. The distribution of the concentration period (Figure 2.7.b) has an identical behaviour with a reduced inter-annual variability for the FP simulations which is more consistent with observations. The concentration period in the FP simulations is mainly distributed between April and May while the distribution of the concentration periods in the NOFP simulations extends over a longer period, between February and May. Thus the FP simulations reduce the inter-annual variability.

The reduced intra-annual and inter-annual variability in the FP simulations indicate that floodplains act as a low-pass filter on river discharge. The presence of floodplains reduces the inter-annual variability of discharge at the outflow of the Pantanal. Floodplains also reduces the impact of the inter-annual variability of precipitation and evaporation onto the discharge.

This result demonstrates that the error of timing and volume in the NOFP simulations at sea-

sonal and inter-annual scale can not be only related to a simple underestimation of the average evapotranspiration over the floodplains. Therefore, the floodplain dynamics needs to be specifically considered by the model to correctly represent the water cycle over Pantanal and the Paraguay River basin.

3.2 Flooded area

The outflow of the Pantanal floodplain is only one facet of the water cycle in the region. Before the river leaves the Pantanal, it floods areas of low topography. The flooded areas in the model have the potential to modify the evapotranspiration by exposing open water to the atmosphere and replenishing soil moisture. The dominant factor for this evapotranspiration enhancement will be the area of open water and the available energy for evapotranspiration. Two different aspects of floodplain representation must be evaluated: the temporal variation of the flooded area and its spatial extension.

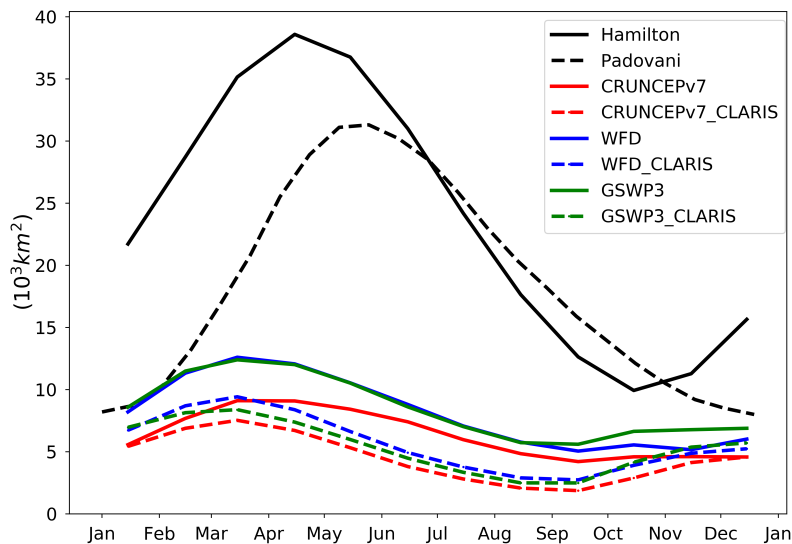


Figure 2.8. Annual cycle of flooded area upstream of Ladário for ORCHIDEE's simulations and Hamilton (2002) averaged over the 1961-2000 period and for Padovani (2010) averaged over the 2000-2009 period.

The flooded area in ORCHIDEE is estimated from the water volume in the floodplains reservoir. A more direct evaluation of the variations of water volumes stored by ORCHIDEE can be performed by comparing them to the Terrestrial Water Storage (TWS) estimates obtained from GRACE observations between 2003 and 2009. The correlation between ORCHIDEE and GRACE of TWS anomalies over Pantanal is high with a value of 0.99 and a confidence level higher than 99% (Not shown). As shown above, the relative bias of the discharge at Porto Murtinho station for the different forcings in the FP simulations ranges between -65% and $+55\%$ (cf. section 3.1). So, in the FP simulations, ORCHIDEE seems to represent well both the annual cycle of the water volume within the Pantanal and the volume of water flowing out of the Pantanal. This leads us to the conclusion that the volume of water present in the floodplains in ORCHIDEE's simulations is realistic. Therefore, comparing flooded area in ORCHIDEE with those proposed by Padovani (2010) and Hamilton (2002) allows to evaluate the

Table 2.2. Correlation between monthly simulated flooded area upstream of Ladário and Hamilton (2002) monthly flooded area for the 1961-2000 period, all correlations have a confidence level higher than 99%

Forcing	Correlation coefficient
CRUNCEPv7	0.589
CRUNCEPv7_CLARIS	0.634
WFD	0.707
WFD_CLARIS	0.653
GSWP3	0.684
GSWP3_CLARIS	0.621

relation between flooded area and water volume in the model.

Figure 2.8 compares the annual cycle of flooded area modeled by ORCHIDEE with Hamilton (2002) between 1961 and 2000 and Padovani (2010) between 2000 and 2009. ORCHIDEE's flooded area is much lower than both estimates but the seasonal variations match well those of Hamilton (2002).

The relationship between volume of water in the floodplains and flooded area is difficult to establish. The conversion from volume to surface, as well as the reverse, requires a high spatial resolution and a high quality topography and river network. These data are not available because of technical limitations but, even if they were available, the coarse resolution of ORCHIDEE cannot capture the complexity of the topography and river network. This means that the conversion of water volumes in the floodplains into flooded area is a major source of uncertainty and in all likelihood ORCHIDEE is underestimating the area.

Despite this, ORCHIDEE's simulations have a similar temporal variation to those found by previous studies, with a maximum between March and May and a minimum around October. This is confirmed in Table 2.2 in which modeled floodplain extents are correlated with Hamilton (2002) over the 1961-2000 period. The correlations range between 0.59 and 0.7 with a confidence level higher than 99 %.

To evaluate the spatial distribution of flooded area, the GFPLAIN250m dataset is used (Nardi et al, 2019). It provides the grid points that can be identified as floodplains based on their geomorphic description. It represents the proportion of area considered as potential floodplains by GFPLAIN250m. ORCHIDEE provides a fraction of the grid which is flooded. Despite this difference, in this paper GFPLAIN250 is interpreted as an extreme maximum for ORCHIDEE. It provides an opportunity to perform a qualitative assessment of the spatial coherence of this variable. Figure 2.9 shows GFPLAIN250m and ORCHIDEE's mean flooded fraction.

The spatial pattern of flooded area in ORCHIDEE for the 1961-2000 period is consistent with the floodplains delineation in GFPLAIN250m. The flooded areas in the Pantanal and in particular along the main Paraguay river are well represented in ORCHIDEE's simulations even if the coarse resolution may affect the construction of the river routing. Some specific grid points are actually not well connected to their upstream area and this is affecting their simulated flooded

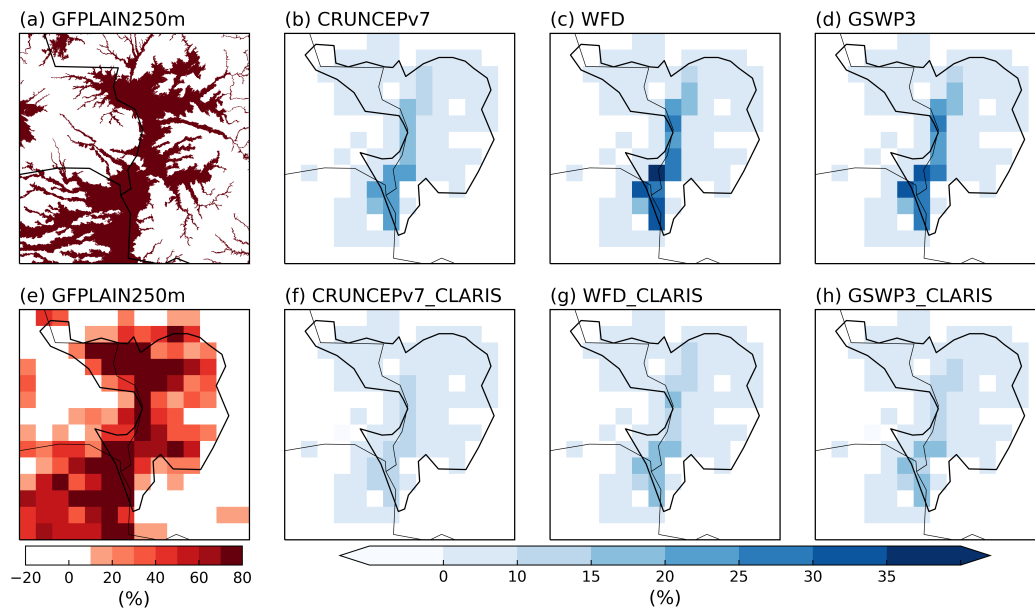


Figure 2.9. Geomorphic description of floodplains from GFPLAIN250m dataset (a) upscaled to 0.5° (b) and mean flooded fraction in ORCHIDEE averaged over the 1961-2000 period for each grid point and all 6 forcing (b-d and f-h).

area. This occurs for example in the north-western part of the Pantanal. Original forcings are more coherent with GFPLAIN250m because they simulate a sharper contrast between the grid points over the main branch of the river and the rest of the area.

3.3 Seasonality of evapotranspiration

The seasonality of evapotranspiration over the floodplains is affected by two main factors: the potential evapotranspiration and the water available for evaporation. Potential evapotranspiration is largely controlled by the atmospheric forcing. Since each pair of simulation FP and NOFP are forced by the same atmospheric conditions they will have comparable potential evapotranspirations. The factor that will most impact the flux of simulations using the same atmospheric forcing is the water available.

The impact of floodplains on the seasonality of evapotranspiration can be evaluated by the difference of evapotranspiration between FP and NOFP in relation with the floodplain extent for each month of the year. Figure 2.10 compares the 40 year average values of mean difference of evapotranspiration ΔE (with $\Delta E = E_{FP} - E_{NOFP}$) and mean flooded fraction. In order to focus attention on grid points where flooding is a dominant process, ΔE only considers the grid points with a mean flooded fraction over 10%.

For each forcing ΔE is positive all along the year meaning that the FP simulations always have a higher evapotranspiration than their respective NOFP simulation since the floodplains provide more evapotranspiration. The results show that between December and May (wet period) the flooded area expands, rising from 30% to almost 60% of the surface, and reduces during the rest of the year (dry period). The difference of evapotranspiration between the FP and the NOFP simulations remains stable at its lower values during the wet period (around 0.5 mm/day) and is more pronounced during the dry period, reaching a maximum of 2.5-4

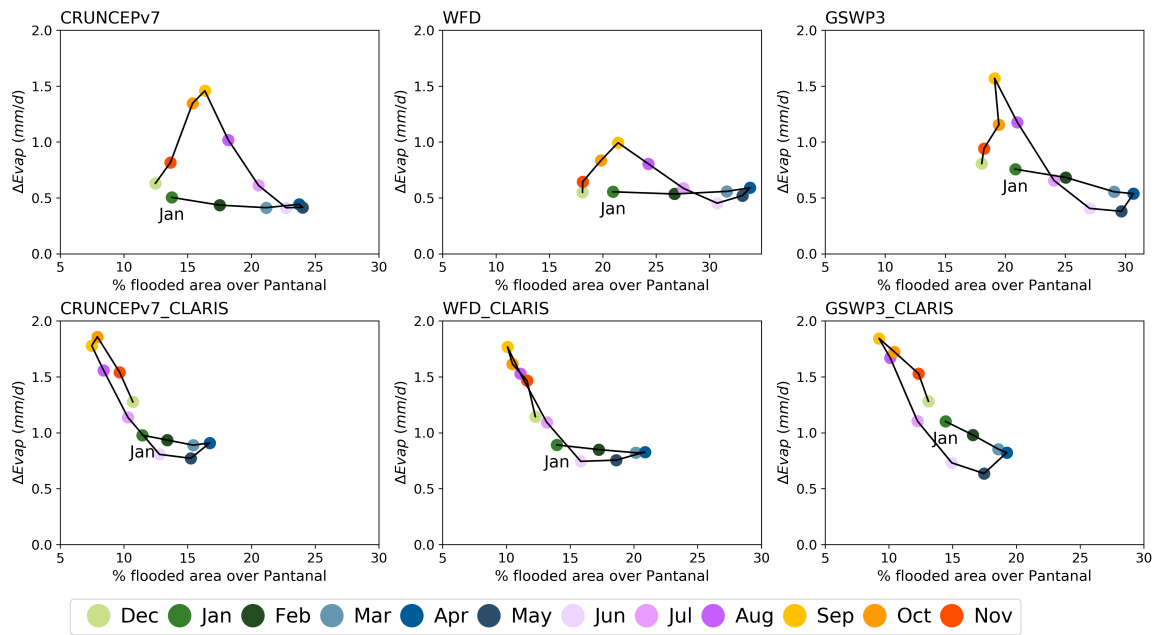


Figure 2.10. Distribution of mean monthly flooded fraction upstream of Porto Murinho (x-axis) in relation with the mean difference of evapotranspiration between the FP and the NOFP simulations ($\Delta E = E_{FP} - E_{NOFP}$, y-axis) among the grid points with mean flooded fraction up to 10 %.

mm/day. Being at a tropical latitude, the radiation provides sufficient energy all along the year and gives favourable evapotranspiration conditions during both dry and wet seasons. During the wet period, both simulations have enough water to evaporate, for this reason the difference of evapotranspiration between the FP and the NOFP simulations is low and stable. The difference is exacerbated during the dry season since evapotranspiration in the NOFP simulations is limited by local precipitation, while the FP simulations can also evaporate water which has fallen upstream during the wet season.

The forcings corrected with CLARIS-lpb have a lower precipitation during the wet season than their respective original forcing, and thus have a smaller flooded area in their FP simulations compared to the FP simulation of their respective original forcing. Regarding the NOFP simulations of the CLARIS-lpb forcings, the lower precipitation affects soil moisture, and thus the transpiration. This lower transpiration further enhances the difference of evapotranspiration with the FP simulation of the same forcing in September / October. This may explain the higher δE in the forcings corrected by CLARIS-lpb compared to the original product.

On top of the importance of precipitation, differences in other forcing atmospheric variables may also impact the potential evapotranspiration. For instance comparing WFD and CRUNCEPv7, the flooded area in WFD is higher than in CRUNCEPv7 because the precipitation is higher in WFD. In contrast, the atmospheric conditions from CRUNCEPv7 provide a higher potential evapotranspiration than WFD (not shown) which means that even with a larger free-water surface available, the difference between the FP and the NOFP evapotranspiration in CRUNCEPv7 is higher than in WFD.

The vegetation cover may also control the evapotranspiration as it facilitates the access to soil moisture. During the flooded period, from January to July, the NOFP simulations have

a higher transpiration than the FP simulations while, from August to December, transpiration is higher in the FP simulations (not shown). The floods between January and July limits the transpiration in the FP simulations because energy is mostly used to evaporate water in contact with the atmosphere. After July, the FP simulations have a higher soil moisture than the NOFP simulations as it has been consumed previously for transpiration. Moreover, soil moisture in the FP simulations is increased by the infiltration from the floodplains. Therefore the FP simulations have a higher transpiration than the NOFP from July to December explaining the increased difference of evapotranspiration from September to October.

The increase of evapotranspiration over the floodplains impacts the land-atmosphere fluxes by increasing latent heat fluxes at the expense of sensible heat fluxes over the flooded area, and thus decreasing the Bowen ratio. The changes in Bowen ratio follow the same spatial pattern as changes in evapotranspiration. This may generate horizontal gradient of temperature and humidity in the atmospheric boundary layer and then may affect low level circulations.

3.4 Water Balance

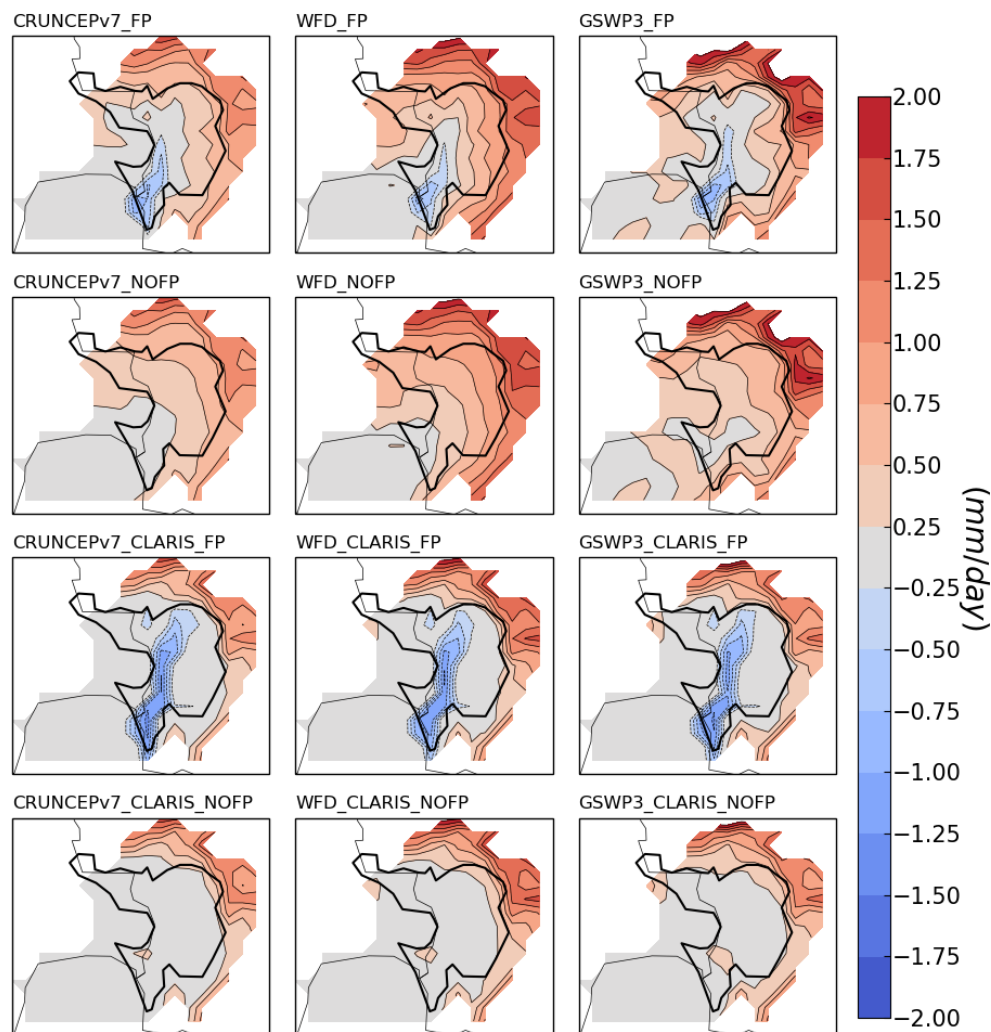


Figure 2.11. Mean difference between precipitation and evapotranspiration ($P-E$) for all 6 forcings with the FP and the NOFP configurations between 1961 and 2000.

The difference between mean precipitation and mean evapotranspiration ($P-E$ flux) is a measure of the exchanges of water between the atmosphere and the surface. A positive $P-E$ flux means that the surface acts as a sink, receiving more water from the atmosphere than it loses through evapotranspiration. A negative $P-E$ implies that the region is a source of water for the atmosphere. The $P-E$ flux in the FP and the NOFP simulations between 1961 and 2000 is shown in Figure 2.11. For each forcing, the FP simulation has a higher evapotranspiration over Pantanal than the NOFP simulation and thus a lower $P-E$. Over the most flooded part of the Pantanal i.e along the main Paraguay river, the activation of the floodplain module leads to a negative $P-E$ for the FP simulations, which means that mean annual evapotranspiration exceeds local mean annual precipitation. This source of water for the atmosphere will generate gradients of temperature and humidity in the planetary boundary layer between the floodplains and the surrounding areas.

The annual cycle of $P-E$ is also an interesting indicator of the inherent mechanisms of the Pantanal. The Figure 2.12 displays the mean annual cycle of $P-E$ over the most flooded areas of the Pantanal, defined as the grid points with a mean flooded fraction up to 10 %. Mean annual $P-E$ is always positive for the NOFP simulations while it is negative for the FP simulations with the lowest basin-wide rainfall, i.e. CRUNCEPv7 and all CLARIS-lpb corrected forcings. $P-E$ in the NOFP simulations can reach negative values during the dry season (July-September). This is due to the combination of: (1) the high local precipitation during wet season that is stored in the ground and remains available during dry season for plant transpiration with (2) low precipitation and dry conditions leading to an evapotranspiration exceeding precipitation. It should also be noted that floodplains may exacerbate this process because of the infiltration from their reservoirs.

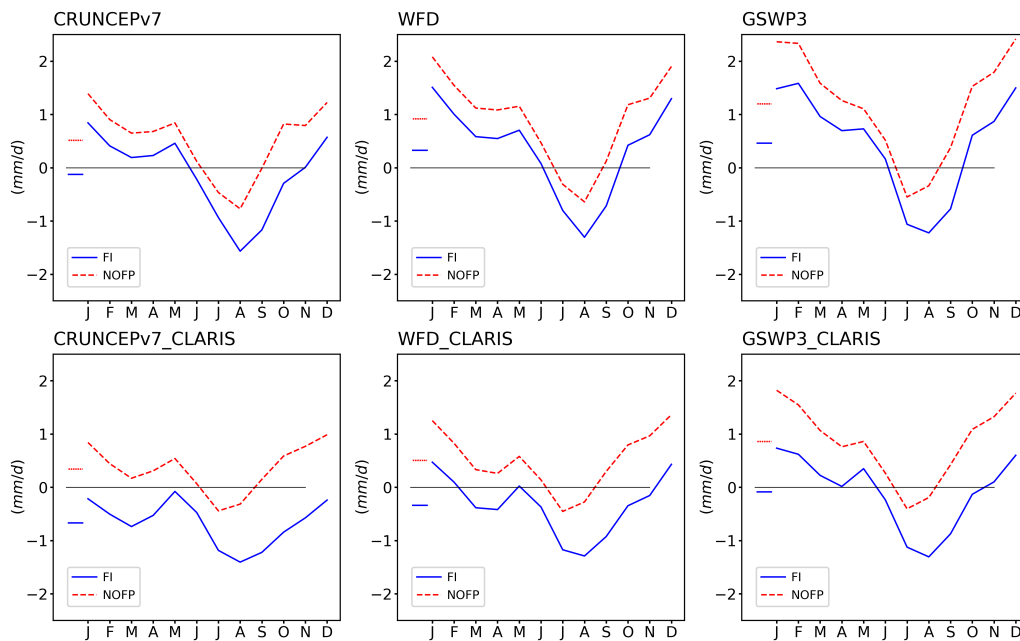


Figure 2.12. Mean annual cycle of monthly $P-E$ flux between 1961 and 2000 for the 6 different forcings with the FP simulation (solid blue line) and the NOFP simulation (dashed red line) among the grid points with mean flooded fraction up to 10 %. The mean value is also displayed by a line left of each annual cycle.

For each forcing, the annual cycle of P - E in the FP simulations and in the NOFP simulations show a similar evolution. It must be taken into account that these simulations are forced by atmospheric conditions extracted from re-analysis models which do not include floodplains. This may impact the evapotranspiration which depends on near-surface air humidity and temperature. This is one of the limitation of this study. Nevertheless future planned simulation coupling ORCHIDEE with an atmospheric model may allow to study more in depth the feedbacks between floodplains and the atmosphere.

4. Discussion

This study has shown that considering floodplains in a Land Surface Model improves the representation of the water cycle and leads to an increased evapotranspiration over Pantanal. This extra evapotranspiration is missed by all Earth System Models as surface parameterization usually do not consider floodplains. In order to quantify this flux which is neglected, we provide a model-guided observational estimation of how much water evaporates annually over Pantanal.

Estimating evapotranspiration is difficult at large scale for regions with sparse observations such as the Pantanal. Empirical formulations of evapotranspiration used in satellite products are based on an approximated surface energy balance and have not been calibrated over the open water surfaces generated by flooding. Therefore these estimates might not provide reliable fluxes over temporarily flooded areas such as floodplains. The scarcity of ground observations complicates the assessment of the reliability of satellite products and limits their adjustment. The formulations of evapotranspiration in LSMs also faces uncertainties from a combination of different factors related to the atmospheric forcings, to the internal uncertainty of the models and their coarse resolutions. Previous studies have attempted to close the water budget from satellite data, with at least one over Pantanal (Penatti et al, 2015). They faced issues with the budget closure due to the inconstancy between the different satellite products used.

The water continuity equation (Eq. 7) for the Pantanal gives a relationship between the main components of the water cycle: the precipitation (P), the river discharge (Q), the evapotranspiration (E) and the groundwater storage (W). The Pantanal is not a closed catchment, thus the equation considers the various inflow ($\sum Q_{inflow}$) and the outflow ($Q_{outflow}$) of the Pantanal.

$$\frac{\partial W}{\partial t} = P + \sum Q_{inflow} - E - Q_{outflow} \quad (2.7)$$

Over the 40 year period considered here, the water storage dynamics can be assumed to be negligible so $\frac{\partial W}{\partial t} = 0$. From this consideration the evapotranspiration can be estimated as a residual of the water continuity equation:

$$E = P + \sum Q_{inflow} - Q_{outflow} \quad (2.8)$$

However, this method has some limitations: (1) the inflow observations are not always available, some do not have a fluviometric station and many hydrological stations have missing

data; (2) there are large differences among the precipitation datasets. We propose to use the internal structure of a model such as ORCHIDEE ensure coherence between the different variables and close the water budget to deduce the missing information.

Discharge is a key output of the simulations and, despite its uncertainty among the different simulations, it can easily be assessed in comparison with fluviometric stations. The outflow of the Pantanal is represented by the Porto Murtinho station. For the inflows, a total of 6 fluviometric stations have been selected because they can be localized in the grid of ORCHIDEE. These stations are Caceres, Cuiaba, São José do Borireu, São Jeronimo, Coxim and Aquidauana, see Figure 2.1. A station is considered as possible to localize if we find a grid point in the grid of ORCHIDEE that fulfills the following criteria: (1) it is at less than 100km of the station actual location, (2) it is at an equivalent position in the river network and (3) has less than 10% of difference in upstream area. It should be noticed that not all inflow branches of the Pantanal have a localized station to evaluate the discharge simulated by ORCHIDEE (See Figure 2.1).

Because of the coarse resolution of ORCHIDEE, the upstream area for some station can differ substantially between the observed and modeled values. This occurs in particular when the upstream area is small (a few grid points of ORCHIDEE). Therefore, we use the differences in upstream area to scale the observations so that it matches the one of ORCHIDEE before comparing the discharge. This implies the assumption that the discharge is proportional to the catchment area.

$$Q_{obs,scaled} = Q_{obs} * \frac{upstream\ area\ ORCHIDEE}{upstream\ area\ REAL} \quad (2.9)$$

Based on the comparison between the simulated and observed discharge for the different inflow stations that could be localized in ORCHIDEE and for the outflow (Porto Murtinho), CRUNCEPv7_FP is the better performing simulation for both inflow and outflow. This simulation is thus considered as our best estimate of the water cycle of the Pantanal and will be used to perform the observational estimate of evapotranspiration. For this reason, the precipitation dataset that will be used for the estimation is CRU TS3.24 as it was used for the bias-correction of CRUNCEPv7.

When estimating evapotranspiration from the water balance equation, it is important to correct the discharge from the simulations with the available observations. Inflow and outflow discharge simulated by ORCHIDEE are thus bias-corrected by the observations from the localized hydrological stations.

For an inflow point corresponding to a localized hydrological station, the discharge is corrected directly by the relative bias over the period with available observations. The discharge bias is related to the P-E error over the upstream catchment, this P-E error is assumed to be comparable in neighbouring regions. So the correction of an unmonitored catchment can be obtained by the interpolation of the relative bias from the surrounding localized fluviometric stations. The western side of the Pantanal doesn't have any fluviometric station, the closest one to the North displays an underestimating discharge while the closest station to the South is overestimating the flux. Therefore, the western inflow to Pantanal is difficult to correct. Since this is a semi-arid area the contribution to the Pantanal inflow is small and its biases should not affect the results.

Table 2.3. Water closure budget with CRUNCEPv7_FP and CRUNCEPv7_NOFP simulations to perform a residual estimation of evapotranspiration over Pantanal region upstream of Porto Murtinho and downstream of the different inflows. The error of P is the standard deviation of the 4 observational datasets used in the forcings (CRU TS3.24, CRU TS2.10, GPCC and CLARIS-lpb).

	E	=	P	+	Qin	-	Qout
(m^3/s)	6360 ± 950		6530 ± 950		2230		2400
$(mm/year)$	Precipitation	1250	± 180				
	Evapotranspiration	1220	± 180				

The precipitation used originates from the observational dataset and its uncertainty is estimated from the spread between all precipitation datasets used in this paper, i.e. through the standard deviation of the mean annual precipitation of CRU TS3.24, CRU TS2.10, GPCC and CLARIS-lpb.

Table 2.3 shows the model-guided residual estimation of evapotranspiration from the water budget based on observations. Mean annual evapotranspiration is estimated to be 1220 mm/year which is 2% smaller than precipitation (1250 mm/year). The uncertainty attributable to the precipitation is 180 mm/year, or 15% of the total evapotranspiration estimated.

The difference of evapotranspiration between the FP simulations and the NOFP simulations ($\Delta E = E_{FP} - E_{NOFP}$) over Pantanal represents the quantity of water that evaporates from the floodplains. If we assume the model to represent correctly ΔE even if evapotranspiration is known to have an error, ΔE ranges between 80 mm/year and 150 mm/year between the 6 sets of simulations which represents between 6 and 12 % of the total evapotranspiration estimated previously. Therefore between 6 and 12 % of the total evapotranspiration may be neglected by atmospheric models which do not consider floodplains.

In the re-analysis underlying the forcings used here, the representation of near-surface variables over floodplains could be corrected for the missing floodplains by data assimilation if sufficient and appropriate observations exist. We do not believe this is the case for the Pantanal. As seen in this study, floodplains have a direct impact on the simulated water cycle by increasing evapotranspiration and consequently by modifying near-surface atmospheric variables such as humidity and temperature. Thus, although the floodplain module is able to affect the water cycle, it cannot generate any feedback through the near-surface atmospheric variables. The absence of feedback will impact the potential evapotranspiration. A first-order estimate of the error due to the absence of feedback on potential evapotranspiration can be made evaluating the ratio between potential evapotranspiration in the FP simulations (ETP_{FP}) and the NOFP simulations (ETP_{NOFP}) using the bulk formula method:

$$\frac{ETP_{FP}}{ETP_{NOFP}} = \frac{qs(T_{sFP}) - qa_{FP}}{qs(T_{sNOFP}) - qa_{NOFP}} \quad (2.10)$$

with q_s the saturated specific humidity which is computed from the mean annual soil temperature T_s and with q_a the specific humidity of the air. This assumes that the atmospheric turbulence is not affected by the floodplains. The mean annual soil temperature is 26.7° in the NOFP simulations and 26.3° in the FP simulations. This is a first approximation because considering a specific period of the year, such as the dry season, would increase the difference of temperature between the FP and the NOFP simulations. This leads to a decrease of 8 % of potential evapotranspiration if the mean annual air specific humidity remains the same. This leads to a decrease of 11 % if the mean annual air specific humidity is raised by 10 %. The consequences of floodplains on precipitation are still discussed (Taylor et al, 2018) but there is some evidences that wetlands and their surface flux heterogeneities may affect precipitation in and around the floodplains (Taylor et al, 2018; Rochetin et al, 2017; Lauwaet et al, 2012) through influencing convection. The lack of feedback between the floodplains and the atmosphere is a limitation of this study especially since the errors of potential evapotranspiration are of the same order of magnitude as the increase of evapotranspiration. Performing coupled simulations will allow a more complete study of the impact of integrating floodplains (1) by considering the land-atmosphere feedbacks and (2) by evaluating the impact of floodplains on precipitation and convection.

The coarse resolution at which ORCHIDEE is used is also a source of uncertainty. Following the previous efforts (Nguyen-Quang et al, 2018c), the development of a higher resolution floodplain module is necessary to improve the simulation of the Pantanal through a better representation of the complexity of its river networks. With an appropriate atmospheric resolution, this will also allow for a finer representation of surface flux heterogeneities which could impact the estimation of evapotranspiration and the convective precipitation.

Tropical floodplains generate important processes for the water cycle of the region, related to the water resources, surface-atmosphere feedback. They also have an important ecological value. But the floodplains of the Pantanal are still poorly understood and quantified. The uncertainty from evapotranspiration due to the lack of feedback and from precipitation are within the same order of magnitude as the estimated increase of evapotranspiration due to the floodplain processes. It means that, beyond the necessity to perform coupled simulations, this system is not well enough observed in order to allow us to get a better understanding of these complex processes, but also more quality observations are required.

5. Conclusion

This paper studies the importance of simulating tropical floodplains in LSMs focusing in particular on the Pantanal which is located in the La Plata Basin. By comparing off-line simulations with the ORCHIDEE LSM with and without a representation of floodplains we are able to evaluate the different components of the regional water cycle which are modified such as river discharge, inundated area and evapotranspiration. In order to evaluate the precipitation uncertainties, three different forcings were used in two versions, the original and a bias adjusted version from a regional observational dataset. These simulations are over a long period (1961-2000) which includes dry and wet decades over this region.

Simulating floodplains in LSMs seems an essential step towards a better representation of the water cycle of the Pantanal. The annual cycle of discharge at Porto Murtinho is better simulated in all cases when the floodplain module is activated despite the forcing uncertainty and its impact on the mean discharge. The activation of the floodplain module also lowers the intra-annual and inter-annual variability of the monthly discharge at the outflow of Pantanal by reducing its dependence on the inter-annual variability of precipitation which is in better agreement with observations.

Despite a representation of the water volume in the floodplains in good agreement with GRACE, ORCHIDEE has a coarse resolution limiting its capacity to convert the volume into a floodplain extension. However, the annual cycle of the simulated open water area over Pantanal is in phase with a previous satellite based study over the area even if the total area is underestimated. Also ORCHIDEE with its coarse resolution seems to represent the spatial distribution of flooded grid points when compared to geomorphic data well. However, the underestimation of the total open water surface over Pantanal by ORCHIDEE will possibly lead to an underestimation of evapotranspiration.

The activation of the floodplain module results in an increase of evapotranspiration through a larger water availability. A higher precipitation in the forcings generate larger flooded area in the simulations that include floodplains but evapotranspiration also depends on other variables of the forcings and in particular those which control potential evapotranspiration. The difference of evapotranspiration between the simulations that include versus not include floodplains is higher in September / October because of the water coming from the upstream area which remains during the dry season in the simulations that include floodplains. This increase of evapotranspiration should have an impact on the lower atmosphere. This will lower the Bowen ratio over the flooded areas which may affect the local circulation due to horizontal gradient of temperature and humidity.

The floodplain module changes the balance between precipitation and evapotranspiration over the floodplains. Over the most flooded part of the Pantanal, the increase of evapotranspiration in the simulations that include floodplains is linked to the evapotranspiration of water from the rainy upstream region which has contributed to the flooding. It allows the annual evapotranspiration to exceed the annual local precipitation over parts of the Pantanal.

Once their consistency confirmed, simulations from LSM are a convenient tool for further studies. We used it to perform a model-guided residual estimation of evapotranspiration over the region using observed precipitation and observed river discharge at suitable fluviometric stations. The evapotranspiration over Pantanal is estimated at 1220 mm/year while the precipitation reaches 1250 mm/year. The uncertainty of precipitation is estimated to be 180 mm/year. The difference of evapotranspiration between simulations with and without floodplains is between 6 and 12 % of total evapotranspiration and thus less than the precipitate error. Nevertheless, this is water that Earth System Models do not take into account when floodplains are not represented.

Coupled atmosphere-land system models may bring more information to the role of floodplains in the regional water cycle by including important feedbacks which had to be neglected here. In any case, more observations are needed over this region in order to reduce the uncertainty

of observational products and allow to gain a better process understanding.

The human impact on the local hydrology can be accounted for in ORCHIDEE by using assimilation techniques that correct the P-E error related to human activity by comparing the modeled natural river discharge with observations (Wang et al, 2018). In this study however, the impact of human activities is not taken into account as the aim is to evaluate the contribution of the Pantanal in its natural state to the regional evaporation. The Pantanal hosts some human activities that may affect its hydrology. Although their impact is limited. Small dams built for electric production in the highlands surrounding the Pantanal (Bergier, 2013; Alho and Silva, 2012) may reduce the flood pulse of the Pantanal as the floodplains dynamic depends on the water flowing from the upstream area. The agricultural sector is in expansion in the region with cattle breeding in the plains and rainfed fields in the surrounding highlands (Alho, 2005). Land use changes due to the expansion of these agricultural activities and deforestation may increase the local runoff (Bergier, 2013) which may lead to an increase of the flood pulse of the Pantanal (Bergier, 2013; Alho and Silva, 2012). ORCHIDEE is partially considering this effect through the vegetation map. The vegetation map used in this study is from 1983 (Olson et al, 1985), further studies may be able to integrate the land use changes by changing the vegetation map along the simulated years. The development of the Paraguay river as a waterway freight transport has modified the river channel (Hamilton, 1999) which may also be a source of changes to the river dynamics.

The major challenge for the years to come is a more systematic inclusion of floodplains in Earth System Models through their LSMs. A particular challenge will be to achieve the higher resolution needed to represent well the meanders of the rivers and quantify the overbank flows to complement the new high resolution routing in LSM (Nguyen-Quang et al, 2018c). The higher resolution in climate models also offers opportunities to change the way floodplains are parameterized because it allows to integrate the bifurcating channels to represent floodplains and deltas.

Acknowledgements

This research has been supported by PICT 2014-0887, PICT-2015-3097, PICT-2017-1406 (ANPCyT, Argentina), Belmont Forum/ANR-15-JCL/-0002-01 "CLIMAX" as well as ECOS-A18D04 (MINCyT, Argentina / ECOS-Sud, France).

2.3 Acronyms

ANA	Agencia Nacional de Aguas
CLARIS-Ipb	Change Assessment and Impact Studies in La Plata Basin
CMIP6	Coupled Model Intercomparison Project
CRU	Climatic Research Unit

ERA	ECMWF Re-Analysis
ERA-40	ECMWF Re-Analysis second generation
ESM	Earth System Model
FP	Offline simulations with the floodplains activated
GFPLAIN250m	Gridded dataset of Earth's floodplains at 250-m resolution
GLWD	Global Lake and Wetlands Dataset
GPCC	Global Precipitation Climatology Centre
GRACE	Gravity Recovery and Climate Experiment
GSWP3	Global Soil Wetness Project Phase 3
HEC-RAS 1D	Hydrologic Engineering Center's River Analysis System
HTU	Hydrological Transfer Unit
IPSL	Institut Pierre Simon Laplace
LAI	Leaf Area Index
LSM	Land Surface Model
MGB-IPH	Modelo de Grandes Bacias do Instituto de Pesquisas Hidráulicas
MODIS	Moderate Resolution Imaging Spectroradiometer
NCEP	National Centers for Environmental Prediction
NOFP	Offline simulations with the floodplains deactivated
NSE	Nash-Sutcliffe Efficiency
ORCHIDEE	ORganizing Carbon and Hydrology in Dynamic EcosystEms
PBIAS	Percent Bias Index
PFT	Plant Functional Type
RMSE	Root Mean Square Error
SALLJ	South American Low Level Jet
SAMS	South American Monsoon System

TWS	Total Water Storage
UPRB	Upper Paraguay River Basin
USDA	United States Department of Agriculture
WFD	WATCH forcing data

Estimation of the flooded area over the Pantanal, a South American floodplains, using MODIS data

Contents

3.1 Introduction	63
3.2 Remote sensing of floodplains	64
3.3 Acronyms	81

3.1 Introduction

This chapter details and discuss the development of different simple and easily reproducible methods to estimate of the flooded area over the Pantanal using optical satellite data. One of these estimates is used further in the thesis for the validation of the flooded area in the high resolution floodplains scheme developped in this thesis. This work has been published in the Meteorologica Journal.

The remote sensing of the large tropical floodplains provides information which is difficult to obtain from ground based observations (Ogilvie et al, 2015b). This information can be useful both for monitoring tasks and for investigation to better understand the floodplains. The floods are the major driver of the floodplains hydrology and ecosystem. Thus, the estimate of the flooded area over the floodplains using remote sensing is a meaningful task. There exists a large variety of methods to estimate the flooded area from satellite data (Fleischmann et al, 2021a).

Several Land Surface Models and Hydrological models simulates the floodplains (cf. D’Orgeval et al, 2008; Dadson et al, 2011; Yamazaki et al, 2013; Getirana et al, 2021; Decharme et al, 2019; Bravo et al, 2012). The spatial extension of the floodplains is complex to represent in the model as it relies on the conversion of the volume of water / the river height into a surface.

In the models, the estimate of the flooded area is very sensitive to the local orography, thus, the resolution and the uncertainty may generate large errors. Some local processes which are not taken into account by the models may also have an impact. Therefore, the satellite estimate of the flooded area are very important for the development of the representation of the floodplains in models because it will help to : (1) assess the conversion of volume / river height into flooded area, (2) detect important processes that may be missing in the model and (3) calibrate these models.

Although, before comparing the flooded area simulated by the model to the satellite estimate, it is important to understand the different type of issues of estimating the flooded area through satellite products. The detection of the presence of open-water surface can be complex because, for example, lushy vegetation can be confused as water. The facility to use these methods should also be taken into account so these methods can be accessible and adaptable to different type of study. The optical satellite data can be easily used with a limited preprocessing compared to infrared sensors. This is why this chapter explores the possibility of detecting the presence of open-water over the floodplains using optical data and discuss the difficulties faced, the possible alternative and the perspective of improvement of these methods. One of the estimate generated will serve to assess the floodplains scheme further in Chapter 5.

The paper accepted for publication by the Meteorologica Journal is presented in the following section. It presents the methods based on spectral indexes related to the presence of water calculated from the MODIS MOD09A1 product. It includes different threshold based methods, a Principal Component Analysis based method and a k-means based method. The flood estimate of these methods is then assessed by previous works.

3.2 Estimation of the flooded area over the Pantanal, a South American floodplains, using MODIS data

Anthony Schrapfer^{1,2,3}, Lucía Mará Cappelletti^{1,2,3}, Anna Sörensson^{1,2,3}

(1) *Universidad de Buenos Aires, Facultad de Ciencias Exactas y Naturales. Buenos Aires, Argentina.*

(2) *CONICET – Universidad de Buenos Aires. Centro de Investigaciones del Mar y la Atmósfera (CIMA). Buenos Aires, Argentina.*

(3) *CNRS – IRD – CONICET – UBA. Instituto Franco-Argentino para el Estudio del Clima y sus Impactos (UMI 3351 IFAECI). Buenos Aires, Argentina*

ABSTRACT

Tropical floodplains, such as Pantanal in Central South America, are important features for land-atmosphere interactions. Schemes to account for floodplains should therefore be included in Earth System Models, but this requires observations of flooded area for validation. Satellite data is a possible solution to estimate the flooded area but it is important to evaluate the

different flood detection algorithms available in order to use the most efficient for the region. This work explores different methods to estimate the flooded area from the MODIS MOD09A1 satellite surface reflectance product using spectral indexes (mNDWI, NDMI, NDMI-NDVI) to detect the presence of water. We include the traditional threshold-based methods but also some unsupervised classification methods such as the k-means and the Principal Component Analysis applied on the water-related spectral indexes. The calibration and validation of these methods are based on the hydrological knowledge of the region, coming from land surface models, river discharge observation and from previous satellite estimations of the flooded area. The NDMI index seems too sensitive to the vegetation which leads to error in the estimation of the flooded area. The other methods were spatially and temporally consistent with previous studies over the Pantanal.

Keywords: *Floodplains, flood detection, remote sensing, Pantanal, MODIS.*

RESUMEN

Las llanuras de inundaciones tropicales, como el Pantanal en Suramérica Central, son importantes para las interacciones suelo-atmósfera. Por lo tanto, los esquemas que representan las llanuras de inundación tienen que ser incluidos en los Modelos del Sistema Tierra, pero eso requiere observaciones del área inundada para validación. Los datos satelitales son una posible solución para estimar la superficie inundada, pero es importante evaluar los diferentes algoritmos disponibles para utilizar el más eficiente para cada región de interés. Este trabajo explora diferentes métodos para estimar la superficie inundada con el producto de reflectancia de la superficie MODIS con el uso de índices espectrales (mNDWI, NDMI, NDMI-NDVI) para detectar la presencia de agua sobre Pantanal. Incluimos los métodos más comunes basados en el uso de umbrales y también algunos métodos de supervisión no clasificada como los k-means y el Análisis de Componentes principales aplicados a los índices espectrales relacionados con la presencia de agua. La calibración y la validación de estos métodos está basado en los conocimientos hidrológicos de la región, proviniendo de modelos de superficie, observaciones de caudal y de estimaciones de la superficie inundada por satélite realizada en trabajos anteriores. El índice NDMI parece demasiado sensible a la vegetación lo que lleva a errores en la estimación de la superficie inundada. Los otros métodos son espacial y temporalmente consistente con estudios previos sobre el Pantanal.

Palabras clave: *Llanuras de inundaciones, Detección de inundaciones, Teledetección, Pantanal, MODIS.*

1) Introduction

The floodplains are wetlands which are temporarily or permanently flooded and where there are strong interactions between the different terrestrial hydrological processes such as river discharge, the evapotranspiration from plants, the evaporation from open water surfaces and the vertical movement of water between the surface soil and the saturated zone. These large floodplains are places of rich biodiversity and provide important ecosystem services such as water purification, river stream regulation and carbon sequestration. The monitoring and im-

proved comprehension of these regions are vital for their revalorization and conservation. Remote sensing products are powerful tools to monitor the spatiotemporal evolution of these extensive floodplains with a reasonable frequency. Satellite estimations of the flooded areas are also necessary to develop a correct representation of the hydrology of these regions in Land Surface Models and Earth System Models.

The periodic flooding of the floodplains related to the overflow of the river is fundamental for the local ecosystem as it is driving the lateral exchange of water and nutrients in the river floodplains system (cf. flood pulse concept, [Junk et al, 1989](#)). These exchanges are one of the reasons why the floodplains are very productive ecosystems and considered as biodiversity hotspots. However, large floodplains are also regions where the in-situ observations are not sufficient to reconstruct their full dynamics, as opposed to smaller and more homogeneous wetlands and to unvegetated regions which can be more easily monitored and where the estimation can be carried out more directly by spectral indices. Thus it is difficult to estimate the temporal variability and map the spatial variability of the floods over large floodplains.

Large tropical floodplains, such as the Pantanal in central South America, are regions of strong land-atmosphere interactions due to a high level of evaporation in relation with the presence of open-water surfaces and of transpiration in relation with the increased soil moisture ([Schrapffer et al, 2020](#)). This induces strong gradient of land-atmosphere fluxes and temperature between the floodplains and the neighbouring regions. This is why the floodplains processes tend to be ever more integrated in Land Surface Models ([Schrapffer et al, 2020](#); [Dadson et al, 2010](#); [Getirana et al, 2021](#)) because this improves the representation of the hydrological cycle and it will change the sensible and latent fluxes which may have an impact on atmospheric conditions and, thus on the regional precipitation citeTaylor2010. These are important advances regarding the growing interest of coupled simulations to study the land-atmosphere interactions. In order to be able to calibrate and evaluate the floodplains scheme in Land Surface Models, the estimates of the temporal and the mapping of the spatial evolution of the flooded surfaces are crucial.

Remote sensing has proven to be a helpful tool to estimate large-scale land processes and may be helpful to estimate the flooded area over large tropical floodplains ([Padovani, 2010](#); [Ogilvie et al, 2015b](#)). There are two types of sensors which can be used to estimate the flooded areas: the Optical and Synthetic Aperture Radar (SAR) sensors. SAR data presents some advantages to detect the flooded area as it is not affected by clouds because it uses the microwave bands and because it can provide data during both day and night ([de Almeida Pereira et al, 2019](#)). Despite this, SAR data may be affected by speckle noise ([Inglada et al, 2016](#)) and may be largely impacted by confounding effects associated with the surface conditions. Moreover, the processing of this type of data is more complex compared to optical data ([Niedermeier et al, 2005](#)). On the other hand, optical data are relatively easy to manipulate and allow to obtain both the flooded area and the presence of vegetation or other features in a relatively simple way. Therefore, in this work, we chose to employ optical data. There are two major difficulties to handle in this work: (1) the relatively large extension of the region and (2) the issue of the cloud cover over such a large region. The first point can be managed by using a satellite product with a lower resolution such as a MODIS product. For the second point, a

post-processed product which uses a lower temporal resolution can be used. Some of these lower temporal resolution products are created by merging the different images available to produce images with the lowest cloudiness possible. There are two similar MODIS products which correspond to this type of post processing: MOD09A1 and MYD09A1.

Traditional methods used to estimate the extension of flooded surfaces rely on spectral indices and thresholds (Ogilvie et al, 2015b). Some spectral indices may highlight the presence of water by higher values. However, some other land features may generate noise and make it difficult to directly detect the flooded area using a threshold. For example, the estimation of flooded area over regions containing lush vegetation may be confounded with the vegetation water content due to the large annual variability of water content related to the flood pulse.

This is why, although the presence of water may be overestimated by higher values in some spectral indices, some land features such as the vegetation might generate noise and make it difficult to directly detect the flooded area using a threshold. Thus more sophisticated methods may lead to an improvement of the estimate. The spectral indices considered in this study contain information about the water content and the status of the vegetation such as the modified Normalized Water Index (mNDWI), the Normalized Difference Moisture Index (NDMI) and Normalized Difference Vegetation Index (NDVI).

This study aims to compare the use of different methods based on spectral indexes to estimate the flooded area and to overcome the difficulties of estimating the flooded surface over large and complex regions such as Pantanal. This is done by comparing different traditional approaches: (1) using the classical approach of applying a threshold over spectral indexes and (2) using unsupervised classification methods such as the k-means and the Principal Component Analysis (PCA). We aim at an optimized method that is both as robust and as simple as possible. The estimates obtained are then validated by a previous satellite estimate made by Padovani (2010) and by the river height at Ladário station.

This paper is organized as follows. Section 2 contains the Methodology and Dataset used. Section 3 contains the results and the evaluation of the temporal and spatial estimation of the flooded area by the different methods considered. Section 4 contains the discussion and conclusion.

2) METHODOLOGY AND DATASETS

2.a) REGION OF INTEREST: THE PANTANAL

The Pantanal, the world's largest floodplains, has an extension of 150.000 km² and is located in the tropical region of southwestern Brazil (see Figure 3.1). The flat lands of Pantanal range between 80 and 150 m.a.s.l. of altitude while the surrounding mountain ranges of the Cerrados from its north/northeast to its southeast ranges between 200 and 1.400 m.a.s.l. (Alho, 2005). It has a regular annual cycle of flooding driven by the precipitation over the Cerrados during the rainy season (December to February). Due to the flat slopes of the Pantanal, it takes between 3 and 5 months for the water flowing from the Cerrados to cross the Pantanal. This excess of water flowing into Pantanal through the river system and slowed down by the topography

generates important floods. The climatological season of floods occurs between February and May (Penatti et al, 2015).

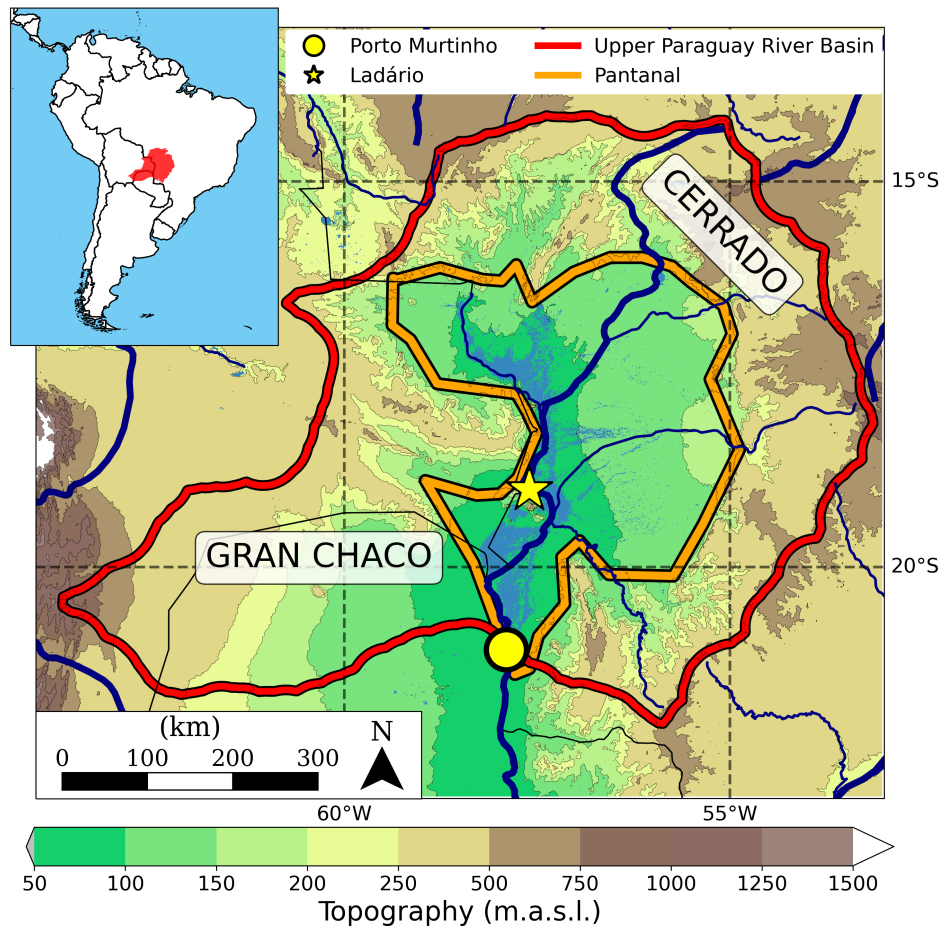


Figure 3.1. Localization and description of the Pantanal wetlands inside the Upper Paraguay River Basin. The blue layer corresponds to the flood extent from WaterMap (Pekel et al. 2016; Source: EC JRC/Google).

2.b) MODIS data: MOD09A1

The Moderate Resolution Imaging Spectroradiometer (MODIS) Terra MOD09A1 and MYD09A1 products have been chosen to perform this study for various reasons. First, they have a resolution of 500m which is higher than some other surface reflectance products such as Landsat (30 m resolution) but it is sufficient and more manageable as we are dealing with an extensive region. The MOD09A1 (MYD09A1) product is constructed from an 8-day composite period and gives an estimate of the surface spectral reflectance for the 7 first bands of Terra (Aqua) MODIS with corrected atmospheric effects (gases, aerosols, Rayleigh scattering). This correction consists in (1) an adjustment to include the effect of the solar zenith angle in order to obtain the top-of-atmosphere value and (2) the correction of the error related to the atmospheric scattering and absorption due to the presence of gases and aerosols in the atmosphere and to the spherical albedo (Vermote and Saleous, 2006). The MODIS satellites provide data for each location each 1-2 days. This permits creating a composite image, selecting for each 8-days

period the highest quality data for each pixel (lower view angle, absence of clouds, clouds shadow and aerosols) to obtain the MOD09A1 and MYD09A1 products. Two tiles were considered to fully include the Pantanal: h12v10 and h12v11. Both products have been retrieved from the NASA Earth Data Search (<https://search.earth.data.nasa.gov>).

The flooding cycle of the Pantanal is annual, thus a temporal resolution from a couple of weeks to a month is acceptable. Thus, both products can be used for this purpose. Although this product intends to avoid clouds and other inconveniences, during the rainy season the images can still be affected by the presence of clouds due to an excessive cloud coverage during the rainy season. The presence of clouds has been assessed in two steps. Firstly, the Quality Bit Flags of the MODIS products over the Pantanal were used to obtain the mask of the Pantanal which is not cloudfree nor covered by clouds shadows. For values of cloud cover fraction over the Pantanal higher than 5%, the image was discarded. After that, all the images retained were checked visually to verify that they didn't contain coarse cloud features over the Pantanal that remained undetected by the Quality Bit Flags. Between 2002 and 2021, 54% of the images available were considered cloudless over Pantanal in MOD09A1 and 35% for MYD09A1. The dates available without clouds for MOD09A1 and for MYD09A1 have been compared. It should be highlighted that the major differences between MOD09A1 and MYD09A1 are the availability of data as MOD09A1 was launched in 2000, two years before MYD09A1 (Savtchenko et al., 2004). During the period they have in common, MOD09A1 has 140 cloudless dates which are considered as cloudy in MYD09A1 while MYD09A1 only has 7 cloudless images which are considered as cloudy in MOD09A1. These 7 images represent the dry season, a period of lower cloudiness and thus of major availability of images also in MOD09A1. For these reasons, only the product MOD09A1 has been retained although the use of both products MYD09A1 may be considered to complete the data in further studies. All the MOD09A1 cloudless images have been confirmed as such by the visual check, while MYD09A1 was not checked visually since this product was not used for this study.

The different methods of flood detection presented in this study have been calibrated over the 2002-2004 period. Figure 3.2 represents for each month the total number of MODIS MOD09A1 images available and the quantity of exploitable images, i.e. cloudless. As expected the number of cloudless images is strongly affected by the wet season (November to March).

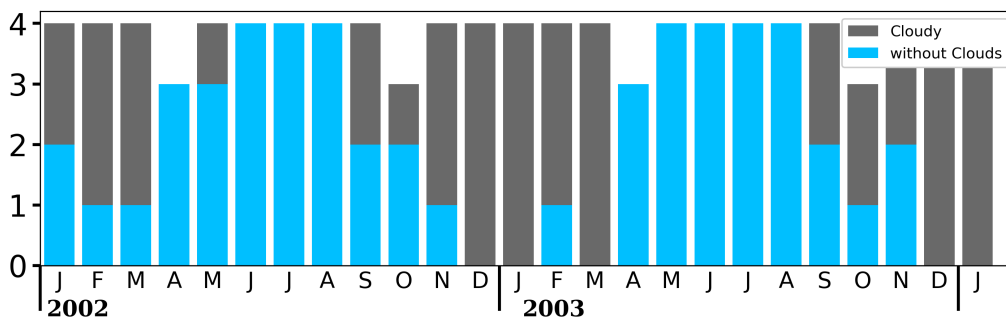


Figure 3.2. Number of monthly available data for this MODIS product and number of dates available without clouds between 2002 and 2004.

2.c) SPECTRAL INDEXES

Table 3.1. Spectral indexes considered in this study with some reference papers and the specificity of these indexes.

Spectral Indexes	References	Specificity
$mNDWI = \frac{Green-SWIR}{Green+SWIR}$	Xu (2006), Ogilvie et al (2015b)	Water detection
$NDMI = \frac{NIR-SWIR}{NIR+SWIR}$	Ogilvie et al (2015b)	Water detection
$NDVI = \frac{NIR-Red}{NIR+Red}$	Rouse et al (1974)	Vegetation and Water detection
NDMI-NDVI	Gond et al (2004), Boschetti et al (2014)	Rice flood mapping, Water bodies and Wetland

The Spectral Indexes have two main objectives: (1) to isolate some specific land features signals such as signals related to the vegetation (Xue and Su, 2017), the presence of water (Acharya et al, 2018) or the soil composition (van der Meer et al., 2012); while (2) they are insensitive to other perturbing signals (Verstraete and Pinty, 1996).

The spectral indices presented here are based on normalized differences between reflectance at different wavelengths. The NDVI emphasizes the presence of vegetation while the rest of the indices try to underline the presence of water bodies. All these indexes are resumed in Table 3.1.

The main spectral indexes are constructed based on some basic processes: the vegetation strongly reflects the Near InfraRed (NIR) and the Green but has a very low reflectance in the Red wavelength. The ShortWave InfraRed (SWIR) is very sensitive to the water content and in particular to the vegetation water content.

These indexes are shown in Figure 3.3 over the Pantanal region for two different dates: one during the dry season (21st August 2002) and one during the wet season (15th April 2003). The NDMI gives a good indication over the flooded vegetation may be falsely detecting highly vegetated regions as flooded. To combine the information contained in NDMI with NDVI seems a possible solution to better distinguish between these two land covers (cf. NDMI-NDVI index in Figure 3.3.d and Figure 3.3.h).

2.d) FLOODED AREA DETECTION

Two methods are tested in this study: (1) a threshold-based method using the indices that seemed to better represent the presence of water (mNDWI; NDMI; NDMI-NDVI) and (2) using two different unsupervised classification methods using 3 indices (mNDWI, NDMI and NDVI).

The first method of unsupervised classification is the k-means (Lloyd, 1982) which is a clustering method to regroup the data into different categories. The number of categories or clusters is given by the parameter "k". number of clusters. Each cluster is defined by its centroid and the membership of each data point to a certain cluster will be determined according to the nearest centroid. The algorithm tries to minimize the total distance between the centroids and the data. The election of the k-value depends on the problem that is being clusterized. Different values have been evaluated. For k-value under 6, the output was not stable while k-values higher than 6 added more complexity to the description of the data which wasn't necessary adding value

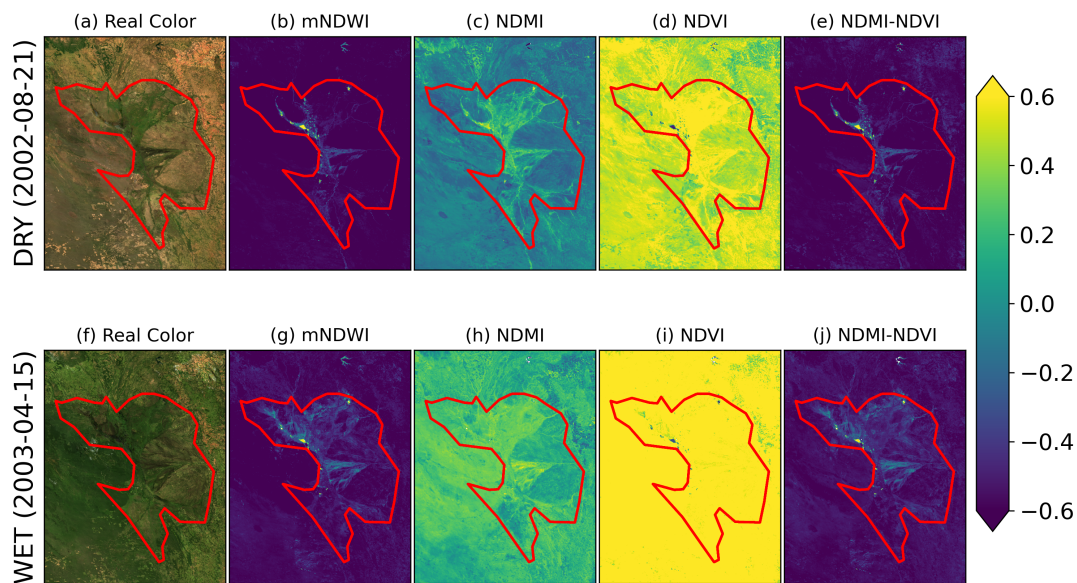


Figure 3.3. Results of the spectral indexes for two different dates: one during the dry period and one during the wet period.

to the discrimination between flooded and not flooded pixels. Thus, the k -value chosen for this study is 6.

The second unsupervised classification method uses the Principal Component Analysis (PCA – Jolliffe and Cadima, 2016) method which finds an orthogonal projection that best fits the data and allows to reduce the number of dimensions. As the data has 3 dimensions (due to the 3 indexes considered), the maximal number of dimensions that can be considered for the PCA is 3. The number of dimensions considered in this study is set at 2. The second dimension refers to the spatial structure of the flooded area. This is not the case for the first dimension of the PCA which seems to be representing other processes such as the vegetation. Higher values in the second dimension of the PCA corresponds with areas with higher values of mNDWI, NDMI and to the spatial structure of the floods (cf. Figure 3.1). The value of the pixels over this axis resumed the flood related information from the 3 indexes. Then, a threshold has to be established to classify each pixel into the flooded / not flooded categories.

2.e) UNSUPERVISED CLASSIFICATION INPUT

In order to have a single model that would take into account the variability of the vegetation along the year and that would underline the flood processes, the sample input data to generate the PCA and the k -means model have been randomly selected from two images. As the Pantanal has a very marked wet and dry season, one of these images corresponds to the dry season (from June to September) and the other one at the end of the wet season (From November to March) which also corresponds to the climatological season of floods. The images chosen correspond to the dates that were used to illustrate the spectral indexes in Figure 3.3 : the 21st of August 2002 for the dry season and the 15th of April 2003 for the wet season. A total of 10000 pixels per image has been used.

The PCA and k-means processes are quite sensitive to the input. In this case, the objective is to represent the variability of the flooded area. The data is mainly composed of not flooded pixels as demonstrated by the distribution in Figure 3.4 whose maximum is located in the low-NDMI / low-mNDWI region. For this reason, although the 10000 pixels per image were randomly selected, pixels with higher values of mNDWI have been favored. Another filter has been applied to avoid selecting the outlier which were mainly pixels with extremely low NDMI value (cf. Figure 3.4).

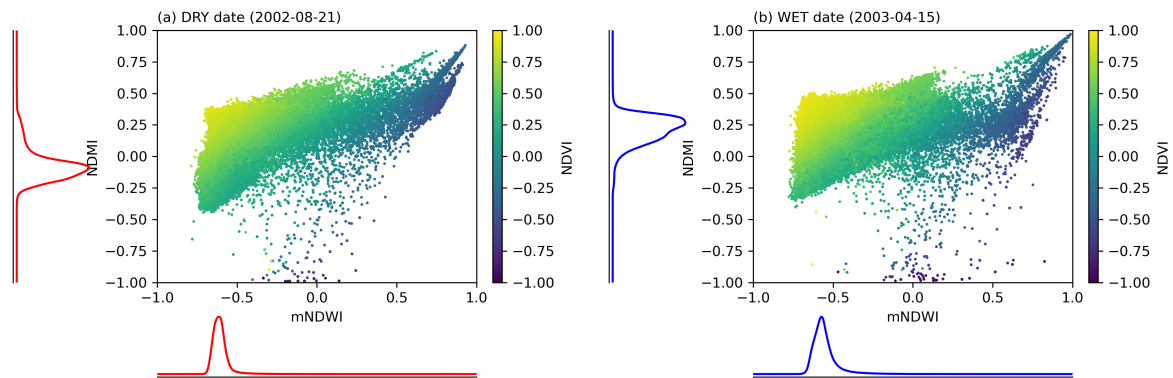


Figure 3.4. Distribution of the mNDWI / NDMI / NDVI values of the pixels.

The k-means clustering with $k=6$ is shown in Figure 3.5. In the spatial location of the clusters in the (mNDWI, NDMI) space (Figure 3.5.c), the cluster number 0 to 3 have a low mNDWI value, reasons why they are considered as not flooded and their NDMI index value is growing from the cluster 0 to the cluster 3. Looking at the difference between the k-means representation of the dry season image (Figure 3.5.b) and the wet season image (Figure 3.5.a) maps, we can see that they may represent different conditions of vegetation and that low vegetation regions in the dry season image become high vegetation region during the wet season. Pixels in the clusters 4 and 5 have a higher mNDWI value and can be considered as flooded. The pixels in cluster 5 include the pixels with maximal mNDWI values, thus we can consider that cluster 5 represents the open water pixels and pixel 4 the flooded vegetation.

The second dimension of the PCA is shown in Figure 3.6. We can deduce that higher values along this dimension represent the flooded pixels.

2.f) VALIDATION DATA

Ground-based observations of the flooded area over such a large area as the Pantanal are scarce. The validation of a flood estimate method may rely on two aspects: (1) the knowledge of the local hydrological network and the characteristics of the regions; (2) the comparison with previous satellite estimates.

[Hamilton et al \(1996\)](#) is a reference for the flooded area estimate over the region. It found a relationship between the flooded area over the Pantanal estimated between 1979 and 1987 and the river gauge at the Ladário station obtained from the Brazilian National Water Agency (Agência Nacional de Águas - ANA). The flooded area has been estimated using the brightness temperature from a satellite passive microwave sensor. [Hamilton \(2002\)](#) further extended this

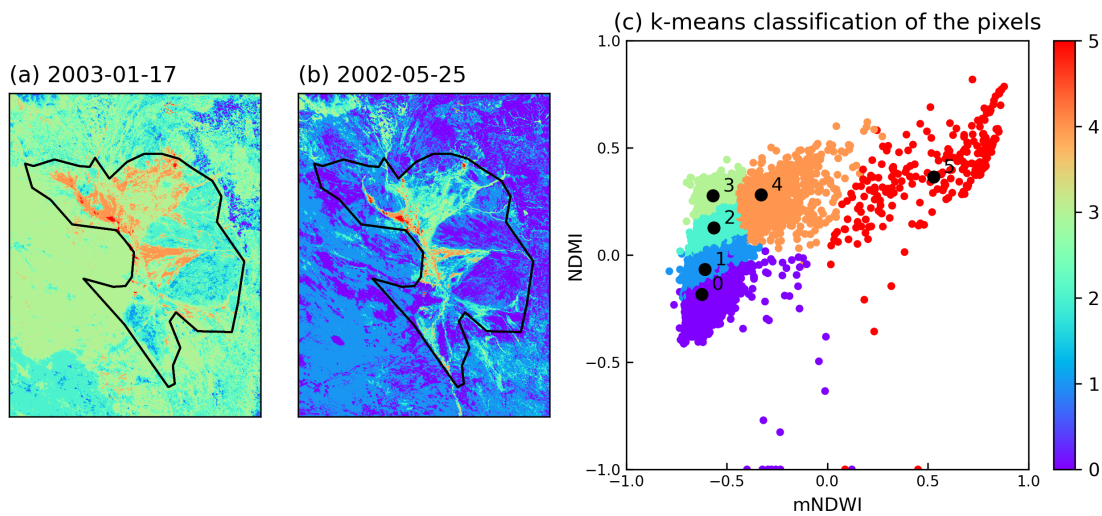


Figure 3.5. Illustration of k -means model output for $k = 6$ for (a) the wet and (b) the dry reference images and (c) distribution of the cluster in the (mNDWI / NDMI space).

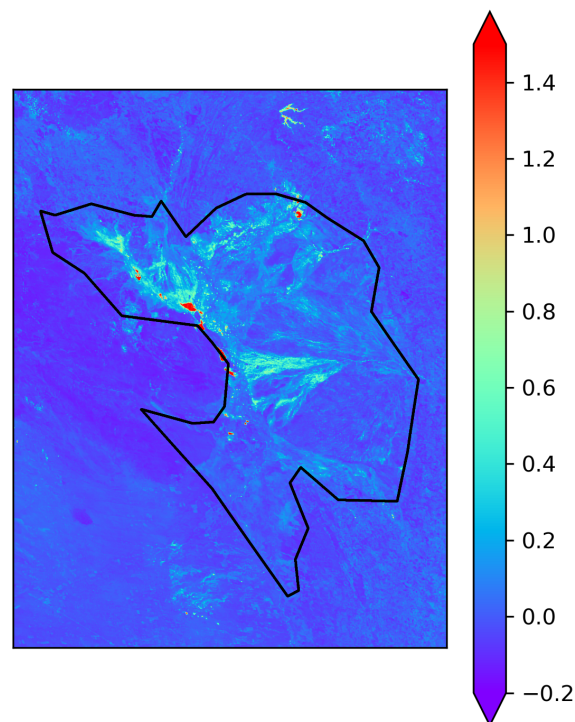


Figure 3.6. Values for the second dimension of the PCA for the wet reference image.

relationship from 1900 to 2000 to obtain an estimation of the evolution of the flooded area. Although these results are not available for the period of availability of MODIS, they point out that the river gauge data from the Ladário station (see Figure 3.1) can be used to assess the flooded area as these data are strongly correlated.

We will also for comparison use the estimation of (Padovani, 2010) which has been validated in comparison with Hamilton (2002). Padovani (2010) applied a Linear Model of Spectral Mixture (LMSM) to MODIS MOD13Q1 images to estimate the temporal and map the spatial evolution

Table 3.2. *Methods and their corresponding threshold values.*

Method	Threshold
Threshold-based mNDWI	-0.465
Threshold-based NDMI	0,32
Threshold-based NDMI-NDVI	-0,45
K-Means	Cluster 4 and 5
PCA	0,09

of the flooded area over the Pantanal. The MOD13Q1 product includes vegetation description (NDVI and EVI indexes) and the corresponding Red, Near Infrared, blue and Mid-Infrared bands from MODIS. A 16-days composite image is created by selecting the highest quality data for each pixel (lower view angle, absence of clouds) and by favoring higher values of NDVI/EVI indexes. Thus, although this product is also constructed from MODIS data, it differs from MOD09A1 because of its focus on vegetation processes and because of the lower temporal resolution (images each 16 days instead of 8). The method developed by Padovani (2010) uses a single image (May 25th 2007) to calibrate by finding a linear relationship between the reflection at different wavelengths available and the soil, vegetation and water cover. By applying this relationship to the other images, it allows estimating the fraction of soil, vegetation and water cover. The flooded area is then determined by applying a threshold on the water cover fraction.

Other types of datasets have been considered for the spatial validation of the methods presented in this study such as WaterMAP (Pekel et al, 2016) and GFPLAIN250m. WaterMAP is a global dataset available between 1984 and 2015 which contains the monthly estimate of the surface water location constructed from optical sensors (Landsat 5 TM; Landsat 7 ETM+ and Landsat 8 OLI), regional datasets and from inventories. GFPLAIN250m is a 250m resolution dataset drawing the delimitations of what can be considered as floodplains based on Digital Elevation Model datasets.

The different thresholds required were calibrated with the Padovani (2010) time series for the period 2002-2004. The respective threshold values for the different methods are resumed in Table 3.2.

3) RESULTS

3.a) EVALUATION OF THE TEMPORAL EVOLUTION

The temporal evolution of the flooded area estimated over the Pantanal by the threshold-based methods are presented in Figure 3.7 and Figure 3.8 shows the evaluation of the results for the unsupervised classification methods. The comparison of the different estimates with Padovani (2010) is summarized through some basic comparative statistical indexes in Table 3.3 (correlation, root mean square error - RMSE - and percentage bias – PBIAS).

Except the NDMI index, the different methods are coherent with the study of Padovani (2010).

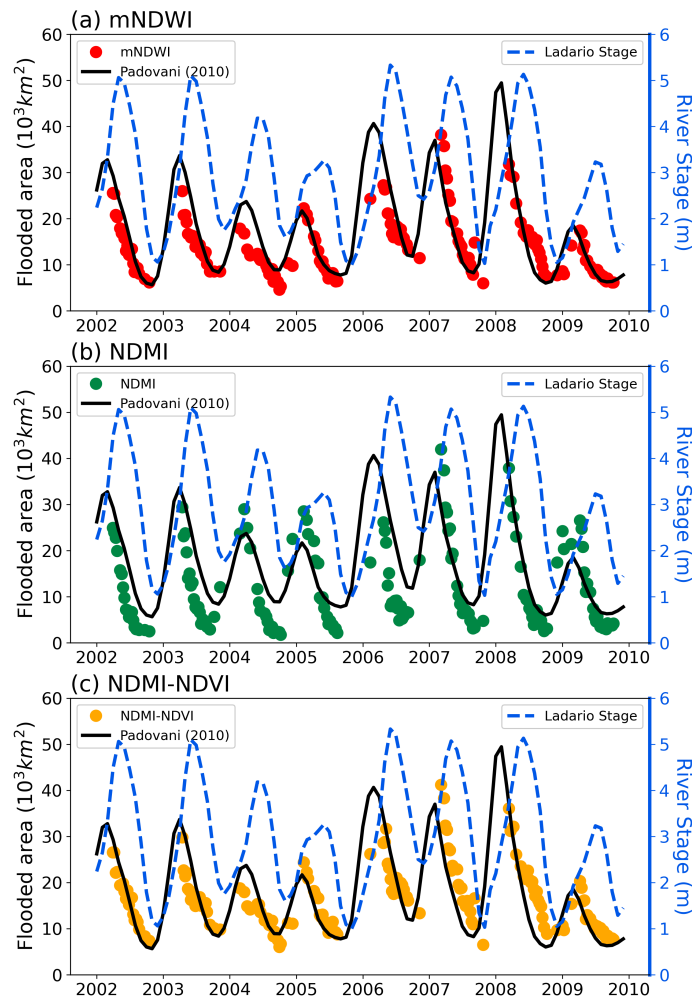


Figure 3.7. Time series of *Padovani (2010)*, the river height at Ladário and of the results from the threshold-based methods using (a) mNDWI, (b) NDMI and (c) NDMI-NDVI.

Among them, the PCA and NDMI-NDVI have higher values of flooded area while the mNDWI index and the k-means have lower values of the flooded area.

The NDMI-based estimation is less correlated than the other methods with *Padovani* but this correlation increases when integrating the information from the NDVI index (Figure 3.7.c). This difference may be related to the influence of the vegetation in the NDMI index.

The river stage at Ladário is delayed compared to both *Padovani (2010)* and the methods evaluated although the amplitude of the river gauge and the estimated flooded area are similar. Following the *Hamilton et al (1996)* estimation of the flooded area, the river stage at Ladário should be strongly correlated. Further analysis should be performed to understand these differences.

3.b) EVALUATION OF THE SPATIAL EVOLUTION

Figure 3.9 shows the comparison of flood frequency between 2002 and 2009 in the different methods presented in this study in order to compare them with the flood frequency map from *Padovani (2010)*, WaterMAP and the floodplains delimitations from GFPLAIN250m.

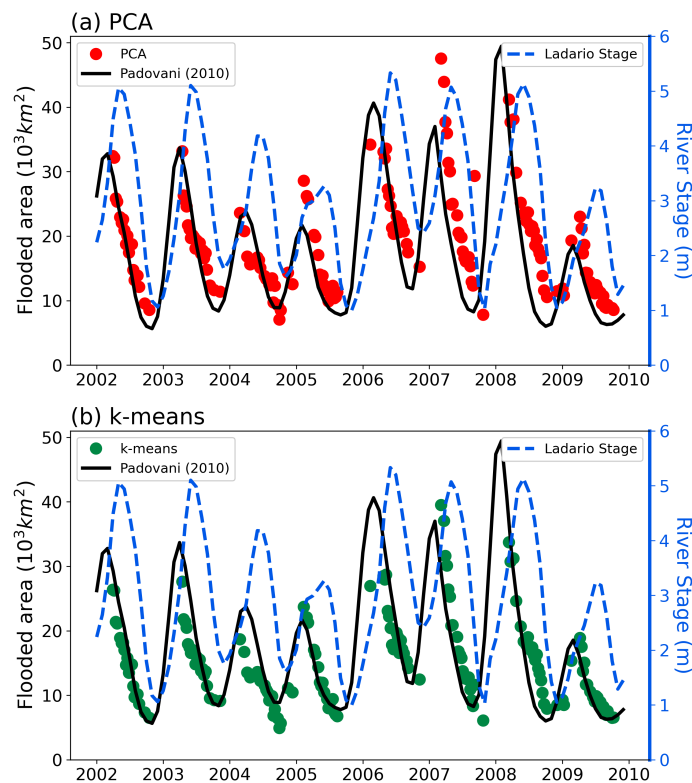


Figure 3.8. Time series of *Padovani* (2010), the river height at Ladário and of the results from the threshold-based methods using (a) the Principal Component Analysis (PCA) method and (b) the k-means algorithm with $k = 6$.

As seen in the first overview of the spectral indexes, the NDMI index is strongly influenced by the vegetation which creates a bias for the detection of flooded areas. For the other estimation methods, the results are more coherent with the flood frequency map from *Padovani* (2010) and WaterMAP although WaterMAP seems to consider only the most flooded area of the Pantanal. Except for the NDMI-based method, the large rivers such as the Main Paraguay River at the North and South of the Pantanal, the São Lourenço river at the northeast and the Taquari river at the East of the Pantanal are clearly visible in the different flood detection methods. All the results are also coherent with the GFPLAIN250m floodplains delimitation which is based on a DEM. The only exception is the central region of the Pantanal, the Taquari Megafan, which may be related to local changes in the orography (*Assine, 2005*).

3.c) EXPLORATION OF A CASE STUDY

The simple flood detection methods presented previously may have a large variety of applications. This subsection aims to illustrate their potential by using the mNDWI-based flood detection method and the NDVI index to explore the evolution of the extent of the floods along the years. The floods are evaluated during the month of march which is one of the most flooded months for the Pantanal. The images chosen have a cloud cover lower than 2% following the quality flag of MODIS. Three dates have been selected to perform this study: 21/03/2004 (t_0), 22/03/2007 (t_1), 06/03/2021 (t_2). t_0 (respectively t_1) corresponds to the year of lower maximum (respectively higher maximum) flood extent over the 2002 and 2010 period. t_2 has been cho-

Table 3.3. Resume of the statistics (Percentage bias - PBIAS, Root-Mean Square Error - RMSE, Correlation) comparing *Padovani (2010)* estimate with the different methods: threshold-based applied to mNDWI, NDMI and NDMI-NDVI, Principal Component Analysis (PCA) method and k-means with $k = 6$. The correlations are significant with a significance level of 99 %.

Method	PBIAS (%)	RMSE ($10^3 m^2$)	Correlation
mNDWI	-12,74	4.894	0,8
NDMI	-23,83	6.839	0,81
NDMI-NDVI	9,89	5.243	0,82
K-Means	11,46	5.119	0,77
PCA	-9,83	4.871	0,78

sen in order to compare the two previous dates to the actual situation which corresponds to drier conditions and with the vegetation cover affected by important wildfires during the 2020 dry season.

Figure 3.10 shows the NDVI index (Fig. 3.10.a) for t_0 over the Pantanal as well as the difference of NDVI between t_1 and t_0 (Fig. 3.10.c) and between t_2 and t_0 (Fig. 3.10.c). Figure 3.10.d-f shows the flooded area estimated with the mNDWI based method for the three dates. Comparing the flooded area in t_0 and t_1 , the floods in t_1 are much more extended but they show similar patterns. The regions where the flood became more important in t_1 are the northwest and central Pantanal. Some flooded areas also appear in the South of the Pantanal. The vegetation seems to be reduced over some of the flooded area which may be related to the floods replacing the vegetation or at least reducing the NDVI. However, the NDVI increases around the shape of the floodplains in t_1 compared to t_0 . A larger extent of flooded area reduces locally the NDVI while the NDVI increases at its border due to the higher water availability.

In t_2 , the floods are at their minimal extent and are principally around the Paraguay river and over the Taquari Megafan in the central region of the Pantanal. The northwest region has almost no floods in t_2 but has increased NDVI compared to t_0 . This means that there is water allowing for the development of the vegetation but there is not enough water so it can be considered as flooded. The NDVI is lower in t_2 compared to t_0 over the regions with higher values of NDVI in t_0 which may be related to the wildfire. It should also be noted that there is an increase of the NDVI values compared to t_0 over the NorthEast of the Pantanal. This region is not usually flooded so this may be more related to the impact of the local precipitation on the vegetation during the wet season.

4) DISCUSSION AND CONCLUSION

The estimation of the flooded area over large floodplains is a difficult task. The satellite products may be precious tools. This paper explored different methods to estimate the flooded area using the surface reflection from optical remote sensing products. The water-related information is extracted by using different spectral indexes related to the presence of water content and vegetation. Then, different methods are developed using directly the spectral indexes to

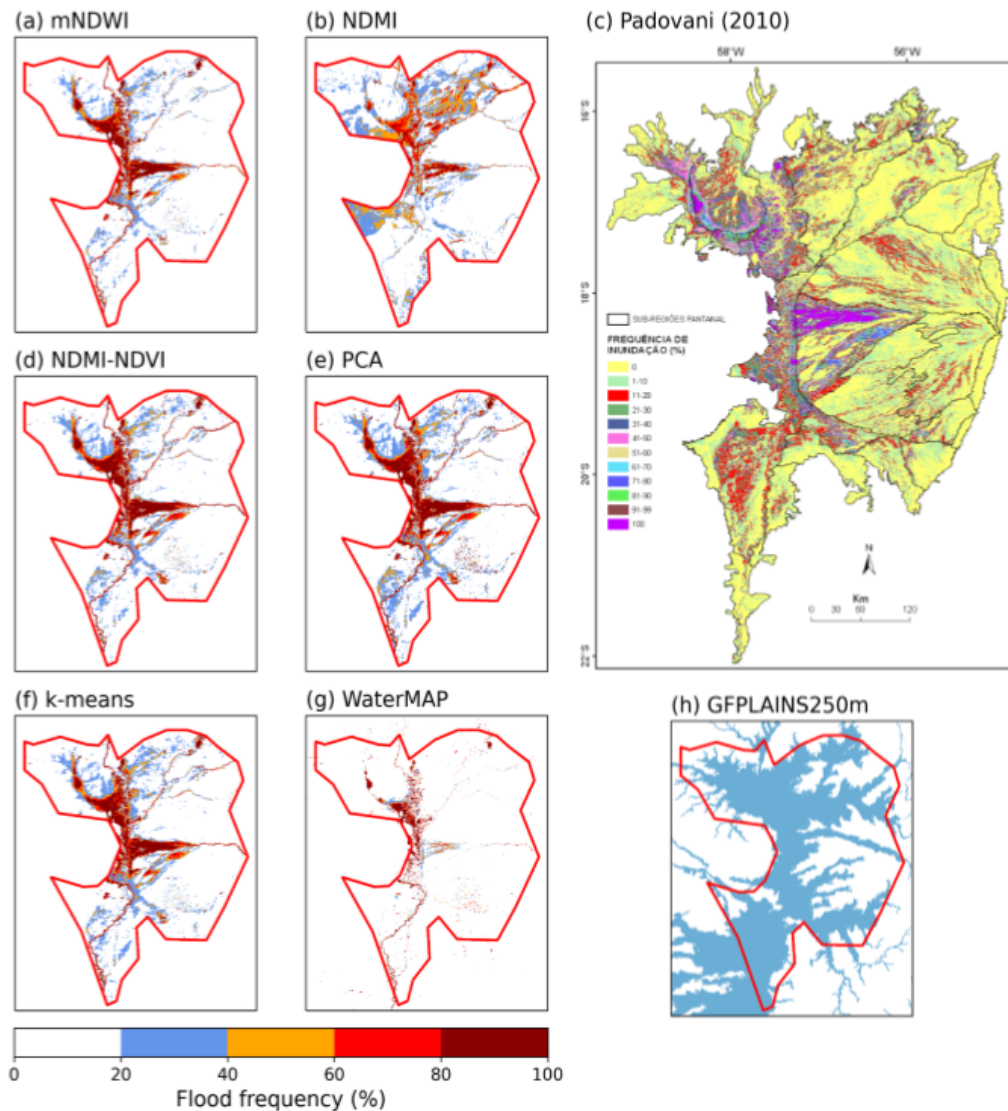


Figure 3.9. Flood frequency between 2002 and 2009 obtained from the different methods presented: 3 threshold-based methods using the (a) mNDWI, (b) NDMI and (d) NDMI-NDVI index and 2 unsupervised classification methods: (e) Principal Component Analysis and (f) k-means. Occurrence of flood from (c) Padovani (2010) and (g) WaterMAP (Pekel et al, 2016; Source: EC JRC/Google) between 1984 and 2015 and floodplains delimitation from GFPLAIN250m (Nardi et al, 2019).

determine the presence of water: threshold-based methods and unsupervised classification to use the information from different spectral indexes at the same time. The different methods evaluated were coherent with the previous works although there is some delay between the temporal evolution of the estimated flood area and the river height at Ladário. The NDMI index has an issue to represent the flooded area as it is influenced by the vegetation during the wet period. However, considering the vegetation through the NDMI-NDVI index seems to improve the representation of the flooded area. The spatial map of the flooded area represents well the known hydrological features of the Pantanal. It should be noted that the threshold based methods have lower computational costs for similar results but the unsupervised classification methods can bring extra information.

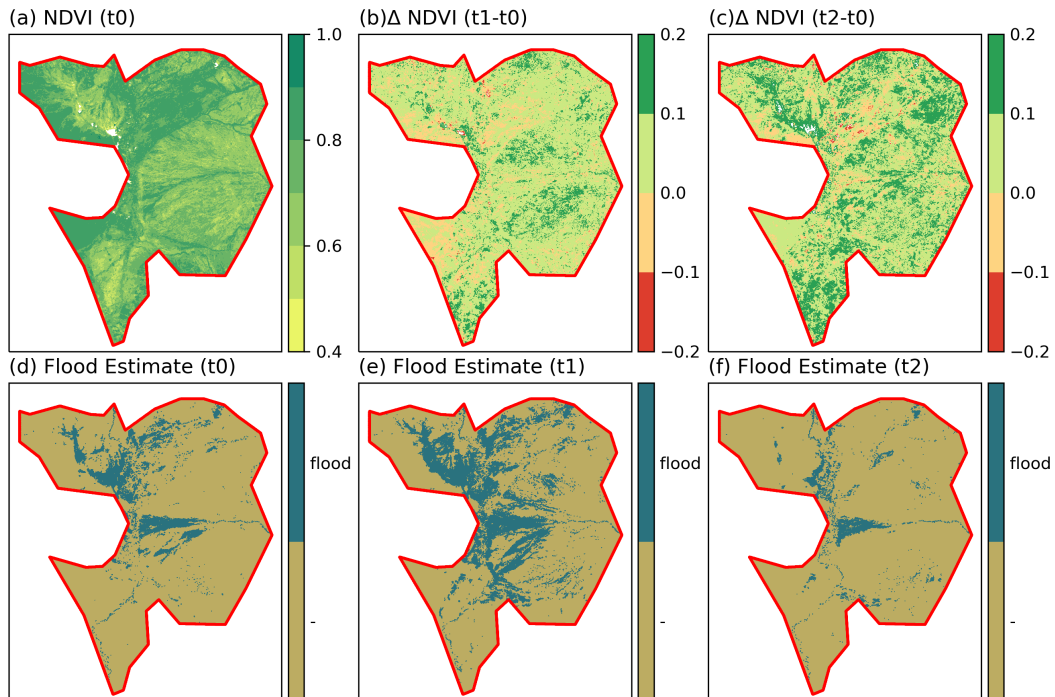


Figure 3.10. NDVI (a,b,c) and flood estimate (d,e,f) and for t_0 (21/03/2004; a and d), t_1 (22/03/2007; b and e) and t_2 (06/03/2021; c and f).

The methods of flood detection presented in this study are simple methods which are based on spectral index and do not require important preprocessing. They may be divided into two categories: the threshold based methods on the one hand and the PCA based and k-means methods on the other hand. The threshold based methods consist in applying a threshold to the spectral indexes to detect the flooded area. This threshold can be determined in comparison with other data which gives an indication either on the flooded area or on the spatial extent of the floods. Different thresholds can be determined depending on the sensibility expected for its use. The PCA and k-means methods use unsupervised classification tools applied to a combination of the spectral indexes related to the presence of water. For the PCA method, the method consists in identifying the dimension related to the presence of water to calibrate and apply a threshold to this dimension. For the k-means, it consists in identifying the clusters which correspond to the flooded area.

The advantage of all the above methods is that they can be easily applicable if the user has some observational data to establish a threshold. Then, it is possible to calculate other spectral indexes corresponding to other processes using the same optical satellite data to obtain a global panorama of the hydrological processes over a certain region quite easily with a reduced pre-processing. Nevertheless, these methods also present some disadvantages. The main disadvantage is related to the presence of cloud cover in optical satellite images which requires the filter of images containing clouds and, thus, may reduce the quantity of images available. Another disadvantage is the fact that the spectral indexes may be affected by other processes which impact the presence of water without being related to floods such as it may be the case with the presence of lush vegetation.

Different solutions can be considered in order to face the issues presented previously although

this may involve more sophisticated methods. Concerning the cloud cover, the combination of optical and SAR satellite data have been proven to improve the flood detection being able to solve both cloud cover issue for the optical satellite and noise from the SAR data (Prigent et al, 2020; Niedermeier et al, 2005; Inglada et al, 2016). Concerning the interaction of other processes with the flood detection when using optical satellite data, there are other methods that can be considered. The simpler process consists of developing customized spectral indexes using a linear combination of the spectral bands in order to better differentiate the vegetation from the flooded water such as it is done in other application such as the Floating Algae Index (FAI) (Dogliotti et al, 2018) used to differentiate the presence of algae in the water. Another option is, instead of evaluating the presence of flood over each pixel individually, to consider the pixels by group of pixels such as it can be done with the Object Based Image Analysis (Blaschke et al, 2014). This may help to better determine if the pixels in an object are flooded by using (1) the distribution of the reflection of the pixels composing each group and (2) the shape of the object (Louzada et al, 2020). The flood detection can also be improved by using additional ancillary data about the local orography using Digital Elevation Models. Finally, some more advanced methods of machine learning classification can be used but they require more precise information on the pixels which are flooded in order to fit the model. Unfortunately, this type of information is not always available.

Finally, we would like to emphasize that the difficulty to detect the flooded vegetation also lies in the difficulty to define a limit to qualify whether a pixel is flooded or whether it is just a pixel representing a moist soil.

Acknowledgements

We would like to gratefully acknowledge the support of the Agencia Nacional de Promoción Científica y Tecnológica (ANPCyT), Argentina (PICTs 2017-1406, 2018-02511); the Consejo Nacional de Investigaciones Científicas y Técnicas (CONICET), Argentina (PIP 1122020010-2141CO); the French-Argentina project ECOS-Sud 2018 co-financed by the Ministerio de Ciencia, Tecnología e Innovación (MINCyT), Argentina and the Université Sorbonne Paris Nord, Francia (ECOS-A18D04); and the French National LEFE program (Les Enveloppes Fluides et l'Environnement; LEFE 12962).

3.3 Acronyms

ANA	Agencia Nacional de Aguas
DEM	Digital Elevation Model
ERA	ECMWF Re-Analysis
GFPLAIN250m	Gridded dataset of Earth's floodplains at 250-m resolution
mNDWI	Modified Normalized Difference Water Index
MODIS	Moderate Resolution Imaging Spectroradiometer
NASA	National Aeronautics and Space Administration
NDMI	Normalized Difference Moisture Index
NDVI	Normalized Difference Vegetation Index
NIR	Near-infrared spectral band
PBIAS	Percent Bias Index
PCA	Principal Component Analysis
RMSE	Root Mean Square Error
SAR	Synthetic Aperture Radar sensor
SWIR	Shortwave Infrared spectral band
WaterMAP	Surface Water Mapping Product

RoutingPP: Parallelized construction of a flexible river routing graph for
Earth System Models

Contents

4.1	Introduction	83
4.2	General Methodology	86
4.2.1	General Objectives and Issues	87
4.2.2	Global methodology	88
4.2.3	Partitioning of the atmospheric grid	89
4.2.4	Overlap of the atmospheric and hydrologic grids	90
4.2.5	Routing construction	91
4.2.6	Truncate	95
4.2.7	Calculation of the upstream area	97
4.2.8	Localization of the fluviometric stations	97
4.3	Validation	98
4.3.1	Hydrological Inputs	98
4.3.2	Methodology	100
4.3.3	Influence of the hydrological input	100
4.4	Discussion and Conclusion	102
4.5	Access to RoutingPP	103
4.6	Acronyms	104

4.1 Introduction

Land Surface Models traditionally compute the water balance locally but they require River Modeling to incorporate the horizontal transport of water. River modeling in Earth System

Models (ESM) connects the atmosphere-land surface-ocean components of the Earth System, allows to close the water budget and may also represent some of the interactions with human activities. Some land-atmosphere interactions arises from the transport of water through river, such as the floodplains, and requires river modelling to be represented. This chapter follows the previous development of [Nguyen-Quang et al \(2018b\)](#) and proposes a parallelized tool to construct a flexible river routing graph able to face the future challenges in Earth System Modeling.

The recent developments of Climate System Models aim at improving the representation of the processes within the different components of the Earth system as well as the interactions between these components. The water cycle is a key process of the Earth System and involves each one of its components (land, atmosphere, ocean, cryosphere). Rivers, the horizontal water transport over land, represent small fluxes compared to the atmospheric and oceanic water fluxes ([Rodell et al, 2015b](#)). However, they are of vital importance for human activities such as: agriculture, industry, electricity production and human water consumption ([Bierkens, 2015](#)) and for climate processes such as the floodplains and lakes. Thus, river modelling is important for both Earth System studies and water resources management ([Van Beek et al, 2011](#); [Beck et al, 2017](#); [Sutanudjaja et al, 2018](#)).

ESMs are numerical coupled models simulating all the component of the climate system. The lateral transport of water from the rivers is part of their Land Surface Model (LSM) because the surface runoff and water drainage into the soil are part of the processes represented in LSMs. But it can interact with the atmospheric and ocean models in case of including some processes such as floodplains or dams ([Sheng et al, 2017](#); [Graham et al, 1999](#); [Arora et al, 1999](#)). Most LSMs either integrate a river routing scheme ([Sheng et al, 2017](#)) such as the ORCHIDEE model ([Polcher, 2003](#)), the JULES model ([Bell et al, 2007](#); [Dadson et al, 2011](#)), ISBA-TRIP ([Decharme et al, 2008](#); [Alkama et al, 2010](#); [Decharme et al, 2010](#)) or can be coupled to an hydrological model such as the JULES LSM coupled with the CAMA-FLOOD model ([Marthews et al, 2021](#)), the coupling of NOAH-MP with the WRF-HYDRO model ([Kumar et al, 2006](#); [Chen et al, 2007](#)) or such as it is done in the NASA Land Information System (LIS, [Kumar et al, 2006](#)) with the coupling between HyMAP global river model and different LSMs ([Getirana et al, 2021](#)).

Closing the water cycle in ESMs through a river routing scheme presents 3 advantages: (1) it is a signal of the water processes occurring over land that can be easily compared to observations; (2) it permits representing the outflow of freshwater from land to oceans; (3) it is a solution to integrate of open-water surfaces related to the river system that may alter the fluxes between land and atmosphere.

Concerning the first point, the river routing is the result of the surface and subsurface runoff thus it reflects the water balance over large regions and gives an integrated signal of the continental water cycle ([Arora et al, 1999](#); [Fekete et al, 2012](#); [Ngo-Duc et al, 2007](#)). Moreover, river discharge observations are available for almost all the world's most important catchments ([Hannah et al, 2011](#)) so river routing is a precious validation and diagnostic tool for the hydrological processes in LSM over large areas ([Arora et al, 1999](#); [Pappenberger et al, 2010](#); [Balsamo et al, 2011](#)).

About the second point, the lateral transport of water affects incoming freshwater from land to sea and, consequently, the boundary conditions for ocean models (Carton, 1991; Huang and Mehta, 2010). The river discharge flowing in the ocean reduces the salinity in the estuaries affecting the ocean circulation (Urakawa et al, 2015; Huang and Mehta, 2010; Verri et al, 2018; Garvine and Whitney, 2006; Hordoir et al, 2008) and having an impact over the heat transport and the ocean temperature (Huang and Mehta, 2010). More locally, the river discharge into the ocean will affect processes occurring in coastal areas through the transport of nutrient and carbon (Borges and Gypens, 2010; Regnier et al, 2013; Lauerwald et al, 2017; Nakhavali et al, 2018) and through changes of the water temperature (Carton, 1991; Masson and Delecluse, 2001).

The third point concerns open water surface processes such as lakes and wetlands that depends on the lateral transport of water. These processes affect the energy and water fluxes between land and atmosphere. For example, large floodplains are directly linked with river runoff and are responsible for large evaporation of land surface water (D'Orgeval et al, 2008; Guimberteau et al, 2012b; Schrapffer et al, 2020). The irrigation processes may also strongly affect the water cycle over land and have a large impact on the evapotranspiration (Zhou et al, 2021a; Wang et al, 2018). From another point of view, river discharge is an important variable for other domains such as Food Security, Economics, Energy and Biodiversity (Bierkens, 2015). A realistic simulation of the river discharge may solve data scarcity issues (missing discharge and river height data, ungauged rivers) making it valuable for other scientific communities.

River routing graphs are generated using the topography information from the Digital Elevation Models (DEMs). The DEM used for this purpose are hydrologically conditioned (HydroDEM). The HydroDEMs resolution has been evolving during the last 20 years. River networks maps had originally a coarse resolution ranging between 1° and 0.25° (Oki and Sud, 1998; Vorosmarty et al, 2000; Döll and Lehner, 2002; Ducharne et al, 2003). More recent global HydroDEMs reach 3 arc-second (90m at the equator) like HydroSHEDS (Lehner et al, 2008) which is based on the SRTM3 DEM (Farr et al, 2007) and MERIT-Hydro (Yamazaki et al, 2019) which is based on the MERIT-DEM (Yamazaki et al, 2017).

Following Kauffeldt et al (2016), hydrological schemes at continental scale need to fulfill various conditions. There are 4 conditions applying particularly to the river routing graph. Anticipating the evolution of atmospheric models, (1) they must be flexible to grid structure. (2) They must also be adaptable to different spatial resolutions. (3) It should be possible to extract the input data directly from existing databases and it should be possible to add extra-information to the river network system. (4) River observation stations should be easily localizable for model validation and data assimilation. Bierkens (2015) advises that in higher resolution models, some of the modeled concepts will have to be more explicitly represented. At hyperresolution, an excessively high resolution, the computational cost for operational use, for long period simulations or for ensemble may be too high at continental-scale (Bierkens, 2015).

The main purpose of LSMs integrated in Regional Climate Models or in ESMs is generally to simulate the land processes (soil and vegetation) interacting with the coupled atmospheric model (Haddeland et al, 2011; Bierkens, 2015; Gong et al, 2011). Although some efforts are

made to combine LSMs with more developed hydrological models (Marthews et al, 2021; Getirana et al, 2020), the hybrid unit-catchment are an interesting alternative. They are based subgrid hydrological units of the atmospheric grid which are constructed from higher resolution hydrological data. It is an interesting solution as it keeps the coherence between the river routing, its processes and the atmospheric model. Thus, it avoids the interpolations between the atmospheric and the hydrological grid (see for example Nguyen-Quang et al, 2018b; Chaney et al, 2016, 2020). The spatial representation of land-atmosphere fluxes have an important impact on the atmospheric models. For example, it is the case for the contrast of latent/sensible fluxes between a wet and a dry area (Taylor et al, 2018). Thus, the interpolation of land-atmosphere fluxes in coupled models may reduce the feedback effects related to these fluxes. Following Beven et al (2015), the study of land-atmosphere interactions needs a more accurate hydrological coupling. It is also important to capture the heterogeneity of the topography, the soil and the vegetation (Wood et al, 2011; Fan et al, 2019). Hybrid unit-catchment may improve both land-atmosphere interaction and sub-grid heterogeneity representation. It would also improve the representation of subgrid processes such as biogeochemical fluxes, wetlands, dams and irrigation (Wood et al, 2011; Bierkens, 2015).

This chapter presents a method of construction of a gridded sub-scale hydrological network based on the concept of HTUs which is used in the latest development of the ORCHIDEE routing scheme (Nguyen-Quang et al, 2018b). This method is flexible because the river routing scheme can be constructed on different types of atmospheric grid and using different high-resolution HydroDEMs. It is currently working for Regular Grids, Lambert Conformal Conic projection and Cassini projection but it can easily be adapted to more complex atmospheric grids such as the icosahedral grids which are used in the DYNAMICO model (Dubos et al, 2015). Moreover, this process has been parallelized to reduce the computational cost. It brings an adequate solution to represent the river routing in coupled land-atmosphere models without requiring any spatial interpolation. Moreover, it opens the door to further aggregate more information in order to integrate additional processes in the river routing scheme of ORCHIDEE such as floodplains, lakes, dams and irrigation.

The general methodology of the river routing construction in RoutingPP is described in Section 2. The routing river graph constructed is then evaluated in Section 3 through simulations of the ORCHIDEE LSM. Section 4 presents the discussion of the methodology and the results, to finally provide some future perspectives and conclude.

4.2 General Methodology

To avoid confusion, the term "pixel" is used for a gridded element of the fine-resolution flow direction maps, while the term "grid box" or "grid point" is used for an element of the atmospheric grid.

4.2.1 General Objectives and Issues

The concept of Hydrological Transfer Units (HTUs), a sub-grid description of the river routing, have been implemented in the ORCHIDEE LSM (Nguyen-Quang et al, 2018b). This river routing graph allows to integrate the information from a high-resolution HydroDEM within the structure of an atmospheric grid. The river routing graph (Fig 4.1.b) is generated from the overlap of the hydrological grid with the atmospheric grid (Fig 4.1.a). It is then simplified by truncation to respect the maximal number of HTUs per grid point defined by the user (Fig 4.1.c).

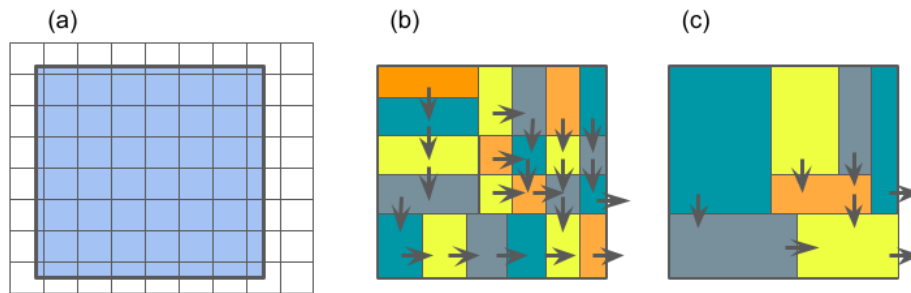


Figure 4.1. (a) *Overlap of the Hydrological grid and the Model grid*, (b) *construction of the HTUs*, (c) *HTUs after truncate*.

Although this representation of the river routing graph leads to some substantial improvement of the rivers representation in ORCHIDEE (Nguyen-Quang et al, 2018b), it is originally constructed in the main code of ORCHIDEE on a unique processor. This carries some issues. Firstly, the construction of the routing is difficult to parallelize inside the ORCHIDEE model because the domain decomposition does not foresee the exchange of information between the processors whose sub-domain are neighbours. The parallelization is essential as we are dealing with a large quantity of data. Secondly, the construction method is difficult to manipulate and to verify because it occurs in the main Fortran code of the ORCHIDEE model. Thus, this makes it more difficult to validate the routing and to integrate of new features. Thirdly, the future evolutions of the river routing scheme will require additional information (floodplains, dams, lakes, irrigation, adduction networks). Their integration requires a flexible code that could be easily modified, and thus it would be complicated and inappropriate to integrate these changes in the main code of the ORCHIDEE model.

This chapter presents a pre-processing tool to construct the river routing graph (RoutingPP; <https://gitlab.in2p3.fr/ipsl/lmd/intro/routingpp/wikis/home>) based on the HTUs concept. RoutingPP is based on a combination of Python and Fortran, this allows to combine the flexibility of Python to the computational efficiency of Fortran. The construction of the river routing graph has been parallelized using specific communication between the processors through a halo communication. The code is flexible and easy to use, the result can be adapted to other models and other uses. It also facilitates the integration of additional information to the HTUs. The river routing graph output is also easy to verify and to visualize (RoutingPP includes an experimental visualization tool: RViewer). An additional module allows to find, when it is possible, the HTU corresponding to the different hydrological stations (Wang et al, 2018). This information is integrated in the river routing graph and may be used further by the hydrological model.

RoutingPP is adaptable to different atmospheric grids, at different resolutions and with different projections. It is possible to use different HydroDEM to construct the river routing graph.

The technical challenges for the parallelized construction of a gridded routing graph are the following:

1. The distribution of the domain must be equilibrated between the processors;
2. The exchange of information between the processors which are neighbours must be handled efficiently so the river routing graph can be coherent;
3. The calculation of the upstream area require information from all upstream HTUs which may be located on different processors;
4. The construction of the routing graph must be done directly from the inputs;
5. The hydrological stations must be localized in the HTUs space.

4.2.2 Global methodology

The workflow of the construction of a river routing graph is illustrated in Figure 4.2. It takes as input the description of the atmospheric grid (Model grid) and its land-sea mask as well as the description of the hydrological network (Hydrological grid). This information is then processed with optional additional ancillary data (hydrological stations, lakes, dams, floodplains, irrigation). Once constructed, the river routing graph on the atmospheric grid is operational to be used by the ORCHIDEE LSM.

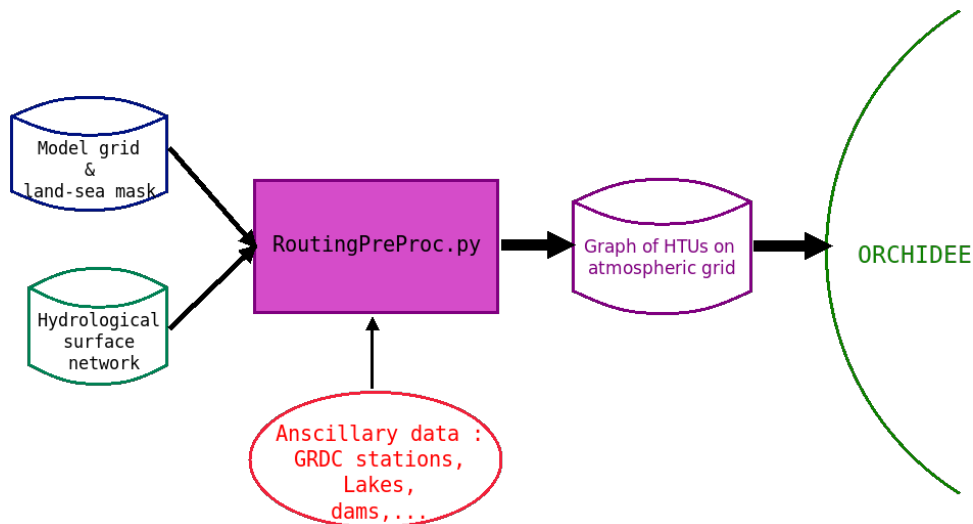


Figure 4.2. Environment of the RoutingPP program.

The construction of the routing river graph is performed through 5 major steps which are the following:

1. **Partition of the atmospheric grid:** the domain is distributed among the different processors with the objective to have the most equilibrated distribution of the land points possible to optimize the parallelization.

2. **Overlap of the atmospheric and hydrological grids:** the overlap between the hydrological pixels and atmospheric grid points are calculated. The result is called "Weights" and can be saved in a netCDF file to avoid repeating this costly operation.
3. **Routing Construction:** the previous Weights calculation is used by the processors to load the hydrological information from the HydroDEM for the land points belonging to their respective subdomain. It permits constructing the routing graph and to calculate the different characteristics of the HTUs composing this routing graph.
4. **Truncate:** the number of HTUs in each grid point is reduced in order to respect the `nbasmmax` parameter chosen by the user.
5. **Finalization:** the hydrological stations are localized in HTU space. All the information is gathered, converting the local indexes to the global indexation, to save the river routing graph in a netCDF file.

4.2.3 Partitioning of the atmospheric grid

The Partition module will distribute the land points of the atmospheric grid over the domain chosen by the user among the processors. The equitable distribution of the grid points between the processors optimizes the computational resources.

The Partition considers the full domain and recuts it into subdomains until there is a subdomain for each one of the processor used. As the subdomains cannot be empty, the number of processors shouldn't be overdimensioned over small domains. The routing construction concerns only the land grid points. This is why once all the subdomains are generated, they are adjusted to reduce the presence of ocean grid points.

The algorithm relies on the iteration of 2 steps:

1. **Selection:** Select the subdomain with the higher number of land points, this domain will be recut perpendicularly to its larger dimension. If it is a vertical (horizontal) rectangular it will be cut horizontally (vertically).
2. **Optimization of the recut:** Partition evaluate how to recut the subdomain so that the two resulting subdomains have the more equilibrated number of land points (cf. Figure 4.3).

The Figure 4.3 shows how a particular subdomain is halved in an optimum way. Then the Figure 4.4 shows the following steps until obtaining 12 subdomains. Each subdomain is allocated to a processor. The processors will consider a halo of 1 grid point around their subdomain. The final domain of a processor is composed by its main core and a halo. The land points in the halo belong to the main core of other processors. Considering, for example, a grid point A which is on the core domain of the processor 1 and on the halo of processor 2, the processor 1 is able to send information about the grid point A to the processor 2. This halo will ensure a coherent routing between the different processors, it is important as a river may cross the domains of different processors. Figure 4.5 illustrates an example of the decomposition of the subdomain attributed to a processor with its core and halo. It should be noticed that, during the

Weight calculation, the halo is not considered to avoid multiple calculation for the same grid point.

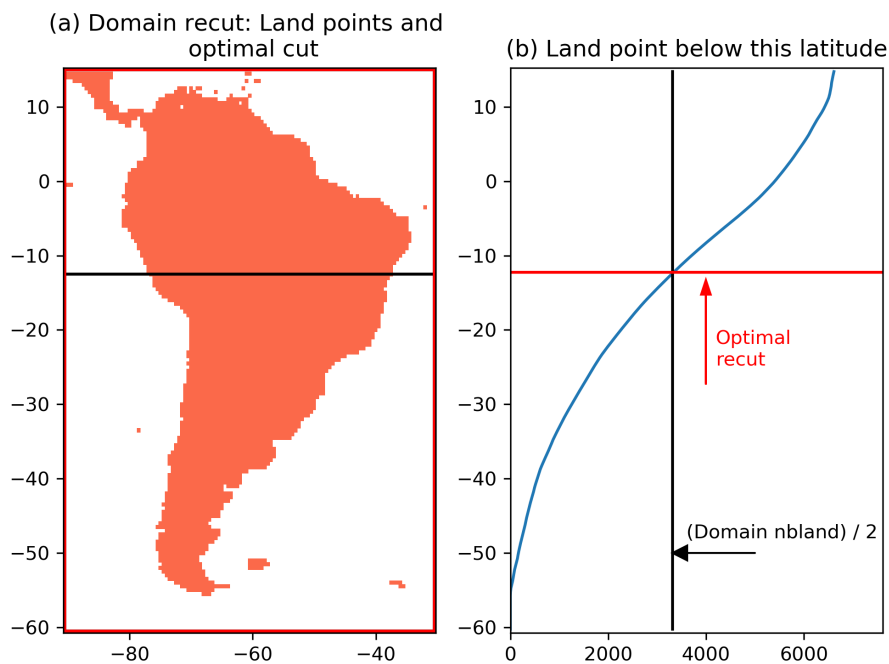


Figure 4.3. Representation of how the optimal recut of a subdomain is done.

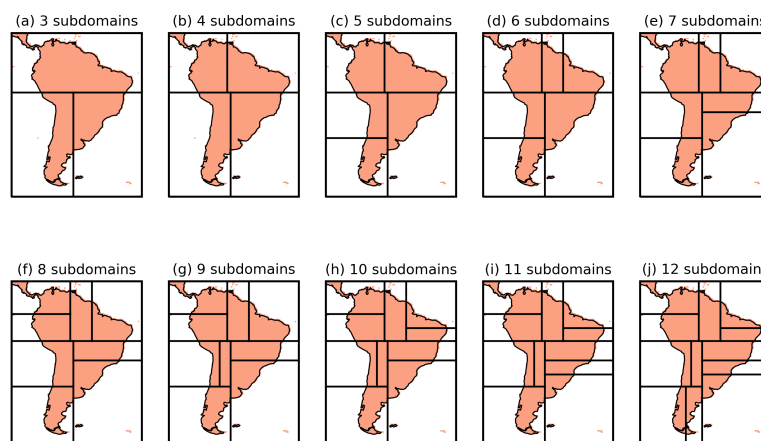


Figure 4.4. Representation of the steps to recut a domain from 3 subdomains to 12 subdomains.

4.2.4 Overlap of the atmospheric and hydrologic grids

At this step, the processors will load the information from the atmospheric grid and from the hydrological grid over their respective subdomains to determine the overlap between the hydrological pixels and the atmospheric grid points as well as the corresponding area of this

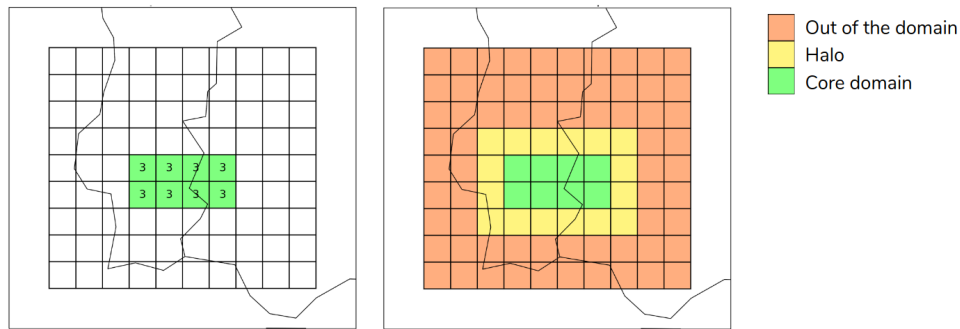


Figure 4.5. Representation of a subdomain with its core domain and halo

overlap (the Weights). The Weights are computed considering the polygons of the grid points and pixels over a sphere using the SphericalGeometry package ([Spherical Geometry GitHub repository](#)). The overlap is illustrated over a grid point in Figure 4.6.

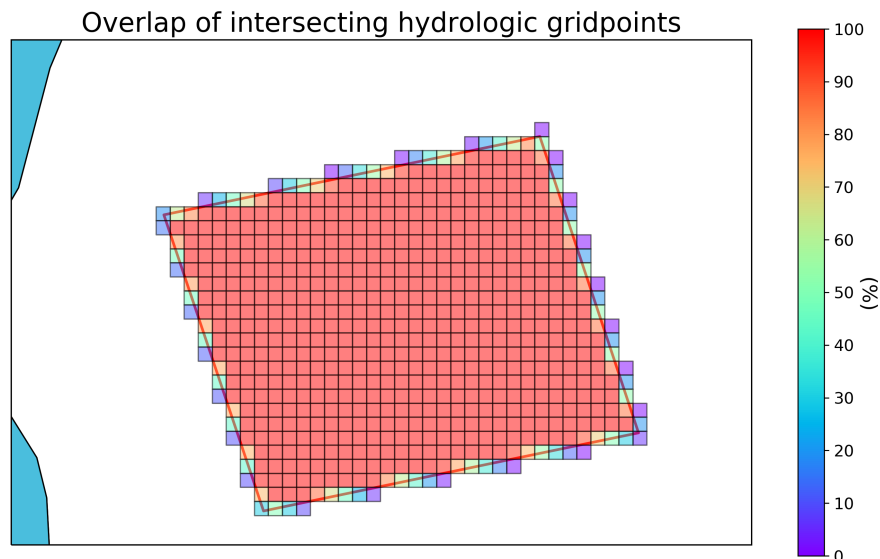


Figure 4.6. Illustration of the fraction of hydrological pixels overlapping with an atmospheric grid point.

The calculation of the overlap is the most time consuming process. This is why the calculation of Weights can be saved in a netCDF file so it can directly be loaded in case of running RoutingPP over the same domain with the same hydrological input. The netCDF Weights file can only be used for the exact same domain; however, it can be used independently of the number of processors used.

4.2.5 Routing construction

The steps of the construction of the HTUs composing the high resolution river routing graph are synthesized in Figure 4.7. Some of these steps are presented with more details in the following subsections.

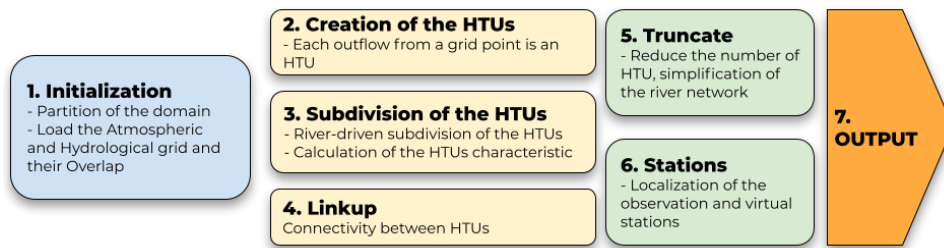


Figure 4.7. Resume of the steps of the construction of the high resolution river routing graph.

Initialization

After the decomposition and the calculation of the overlap between the atmospheric grid and the hydrological grid, each processor can load the HydroDEM data corresponding to the grid points which are in its subdomain using the `Weights (HydroData class)`. Once the fortran grid is initiated (`initatmgrid` subroutine), the hydrological data is converted to be used in the Fortran Subroutines.

The general idea is to generate a sub-grid tiling which preserves the hydrological continuity. The HTUs are initially constructed by considering one HTU per pixel flowing out of the grid point (these pixels are called outflow). Each one of these HTUs contains all the pixels of the grid point flowing to the outflow pixel of the HTU. Some of these HTUs are very large while others only contain one or a few pixels. These very small HTUs are caused by the border effect of the overlap. For each HTU, we define the mainstream river pixels by following the pixels with the largest flow accumulation going upstream from the outflow.

Two methods of subdivision of the largest HTUs have been developed, the original method is the area driven HTU decomposition and the new method developed is the river driven HTU decomposition. These methods are presented in the following subsections.

Area driven HTU decomposition

This method of decomposition has been developed by [Nguyen-Quang et al \(2018b\)](#) and aims to have HTUs with about the same size within an atmospheric grid.

Each HTU with an area larger than 2 % of the atmospheric grid will be subdivided further using the Pfafstetter decomposition ([Verdin and Verdin, 1999](#)). This methodology is illustrated in [Figure 4.8](#). The issue with this method is that, although it will optimise the generation of equal area HTUs, it will divide the major rivers in a large number of segments as shown in [Figure 4.8](#). This may have consequences on the quality of representation of large rivers and the stability of the routing scheme.

River driven HTU decomposition

This methodology, developed in the context of this thesis, has been developed with the aim to preserve the main river segments flowing through the atmospheric grid to better estimate their parameters. It will also increase the stability of the river routing scheme by reducing the

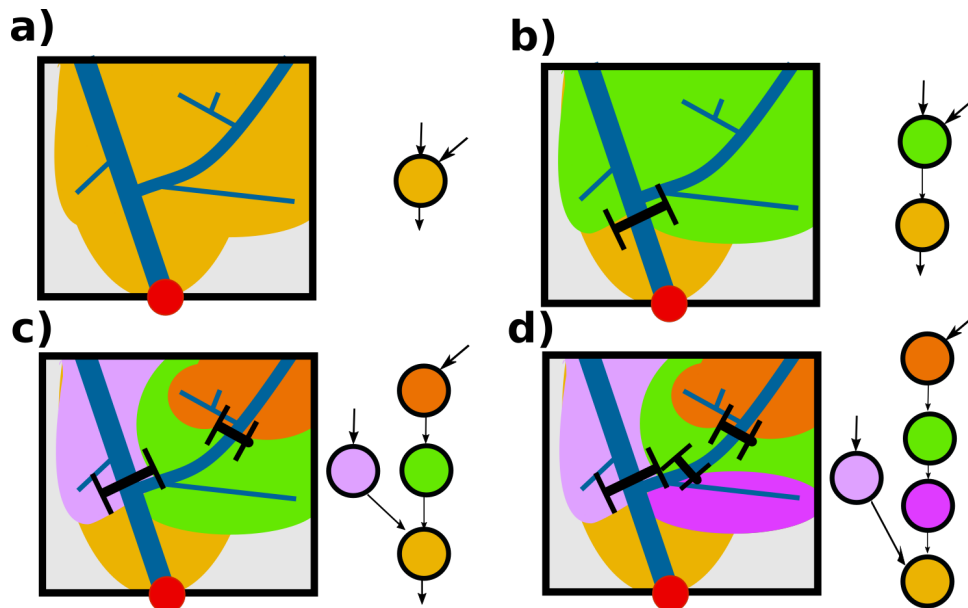


Figure 4.8. Illustration of the decomposition steps of the area driven subdivision of the HTUs.

number of reservoir along the river pathway.

The first step is the same as the area driven HTU decomposition presented above. An initial HTU is constructed for each outflow of the grid point and contains all the pixels flowing to this outflow pixel (cf. Figure 4.9.a).

Then for each HTUs we have 2 level of decomposition:

- division of the HTUs to represent the large-scale structures: create new HTUs containing the tributaries of the mainstream rivers with the largest global flow accumulation (cf. Figure 4.9.b),
if the area of the main river HTU is considered large enough upstream and downstream of the confluence, it is divided in two at the confluence (cf. Figure 4.9.c)
- division of the HTUs to represent the local hydrological structures and create new HTUs containing the tributaries of the mainstream river having the largest local flow accumulation, i.e. the flow accumulation calculated only considering the pixels of the grid point (cf. Figure 4.9.d).

This type of decomposition allows to keep various important features of the river network: (1) it keeps the major river pathway undivided so we limit the instability related to an excessive subdivision of the major river; (2) it better represents the large scale features by generating separated HTUs for the most important tributaries (important in terms of upstream area); (3) it improves the representation of the local HTUs, i.e. the HTU with a small upstream area, that occupy a large fraction of the grid point.

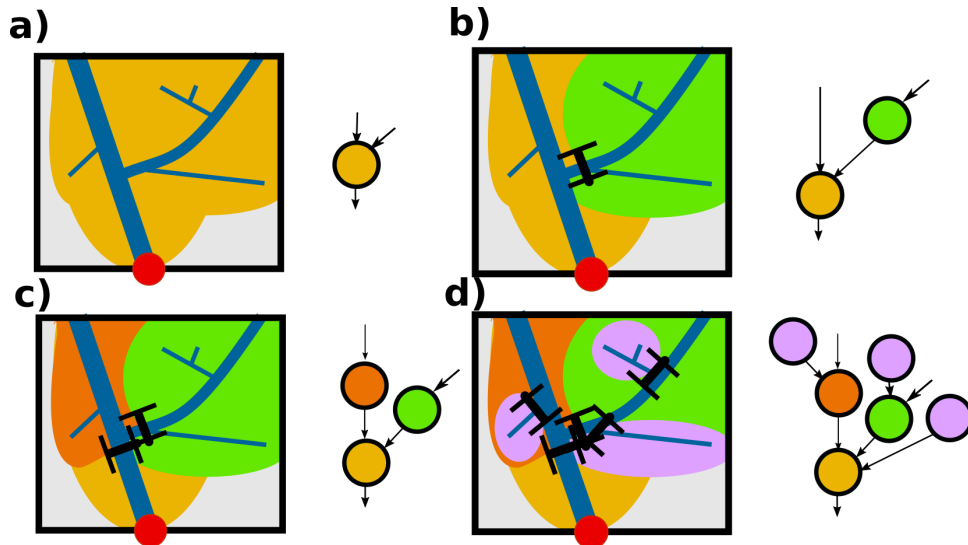


Figure 4.9. Illustration of the decomposition steps of the area driven subdivision of the HTUs.

Extracting the characteristics of the mainstream river

This topographic index (topindex) is the geometric parameter of the routing scheme in ORCHIDEE describes the speed of the water flow and is defined as:

$$\lambda = \sqrt{\frac{d^3}{\Delta z}} \quad (4.1)$$

where d is the length of the river segment considered and Δz the elevation change of that river segment. Both variables are given in meters and the resulting λ is converted to kilometers. λ can also be expressed in terms of river segment length and slope. Multiplying the topindex by a constant, which is in units of an inverse speed, will give the emptying time characteristic of the stores in the routing scheme.

The topindex has been re-adjusted in (Nguyen-Quang et al, 2018b) to render the behaviour of the different hydrological pixels contained in an HTU. It is calculated using the whole river network composing an HTU. This value of the topindex was used for all the ORCHIDEE reservoirs (stream, fast and slow reservoir). The development of the RoutingPP tool has been an opportunity to evaluate other implementations of the topindex. The simulation of the river discharge has been improved by calculating a different topindex for the stream reservoir (Λ_s) and the fast and slow reservoir ($\bar{\Lambda}$). The stream reservoir HTU is mainly affected by the water that flows from the upstream area through the main river of the HTU. Thus, Λ_s is calculated considering the distance of the HTU's mainstream river for d and the difference of altitude over the HTU's mainstream river for Δz . There are different options to calculate $\bar{\Lambda}$. It can consider, for example, the mean distance (resp. the difference of altitude) between the pixel of the HTU and the outflow for d (resp. Δz).

The river driven HTU decomposition allows to take maximum advantage of the Λ_s as it focuses the river description on the largest rivers. Thus instead of having a unique and complex definition of the topindex trying to represent the dynamic of both the local sub-catchment and

the mainstream river, the model can use Λ_s to represent separately the mainstream river flow between one HTUs and its downstream HTU

Figure 4.10.d shows an example of the division of a grid point into HTUs with the flow accumulation and the orography (respectively Figure 4.10.b and Figure 4.10.c). This grid point include the Rhone river near Valence in France (Figure 4.10.a) and its confluence with the Isère river from the East and the Doux river from the West. The HTU including the Rhone river is in yellow with the mainstream river (i.e. the Rhone) is in darker yellow. The Isère is the large HTU in blue while the contribution of the Doux river in the grid point is in red.

Considering the main Rhone HTU (yellow), Λ_s will be calculated using the distance and difference of altitude among the dark yellow path. $\bar{\Lambda}$ can be calculated using different methods that try to combine the property of the pixels composing the HTU. In the following examples, $\bar{\Lambda}$ will be calculated with the average of the distance and the difference of altitude between the pixels and the outflow of the HTU.

Linkup

The linkup is the step that connects the HTUs with each other. This is done using the information from the construction of the HTUs, in particular from the location and flow direction of their outflow pixel. In the case of a coastal outflow, a river outflow, the outflow of an endorheic basin or if the HTU is flowing to the same grid point (HTU from the decomposition operation) the outflow is already given. If it is flowing into another grid point, different solutions are evaluated: (1) the original `outflow_grid`; (2) each consecutive pair of neighbours starting from the original `outflow_grid` point; (3) if no solution is found, a solution is searched in the same grid point; (4) if really no solution is found, the HTUs is set as a coastal flow. The coherence of the routing graph is ensured by two informations: the upstream area of the HTUs and their distance to the ocean. As long as these variables are coherent, there are no loops generated in the graph and, therefore, the graph is ensured to be non-cyclic.

4.2.6 Truncate

The truncation is used to reduce the number to HTUs to respect the `nbasmax` parameter defined by the user. Reducing the number of HTUs allows to simplify the structure of the river routing scheme, to reduce the memory size of the river routing output and to reduce the computational cost in the model using this river routing output. In both methods for the HTU decomposition presented above, we will usually generate a number of HTUs higher than the `nbasmax` parameter. It should be noticed that the procedure is used less often for the "river driven decomposition" as the number of HTU achieved is lower and thus may be closer or lower than the `nbasmax`.

The main objective is to perform the truncation with as little impact as possible on the river graph. The truncate process is performed using 5 criterias presented below. All the operations possible within one criteria are performed before using the following criteria. The HTUs with lower upstream areas are merged into the HTUs of higher upstream areas. Each processor

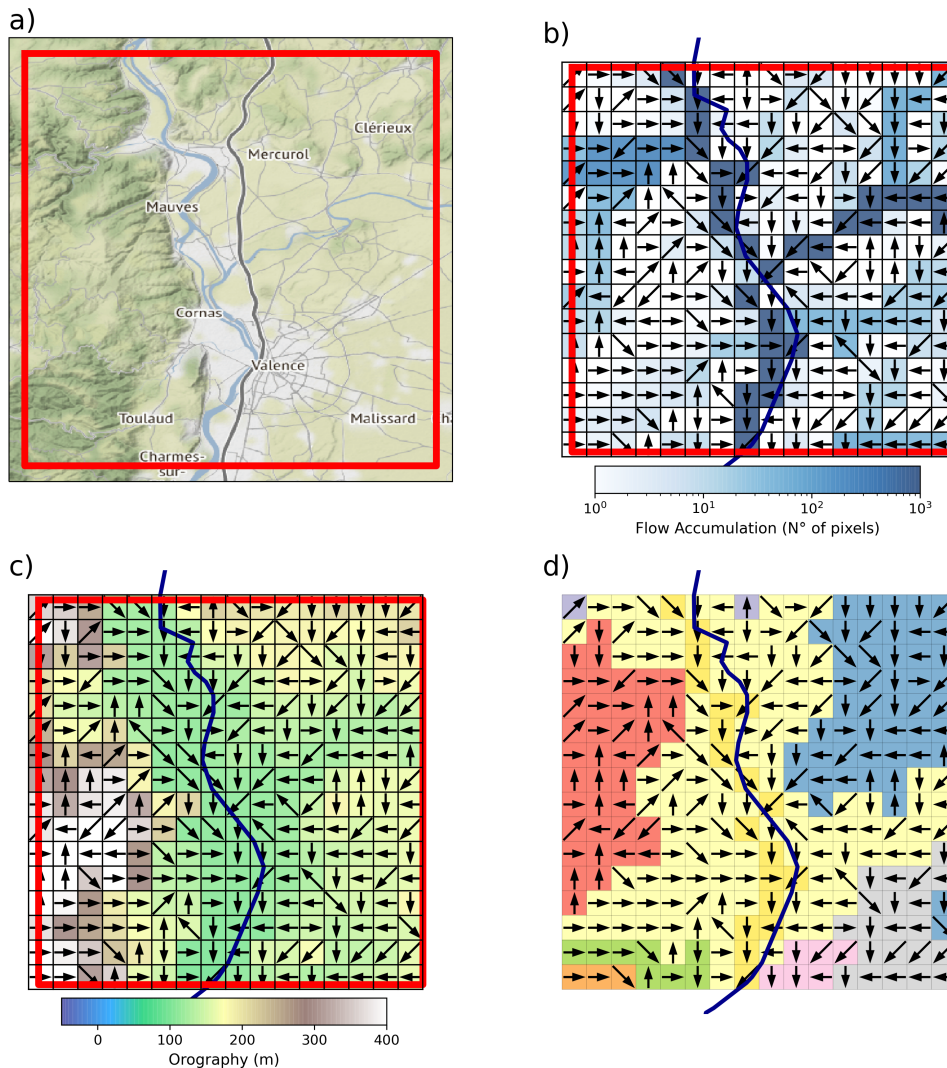


Figure 4.10. Illustration of the the construction of the HTU over the Rhone basin near Valence in France with the map of the region (a), the flow accumulation (b) and orography (c) in MERIT-Hydro and the construction of the HTUs over this grid point (d). In (d), the HTU corresponding to the main river is in yellow and the mainstream river, i.e. the Rhone river, is represented in dark yellow.

evaluates a total of 100 operations over its core, send these operation to the processors with some of these grid point in its halo and the operation over the grid point of its halo. The sending of the operation over the halo allows to conserve the coherence between the processors. Then, these truncation operations are performed and the upstream area is recalculated because it will be used to evaluate the following truncation operations.

The four criterias are the following:

- Merge HTUs which are coastal outflow
- Merge HTUs which flows into the same grid point (outside of the grid point they belong to)
- Merge HTUs of the same basin flowing into different directions

- Merge HTUs in the same grid point with one HTUs flowing into the other. If the exceeding HTUs represent less than 5 % of the grid point, all the exceeding HTUs are merged.

4.2.7 Calculation of the upstream area

The calculation of the upstream area is difficult to implement as it requires a complex exchange of information between the processors. First, each processor partially calculates the upstream area (*fetch*) over its core domain. Then the upstream over the halo is updated from the partial calculation of the other processors and propagated over the core domain. This operation is repeated to propagate the upstream area along the rivers until the upstream area doesn't change anymore (cf. Figure 4.11).

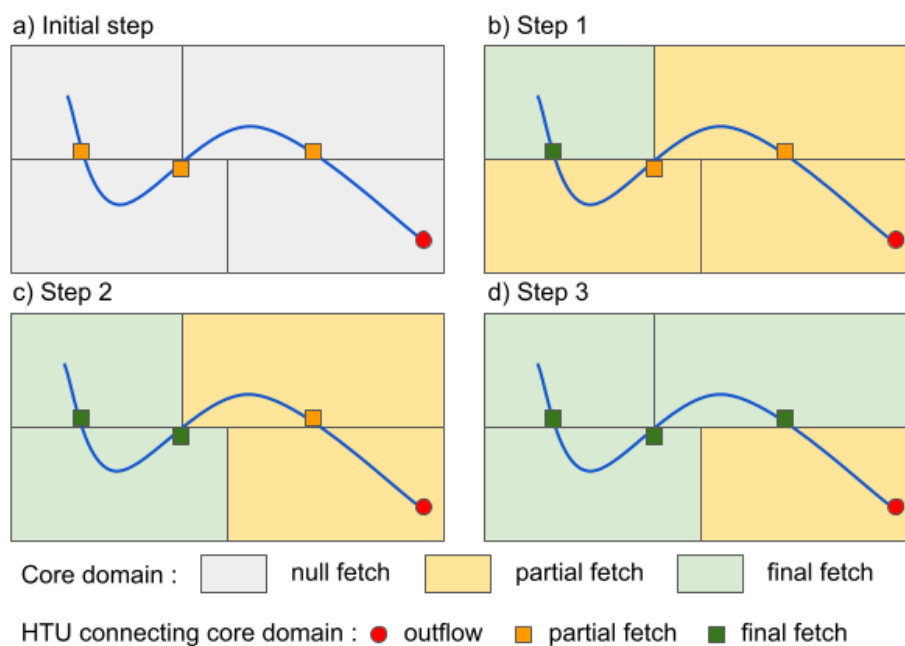


Figure 4.11. Illustration of the calculation of the upstream area within the parallelized structure.

4.2.8 Localization of the fluvimetric stations

The river routing scheme is a very helpful tool in LSMs to validate the simulation of the water cycle at a catchment scale. For this reason, it is important to know the exact location of some stations of interest in the river routing. A module in RoutingPP aims to localize, if possible, the fluvimetric stations in HTU space.

This module further allows the ORCHIDEE model to generate an output with the discharge for all the stations that have been localized in the routing graph. Once the truncation is performed and the final upstream area calculated, each processor will localize the stations which are inside its sub-domain. The stations can be read from a netCDF file or may correspond to virtual stations defined by the user. The informations required to search a station in the river graph are its coordinates and its upstream area.

RoutingPP first evaluates the grid points corresponding to the exact location of the station. These grid points must be inside a pre-defined perimeter (defined with the parameter `TRES_DEGREE`) around the station's exact location. Then, it selects the HTU from these grid points whose upstream area is closer to the exact upstream area of the station. For the HTUs with an absolute relative difference of upstream area lower than a certain threshold defined by the user (`TRES_DIFF`), the localization of the HTUs with the highest correspondence is kept into memory. In addition to the development of the RoutingPP tool, an important work has been carried out to collect and organize the stations discharge observations from different sources. For example, over the Western Europe domain represented in Figure 4.12, the construction of the routing graph over a 0.5° resolution atmospheric grid, a total of 2926 stations has been located in HTU space using the HydroSHEDS dataset (1km resolution), 2923 using the MERIT-Hydro dataset (2km resolution) and 664 using the Fekete-Vorosmarty dataset (0.5°).

4.3 Validation

4.3.1 Hydrological Inputs

Fekete and Vorosmarty

Vorosmarty et al (2000) have been a precursor by presenting a global 0.5° gridded river network dataset: the Simulated Topological Network at 30-minute spatial resolution (STN-30). The river routing scheme of the ORCHIDEE model was originally based on this gridded dataset. This dataset has been constructed by aggregating the ETOPO5 DEM (Edwards, 1989; available in a resolution from 5 to 10 minutes) to a 0.5° resolution. The convergent routing river network has been constructed by finding the flow direction from the topology of the ETOPO5 data.

HydroSHEDS

HydroSHEDS is a near-global gridded hydrological map (Lehner et al, 2008) based on high resolution elevation data from the Shuttle Radar Topography Mission at 3 arc second resolution (SRTM3). HydroSHEDS data gives hydrological information over land points from 56°S to 60°N due to the spatial availability of the SRTM3 data. It is available at different resolutions, from 3 arc-second to 30 arc-second. It provides a complete description of the river network: hydrologically conditioned elevation, drainage direction, watershed boundaries.

HydroSHEDS face some limitations such as elevation biases due to the canopy in forested areas (Yamazaki et al, 2019). Although it is a reference for large-scale hydrological modelling (Gong et al, 2011; Nguyen-Quang et al, 2018b; Yamazaki et al, 2019) its development needed some manual editing which inhibited the reproduction / improvement of its construction.

The HydroSHEDS dataset used to construct the routing graph has a 30 Arc-Second resolution ($\sim 1\text{km}$).

MERIT-HYDRO

The Multi-Error-Removed-Improved-Terrain (MERIT; Yamazaki et al, 2019) Hydro is the global hydrological DEM based on the MERIT DEM (Yamazaki et al, 2017) at 3-arcsec resolution. The MERIT DEM dataset has been constructed by applying a multiple error correction on pre-

existing spaceborn DEMs (SRTM3 v2.1 and AW3D-30m v1) The algorithm used to construct MERIT HYDRO tries to avoid as much as possible manual editing to ensure the reproducibility of the final product. The MERIT-HYDRO dataset used to construct the routing graph has a 1 Arc-Minute resolution (~ 2 km).

Stations localized

Figure 4.12.a compares the stations localized in the river graph between the MERIT based and the Fekete-Vorosmarty based routing graph. The higher resolution of MERIT allows to locate a larger quantity of hydrological stations but still, some stations can only be located in the Fekete-Vorosmarty based routing graph. Figure 4.12.b compares the MERIT based and the HydroSHEDS routing graph. It can be seen that most of the stations are located in both dataset although each routing graph is able to locate some stations that cannot be located by the others due to the differences between the resulting HTU graphs.

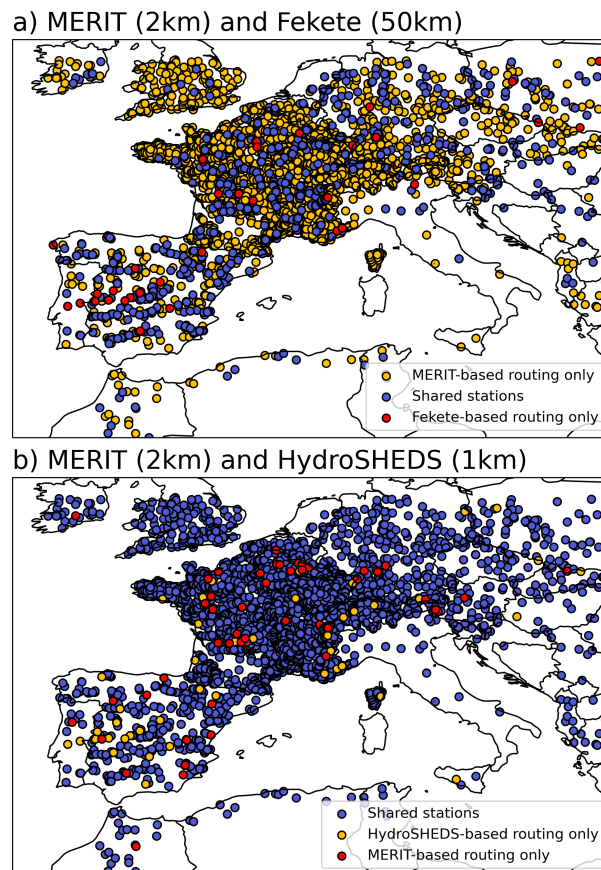


Figure 4.12. Localization of stations in the routing graph using MERIT compared to Fekete-Vorosmarty (a) and using MERIT compared to HydroSHEDS for Western Europe over a 0.5° atmospheric grid.

4.3.2 Methodology

In order to validate the routing graph and its sensibility to the different configurations, three offline simulations have been performed, i.e. simulations which are not coupled to an atmospheric model but forced by an atmospheric forcing. The forcing used to assess the routing description from the RoutingPP pre-processing tool is WFDEI_GPCC. It is a 0.5° resolution atmospheric forcing (Weedon et al, 2014). WFDEI is issued from the ERA-Interim reanalysis (Dee et al, 2011) which is a 3-hourly re-analysis with 0.5° resolution which has been processed by the WATCH Forcing Data methodology. WFDEI_GPCC corresponds to the version of WFDEI whose precipitation has been bias-corrected by the GPCC dataset (Schneider et al, 2017).

A set of three simulations has been performed over the Western Europe and Mediterranean to evaluate the three hydrological inputs (Fekete, MERIT and HydroSHEDS). This region is an adequate place to evaluate the routing as it contains numerous mid-sized catchment and a large quantity of discharge data to assess the simulations. The same atmospheric forcing (WFDEI_GPCC) has been used for the three simulations over the 1990-2010 period. Each one of these simulation is launched after a previous ten year spin-up in order to properly initialize the routing reservoirs. The representation of the discharge at key stations is then evaluated in comparison with the observations.

The key stations are available in the three routing graph and intend to include some of the major basins over this region with available observations for the period of the simulations: the Loire (Monjean sur Loire), the Ebre (Tortosa), the Rhone (Beaucaire), the Po (Pontelagoscuro), the Rhine (Rees), the Moselle (Cochem), the Seine (Poissy), the Thames (Kingston). It should be highlighted that none of these basins is natural anymore. The infrastructures built on them can affect significantly the river flow. Hence, only a qualitative evaluation is performed.

4.3.3 Influence of the hydrological input

Figure 4.13 compares the annual cycle of the discharge simulated with at the different key stations with the observations. The three simulations have a similar evolution at the different stations although there may be higher differences between Fekete simulation and the others such as in the Ebre, Rhone, Rhine and Moselle. This must be linked to the resolution of the Fekete-Vorosmarty dataset which may lead to a coarser representation of the upstream area and thus to a different representation of the discharge.

The three simulations having a similar representation of the discharge over the key stations, the simulation with the MERIT-based routing has been chosen to perform further analysis through a Normalized Taylor diagram (Figure 4.14). This diagram shows us that the simulations have a good correlation with the observation with values between 0.7 and 0.9. The behaviour of the Centered Root Mean Square Error (CRMSE) and of the standard deviation depends on the station. The stations of the Po, Rhone and Rhine have standard deviation close to the value of the observations and have a CRMSE around 0.4. Meanwhile the stations over the Thames, the Moselle, the Ebre and the Seine are strongly underestimating the standard deviation have a CRMSE between 0.8 and 1.

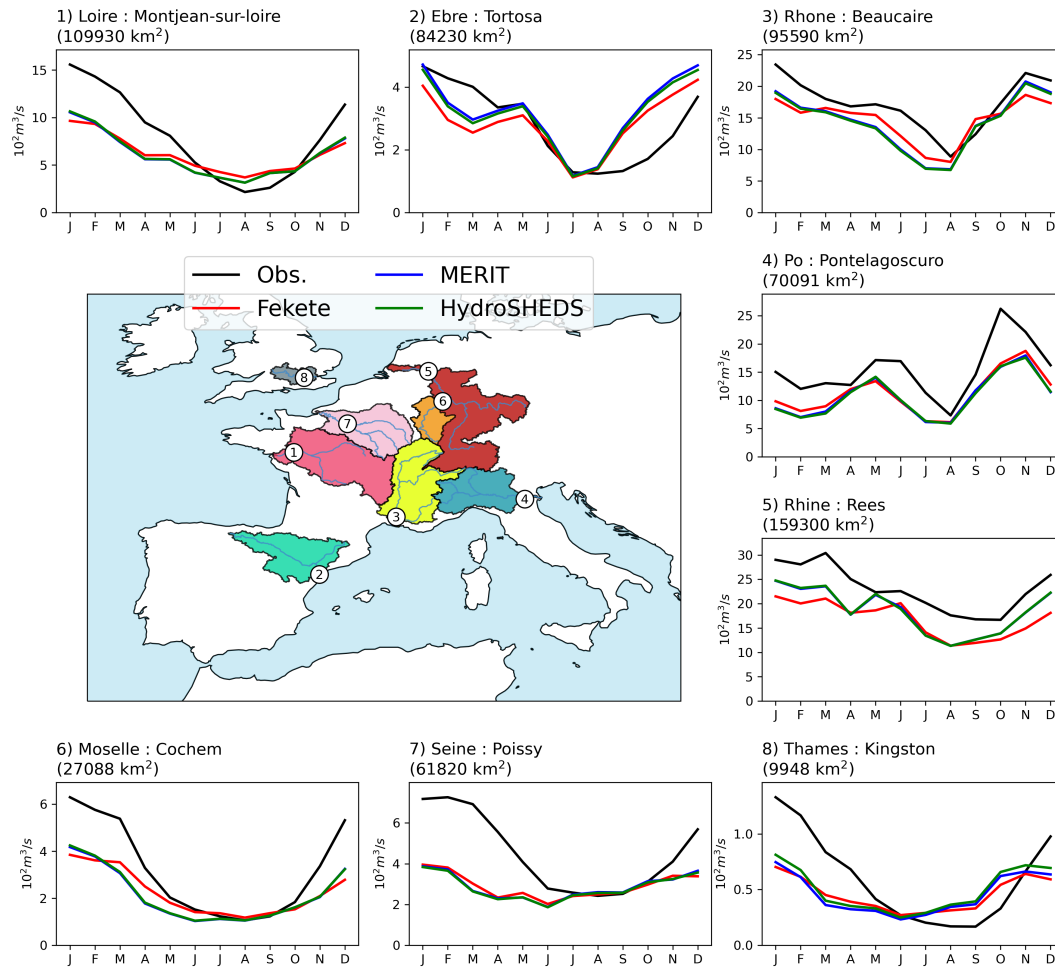


Figure 4.13. Map of the Western Europe with the representation of the 8 basins considered and their respective key stations emplacement. The annual cycle of the observed and discharge of the 3 simulations with different routing graph (Fekete-Vorosmarty, MERIT and HydroSHEDS) are represented using the reference at their emplacement on the map.

We may conclude that the behaviour of the discharge in the simulations have a similar evolution compared to the observations although there may have some errors. This shows the robustness of the construction method as the results do not depend strongly on the hydrological forcing used to construct the routing. These errors may be related to (1) the impacts of human activity on the rivers which are not considered in these simulations such as human consumption, dams or irrigation, (2) the uncertainty of the atmospheric forcing and, in particular, of the precipitation (Ngo-Duc et al, 2005), (3) errors related to the construction of the graph such as differences of upstream area between the HTU considered for a specific station and real upstream area of the station and (4) errors related to the river routing in the ORCHIDEE model.

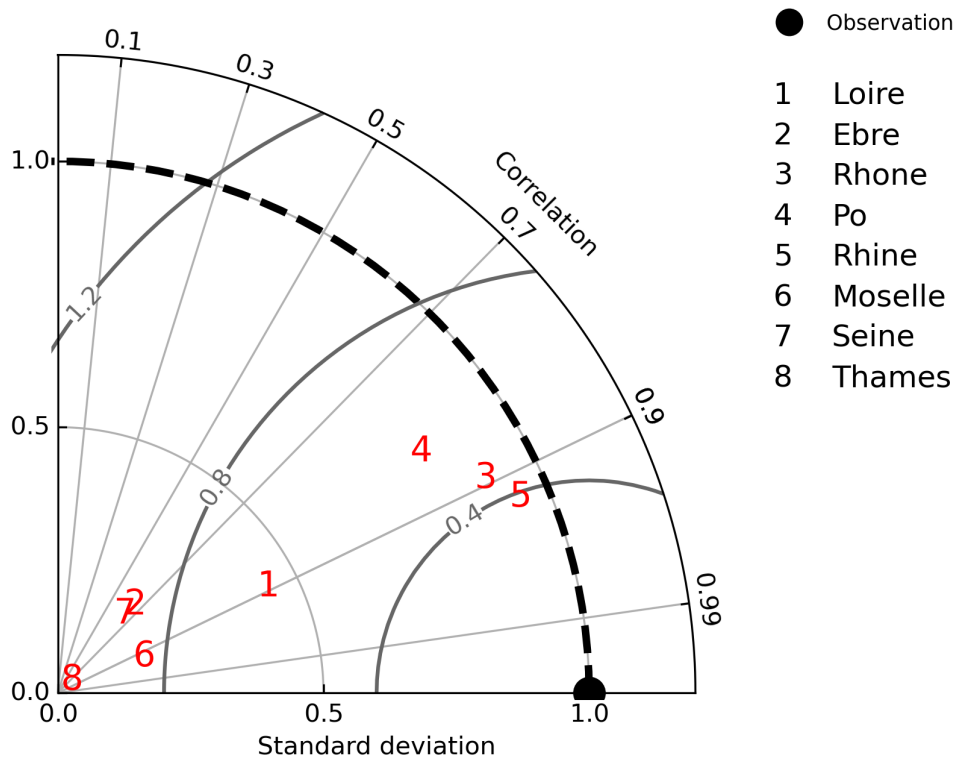


Figure 4.14. Normalized Taylor Diagram for the discharge at the key stations over Western Europe for the simulation forced by WFDEI.GPCC with the routing scheme based on MERIT during the 1990-2010 period.

4.4 Discussion and Conclusion

This chapter presented the development of RoutingPP, a parallelized pre-processing tool to construct the river routing based on the HTU concept introduced by [Nguyen-Quang et al \(2018b\)](#) which is a sub-grid parameterization of the river routing scheme.

The objective of developing a high resolution routing scheme required the development of a parallelized flexible pre-processing tool (RoutingPP) to construct the HTUs from different types of atmospheric grid based on different hydrological dataset.

The methodology of construction of the routing graph has been presented as well as its different specificities including the optimization of the grid partition and the calculation of the overlap between the atmospheric and hydrological grid. The improvement of the HTUs construction are also presented such as: (1) the new river-driven method to divide the large HTUs, (2) the calculation of the upstream area with the parallelization, (3) the integration of a different topindex for the mainstream river to be used for the stream reservoir in ORCHIDEE, (4) the truncation method to reduce the number of HTUs and (5) the localization of hydrological stations in HTU space.

The construction of the HTUs has been assessed by comparing 3 simulations performed over

Western Europe forced by the same atmospheric forcing (WFDEI_GPCC) between 1990 and 2000 using the routing graph constructed from 3 hydrological datasets at different resolutions: Fekete-Vorosmarty at 0.5° , MERIT-Hydro at 2km and HydroSHEDS at 1km. These simulations were evaluated over the main basins in Western Europe at key stations. The discharge at the different stations were coherent with the observations. Although the discharge in the three simulations have a similar behaviour, some differences can be observed between the simulation using the Fekete-Vorosmarty based routing graph and the others. This can be related to the resolution of Fekete-Vorosmarty. The coarser resolution of Fekete-Vorosmarty also reduces the quantity of stations localized over the HTU graph compared to MERIT-Hydro and HydroSHEDS. This affects in large part the stations over the small catchment which reduce the possibility to evaluate the performance over these catchment. Nevertheless, we suppose that these differences may be increased over small catchment (such as over the Cochem station - Moselle).

RoutingPP allows a fast and robust construction of the HTUs which may be used in different Land Surface Models. It opens the possibility to easily includes new processes in the routing graph such as the floodplains, the irrigation of the lakes. However, some elements may be improved such as the time calculation of the overlap between the atmospheric grid and the hydrological grid. The calculation of the topindex from the different pixels of a HTU may also be discussed. There are also some developments to be done in order to be able to construct the routing graph over more complex atmospheric grid projection such as Icosahedral grids.

River modeling in ESM has to be adapted to the future challenges to come. This requires the ability to adapt the river routing graph to the diversity of atmospheric grid projections and the possibility to use indifferently the different hydrological description available. It will also need to solve the memory issues related to large domains at high resolution such as, for example, simulations over the South American domain at a 4km resolution. The development of the pre-processing routing graph is a first step to better capture the land-atmosphere feedbacks in the Land Surface Models as it facilitates the integration of the processes interacting with the river network such as human activities and floodplains.

4.5 Access to RoutingPP

The code of the Routing Pre-Processing (RoutingPP) is available at the following link:

<https://gitlab.in2p3.fr/ipsl/lmd/intro/routingpp>

4.6 Acronyms

CAMA-FLOOD	Catchment-based Macro-scale Floodplain model
CRMSE	Centered Root Mean Square Error
DEM	Digital Elevation Model
DYNAMICO	Icosahedral Dynamical Core atmospheric model of the Institut Pierre Simon Laplace
ERA	ECMWF Re-Analysis
ESM	Earth System Model
ETOPO5	Earth topography five minute grid
GPCC	Global Precipitation Climatology Centre
HTU	Hydrological Transfer Unit
HyMAP	Hyperspectral Mapper sensor
HydroDEM	Hydrologically coherent Digital Elevation Model
HydroSHEDS	Hydrological data and maps based on SHuttle Elevation
JULES	Joint UK Land Environment Simulator
LSM	Land Surface Model
MERIT DEM	Multi-Error-Removed Improved-Terrain Digital Elevation Model
NASA	National Aeronautics and Space Administration
NOAH-MP	Noah-Multiparameterization Land Surface Model
ORCHIDEE	ORganizing Carbon and Hydrology in Dynamic EcosystEms
RoutingPP	Pre-Processor of the routing input for ORCHIDEE high resolution routing scheme
SRTM3	Shuttle Radar Topography Mission 3 arcseconds
STN-30	Simulated Topological Network 30 arcseconds
WFDEI	WATCH forcing data bias corrected by ERAI
WRF-HYDRO	Weather Research and Forecasting Hydro Modeling System

Development of a high resolution floodplains scheme

Contents

5.1	Introduction	106
5.2	Floodplains scheme description	106
5.2.1	Representing the water flow on a graph	106
5.2.2	Water Continuity Equation: stream reservoir	108
5.2.3	Water Continuity Equation: floodplain reservoir	110
5.2.4	Floodplains geometry	112
5.2.5	Ancillary data	114
5.2.6	Workflow of the Module	116
5.3	Methodology and Dataset	116
5.3.1	Model Description: ORCHIDEE	116
5.3.2	Methodology of Validation	117
5.3.3	Discharge	118
5.3.4	Statistical indexes	119
5.3.5	Flooded area	120
5.3.6	Water Storage	121
5.4	Results	122
5.4.1	Comparison with the previous version	122
5.4.2	Assessment of the floodplains at different resolutions	126
5.5	Discussion and Conclusion	134
5.6	Acronyms	137

5.1 Introduction

To summarize, the development of the floodplains at higher resolution intent to: (1) answer to the lack of data over large floodplains and help to better understand the processes occurring at large scale over these regions, (2) represent the impact of floodplains on the local land water cycle, on the river discharge and on the land-atmosphere energy balances and (3) obtain a representation of floodplains that can be used in land-atmosphere coupled simulation to estimate the floodplains-atmosphere feedbacks.

The sub-parametrization of the routing scheme require to reconsider some of the modeled concepts and to represent them more explicitly. This is the case of floodplains which were handled at a 0.5° resolution in ORCHIDEE (D'Orgeval, 2006; Guimberteau et al, 2012a; Schrapffer et al, 2020). In this particular case, the higher resolution will exacerbate the difficulty to simulate the correct extent of floods. This is related to the fact that, in modelling, floods are usually well estimated over the main river but underestimated over the adjacent areas (Decharme et al, 2019). However, the HTU representation is also useful to overcome this difficulty as (1) it gives the opportunity to define floodplains with more details and (2) the increased information on river network connectivity brings solutions to model the flooding of the area of floodplains which are adjacent to the main rivers. Nevertheless, the floodplains scheme needs to be adjusted to the HTUs description by changing its dynamic and the volume / flooded area relationship.

This chapter contains the description of a high resolution floodplains scheme for the Organising Carbon and Hydrology In Dynamic Ecosystems (ORCHIDEE - Krinner et al, 2005) Land Surface Model developed by the Institut Pierre Simon Laplace (IPSL) and its validation over the Pantanal, the world's largest continuous floodplains located in South America. In this chapter, Section 2 presents the description of the floodplains scheme implementation in the river routing scheme of ORCHIDEE and the different equations ruling the exchange of water. Section 3 presents the methodology of the validation and the observational datasets used for this purpose. Section 4 contains the validation. This validation is performed based on the variables directly linked with the river routing scheme (discharge, flooded area, volume of water in the routing reservoirs). The floodplains scheme is assessed by (1) a comparison with the previous version at 0.5° and (2) a more complete evaluation based on simulations at different resolutions using a 0.5° atmospheric forcing and a 20-km atmospheric forcing. The last section presents a conclusion for this chapter.

5.2 Floodplains scheme description

5.2.1 Representing the water flow on a graph

The Hydrological Transfer Units (HTUs) in the ORCHIDEE LSM are basic hydrological units used to represent the river routing system. They can be represented by a forest of directional rooted tree graphs (Foulds, 1992). Each tree represents a river basin described by $D = (V, E)$ where V are the vertices, and E are the edges that connect the vertices. The HTUs in ORCHIDEE correspond to the river system vertices. Each tree has a root which is either

located at the coast (the river mouth) or in a lake when it is an endorheic basin. There cannot exist any loop in the river graph. The graphs in the routing are said convergent because each vertex V has only one edge that goes to another vertex.

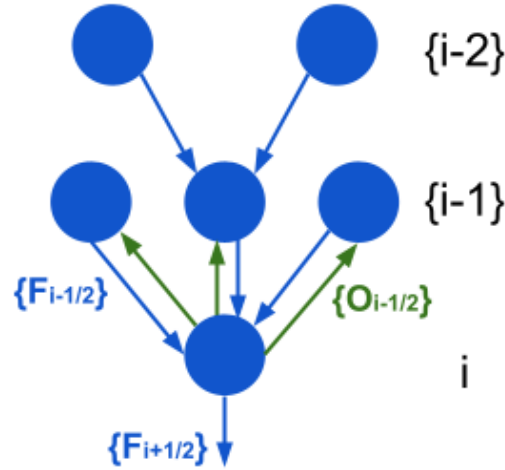


Figure 5.1. A sample graph to illustrate the indexing convention and the placement of fluxes out the vertices (F) as well as the overflow fluxes (O).

In ORCHIDEE's implementation, each vertex/HTU is fully contained in one cell of the grid used. The cells of ORCHIDEE can contain more than one HTU and can be crossed by more than one graph. The grid point of a vertex i is noted \hat{i} . The surface of the HTU is described by the term S_i and the surface of the grid point to which this HTU belong is noted $S_{B,i}$. The fraction of the grid point associated with each HTU is needed to know the water source and sink terms which are computed by ORCHIDEE on the atmospheric grid for the routing scheme. The fraction of the mesh \hat{i} occupied by the HTU i is noted as $\delta_{\hat{i},i}$ and is equal to $S_i/S_{B,i}$.

Each vertex contains four water reservoirs used by the river routing scheme to represent processes with different time constants: the river flow (stream reservoir), the runoff (fast reservoir), the drainage (slow reservoir) and the floodplains (floodplain reservoir). The local properties of the vertexes are defined by the local slope and tortuosity of the river segment represented by the downstream edges. The local properties of the HTU and the characteristics of the water reservoirs govern the residence times of the water in this HTU and thus govern the flow passing through the edge towards the downstream HTU.

For example, the discharge from the reservoir j of the HTU i ($Q_{j,i}$) depends on the time constant of the reservoir (τ_j in s/km) and the topographic index (topoindex) of the reservoir j of the HTU i ($\Lambda_{i,j}$ in km) expressed in equation 5.1. There are two different topoindex: (1) one based on the properties of the pixels composing the HTU which is used for the slow and fast reservoirs (cf. Chapter 4, $\Lambda_{i,j} = \Lambda_{S,i}$) and (2) another one based on the properties of the main river of the HTU which is used for the stream and floodplains reservoirs (cf. Chapter 4, $\Lambda_{i,j} = \bar{\Lambda}_i$).

$$Q_{j,i} = \frac{V_{j,i}}{\tau_j * \Lambda_{i,j}} \quad (5.1)$$

A sample segment of a river graph is shown in Figure 5.1. F (respectively O) represents the fluxes of water going downstream (resp. upstream) and is detailed in the subsection 5.2.2 (resp. at the end of the subsection 5.2.3). The relations between the vertices of the river graph are represented by an integer index. The natural flow direction of the river is used to order the indices of the water stores on the graph where the index increases as the HTU are closer to the river outflow. We note $\{i - 1\}$ the ensemble of all the upstream vertex of vertex i . $i + 1$ is the unique downstream vertex of i . The flux of water between the vertex are placed on the edges of the graph and are indexed with half indices. Each vertex is linked to an ensemble of upstream vertices but only to one downstream. For example, the outflow edge of the HTU i is unique and noted $i + 1/2$, but is part of the ensemble of upstream edges of the HTU $i + 1$. Thus we have $i + 1/2 \in \{(i + 1) - 1/2\}$. The water flowing into the vertex i is given by the ensembles of fluxes on edges $\{i - 1/2\}$ while the outflow is given on the edge $i + 1/2$. It should be noticed that, for an HTU i , its associated atmospheric grid point \widehat{i} can be different or the same as the grid point of the downstream HTU $\widehat{i + 1}$.

5.2.2 Water Continuity Equation: stream reservoir

The approach for the high resolution floodplains scheme is adapted from the PhD thesis of Tristan d'Orgeval (D'Orgeval, 2006) who has established the floodplains scheme for the 0.5° routing scheme. It consists in using an additional reservoir in the HTUs containing floodplains. The slow, fast and stream reservoir are active in the ORCHIDEE routing whether the floodplains are activated or not. However, the floodplains scheme will only impact the functioning of the stream reservoir. The floodplains scheme is based on the characteristic of the HTUs and the maximum flooded fraction (noted $f_{max,i}$ for a HTU i) which have a value between 0 and 1. This fraction is obtained from the Global Lake and Wetland dataset (GLWD - WWF, 2004), see subsection 5.2.5 for more details. The maximum flooded surface for an HTU i is $S_{fmax,i} = S_i * f_{max,i}$. We consider that an HTU i is a floodplains if $f_{max,i} > 0$. The flooded fraction and the flooded surface are noted respectively $f_i \in [0, f_{max,i}]$ and $S_{f,i} \in [0, S_{fmax,i}]$.

The water continuity equation provides the basis for the time evolution of the water volumes in the floodplain reservoir. In Figure 5.2, the different components of the water continuity equation in the case of an HTU with floodplains (Figure 5.2.a) and without floodplains (Figure 5.2.b) are resumed.

The volume of water in the stream reservoir of an HTU i ($V_{stream,i}$) follows the water continuity equations in equations 5.2 differentiating whether it is a HTU with or without floodplains.

$$\frac{\partial V_{stream,i}}{\partial t} = \begin{cases} \sum_{j \in \{i-1/2\}} (F_{out,j}) - F_{out,i+1/2} & \text{if } S_{fmax,i} = 0 \\ Q_{f,i} - F_{out,i+1/2} & \text{if } S_{fmax,i} > 0 \end{cases} \quad (5.2)$$

With:

- $F_{out,j}$ with $j \in \{i - 1/2\}$: Water flowing from the stream reservoir of the upstream HTUs to the HTU i .
- $F_{out,i+1/2}$: Outflow from the stream reservoir of HTU i into the stream reservoir of the

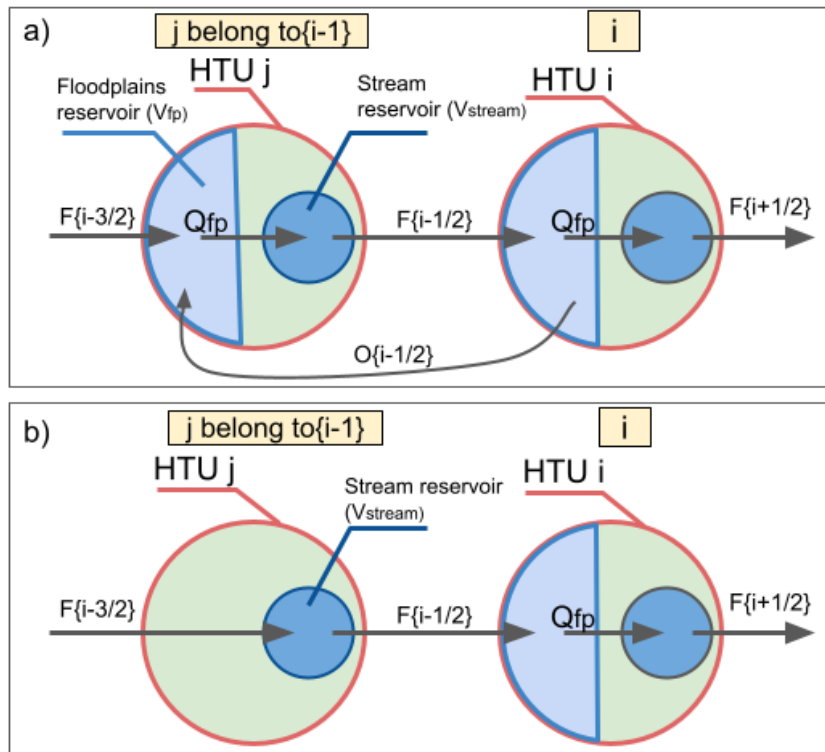


Figure 5.2. Scheme resuming the movement between the different reservoirs for a HTU which has floodplains and its upstream HTUs depending if (a) the upstream HTU has floodplains or if (b) the upstream HTU doesn't have floodplains.

downstream HTU $i + 1$.

- $Q_{f,i}$: Water flowing from the floodplains reservoir of the HTU i to the stream reservoir of the HTU i . This variable will be explain in the following subsection.

The outflow from the stream reservoir $F_{out,i+1/2}$ is also affected by the presence of floodplains but the time constant of this reservoir (τ_{stream}) remains constant for all the HTUs. Thus, a reduction factor based on the fraction of the HTU which is flooded has been introduced to reduce the flow of the stream reservoir depending the importance of the floods. This factor aims to represent the impact of the floodplains on the reduction of the river discharge that flows from the stream reservoir. It should be noticed that it is not affecting the HTUs without floodplains. The floodplains reservoir has its own time constant, therefore, this factor is exclusively used for the stream reservoir. Due to the HTUs structure, some small HTUs over the main river can have a flooded fraction close to 1 that impeach the river from flowing. Therefore a parameter R_{limit} has been implemented to limit the flow reduction. This parameter is the same for all the HTUs. The reduction factor can be deactivated with a value of $R_{limit} = 0$. Therefore, the formulation of the outflow from the stream reservoir of an HTU i which has floodplains ($F_{out,i+1/2}$) differs from the equation 5.1 and is represented in equation 5.3.

$$F_{out,i+1/2} = \frac{V_{stream,i}}{\tau_{stream} * \Lambda_{S,i}} * (1 - max(f_i, R_{limit})) \tag{5.3}$$

The flooded fraction f_i used in equation 5.3 is calculated from the area of the HTU which is

flooded ($S_{f,i}$). This value is diagnosed using the equation 5.4.

$$S_{f,i} = \min(\Gamma(V_{f,i}), S_{fmax,i}) \quad (5.4)$$

The appropriate function to be used for Γ will be discussed further in this chapter in subsection 5.2.4.

5.2.3 Water Continuity Equation: floodplain reservoir

This subsection focuses on the definition of the different water fluxes related to the floodplains reservoir. The water continuity equation ruling the temporal changes of the volume of water in the floodplains reservoir ($V_{f,i}$) is presented in equation 5.5. The different components of this equation will be described with more details further in this subsection.

$$\frac{\partial V_{f,i}}{\partial t} = (P_{f,i} - E_{f,i} - I_{f,i}) - Q_f + \sum_{j \in \{i-1/2\}} (F_{out,j} - O_j) \quad (5.5)$$

With:

- $F_{out,j}, j \in \{i - 1/2\}$: Water inflow into the floodplains from the upstream HTUs,
- $O_j, j \in \{i - 1/2\}$: Overflow of HTU i into the floodplains reservoir of the upstream HTUs.
- $P_{f,i}$: Rainfall onto the floodplain,
- $E_{f,i}$: Evaporation from the flooded surface,
- $I_{f,i}$: Infiltration from the floodplain into the soil moisture reservoir,

The precipitation over the flooded area goes directly to the floodplains reservoir. Considering an HTU i within the grid point \hat{i} , the precipitation going directly to the floodplains reservoir is

$$P_{f,i} = P_{\hat{i}} * S_{f,i} / S_{\hat{i}} \quad (5.6)$$

Over the floodplains, the water in the flooded area is able to evaporate at its potential rate. The potential rate of evaporation is defined from the characteristics of the land surface variables of the grid point to which the HTU belongs. However, the effect of vegetation and interception are taken into account through their respective beta coefficient as they will lower the evaporation from the floodplains. The evaporation from the floodplains is represented in equation 5.7.

$$E_{f,i} = f_i * (1 - \beta_{vegetation} - \beta_{interception}) * E_{pot_{\hat{i}}} \quad (5.7)$$

With:

- $E_{pot_{\hat{i}}}$: potential evaporation rate over the grid point \hat{i}
- $\beta_{vegetation}$: beta coefficient of vegetation

- $\beta_{interception}$: beta coefficient of interception

The water in the floodplains reservoir is able to infiltrate. It is a one-way flux from the floodplains to the soil moisture of the grid point. The infiltration term is calculated based on the averaged conductivity for saturated infiltration in the litter layer (k_{litt} in $kg/m^2/s$). This k_{litt} parameter has been established for the soil infiltration processes but not especially for floodplains. Therefore, the infiltration can be larger than what occurs over the floodplains. This is why a reduction factor (C) has been introduced to reduce the floodplains infiltration if necessary.

$$I_{f,i} = S_{f,i} k_{litt} C \quad (5.8)$$

The infiltration plays an important role because the water flooding the HTU can infiltrate and further be redistributed in the soil of the whole grid point. Then, it will progressively flow back into the river routing network of the HTUs belonging to the grid point through drainage (i.e. through the slow reservoir).

Within a HTU i with floodplains, the flow of water from the floodplains reservoir to the stream reservoir ($Q_{f,i}$) has the same type of formulation as the equation 5.1. This formulation is presented in equation 5.9. It uses a time constant τ_f which is a slower than the stream reservoir time constant.

$$Q_{f,i} = \frac{V_{f,i}}{\tau_f * \Lambda_{S,i}} \quad (5.9)$$

The floodplains scheme allows a specific HTU to "overflow" the content of its floodplains reservoir into the upstream HTUs with floodplains which are directly connected to the concerned HTU as shown in Figure 5.3. This process is driven by the difference in height between the elevation of the water and that of the neighbouring HTUs:

$$\Delta h_{i,j \in \{i-1/2\}} = \max((z_i + h_i) - (z_j + h_j), 0) \quad (5.10)$$

with:

- z : the orography at the outflow of the HTU
- h : the height of the floodplains

As long as $\Delta h_{i,j \in \{i-1/2\}} = 0$, there is no overflow ($O_{i,j \in \{i-1/2\}} = 0$). When the water rises over the elevations of the upstream HTU, the overflow is enabled. The flux is proposed to be:

$$O_{i,j \in \{i-1/2\}} = \Delta h_{i,j} \frac{S_{f,i} S_{f,j}}{S_{f,i} + S_{f,j}} \frac{1}{OF} \quad (5.11)$$

with OF the time constant of the overflow (in seconds).

The term $\frac{S_{f,i} S_{f,j}}{S_{f,i} + S_{f,j}}$ allows to give an estimate of an equivalent surface considering both HTUs. It avoids some undesirable effects of excessive overflow value in case the HTU considered has a very small surface due to a border effect. This is implemented in order to (1) consider the size of both HTUs and (2) avoid instability issues.

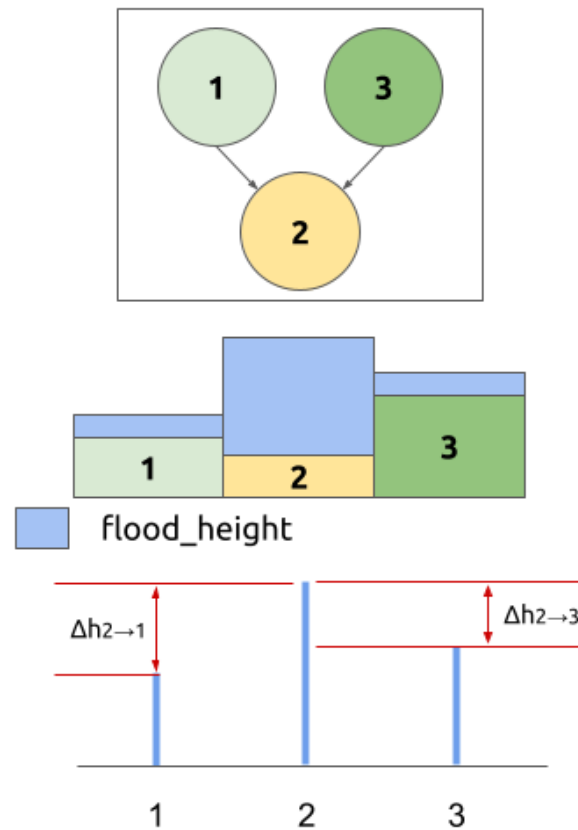


Figure 5.3. Schematic representation of the definition of the water involved in the overflow.

If the values of the OF time constant are too low, this generates instabilities (the lower OF , the more important the overflow). For example, if the HTU i overflow in various upstream HTUs, an excessive transfer of water at once will leave a negative volume in the floodplains reservoir. It is possible to increase the overflow without generating instabilities by using a slower time constant OF and by repeating the overflow operation several times during the same time step. The number of repetition of the overflow water transfer within a single time step is defined by the parameter OF_{repeat} .

5.2.4 Floodplains geometry

Another crucial aspect of the floodplains scheme is the relationship between the volume of water in the floodplain reservoir ($V_{f,i}$), the surface of open water and the height of water. In order to establish a simple but meaningful relationship, some assumptions have to be made on the geometry of the floodplains.

As the HTUs are constructed from higher resolution hydrological data, it is possible to construct a direct and detailed relationship using the topography data from the hydrological pixels (Dadson et al, 2010; Zhou et al, 2021c; Fleischmann et al, 2021b; Chaney et al, 2020). But this method would bring two different issues: (1) the uncertainty of the topography over lowlands such as floodplains and (2) the high computational memory cost. The memory cost involved may not necessarily be worth the improvement it would bring to the simulation.

For this reason, the definition of the floodplains shape has been simplified by using two variables controlling the shape of the floodplains such as proposed by D'Orgeval (2006) and shown in Figure 5.4.a. These variables are the following:

- $h_{0,i}$: the height at which the floodplains of the HTU are fully covered, i.e. $S_{f,i} = S_{f,max}$.
- β_i : the shape of the floodplain which will control how quickly it fills. $\beta_i > 1$ corresponds to a floodplain with a concave cross section (as figure 5.4.a) whereas $\beta_i < 1$ corresponds to a floodplain with a convex cross section. $\beta_i = 1$ represents a triangular cross section which fills linearly.

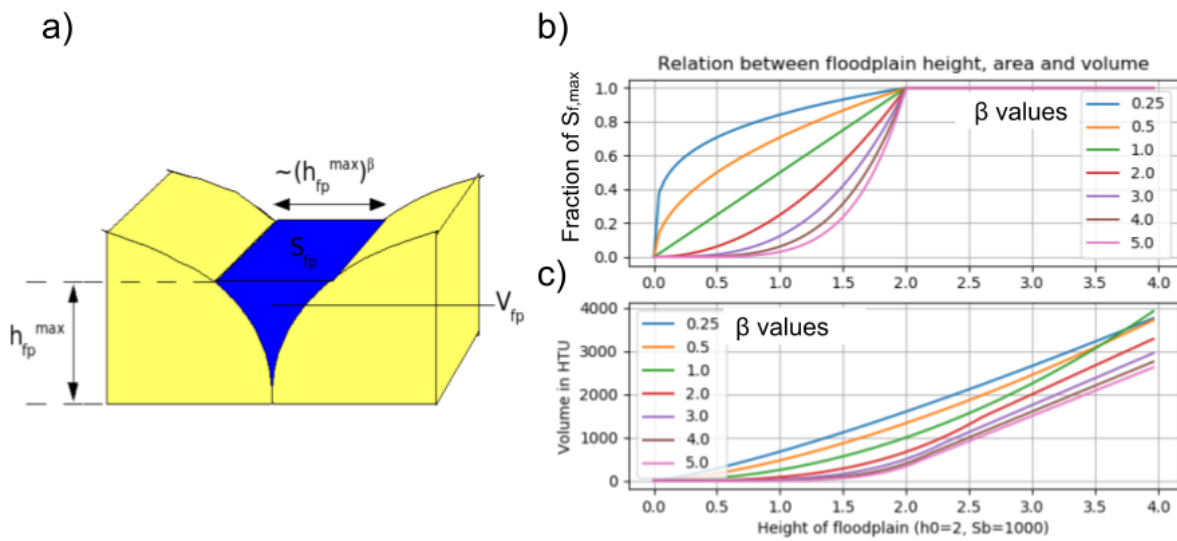


Figure 5.4. (a) Figure 4.9 from Tristan d'Orgeval's thesis representing the parameterization of the floodplains shape, (b) relationship between the floodplains area and floodplains height depending on β parameter with $h_0 = 2m$ and $f_{max} = 1$ and (c) relationship between the volume in the floodplains reservoir and the height of the floodplains depending on the value of the β parameters for $h_0 = 2m$.

In D'Orgeval (2006), both variables have been set to constant values: $\beta = 2$ and $h_0 = 2m$. With the high resolution floodplains scheme, it is possible to define β and h_0 with more precision using the characteristics of the hydrological pixels combined within an HTU.

The spatial representation of the floodplains in an HTU i is defined by the relationship between the volume of water in the floodplains $V_{f,i}$, the surface of the floodplains $S_{f,i}$ and the height of the floodplains h_i . It is considered that at a certain height h_0 , the whole floodplain is flooded, i.e. $S_f = S_{f,max}$ and that, even if the floodplains height is higher than h_0 , the flooded area cannot exceed this limits (cf. equation 5.12). The shape of the floodplains will have an influence only for $h_i < h_0$ because above h_0 , the height is considered to increase linearly with the volume.

$$f_i = \frac{\min(S_{f,i}, S_{f,max,i})}{S_{B,i}} \quad (5.12)$$

If we consider a HTU i which is fully considered as floodplains, i.e. with $f_{max,i} = 1$ or $S_{f,max,i} =$

S_i , the relationship between the flooded area $S_{f,i}$ and the height of the floodplains h_i for $h_i < h_0$ is represented in equation 5.13.

$$S_{f,i} = S_{B,i} \left(\frac{h_i}{h_{0,i}} \right)^{\beta_i} \quad (5.13)$$

This assumes that the shape of the HTU is an exponential function and with the choice of β it can be decided how quickly it fills. The relation between the floodplains height and the volume in the floodplains reservoir is obtained by integrating this function between 0 and h_i :

$$V_{f,i} = \frac{S_{B,i}}{\beta_i + 1} \frac{h_i^{\beta_i + 1}}{h_{0,i}^{\beta_i}} \quad (5.14)$$

This provides the Γ function introduced above to calculate the surface from the volume. The above equations are only valid for $h \leq h_{0,i}$. If $h_i > h_{0,i}$, we have $S_{f,i} = S_{fmax,i}$. The equation 5.15 shows the relationship between the flooded surface and the volume in the floodplains reservoir by combining the equations 5.13 and 5.14.

$$S_{f,i} = \Gamma(V_{f,i}) = \max\left(\frac{S_{B,i}}{h_{0,i}^{\beta_i}} \left[\frac{(\beta_i + 1) h_{0,i}^{\beta_i} V_{f,i}}{S_{B,i}} \right]^{\frac{\beta_i}{\beta_i + 1}}, S_{fmax,i} \right) \quad (5.15)$$

In order to generalize, the floodplains height above h_0 increases linearly with the volume. Considering $V_{fmax,i}$ the volume at which $\Gamma(V_{fmax,i}) = S_{fmax,i}$. For $V_{f,i} > V_{fmax,i}$, the flooded surface and the floodplains height in the HTU i follows respectively the equation 5.16 and 5.17.

$$S_{f,i} = S_{fmax,i} \quad (5.16)$$

$$h_i = h_0 + \frac{(V_{f,i} - V_{fmax,i})}{S_{fmax,i}} \quad (5.17)$$

5.2.5 Ancillary data

ORCHIDEE's high resolution routing

The routing in ORCHIDEE has been constructed by the routing preprocessor (RoutingPP) presented in the Chapter 4. It allows combining different high resolution hydrological information to construct the HTUs and calculate their characteristics. In this case, the routing graph have been constructed using the MERIT-Hydro dataset.

Spatial description of the floodplains

The Global Lake and Wetland Database (GLWD - WWF, 2004) available at a 1 km resolution has been interpolated at the MERIT-Hydro resolution in order to define a floodplains mask using the three following categories: (1) Freshwater Marsh, Floodplains; (2) Reservoir; (3) Pan, Brackish Saline Wetland. Therefore, the floodplains mask is available for each pixel of the hydrological data. This data allows the calculation of the maximal flooded area within each HTU

during the routing construction.

Orography and shape of the floodplains

The orography is a variable available for each pixel in the hydrological datasets. Therefore, the orography of the different pixels within a HTU is known. Considering a HTU i , the reference orography is defined by the orography of the outflow pixel (z_i) meanwhile $h_{0,i}$ is the lowest difference of orography between z_i and its upstream HTUs reference orography (cf. equation 5.18).

$$h_{0,i} = \min_{j \in \{i-1\}} (z_j - z_i) \quad (5.18)$$

The β variable has been estimated using the standard deviation of the distribution of the orography including the values for all the pixels being part of each HTU. The different values of standard deviation are bounded by $\text{lowlim_std} = 0.05m$ and $\text{uplim_std} = 20m$ and are then converted to obtain the β variable which ranges between values of $\text{lowlim_beta} = 0.5$ and $\text{uplim_beta} = 2$.

$$\text{std_orog_bounded}(i) = \begin{cases} \text{lowlim_std} & \text{if } \text{std_orog}(i) < \text{lowlim_std} \\ \text{uplim_std} & \text{if } \text{std_orog}(i) > \text{uplim_std} \\ \text{std_orog}(i) & \text{elsewhere} \end{cases} \quad (5.19)$$

$$\beta_i = \frac{\text{std_orog_bounded}(i)}{\text{uplim_std} - \text{lowlim_std}} (\text{uplim_beta} - \text{lowlim_beta}) \quad (5.20)$$

With the hypothesis that $h_{0,i}$ is the height at which the floodplain of the HTU i is totally covered, this height is assumed to be the minimum of the difference between elevation of the vertex i and the ensemble of its inflows which have floodplains ($\{i-1\}$). When h_i is larger than this difference, it means that the floodplain of i will be able to overflow to the upstream vertices.

Calibration of the parameters

The different parameters of the floodplains scheme have been adjusted based on the simulated discharge at the Porto Murtinho station considering to the observations considering : (1) the temporality of the discharge through its correlation with the observations and (2) the mean value and variability of the discharge. The parameters have been adjusted in the following order :

1. τ_f and R_{limit} : the floodplain reservoir time constant and the discharge limiter which have the greater influence on the discharge (temporality, mean value and variability). The interval considered for τ_f is $[\tau_{stream}, \tau_{fast}]$ because the flow from the floodplains is considered as slower than the stream reservoir but faster than the fast reservoir. R_{limit} was searched in the interval $[0,1]$. The best combination of parameter has been established through a grid-search method which consists in evaluating the different combination of parameters within their respective interval of definition.

2. OF and OF_{repeat} : these parameters slightly influence the temporality of the discharge. The interval considered for OF was [0.5 day, 2 days] and for OF_{repeat} it was [1,5].
3. C : the infiltration constant which has no influence on the temporality of the discharge but which is able to reduce / increase it. The interval considered for C is [0,1].

The values of the parameters found depended on the resolution of the atmospheric forcing and are shown in Table 5.1. The parameterization for the 0.5° resolution has been established with WFDEI_GPCP and the 20 km resolution with AmSud_GPCP which are both described with more details in the following section.

Resolution	0.5°	20 km
τ_f	15	20
R_{limit}	0.4	0.4
OF	0.5	0.5
OF_{repeat}	3	3
C	0.7	1

Table 5.1. Parameterization of the floodplains scheme depending on the resolution of the atmospheric grid.

5.2.6 Workflow of the Module

The workflow of the high resolution floodplains scheme in ORCHIDEE is presented in Figure 5.5. First the transport of water from fluxes flowing downstream is performed. It concerns all the fluxes except the overflow. Then the floodplains height and flooded fraction of each HTU are calculated and then the overflow is calculated. After transferring the water of the overflow, the flooded fraction of the HTU is re-estimated with the adjusted volume of the floodplains reservoir. If the overflow is repeated more than once, the floodplains height and floodplains fraction are updated between each operation.

5.3 Methodology and Dataset

5.3.1 Model Description: ORCHIDEE

The simulations presented here are offline simulations forced by an external atmospheric dataset containing the atmospheric informations required to run the model (downward long and shortwave radiations, precipitation, 2-m air temperature, wind speed, 2-m specific humidity, snowfall and rainfall).

Extra ancillary datasets provide the information about the vegetation cover and the soil composition. The vegetation cover is described for each grid cell by the fraction of each one of

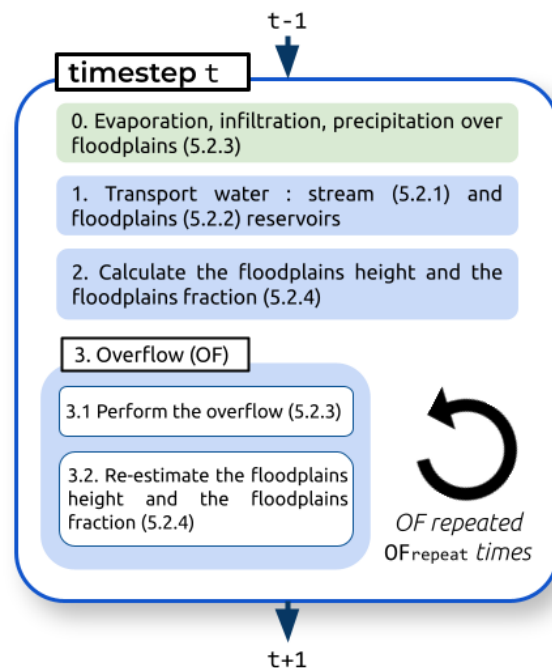


Figure 5.5. Workflow of the floodplains processes over a time step.

the 12 Plant Functional Types (PFT) representing different types of vegetation and the proportion of bare soil. The soil composition is described by the combination of the three main soil textures: coarse, medium and fine from the USDA soil description (Reynolds et al, 2000). For vegetation, the ESA 2.0.7 dataset (used for the IPSL's CMIP6 simulations) has been used.

The hydrology in ORCHIDEE is represented through a 11-layer soil scheme (De Rosnay et al, 2000; de Rosnay et al, 2002; Campoy et al, 2013) representing the vertical movement of the water in the soil and the transfer of heat.

5.3.2 Methodology of Validation

The evaluation of the high resolution floodplains module consists of two different evaluations which include various experiments. Each experiment is composed by a pair of simulations forced by the same atmospheric forcing. Each pair of simulations contains one simulation with the floodplains scheme deactivated (NOFP) and the other with the floodplains scheme activated (FP). As these simulations are forced by an offline atmospheric forcing, it should be reminded that the atmospheric conditions are fixed and the model does not interact with the atmosphere and don't affect the atmospheric conditions.

The first evaluation consists in the comparison of 4 experiments: two are using the previous 0.5° floodplains scheme of ORCHIDEE (based on the low resolution version of the routing scheme) and two are using the high resolution floodplains scheme presented here (based on the high resolution routing scheme). Two different forcings are used. Each forcing is used for one experiment using the low resolution floodplains scheme and one experiment with the high resolution floodplains scheme. The second evaluation evaluates with more details the representation of the high resolution floodplains scheme by comparing (1) an experiment with

a 0.5° atmospheric forcing and (2) an experiment with a 20km resolution forcing.

For the first evaluation, the atmospheric forcings includes the third phase of the Global Soil Wetness Project (GSWP3; Kim, 2017) and the CRUNCEP version 7 (Viovy, 2018). GSWP3 is based on the second version of the twentieth century Reanalysis (20CR) which is a six hourly global product at a 2° resolution from the NCEP land-atmosphere model (Compo et al, 2011). GSWP3 is constructed by (1) a dynamic downscaling of CR20 at a 0.5° resolution with a spectral nudging technique and (2) a bias correction of the precipitation by the GPCC v6 monthly data. CRUNCEPv7 is an interpolation at a 0.5° resolution of the National Center for Environmental Prediction National Center for Atmospheric Research (NCEP-NCAR) 6-hourly reanalysis. The precipitation in CRUNCEPv7 is bias corrected using the monthly data at 0.5° from the Climatic Research Unit (CRU TS3.24, Harris et al, 2014). This first evaluation is performed for the 1960-2000 as it will permit the comparison of the results from the high resolution floodplains scheme to the simulation performed with the 0.5° floodplains scheme in Schrapffer et al (2020). It should be noticed that the ancillary data used to define the floodplains over the Pantanal region differs between the LR and HR version. The main difference concerns the region at the Northwest of the Pantanal considered as floodplains only in the LR version.

For the second evaluation, the 0.5° resolution atmospheric forcing is the WFDEI.GPCC forcing data (Weedon et al, 2014) which is already described in Chapter 4 and the 20km atmospheric forcing AmSud_GPCC (see more details here: <https://gitlab.in2p3.fr/ipsl/lmd/intro/regipsl/regipsl/wikis/AmSud>), based on the bias-correction of the AmSud simulation by the GPCC dataset. AmSud_GPCC is based on AmSud, a 30 years simulation performed with the RegIPSL regional model which couples the Weather Research and Forecasting (WRF v3.7.1; Skamarock et al, 2008) and the ORCHIDEE land surface model from 1990 to 2019 and forced with ERA5 re-analysis data. The configuration of this simulation is presented with more details in Chapter 4. The AmSud simulation didn't include any type of floodplains scheme. The precipitation in AmSud_GPCC is the precipitation from AmSud which has been bias-corrected by GPCC monthly precipitation adjusting the monthly precipitation total by a multiplicative factor for each grid point. This is principally to correct the negative biases of precipitation over the Southern Amazon and Northern La Plata Basin (i.e. the Upper Paraguay River Basin). This evaluation will be performed over the 1990-2013 period as it is the common period for both forcings. It must be emphasized that none of these forcings includes the impact of the floodplains and, thus, includes possibly large biases in the temperature and humidity provided. The annual cycle of the different variables over the UPRB in the AmSud_GPCC and the WFDEI_GPCC forcings are presented in Figure 5.6. Although they have a similar precipitation, AmSud_GPCC has a much higher downward shortwave radiation, a lower near-surface specific humidity and an higher near-surface temperature. These will results in an higher evaporative demand in the simulations forced by AmSud_GPCC.

5.3.3 Discharge

The National Hydro-meteorological Network managed by the Brazilian National Water Agency (Agência Nacional de Águas - ANA) has provided the monthly river discharge observations for

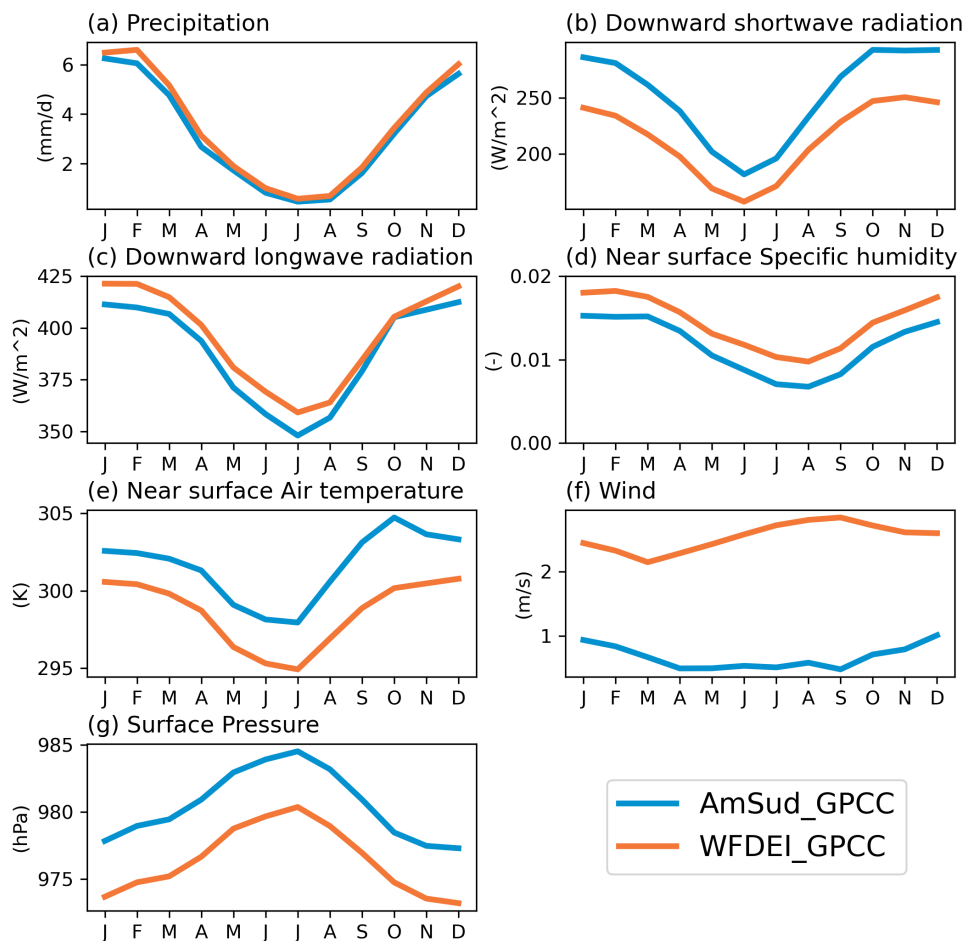


Figure 5.6. Annual cycle of the variables in the atmospheric forcings WFDEI_GPCC and AmSud_GPCC between 1990 and 2013 over the Upper Paraguay River Basin (UPRB).

the Porto Murtinho station.

This station is considered as the reference outflow for the Pantanal (Schrapfer et al, 2020; Penatti et al, 2015). Moreover, its large continuous data record allows more freedom to choose the period of simulation to evaluate the floodplains scheme.

5.3.4 Statistical indexes

Statistical indexes are precious tools to quantify and discuss the performance of a model. For this reason, different statistical indexes are used in this chapter to evaluate the behaviour of the simulated discharge at the Porto Murtinho station compared to the observed values. The statistical indexes used in this chapter are described in the present section, the mathematical formulations of these indexes use the following nomenclature: N is the total number of time steps considered, M_t represent the model value at the timestep t and O_t the observation corresponding to this time step, \bar{O} will represent the mean value of the observations over the interval of timesteps $[1, N]$.

The Nash-Sutcliffe model efficiency coefficient (NSE) allows to compare the performance of the model to the mean value of the corresponding observed variable. It can be calculated

by the equation (5.21). Its values are in the range $]-\infty, 1]$ with 1 corresponding to a model perfectly representing the observed variable. For values of NSE lower than 0, the variable might be better estimated by the mean value of the observations.

$$NSE = 1 - \frac{\sum_{t=1}^N (M_t - O_t)^2}{\sum_{t=1}^N (M_t - \bar{O})^2} \quad (5.21)$$

The Percent Bias (PBIAS) is an indicator allowing to evaluate systematic bias in the model compared to the observations. Positive values means that the model might be overestimating the variable while negative values mean the opposite. The equation of the PBIAS index is represented in the equation (5.22).

$$PBIAS = 100\% * \frac{\sum_{t=1}^N (M_t - O_t)}{\sum_{t=1}^N O_t} \quad (5.22)$$

The Root Mean Square Error (RMSE) is a classical index which is used to evaluate the performance of the model. The RMSE is a positive number representing the error in the same unit as the variable evaluated. It can be calculated by the equation (5.23).

$$RMSE = \sqrt{\frac{\sum_{t=1}^N (M_t - O_t)^2}{T}} \quad (5.23)$$

The correlation between the simulated and observed discharge is also presented along with the information of the significance of this correlation at a 95% level using a two-tails test.

5.3.5 Flooded area

Another important aspect of the floodplains scheme is the representation of the flooded area that will further impact the surface fluxes and thus the atmosphere. Depending on the period of the simulations, the flooded area simulated will be assessed by different estimates of the flooded area over the Pantanal.

The evolution of the flooded area over the 20th century has been estimated by [Hamilton et al \(1996\)](#) and [Hamilton \(2002\)](#) extrapolating the correlation between river height and the flooded area established between 1979 and 1987. [Padovani \(2010\)](#) performed a satellite estimate of the flooded area by applying a Linear Spectral Mixture Model to using MODIS data between 2002 and 2009. Their detection techniques are discussed in more detail in Chapter 2. Apart from [Hamilton \(2002\)](#) [Padovani \(2010\)](#), the satellite estimate of the flooded area based on the mNDWI index presented in Chapter 3 is also used to assess the flooded area in the FP simulations.

The Global Inundation Extent from Multi-Satellites database version 2 (GIEMS-2; [Prigent et al, 2020](#)) is a satellite estimate of flooded areas (agricultural irrigation and wetlands) which is principally constructed using passive microwaves observations but also using visible and near-infrared reflectance data from optical satellites. GIEMS-2 is a global monthly dataset available at a 0.25° resolution between 1992 and 2015. As for the GIEMS version 1, the GIEMS-2 is

largely use to validate the floodplains representation in different models (Zhou et al, 2021c; Marthews et al, 2021).

Fluet-Chouinard et al (2015) generated a downscaled version at a 15-arcsecond resolution of the Global Inundation Extent from Multi-Satellites database version 1 (GIEMS-D15). Figure 5.7 shows a high resolution map over the Pantanal of the climatological number of month for which each pixel is flooded. It has been elaborated considering the period between 1993 and 2004. This climatological map will serve to complete the comparison of the spatial representation of the flooded area.

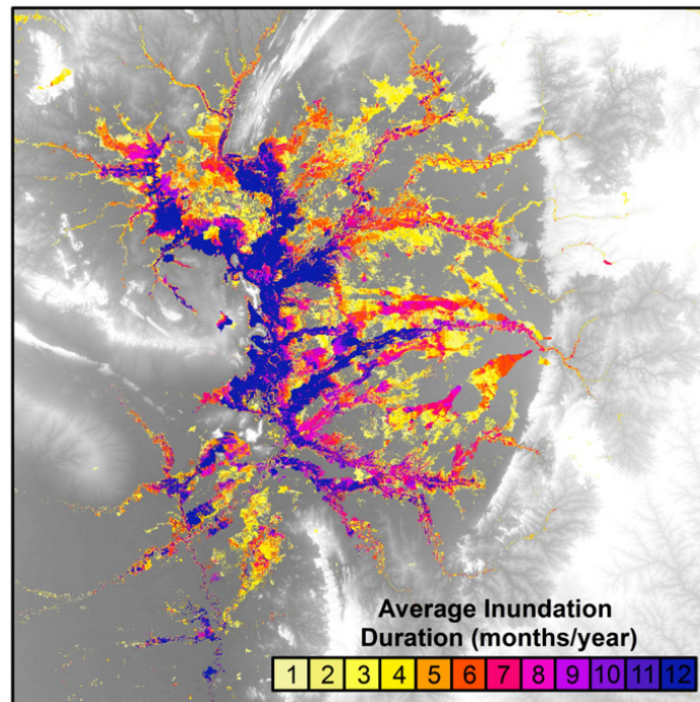


Figure 5.7. Mean duration in months of the floods over the Pantanal in the monthly GIEMS-D15 product over the 1993-2004 period (extracted from Fluet-Chouinard et al, 2015).

5.3.6 Water Storage

The evaluation of the discharge and the flooded area will be completed for AmSud_GPCC and WFDEI_GPCC by the evaluation of the total water storage (TWS) over the region.

This evaluation can be done by comparing the evolution of the water available in ORCHIDEE over the Pantanal by considering the different reservoirs of the routing scheme (slow, fast, stream and floodplains) and the soil moisture, to the estimate of the water storage from the GRACE satellite.

The Gravity Recovery And Climate Experiment (GRACE; Schmidt et al, 2008) satellite mission is an US-German collaboration launched in March 2002. The GRACE twin satellite aims to estimate the changes of the mass redistributions near the surface which are related to different processes by evaluating the changes of the gravity fields (using 2 satellites in motion). The

use of the GRACE satellite product for hydrology requires a large spatial resolution in order to reduce the error. In order to reduce the signal to noise ratio, it is recommended to use GRACE at spatial scale of 90000 km² (Vishwakarma et al, 2021). The extension of the Pantanal is large enough to be able to use GRACE. GRACE data represents the anomaly of water storage normalized by the values obtained during the 2004-2010 period. The data from GRACE is available between 2002 and 2016.

5.4 Results

This section will refer to the simulations using their forcing, the version of the routing scheme used in ORCHIDEE and to the activation or not of the floodplains scheme (FP or NOFP). The previous routing scheme will be referred to as "low resolution routing scheme" (LR) while the new version of the routing will be referred to as "high resolution routing scheme" (HR).

5.4.1 Comparison with the previous version

a) Discharge

The pair of simulations forced by CRUNCEPv7 and GSWP3 between 1961 and 2000 using the previous version of the floodplains scheme (presented in Chapter 2) are compared to a pair of simulations forced by the same forcings but using the high resolution routing scheme.

Firstly, the discharge at the outflow of the Pantanal must be assessed as it represents the different aspects of the hydrology of the upstream region, i.e. the Pantanal and the Cerrado. In order to have a global view of the representation of the floodplains in the model, Figure 5.8 shows the Taylor diagram for the full periods (1961-2000) for the different simulations. The performance of the high resolution simulations without floodplains (HR_NOFP, circles) is degraded in comparison to the low resolution simulations without floodplains (LR_NOFP, stars). The correlation is the most affected as it decreases from around 0.5 to -0.1/0.1. However the performance of the simulation of the river discharge at Porto Murtinho in the simulations with the floodplains scheme activated is similar in both low (LR_FP, cross) and high resolution routing scheme (HR_FP, square). The NOFP simulations were all strongly overestimating the standard deviation of the discharge (between 50% and 150%) while the FP simulations are closer to the observations and distributed around the observed value. The LR_FP simulations have a higher standard deviation than the HR. As the standard deviation is strongly overestimated for GSWP3_LR_FP, the reduced standard deviation in GSWP3_HR_FP is closer to the observation. However, the standard deviation in CRUNCEPv7_LR_FP is already close to the observations so the reduction of the standard deviation in CRUNCEPv7_HR_FP leads to an underestimation of the standard deviation. In conclusion, although the difference between the simulations are partly influenced by the version of the routing scheme, the uncertainty of the forcing used is playing an important role in these differences.

This first analysis of the discharge over the full period can be completed by an analysis of the concentration period and concentration degree of this variable in Figure 5.9. The con-

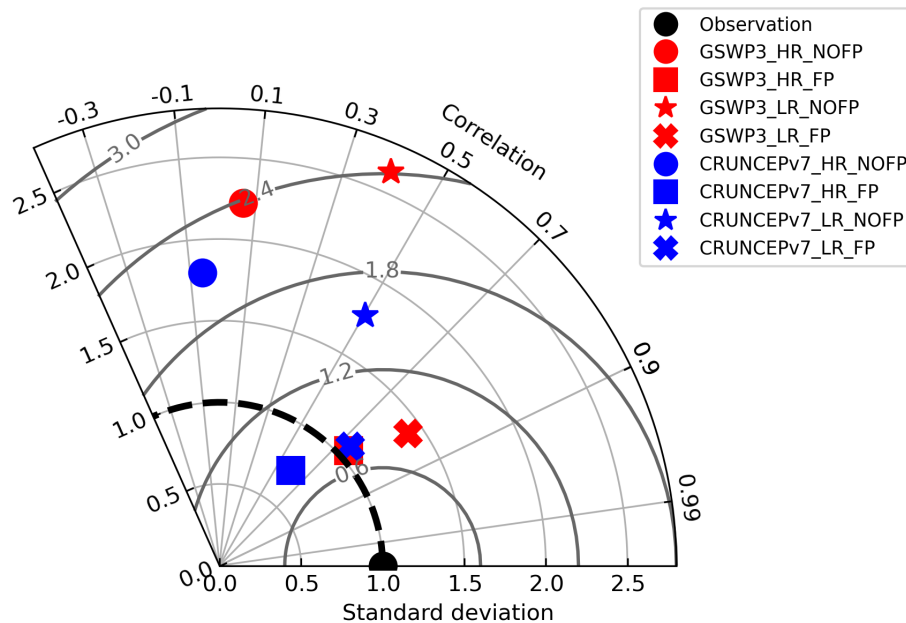


Figure 5.8. Normalized Taylor Diagram for the discharge at Porto Murtinho between 1961 and 2000 for the pair of simulation (with -FP- and without -NOFP- floodplains) forced by the GSWP3 and CRUNCEPv7 with the previous floodplains scheme (LR) and the high resolution floodplains scheme (HR).

concentration period and concentration degree have already been introduced in Chapter 2. The Concentration Period and Concentration Degree diagram (Figure 5.9.a) shows similar results as the Taylor diagram from the Figure 5.8. The observed concentration period is around June and the concentration degree of the LR_NOFP simulations has a concentration degree which is closer to the observations (March/April) than the HR_NOFP simulations (February). The Concentration Period of the FP simulations are in June and, thus, are closer to the observations. For the concentration degree, the NOFP simulations are all overestimating it with values around 0.3 while the FP simulations are closer to the observed value which is around 0.15. For GSWP3, the concentration degree with the floodplains is improved with the HR river routing scheme compared to the LR river routing scheme.

In order to better understand how the model performs under different conditions, the Figure 5.9.b-e shows the annual cycle of the discharge in two different periods: 1961-1975 (b and d) which corresponds to a dry period (Bergier, 2010; Alho and Silva, 2012) and 1980-2000 (c and e) which corresponds to a wet period (Padovani, 2010). The annual cycle of the discharge for the FP simulations is always well correlated with the observations but we observe some differences between GSWP3 and CRUNCEPv7. Considering only the LR routing, the result for the FP simulations seems to depend strongly on the forcing. For example, the better performance of CRUNCEPv7_LR_FP compared to GSWP3_LR_FP during the dry and wet period is related to the differences in precipitation between both forcings. This can be related

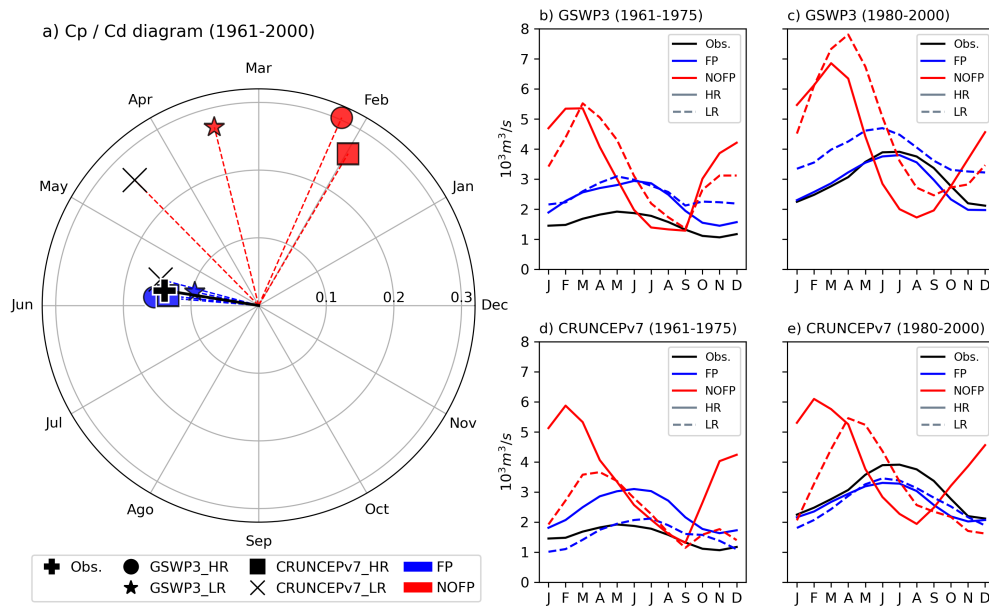


Figure 5.9. (a) C_p / C_d diagram for the discharge at Porto Murtinho between 1961 and 2000 for the pair of simulation (with and without floodplains) forced by the GSWP3 and CRUNCEPv7 with the previous floodplains scheme (LR) and the high resolution floodplains scheme (HR). Annual cycle for the discharge at Porto Murtinho for the simulations forced by GSWP3 (b and c) and CRUNCEPv7 (d and e) for the dry period from 1961 to 1975 (b and d) and for the wet period from 1980 to 2000 (c and e).

to the fact that CRUNCEPv7 has a lower precipitation than GSWP3 (cf. lower mean discharge for all the simulations during the dry and the wet period). Considering the differences between the LR and HR simulations, the results for the FP simulations depends on the forcing and on the period. For example during the dry period, the annual cycle of the discharge is similar between the HR_FP and LR_FP simulations forced by GSWP3 while, in the simulation forced by CRUNCEPv7, the HR_FP simulation overestimates the discharge compared to the LR simulation. During the wet period the opposite happen, the floodplains simulations forced by CRUNCEPv7 are similar while the GSWP3_LR_FP overestimates the discharge compared to GSWP3_HR_FP.

To complement the analysis of the discharge, some statistical indexes have been calculated and are presented in Table 5.2. The NSE and the correlation are higher in the FP simulation compared to the NOFP for all simulations except for the NSE index in the CRUNCEPv7_HR simulations. The PBIAS and the RMSE are lower in FP compared to the NOFP in all pair of simulations. The decrease of the PBIAS leads in all cases to values closer to 0, thus the bias of the discharge compared to the observations is reduced due to the floodplains scheme. For the CRUNCEPv7_HR simulations, the decrease of the NSE between NOFP and FP can be related to the strong overestimation of the discharge in FP during the dry period (cf. Figure 5.9).

As seen previously, representation of the discharge is degraded in the HR_NOFP simulations compared to the LR_NOFP simulations. It seems to be principally due to an increased delay between the annual cycle of the simulated and observed discharge which affects the correlation, PBIAS and NSE indexes. The peak in the annual cycle of HR_NOFP is sooner than in

Forcing	NSE	PBIAS	RMSE	Corr %
CRUNCEPv7_LR_NOFP	0.22	16.84	334.93	0.51*
CRUNCEPv7_LR_FP	0.42	-8.32	175.13	0.75*
GSWP3_LR_NOFP	0.11	71.26	622.90	0.41*
GSWP3_LR_FP	0.45	40.15	266.72	0.82*
CRUNCEPv7_HR_NOFP	-0.32	52.79	533.33	-0.05
CRUNCEPv7_HR_FP	-0.72	2.53	199.52	0.59*
GSWP3_HR_NOFP	-0.15	52.94	578.09	0.07*
GSWP3_HR_FP	0.39	7.61	174.66	0.74*

Table 5.2. Comparison of the simulation between the high resolution floodplains scheme and the previous version of the floodplains scheme using statistical index (NSE, PBIAS, RMSE, Corr). The asterisk is used next to the value of the correlation if the confidence of the correlation is higher than 99%.

LR_NOFP Moreover, the correlation between the discharge in the HR_NOFP simulations and the observations is not even significant. It is difficult to evaluate if the HR_FP or LR_FP simulations have a better representation of the discharge because the conclusion would depend on the index considered and the atmospheric forcing used to force the simulation. For example, although LR_FP have higher NSE, HR_FP have a PBIAS value closer to 0. LR_FP has a lower RMSE for CRUNCEPv7 while HR_FP has a lower RMSE for GSWP3.

b) Flooded Area

Once the discharge has been assessed, another important aspect of the simulation of the floodplains is the representation of the flooded area. Over this specific period, the simulated flooded area can be compared to the [Hamilton \(2002\)](#) satellite estimate. The temporal evolution of the flooded area over the Pantanal is assessed in [Figure 5.10](#). The flooded area in the HR simulations is higher than the LR simulations. Nevertheless it doesn't seem to change between the wet and dry period in the HR simulations while it slightly increases in the LR simulations during the wet period ([Fig. 5.10.b](#)) compared to the dry period ([Fig 5.10.a](#)). The flooded area regime in all simulations corresponds to the value of the flooded area during the dry period (between 10 and 20 10^3 km²) and doesn't reach the higher flooded area during the wet period (30-70 10^3 km²).

It is also important to assess the spatial representation of the floodplains. As there aren't any gridded dataset available for the whole period, this aspect is assessed by comparing the different simulations with regards to the knowledge of the flood frequency over the region. [Figure 5.11](#) shows the flooded area for each forcing for the dry and wet period as well as the anomaly for the dry season (SON) and the flood season (MAM). The change of the mean flooded area between the dry and the wet period seems to be more important in the LR simulations and principally in the south of the Pantanal over the main Paraguay river. On the contrary, the difference between the dry season and the flood season is marked in every simulation

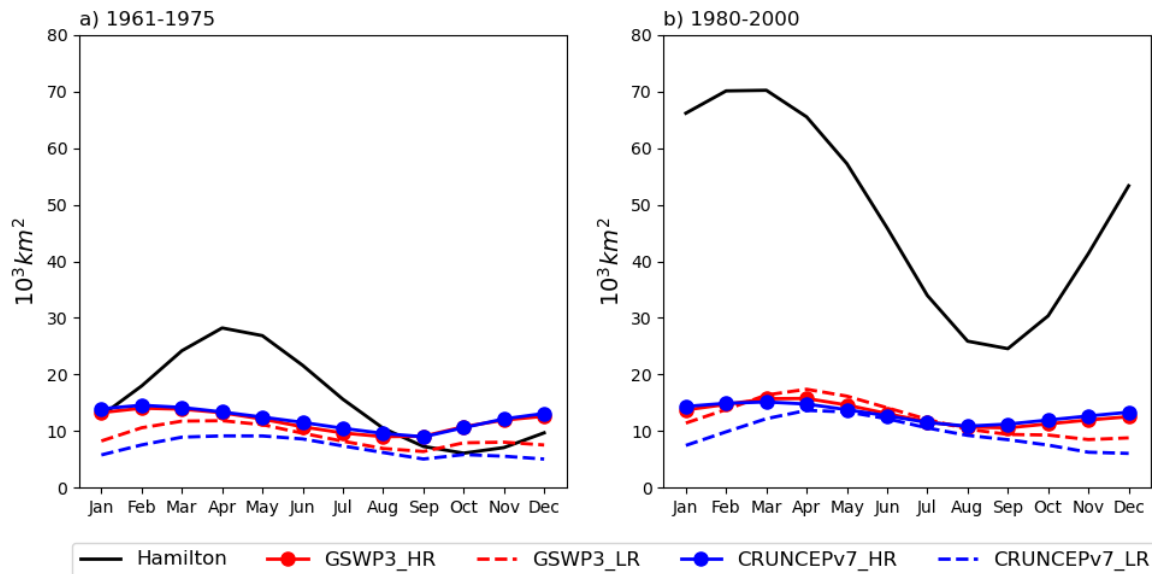


Figure 5.10. Annual cycle of the flooded area over the Pantanal for the different FP simulations (GSWP_HR, GSWP_LR, CRUNCEPv7_HR and CRUNCEPv7_LR) and the flooded area estimated by Hamilton (2002) for the dry period from 1961 to 1975 (a) and for the wet period from 1980 to 2000 (b).

although it seems to principally affect the South of the Pantanal in the LR simulation while it affects a much larger area in the HR simulations.

The main difference between the HR and the LR simulations is that the pattern of flooded area is more diffuse in the HR simulations while it remains over the main Paraguay river in the LR simulation. This difference is more important in the Central North Pantanal, this is related to the improved description of the river network and to the possibility of overflow in the high resolution floodplains scheme.

5.4.2 Assessment of the floodplains at different resolutions

a) Discharge

In this subsection, the main objective is to assess the floodplains scheme using two atmospheric forcings with different resolutions. The simulations are forced by AmSud_GPCC and WFDEI_GPCC. Both of these forcings have a similar precipitation climatology as they are both corrected by the GPCC dataset although the other atmospheric variables differ. The pair of simulations for each forcing are compared over the period they have in common: 1990-2013.

First, the simulations are assessed by the discharge over the entire period through a Taylor diagram in Figure 5.12. The correlation, RMSE and standard deviation of the simulations are improved for both forcings when activating the floodplains scheme. The correlation passes from -0.3 (AmSud_GPCC_HR_NOFP) and -0.1 (WFDEI_GPCC_HR_NOFP) to 0.55 (AmSud_GPCC_HR_FP) and 0.7 (WFDEI_GPCC_HR_FP). The RMSE decreases for both simulations from 3 to 1.1. In both cases, the standard deviation was strongly overestimated in the NOFP simulations and it decreased in the FP simulation reaching values closer to the observed standard

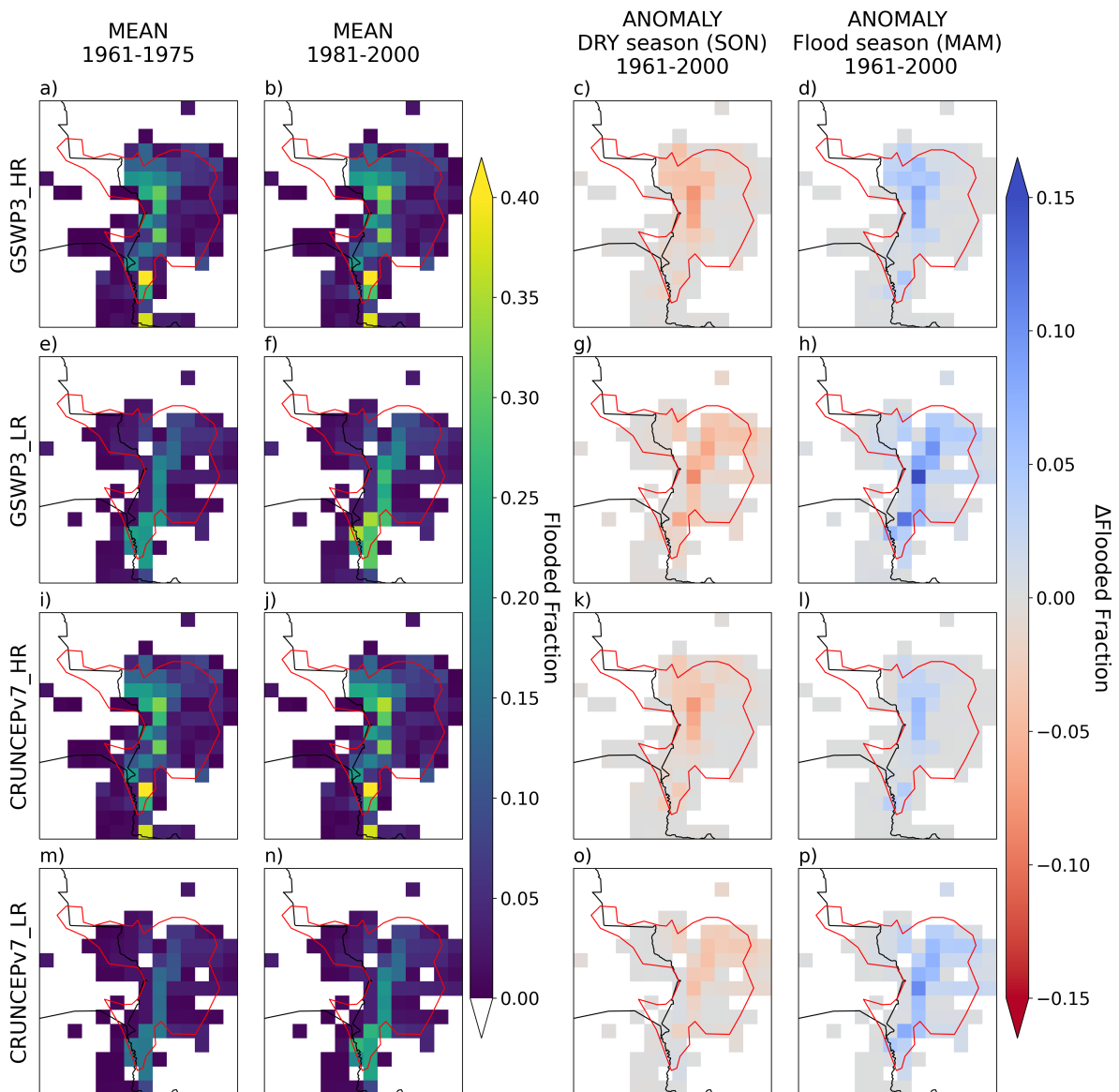
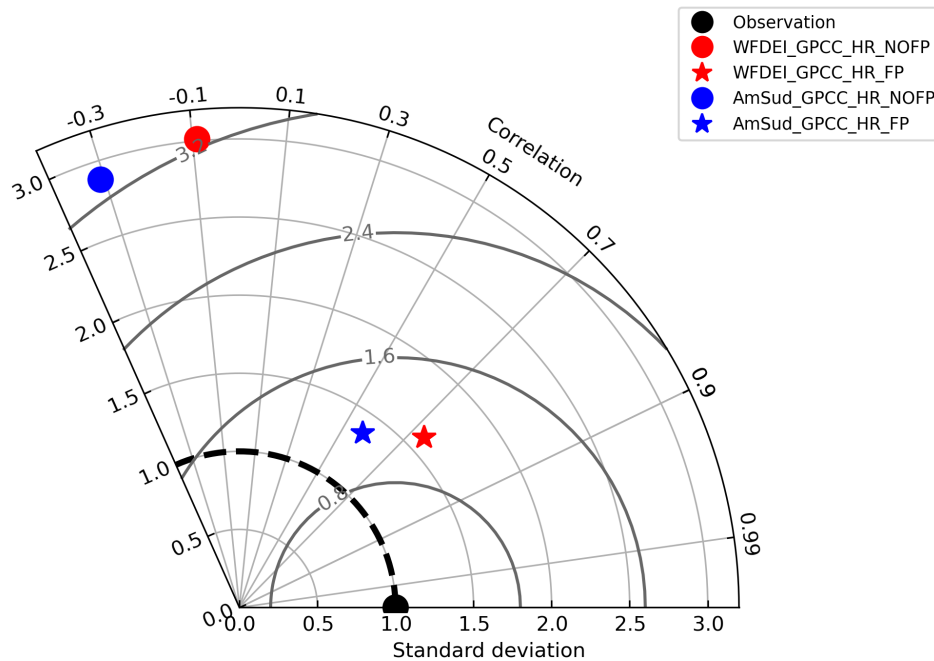


Figure 5.11. Map of the flooded area forced by GSWP3 (a-h) and CRUNCEPv7 (i-p) with the high resolution version of the floodplains (a-d; i-l) and with the previous version of the floodplains (e-h; m-p). The mean flooded area is presented for the period 1961-1975 (a,e,i,m), for the period 1981-2000 (b,f,j,n), the anomaly for the dry season - SON - between 1961 and 2000 (c,g,k,o) and the anomaly for the flood season - MAM - between 1961 and 2000 (d,h,l,p).

deviation.

This Taylor Diagram analysis is completed by Figure 5.13.a which presents the Concentration Period and Concentration Degree of the simulations as well as the annual cycle of the discharge at Porto Murinho. The observed Concentration period is by the end of May and the Concentration Period in the simulation is improved by the activation of the floodplains scheme as it goes from the end of January (AmSud_GPCC_HR_NOFP) and mid-February (WFDEI_GPCC_HR_NOFP) to the beginning of May for WFDEI_GPCC_HR_FP and end of May for AmSud_GPCC_HR_FP. The Concentration Degree is over 0.3 in both NOFP simu-



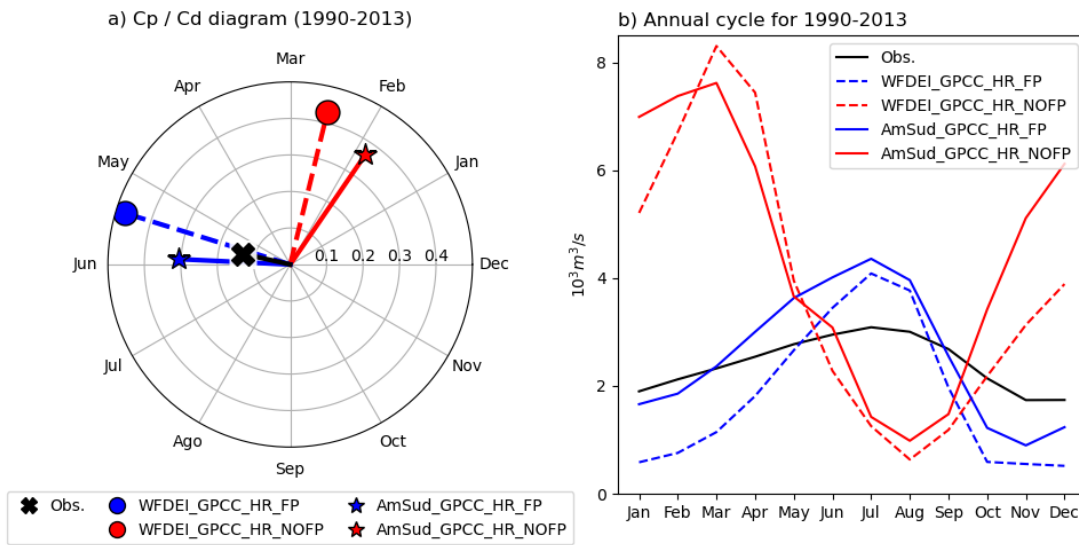


Figure 5.13. (a) Taylor Diagram and (b) annual cycle of the discharge at Porto Murtinho between 1990 and 2013 simulated by each pair of simulations (with -FP- and without floodplains -NOFP-) forced by WFDEI_GPCC and AmSud_GPCC with the high resolution floodplains scheme (HR).

in the representation of the discharge and, therefore, of the water cycle over the basin. For the same floodplains scheme, the lower resolution forcing has more difficulty to represent the baseflow and it results in a strong overestimation of the difference between the high and low value of discharge compared to the observations.

Forcing	NSE	PBIAS	RMSE	Corr
WFDEI_GPCC_HR_NOFP	-0.10	58.46	1213.59	-0.09
WFDEI_GPCC_HR_FP	0.44	-24.90	448.20	0.74*
AmSud_GPCC_HR_NOFP	-0.17	83.07	1321.88	-0.31
AmSud_GPCC_HR_FP	0.36	5.53	383.30	0.60*

Table 5.3. Evaluation of the discharge at the outflow of the Pantanal for the simulations with the high resolution routing scheme with and without the floodplains scheme activated forced by two atmospheric forcings with a different resolution (WFDEI_GPCC and AmSud_GPCC) using statistical index (NSE, PBIAS, RMSE, Corr).

b) Volume of Water

The evaluation of the volume of water in the WFDEI_GPCC and AmSud_GPCC pairs of simulations will help to understand the dynamic of the model in its representation of the water cycle at different resolutions. The volumes of water involved are also interesting to observe the impact of the floodplains scheme on the dynamic of the hydrology of the Upper Paraguay River Basin. The evolution of the total water storage over the Pantanal region in the simulations can be compared to the anomaly of Total Water Storage from GRACE. Due to its resolution, GRACE is a

coarse estimate but, compared to the simulations, it gives general overview of the representation of the water cycle in the model. This is a qualitative comparison because of GRACE resolution compared to the simulations. Therefore, the area considered to calculate the anomaly of the normalized Total Water Storage for GRACE and the simulation is a rectangle which goes from 61 to 53°W and from 15 to 21°S and which includes the Pantanal.

Table 5.4 shows the correlation between anomaly of total water storage from GRACE and the total volume of water in the simulations normalized by the values between 2004 and 2010 such as it is done in GRACE to calculate the anomaly. It shows that both FP and NOFP simulations have the same evolution as GRACE with a high and significant correlation. This means that the model is representing well the general evolution of the water over the Pantanal but that the floodplains has little impact on this balance.

Forcing	Correlation
WFDEI_GPCC_NOFP	0.951*
WFDEI_GPCC_FP	0.958*
AmSud_GPCC_NOFP	0.711*
AmSud_GPCC_FP	0.701*

Table 5.4. *Correlation between the anomaly of total water storage from GRACE and the volume of water in the different reservoir over the Pantanal region between 2003 and 2013 normalized by the mean and standard value between 2004 and 2010. The asterisk signals that the correlation has a level of significance higher than 99%.*

The volume of water in the Pantanal is explored with much details in Figure 5.14 which contains the annual cycle of the water volume within the different water reservoirs in the simulations average over the Pantanal. The floodplains scheme has the same impact on the reservoir for both forcings. The content of water in the slow reservoir (cf. Figure 5.14.a and b) is higher in the floodplains simulation. This is related to the floodplains infiltration increasing the water content of the slow reservoir. The water from the floodplains infiltration goes first into the Soil Moisture, this is why the water content of this reservoir increases in the FP simulation compared to the NOFP simulation (cf. Figure 5.14.i and j). Concerning the stream reservoir (cf. Figure 5.14.c and d), we observe a change that is similar to the change of the discharge at the Porto Murtinho station because this is the reservoir that drives the discharge. The water content in the fast reservoir (cf. Figure 5.14.e and f) is higher in the FP simulation compared to the NOFP simulation. This is related to the increase of the Soil Moisture that enhances the runoff. The floodplains reservoir (cf. Figure 5.14.g and h) has logically a value of 0 in the NOFP simulation and follows the evolution of the stream reservoir in the FP simulation because these reservoirs are connected.

The volumes of water are higher in WFDEI_GPCC for the fast, slow and stream reservoirs. This can be related to (1) the impact of the resolution of the atmospheric forcing on the hydrological dynamic and (2) to the higher evapotranspiration in AmSud_GPCC compared to WFDEI_GPCC. This higher evapotranspiration would decrease the soil moisture, the drainage and the runoff and, therefore, the fast and slow reservoirs. The stream and flood reservoir

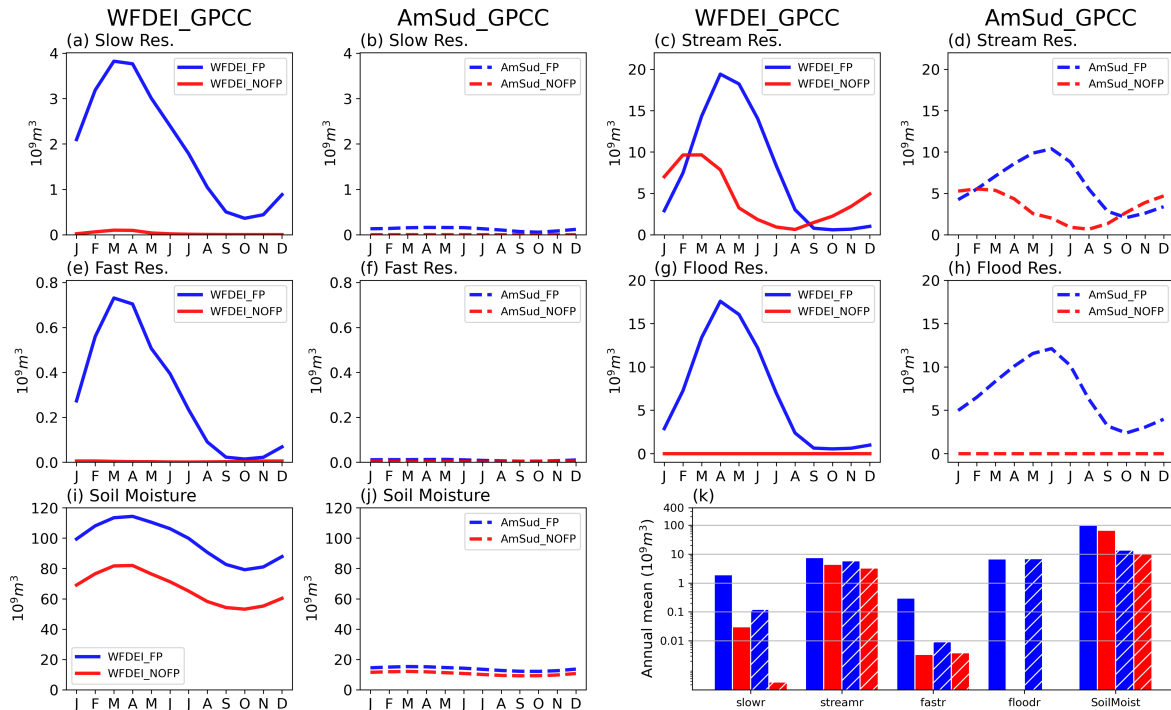


Figure 5.14. Annual cycle of the content of water in the different reservoir: slow (a-b), stream (c-d), fast (e-f), flood (g-h), integrated Soil Moisture (i,j) for the pair of simulations FP and NOFP forced by WFDEI_GPCC (a,c,d,e,g,i) and AmSud_GPCC (b,d,f,h,j). (k) shows the annual mean value of the water storage in the different reservoirs, a logarithmic scale is used to facilitate the comparison.

are less affected by an higher evapotranspiration over the Pantanal as their dynamic is more influenced by the water from the upstream areas that flows into the Pantanal. The origin of the issue with the overestimated variability of the discharge at Porto Murtinho in WFDEI_GPCC can be observed in the slow, fast, stream and floodplains reservoirs which have an annual cycle much more pronounced than AmSud_GPCC. The volumes of the fast, slow, stream and floodplains reservoirs reaches almost 0 during the dry period in WFDEI_GPCC_FP while it is not the case in AmSud_GPCC_FP. This allows AmSud_GPCC_FP to have a higher discharge during the dry period and, thus, a more realistic discharge.

The Soil Moisture over the Pantanal is the largest contribution to the total water storage followed by the stream reservoir and the floodplains reservoir in the FP simulations. The activation of the floodplains increases the Soil Moisture but is not impacting its temporal evolution. This explains why the floodplains scheme doesn't have an impact on the evolution of the total water storage over the Pantanal.

In conclusion, the floodplains involves relatively small volume of water compared to the total water storage over the region but these volumes are of great importance as they directly affect the river discharge and as they concern open-water surfaces which will impact the land-atmosphere interaction.

c) Flooded Area

The relatively small volumes of water in the floodplains are, in part, important because they are open water surfaces. Hence the importance of the assessment of the estimated flooded area. The resolution of the simulation will influence the estimated flooded area due to the hydrological dynamic changes and due to the different size / characteristics of the HTUs.

The evolution of the flooded area for the FP simulations is presented in Figure 5.15. In this case, the flooded area is compared to the observations over the period 1992-2013 as it allows to compare directly the simulations with different satellite estimates of the floodplains: GIEMS-2 (Prigent et al, 2020), Hamilton (2002) and Padovani (2010). The flooded area in WFDEI_GPCC is slightly lower than in AmSud_GPCC but the variability of the flooded area is higher in the WFDEI_GPCC simulation. This difference is related to: (1) the higher discharge in AmSud_GPCC and/or (2) to the difference of the volume/discharge relationship due to the grid resolutions. Despite the differences, the mean value of the flooded area is coherent in both simulations. There are discrepancies between the different satellite estimates, Hamilton tends to have higher values compared to GIEMS-2 while the opposite happens with Padovani and the mNDWI based satellite estimate from Chapter 3. The variability of the flooded area is underestimated for both forcings compared to the different observations. However, in some cases the mean value of the simulated flooded area corresponds to the lowest value of the satellite estimates such as it happens in the 1990's. After 2000, the mean value is more coherent with the mean annual value of the satellite estimates. The underestimation of the variability can be related to: (1) the volume of water in the floodplains / flooded area conversion, (2) different definitions for the flooded areas in the model and in the satellite estimates and (3) to the lack of flood in the grid cells adjacent to the main river.

GIEMS-2 also allows direct spatial evaluation of the flooded area in ORCHIDEE. Figure 5.16 represents the spatial representation of the flooded area averaged over the 1992-2013 period considering (1) all the months, (2) the anomaly during the dry season and (3) the anomaly during the flood season. The structure of the mean flooded area in AmSud_GPCC_HR_FP and WFDEI_GPCC_HR_FP is coherent with GIEMS-2 and, in particular, concerning the northern region and the central flood over the main Paraguay. The central flooded area is not well represented in the model, this is related to the presence of the Taquari Megafan which is based on a divergent process very sensitive to the orography and cannot be represented in this model (Louzada et al, 2020; Assine, 2005). Due to the higher resolution of the atmospheric forcing, the influence of the river network over the flooded area is clearly observable in AmSud_GPCC. The increased flooded surface in AmSud_GPCC compared to WFDEI_GPCC seems to be related to the fraction of flooded area over the main rivers and their adjacent grid points. The higher resolution is the cause of these differences because it facilitates the concentration of the flooded area over the main rivers and this concentration allows for more important overflow fluxes that flood the adjacent HTUs.

The anomaly during the dry season is higher in the simulations with values for the differences of flooded fraction reaching -0.3 to -0.4 compared to the mean while in GIEMS-2 the differences remain higher than -0.3. On the contrary, during the flood season the difference is almost not visible in the simulations while the flooded fraction increases up to 0.3 in GIEMS-2. The

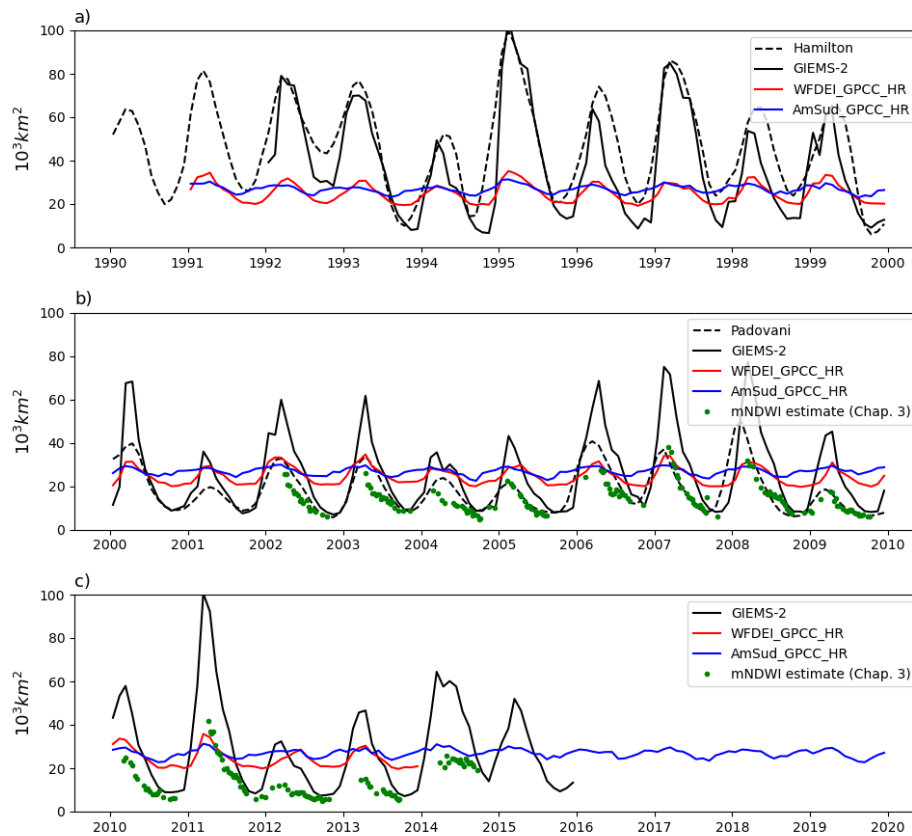


Figure 5.15. Time serie of the flooded area in the simulations with the high resolution floodplains scheme (HR) forced by WFDEI_GPCC and AmSud_GPCC for the 1990's (a), 2000's (b) and 2010's (c) in comparison to the different satellite estimate available over the region: [Hamilton \(2002\)](#) until 2000, [Padovani \(2010\)](#) between 2000 and 2010, [GIEMS-2 \(Prigent et al, 2020\)](#) for the period 1992-2015 and the flood estimate based on MODIS MOD09A1 using the mNDWI spectral index (cf. Chapter 3).

floodplains scheme has a strong reduction of the flooded area during the dry season but the flooded area remains in a small range of value during the rest of the year and do not have an important increase such as in GIEMS-2. The lack of variability of the flooded area in the floodplains simulation is mainly related to the smaller spatial extension of the floodplains in the model.

In GIEMS-2, the eastern region has a negative anomaly of flooded fraction during the flood season and has a positive anomaly during the wet season (not shown). There are not important floodplains over this region, thus the variability of the flooded area can be related to the possible confusion between high soil moisture and flooded area in the satellite estimate of the floodplains (cf. Chapter 3).

Although the variability of the floodplains seems underestimated in the model, the spatial representation of the flooded area is well represented in the model. The high resolution forcing allows to have a precise description of the flooded area which is coherent with the river network.

The satellite estimate of the flooded area may erroneously consider saturated soils as water

surface (Zhou et al, 2021c; Aires et al, 2018). Therefore the flooded area in the satellite estimate represent the open water surfaces, the surfaces with a high soil moisture content and the flooded vegetation while the model considers separately the soil moisture and the open-water surface in the floodplains.

The conversion of the water in the floodplains reservoir into flooded area has been assessed by testing different definition of the parameters defining the floodplains shape (β and h_0). It results that, although these parameters can lead to important changes over a single HTU, they have a very reduced influence on the total flooded area. Therefore, the representation of the flooded area is more affected by the definition of the flooded area or, in other terms, if the regions with high soil moisture content are considered within the definition of flooded area.

The extension of the floodplains could also be strongly affected by the possibility of the floodplains to affect the neighbouring regions through the aquifers. The ORCHIDEE LSM doesn't include the transfer of water between grid points through the groundwater reservoirs (slow reservoir, soil moisture). However, the floodplains infiltrate into the soil moisture of the grid point and, therefore, affect an area which is larger than the flooded area. This partially compensate the absence groundwater transport in the model. This effect will be enhanced at lower resolution because the grid points have larger area and, therefore, the increase of soil moisture related to the floodplains infiltration will affect larger areas.

5.5 Discussion and Conclusion

This chapter presented the high resolution floodplains scheme developed for the high resolution river routing scheme of ORCHIDEE and its evaluation over the Pantanal before leading further analysis on the impact of the floodplains on the surface variables.

The floodplains scheme presented in this chapter exploit the high resolution information of the hydrological file to construct the HTUs. This allows to describe the shape of the floodplains with more precision. The resolution of the hydrological units increases compared to the previous version of the floodplains scheme. This carries with it the necessity to adjust the processes already available and to implement some extra processes such as the overflow. The infiltration of the floodplains into the soil is a crucial aspect as it permits the floodplains to affect a larger area.

The representation of the water cycle over the Pantanal has been assessed by comparing the discharge simulated at the station of Porto Murtinho which is at the outflow of the Pantanal. At first, the performance of the high resolution floodplains has been assessed in comparison with the previous version by using the same atmospheric forcings. The activation of the floodplains scheme improves the representation of the discharge in both versions. The flooded area is similar in both high and low resolution versions of the routing scheme although the flooded area seems more realistic in the high resolution version as it reaches larger areas such as the North of the Pantanal while the flooded area in the low resolution version remains over the main Paraguay river.

A more detailed assessment has been performed using two different resolution forcings. It

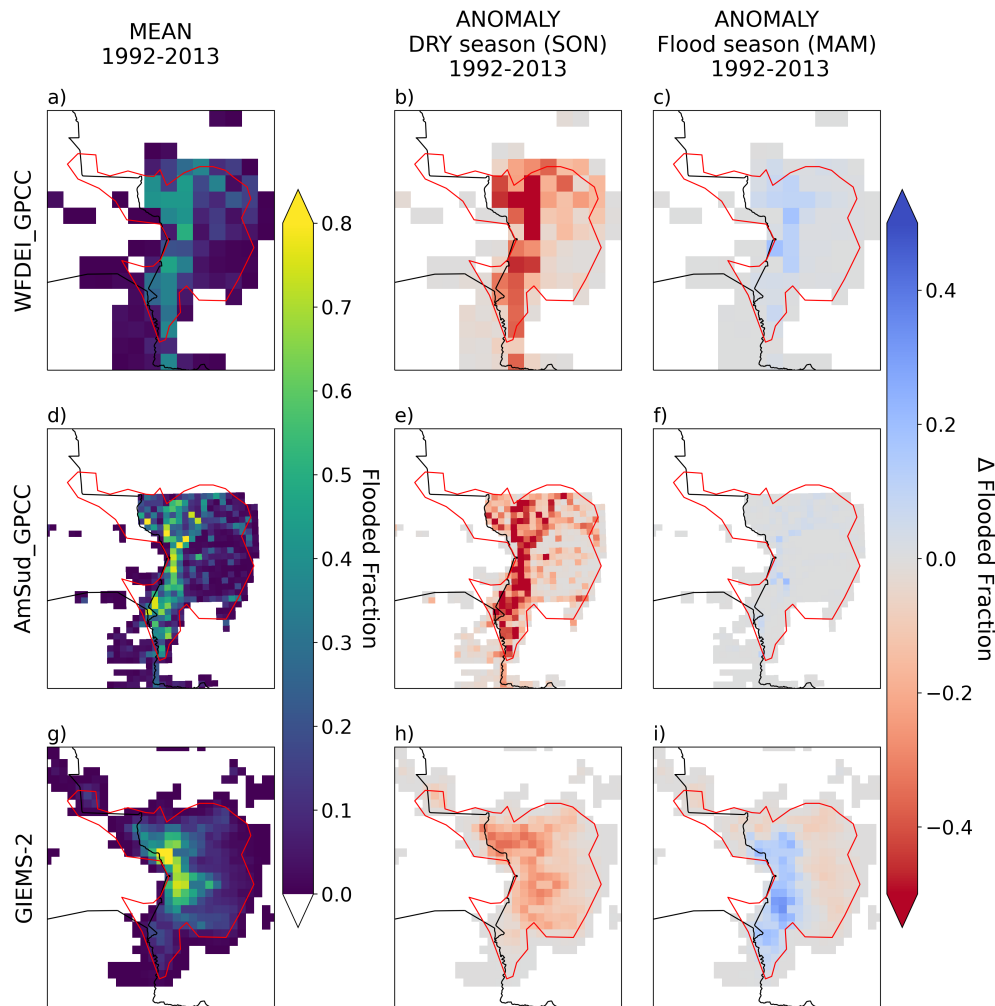


Figure 5.16. Evaluation of the spatial representation of the floodplains in ORCHIDEE in the simulation forced by WFDEI_GPCC (a-c), by AmSud_GPCC (d-e) and estimated by GIEMS-2 (g-i) for the full 1992-2013 period (a,d,g) and over two specific seasons over the same period: the dry season - SON - over the same period (b,e,h) and the flood season - MAM - (c,f,i).

also allowed to assess the impact of the atmospheric grid on the dynamic of the floodplains scheme. These forcings include a 0.5° resolution forcing (WFDEI_GPCC) and a model-based 20 km resolution forcing (AmSud_GPCC). It should be noticed that the precipitation in both forcings is bias-corrected by the GPCC gridded dataset, this reduces the differences related to the precipitation. Both forcings underestimates the near-surface humidity and temperature because they didn't consider the impact of the floodplains on the atmosphere, however, the 20 km forcing have a higher atmospheric evaporative demand due to its lower near surface humidity and higher near surface air temperature and incoming radiation. In both cases, the activation of the floodplains scheme improves the simulation of the discharge at the outflow of the Pantanal. The intra-annual variability of discharge is overestimated in both forcings but this is improved in the higher resolution simulation. The water in the floodplains has only a reduced impact on the total water storage and, thus, has only a small impact on the evolution of the total water storage when compared to GRACE. Although the floodplains represents a

relatively small volume of water, they have an important impact on the discharge and on the surface variables. This is why it is important to represent correctly the flooded area.

The mean flooded area is coherent between both AmSud_GPCC_FP and WFDEI_GPCC_FP simulations and the variability of the flooded area is underestimated in both forcings compared to the different satellite estimates. However, there are large discrepancies between the different satellite estimates considered so it is difficult to correctly assess the flooded area (cf. conclusion of Chapter 3). The representation of the flooded area is a major issue for the floodplains scheme. As it has been evaluated that the water cycle is correctly represented in the model, the issue can come from: (1) the conversion of the volume of water in the floodplains to flooded area, (2) some missing processes and (3) the fact that there exists different ways to define what is a flooded area (cf. Chapter 3).

For the first point, the relationship between the volume of water and flooded area is simplified in the model in order to reduce the memory use. Some more realistic and complex relationships between the volume / height of the floodplains and the flooded area could be considered. Yet, it should be reminded that there are still large uncertainties in the DEM over the floodplains and even more if the vegetation cover is important. Several tests have been performed to evaluate the sensibility of the estimate of the flooded area from the water in the floodplains reservoir. These tests have shown that this conversion doesn't seem to play an important role at a large scale on the estimate of the total flooded area over the region. The major source of error is more related to an underestimation of the grid points affected by floods than to the underestimation of the flooded fraction within each grid point.

For the second point, the water processes over the floodplains can not always be represented by the current river network description in ORCHIDEE which is a convergent model because, in some cases, the floodplains can be caused by a divergent flow such as the Taquari Megafan over the Taquari river in the central region of the Pantanal. The representation of this type of process would require a high precision HydroDEM as the floodplains in this region are very sensitive to the small differences of orography. The Taquari floodplains are also based on a divergent river network which is not implemented in ORCHIDEE. The groundwater fluxes between grid points are not considered neither in the version of ORCHIDEE used for these simulations. The water that infiltrates from the floodplains reservoir of an HTU affects the soil moisture of the whole grid point. However, this increase of the soil moisture should be able to affect the neighbouring grid points but this is not the case in the actual version of ORCHIDEE. This is more important as the resolution is higher. In absence of groundwater transport between grid points, using a lower resolution allows to represent better this type of water transport.

The third issue concerns the following question: what should be considered as a flooded area? The estimate of the flooded area over the floodplains is quite complex (cf. Chapter 3) as it can take different forms such as the presence of shallow water or flooded vegetation and can be related to some groundwater processes. Regarding the representation of the floodplains from a land-atmospheric coupled model point of view, a higher soil moisture can have similar impacts on the atmosphere as a flooded vegetation region which limits the issue of the flooded area underestimation. Therefore, it should be reminded that the satellite products consider

altogether the open-water surfaces and the regions with high soil moisture content while they are considered separately in the model. The changes in soil moisture related to the activation of the floodplains scheme are shown in the following Chapter.

Over the Pantanal, the floodplains scheme seems to be well adapted to the hydrological processes involved but, looking at the subject from a wider angle view, other types of processes can be involved in what we referred to as floodplains. For example, they can be related to some ponds or lakes, to different types of flooded forest or to swamp. This configuration is not the optimum for these other types of wetlands. Some other schemes can be constructed from the spatial description of these other types of region and then be processed differently. For example, the ponds are related to the water remaining after the recedence of water and to the local precipitation. They can be represented by filling some pond reservoirs by a fraction of the local precipitation. The swamps and flooded forest can be managed by redirecting a small fraction of the river flow into the soil moisture. Another difficulty lies in defining an adequate map for the type of floodplains concerned by the scheme. In Guimberteau et al. (2012), different floodplains maps have been compared for the 0.5° resolution of the floodplains scheme. The GLWD map used for the simulations is well adapted for the Pantanal but this description have to be checked as well as the process involved in the region of interest before using it in another region. The inclusion of the lakes should allow to improve the floodplains lakes but will also cause other difficulties such as the interaction between lakes and floodplains which will have to be represented.

5.6 Acronyms

ANA	Agencia Nacional de Aguas
AmSud	RegIPSL simulation at 20 km over the South American domain
AmSud_GPCC	Atmospheric forcing based on a RegIPSL simulation at 20 km over the South American domain which precipitation is bias-corrected by GPCC
CMIP6	Coupled Model Intercomparison Project
CRU	Climatic Research Unit
DEM	Digital Elevation Model
ERA	ECMWF Re-Analysis
ERA5	ECMWF Re-Analysis fifth generation
ESA	European Spatial Agency
FP	Offline simulations with the floodplains activated

GIEMS-2	Global Inundation Extent from Multi-Satellites version 2
GIEMS-D15	Global Inundation Extent from Multi-Satellites downscaled 15 arcseconds
GLWD	Global Lake and Wetlands Dataset
GPCC	Global Precipitation Climatology Centre
GRACE	Gravity Recovery and Climate Experiment
GSWP3	Global Soil Wetness Project Phase 3
HR	Offline simulations with the high resolution river routing scheme in ORCHIDEE
HTU	Hydrological Transfer Unit
HydroDEM	Hydrologically coherent Digital Elevation Model
HydroSHEDS	Hydrological data and maps based on Shuttle Elevation
IPSL	Institut Pierre Simon Laplace
LR	Offline simulations with the low resolution river routing scheme in ORCHIDEE (cf. routing scheme at °)
LSM	Land Surface Model
mNDWI	Modified Normalized Difference Water Index
MODIS	Moderate Resolution Imaging Spectroradiometer
NCEP	National Centers for Environmental Prediction
NOFP	Offline simulations with the floodplains deactivated
NSE	Nash-Sutcliffe Efficiency
ORCHIDEE	Organizing Carbon and Hydrology in Dynamic Ecosystems
PBIAS	Percent Bias Index
PFT	Plant Functional Type
RMSE	Root Mean Square Error
RegIPSL	Institut Pierre Simon Laplace's Regional Earth System Model

RoutingPP	Pre-Processor of the routing input for ORCHIDEE high resolution routing scheme
TWS	Total Water Storage
UPRB	Upper Paraguay River Basin
USDA	United States Department of Agriculture
WFD	WATCH forcing data
WFDEI	WATCH forcing data bias corrected by ERAI
WRF	Weather Research and Forecasting

Evaluation of the impact of the high resolution floodplains scheme on
the surface variables in ORCHIDEE

Contents

6.1	Introduction	141
6.2	Methodology	142
6.2.1	Simulations	142
6.2.2	Overview	143
6.2.3	Water Cycle and Vegetation	143
6.2.4	Land atmosphere fluxes	144
6.2.5	Evapotranspiration and Budyko Diagram	145
6.3	Results	146
6.3.1	Impact on the surface variables	146
6.3.2	Changes in Surface Energy Budget	153
6.3.3	Evapotranspiration	155
6.3.4	Budyko Diagram	157
6.4	Conclusion	159
6.5	Acronyms	163

6.1 Introduction

The previous chapter presented the floodplains scheme developed for the ORCHIDEE high resolution routing scheme and its validation over the Pantanal region. Thereafter, the high resolution floodplains scheme can be used to study, in the present chapter, the impact of the presence of floodplains in the model regarding the surface conditions and the different land-atmosphere fluxes.

The presence of floodplains in the model impacts the local surface conditions in different ways. Without the floodplains scheme activated, the water flowing through the Pantanal in the river routing of the ORCHIDEE model do not interact with the surface variables over the floodplains. The floodplains scheme allows to improve the realism of the dynamic of the water flowing through these regions as the flow is slowed and it may follow paths that would not be considered in a traditional and purely convergent routing scheme. Moreover using these recent developments, the water in the floodplains can interact with the land surface variables. Thus, it will alter the land-atmosphere fluxes in a variety of ways driven by: (1) the direct evaporation of the flooded area, (2) the infiltration of the floodplains water into the soil moisture and (3) an enhanced vegetation. These interactions have indirect consequences on the surface conditions as they enhance the soil moisture which remains high during the dry period. This would help to sustain the vegetation during the dry period. The quantity and distribution of the different categories of land-atmosphere fluxes will also be impacted altogether with other surface variables such as the surface humidity or the surface temperature.

This chapter investigates the differences between the simulations with and without floodplains to underline what are the impacts of the presence of the floodplains on the surface conditions. Section 2 contains the Methodology and presents the observational datasets used for the analysis. Section 3 will present the results and the last Section will discuss the results and draw a conclusion of the chapter.

6.2 Methodology

6.2.1 Simulations

Two pairs of ORCHIDEE simulation using the high resolution routing are used to perform this analysis. Each pair is forced by a different forcing: WFDEI_GPCC at 0.5° resolution and AmSud_GPCC at 20 km resolution. These forcings are presented with more details in the Chapter 5. The analysis is performed between 1990 and 2013 which is the period that both forcings have in common. Each pair of simulations is composed by a simulation with the floodplains scheme activated (FP) and another one without the floodplains scheme (NOFP).

These four simulations are used to evaluate the impact of the floodplains scheme on the variables of the water cycle (other than the discharge and the flooded area) and the land-atmosphere fluxes in the ORCHIDEE Land Surface Model. As we consider two sets of simulations forced by two forcings with different resolutions, this can also give an idea of the influence of the resolution on the floodplains scheme. Both simulations have a comparable precipitation as they are both bias-corrected by the GPCC gridded observation dataset. Due to the absence of feedbacks in the simulations, these forcings will be source of errors for the near surface temperature and humidity because they will not react to the changes related to the presence of flooded areas in the model. It should also be noticed that, compared to WFDEI_GPCC, AmSud_GPCC have a higher evaporative demand due to the higher near-surface temperature, incoming shortwave radiation and the lower near surface humidity (cf. Chapter 5). This is partly related to the fact that the AmSud_GPCC forcing is only bias corrected as to the precipi-

tation, the other variables remain unchanged. Therefore, as the precipitation is underestimated over the region in AmSud, the other variables represents a drier atmosphere over the Pantanal. This section will focus on the mean value of the variables between 1990 and 2013 but will also consider their mean values over two different seasons during this period: the dry season from September to November (SON) and the flood season from March to May (MAM). This will allow to have a global view of the climatological behaviour of these variables and to evaluate the seasonal dynamics of the floodplains.

6.2.2 Overview

The presence of the floodplains will affect the hydrological cycle and the surface energy balance which are both closely related through the evapotranspiration.

The activation of the floodplains scheme is expected to increase the water availability over the Pantanal. The evaluation of the impact of the floodplains will be performed in three steps:

1. impact on the surface variables: Soil Moisture, Surface Temperature and Vegetation,
2. impact on the surface energy budget,
3. impact on the evapotranspiration.

6.2.3 Water Cycle and Vegetation

The evolution of the vegetation is partly driven by the water availability in the soil. So, as the floodplains can alter the local soil moisture, the floodplains also indirectly impact the vegetation. The vegetation in ORCHIDEE is described in the model's input by the potential vegetation cover (maxvegetfrac) which is the maximal cover per grid point of 13 different Plant Function Types (PFTs). For each grid point, the sum of the maxvegetfrac of the different PFT is equal to 1. In these simulation, the PFT are constructed from the ESA-CCI database (European Space Agency-Climate Change Initiative; [ESA, 2017](#)). The realised vegetation cover is defined by the fraction of the grid cell occupied by each PFT (vegetfrac) which upper limit is maxvegetfrac . If $\text{vegetfrac} < \text{maxvegetfrac}$, the remained surface not occupied by the PFT in the simulation is considered as bare soil.

In order to explore further the changes related to the vegetation, it is important to know the description of the location of the different vegetation type over the Pantanal in the simulation. The maximal vegetation cover for the different PFT categories existing over the Pantanal is represented in [Figure 6.1](#).

There is a high presence of Tropical Broadleaf Evergreen on the Western and Northeastern part of the Pantanal covering more than 50% of the grid points concerned. The Tropical Broadleaf Raingreen are present over all the Pantanal with a cover of around 20% of each grid points. The rest of the Pantanal is mainly covered by Natural Grassland of C3 (in the Northwest, the South and the East) and C4 type (in the North and the South/Southeast). It should be noted that there is a presence of bare soil over the main Paraguay and the Taquari river. These

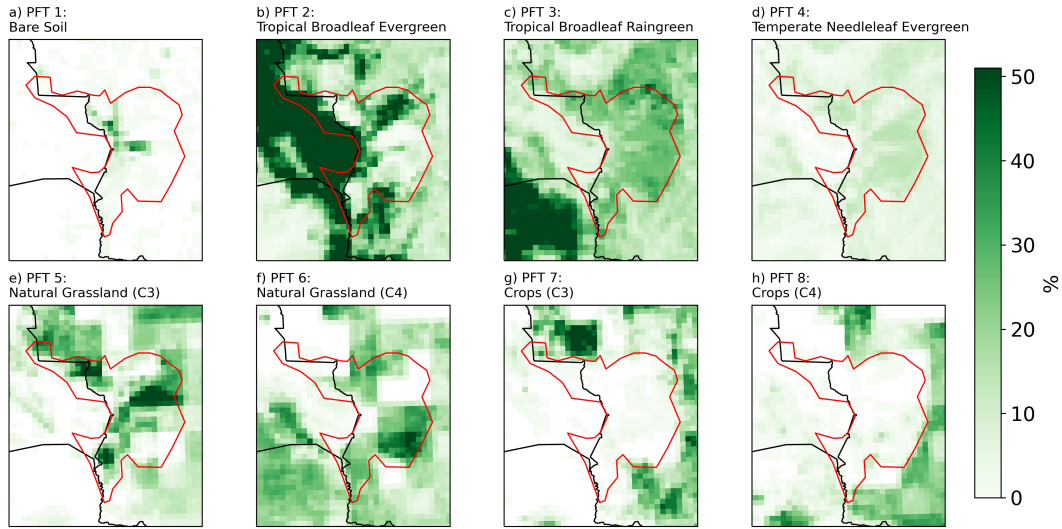


Figure 6.1. Description of the potential vegetation cover (maxvegetfrac) for all the vegetation types (PFT) existing over the Pantanal in the simulations. The PFT are constructed from the ESA-CCI database (European Space Agency-Climate Change Initiative; ESA, 2017).

regions are strongly affected by the presence of open-water and, therefore, are described as area without vegetation in the PFT description by the bare soil cover.

6.2.4 Land atmosphere fluxes

The surface energy budget is the partitioning of the total net radiation composed by the net longwave and shortwave radiations ($R_n = LW_n + SW_n$) into latent heat fluxes (LE), sensible heat fluxes (H) and ground heat fluxes (G), cf. eq. 6.1. The net shortwave radiation is strongly influenced by the albedo (α) at the surface because $SW_n = (1 - \alpha)SW_{in}$ with SW_{in} the incoming shortwave radiation. In the model, the direct impact of the flooded area on the albedo is not considered, but the changes in soil moisture and vegetation directly affect this parameter and, therefore, impact the net radiation.

$$R_n = LE + H + G \quad (6.1)$$

The latent heat fluxes is represented by the latent heat of vaporization (L) and the evapotranspiration (E) which is estimated from the bulk formulation, cf. equation 6.2. In this formulation, the evapotranspiration is described as the fraction β (the moisture availability function) of the potential evaporation (E_{pot}). E_{pot} is estimated with ρ the air density, r_a the aerodynamic resistance, q_s the specific humidity of the air when it is saturated, q_a the specific humidity of the air at the surface and T_s the surface temperature.

$$E = \beta E_{pot} = \beta \frac{\rho}{r_a} [q_s(T_s) - q_a] \quad (6.2)$$

On the other side, the sensible heat fluxes in the ORCHIDEE LSM are driven by the difference

between the surface temperature (T_s) and the temperature of the air at the surface (T_a). It is calculated from the equation 6.3 with c_p the specific heat.

$$H = \frac{\rho c_p}{r_a} [T_s - T_a] \quad (6.3)$$

Over a large period of time, the ground heat fluxes can be neglected and, then, R_n is only partitioned into LE and H ($G=0$). Thus, the relative distribution of LE and H is important to quantify the changes in the surface energy budget and the changes in temperature. This can be expressed with the Evaporative Fraction (EF) which is the ratio of latent heat (LE) over the total land atmosphere fluxes, i.e. the sum of the latent heat and of the sensible heat (LE+H):

$$EF = \frac{LE}{LE + H} \quad (6.4)$$

The EF index gives an indication of the distribution of the heat fluxes over land. The value of this index tends to 0 when there are no latent heat fluxes such as in arid areas. It can take the value of 1 if there are only latent fluxes and take values over 1 when the land surface is cooled because in this case $H < 0$.

6.2.5 Evapotranspiration and Budyko Diagram

The latent heat flux is the conversion of the total evapotranspiration into an energy flux through its multiplication by the latent heat of fusion. Therefore, to analyze the origin of the changes in latent heat flux, it is interesting to detail the origins of the changes in evapotranspiration using its different components: evaporation over bare soil, evaporation from the floodplains, transpiration from the vegetation and interception loss (the evaporation of the water on the canopy).

The Budyko diagram (Budyko, 1974) aims to synthesize the surface conditions as depending on the precipitation (P), the actual evapotranspiration (AET) and the potential evapotranspiration (PET). On the vertical axis, it considers the Evaporative Index ($= AET/P$) for which higher values means that a higher proportion of the local precipitation is evaporated instead of being infiltrated or increasing the runoff. The Aridity index is represented on the horizontal axis. It is the ratio of potential evapotranspiration to precipitation. The higher this index, the drier the local conditions. The Budyko framework is usually applied to a closed catchment and averaging the variables over a long term period (at least 1 year). The annual mean over the catchment can also be analyzed to observe the inter-annual variability.

In theory, two zones can be distinguish in the diagram: (1) an energy limited zone and (2) a water limited zone. The energy limited zone refers to a condition where there is not enough energy to evaporate all the water from the precipitation ($PET < P$), thus the AET is equal or close to the PET. In the water limited zone, all the water from precipitation can be evaporated ($PET > P$ and $AET = P$) but there is still more energy available to evaporate water.

The black line of the energy and water limitation (cf. Figure 6.2) are the theoretical limits that cannot be exceeded by the a closed catchment catchment with a conservative total water storage.

In reality, the values for a closed catchment in a steady state are located below these black lines and are approximated by the Budyko curve. There are numerous formulations of the Budyko curve which are all defined empirically (Mianabadi et al, 2019; Gerrits et al, 2009). In certain cases, when the total water storage is not conservative, the values over a catchment are above the Budyko limits. This is the case when there is water depletion from the soil moisture or groundwater through evapotranspiration or from the transfer of water from another region which increases locally the evapotranspiration (Zaninelli et al, 2019; Greve et al, 2016). The present chapter uses a classical Budyko diagram with the mean values over the 24 years period of simulation and also the mean annual values over the Upper Paraguay river basin catchment. Along with it, a Budyko-inspired diagram will be used to show the mean value over flooded grid points of the Pantanal (unclosed catchment) averaged over the different seasons to understand the annual cycle of the evaporative process over the Pantanal through an hysteresis graph.

6.3 Results

6.3.1 Impact on the surface variables

Soil Moisture

The presence of the floodplains induces an additional infiltration of water into the soil which affects the soil moisture. Figure 6.3 shows the mean soil moisture for the FP simulations and the relative difference with the NOFP simulations averaged between 1990 and 2013 considering: the dry period, the flood period and the whole year.

The floodplains integration in ORCHIDEE increases the soil moisture over the most flooded

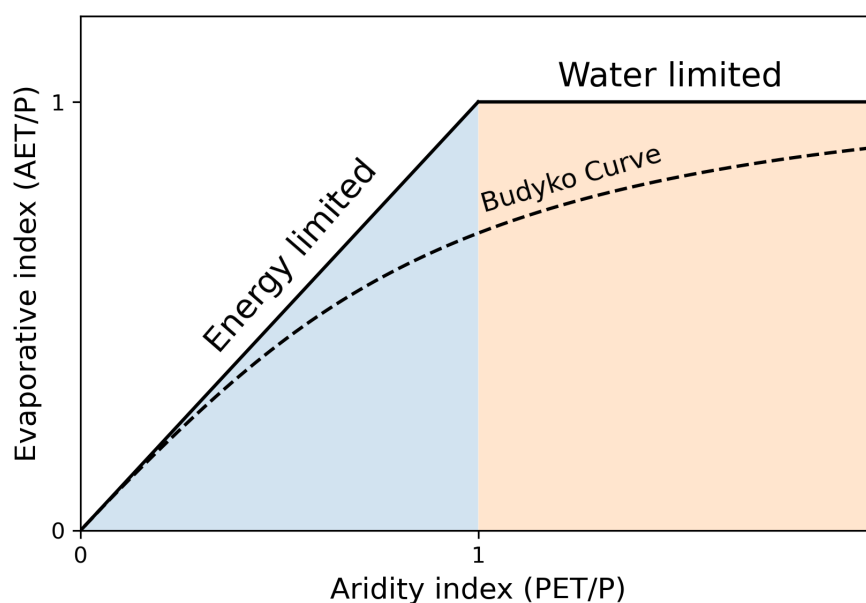


Figure 6.2. Illustration of the Budyko diagram.

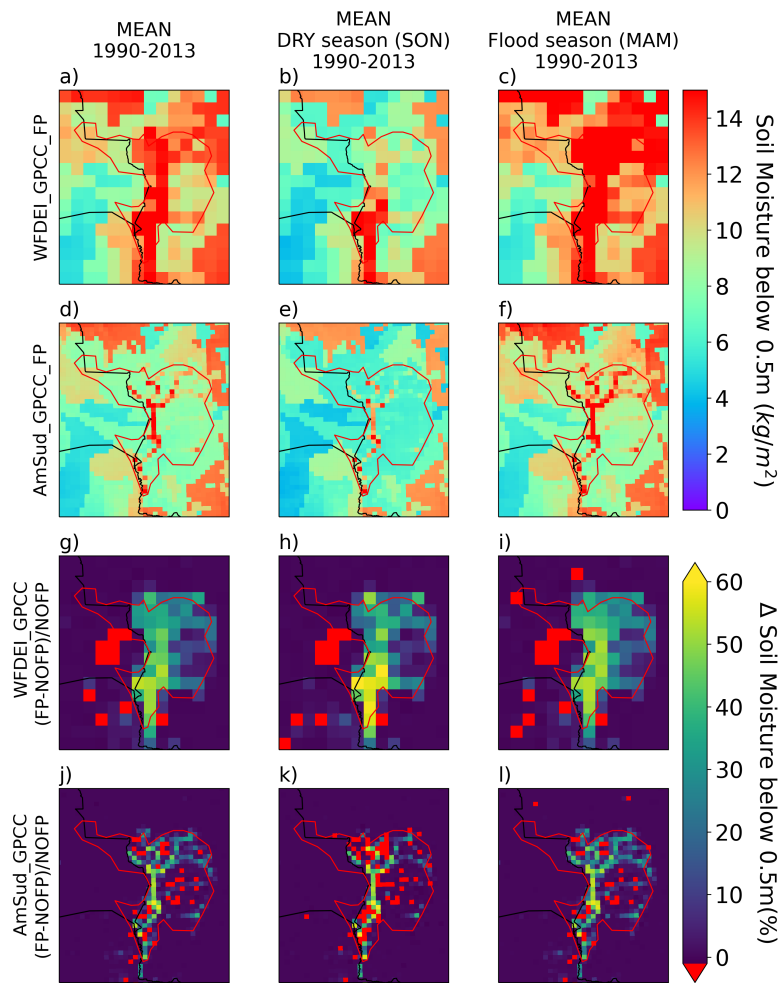


Figure 6.3. Mean of the soil moisture over the upper level (below 0.5m depth) during the 1990-2013 period considering the full year (a,d,g,j) the dry season - SON (b,e,h,k) and the flood season - MAM (c,f,i,l) for the WFDEI_GPCC_FP simulation (a,b,c) and the AmSud_GPCC_FP (d,e,f) as well as the difference between the FP and NOFP simulations for WFDEI_GPCC (g,h,i) and AmSud_GPCC (j,k,l).

areas. Therefore, the increase of the soil moisture in the FP simulation reflects the structure of the hydrological network in the Pantanal. The comparison with the NOFP simulation shows that these changes occur over a larger area during the flooded season compared to the rest of the year. However, the relative differences between the FP and the NOFP simulations are higher during the dry season where the positive anomaly in soil moisture remains until the dry period.

The extension of the floodplains through the soil moisture is more important at lower resolution because the grid cells are covering a larger area. This issue is related to missing processes in the model such as the lateral transport of the groundwater which is not included in ORCHIDEE. The higher the resolution, the more these missing processes are affecting the impact of the floodplains on the soil moisture. This can be solved by including another type of water transfer between the grid cells through, for example, a groundwater routing which will transfer the water

from the floodplains reservoir to the neighbours grid cell that have a lower water table in order to simulate the transport of water through the aquifers.

Some regions have a lower soil moisture in the FP simulation compared to NOFP. This can be related to the balance between the two type of interactions existing between the floodplains and the soil moisture: (1) the floodplains provide water to the soil through infiltration but (2) they decrease the soil moisture because the precipitation falls into the floodplains instead of the soil. If the infiltration from the floodplains is low but the floodplains receives the water from precipitation, the soil moisture can slightly decrease locally. This will principally occur when the volume in the floodplains and the precipitation are lower (cf. dry period in Figure 6.3) and in region with a lower infiltration coefficient which is related to the soil type. Over the Pantanal, this occurs principally in the higher resolution forcing. This is related to the resolution because there are more grid point which do not contain large rivers which will increase the soil moisture when flowing through the floodplains reservoir. This is confirmed by the fact that the grid points affected are around the main rivers: along the Paraguay river in an North-South axis and along the Taquari river in the Central region.

Temperature

The surface temperature (T_s) is a variable that reflects the energy balance at the surface and thus will be directly affected by the impact of the floodplains on the land-atmosphere fluxes.

Figure 6.4 shows the temperature in the NOFP simulations for the period 1990-2013 as well as the differences between the FP and NOFP simulations. The Pantanal is in a tropical region; therefore, when the model is not considering the impact of floodplains, the mean surface temperature remains relatively high during all the year and principally over the Pantanal with a mean annual temperature higher than 20°C. The mean temperature over the Pantanal is higher in AmSud_GPCC which is mainly due to the higher values of the radiative input and the near surface temperature as well as the lower values of specific humidity compared to WFDEI_GPCC.

The activation of the floodplains scheme reduces the temperature over the Pantanal. This reduction of the temperature is more important during the dry season because during the flood season the soil is wet in both FP and NOFP simulations due to the precipitation that occurs locally during the rainy season (DJF). The flood water that remains during the dry season in the FP simulations makes a larger difference of temperature compared to the much drier soil of the NOFP simulation. The difference of temperature is lower in WFDEI_GPCC (around -1°C) compared to AmSud_GPCC (with differences up to -3°C during the flood season and up to -6°C during the dry season). Contrary to the differences observed between FP and NOFP for soil moisture, the area concerned by these temperature changes is more important in the high resolution simulation.

Contrary to its limited impact on soil moisture, the higher concentration of the flooded area in AmSud_GPCC_FP have an important impact on the land-atmosphere fluxes which impacts the temperature. The higher temperature over the Pantanal in the AmSud_GPCC simulation will also make the temperature of the region more sensitive to the increased water availability for

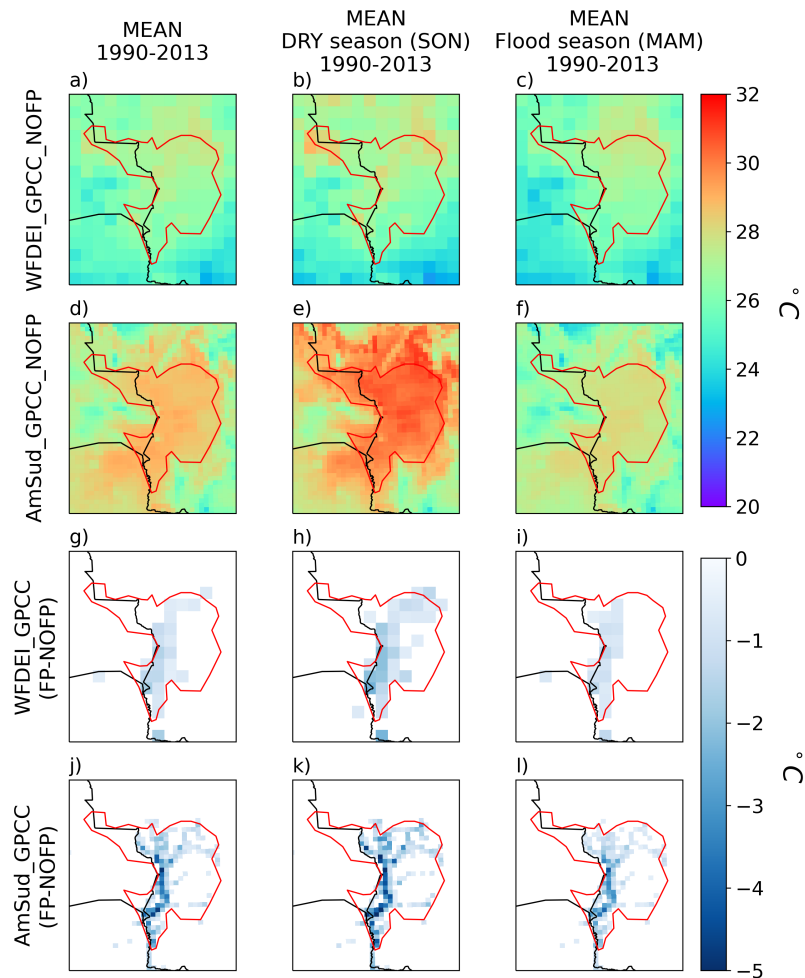


Figure 6.4. Average Surface Temperature in the NOFP simulation forced by WFDEI_GPCC (a,b,c) and AmSud_GPCC (d,e,f) and the difference between the FP and NOFP simulation for WFDEI_GPCC (g,h,i) and AmSud_GPCC (j,k,l) between 1990-2013 period considering the full period (a,d,g,j), the dry season (b,e,h,k) and the flood season (c,f,i,l).

evaporation compared to WFDEI_GPCC.

The distribution of the average daily temperature over the most flooded parts of the Pantanal (with a mean flood_frac > 0.1) in both forcings is represented in Figure 6.5. During the austral summer (Figure 6.5.a), the activation of the floodplains module reduces both maximum and minimum values for AmSud_GPCC but only the minimum value for WFDEI_GPCC because its maximum is higher. This can be related to a particular event over a single grid point because the percentile 90 is lower in WFDEI_GPCC_FP compared to WFDEI_GPCC_NOFP. But in both cases, the body of the distribution (the distribution between percentile 10 and 90) is shifted toward lower temperature and is more concentrated.

During the austral winter (Figure 6.5.b), the body of distribution of the temperature as well as the extremum are shifted toward lower values. This is more important in AmSud_GPCC whose minimum is 2° lower than the minimum of AmSud_GPCC_NOFP.

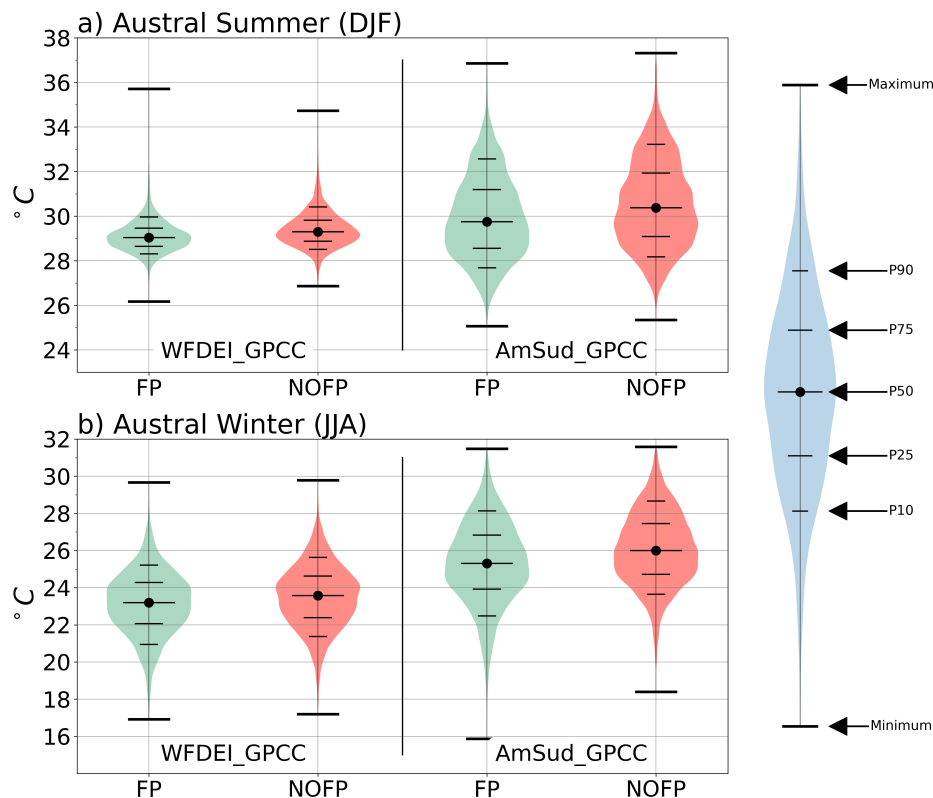


Figure 6.5. Representation of the distribution of the average daily temperature over the most flooded part of the Pantanal for the pair of simulation with and without floodplains forced by WFDEI_GPCC and AmSud_GPCC during the period 1990-2013. The extremas, the median as well as the percentile 10, 25, 75 and 90 are represented.

The floodplains acts as a buffer for temperature as they lower the temperature over the flooded area and, not considering the extremums, reduce the variability of the temperature. The temperature over the floodplains in AmSud_GPCC has a larger variability than WFDEI_GPCC during both austral winter and summer which is mainly related to the difference resolution because a higher resolutions brings more spatial and temporal variability.

Vegetation

In the model, the state of the vegetation is defined by the Leaf Area Index (LAI) which characterize its concentration and by the fraction of the grid points occupied by the different PFT (*vegetfrac*). These variables depend on the surface conditions and, in particular, on the soil moisture availability. This is why it can also be affected by the floodplains scheme. To better assess the differences between the FP and the NOFP simulations, Figure 6.6 shows, for each vegetation type existing in the Pantanal, the ratio of surface they occupy to the maximum surface they can occupy (*vegetfrac*/*maxvegetfrac*) during the flood season (no hatch) and the dry season (hatched) for the FP and NOFP simulation, respectively in blue and orange for the WFDEI_GPCC (Figure 8.a) and the AmSud_GPCC simulations (Figure 6.6.b).

All the vegetation types are strongly affected by the floodplains except the crops C3 in Am-

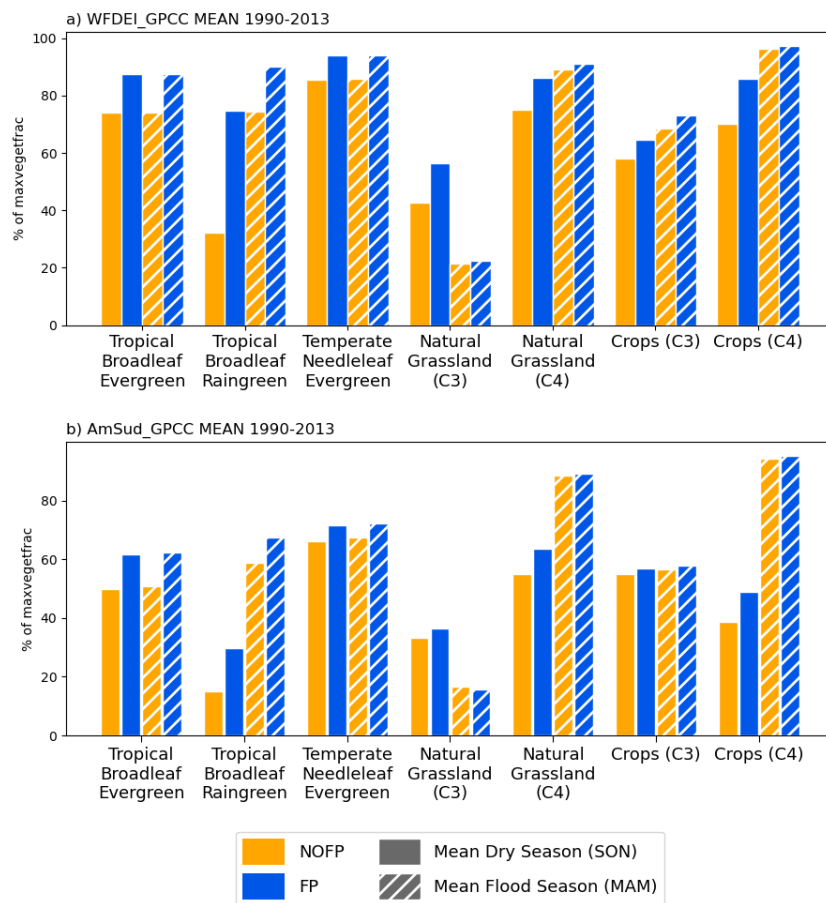


Figure 6.6. Bar plot of the percentage of the maximum vegetation cover in the model for the FP (blue) and NOFP (orange) simulations during the dry season - SON (no hatch) and during the flood season - MAM (hatched) for the simulations forced by WFDEI_GPCC (a) and AmSud_GPCC (b).

Sud_GPCC. The percentage increases for all the affected vegetation types. For most of these PFTs, the difference only occurs during the dry season such as for Natural Grassland C3 and C4 and Crops C4. For the Tropical Broadleaf (evergreen and raingreen) and for the temperate Needleleaf Evergreen, this change occurs during both flood and dry seasons.

The ratios of surface occupied by the PFT to the maximum surface that can be occupied are generally higher in the simulations forced by WFDEI_GPCC which is related to the higher soil moisture (cf. Figure 6.3). The changes between the FP and NOFP simulations are also higher for WFDEI_GPCC compared to AmSud_GPCC which is related to the major impact of the floodplains on soil moisture in WFDEI_GPCC. The tropical broadleaf raingreen are particularly affected by the floodplains scheme. This vegetation type has an important presence in the North of the Pantanal (cf. Figure 6.1). It is a region in which the increase of the soil moisture is relatively important in WFDEI_GPCC (cf. Figure 6.3). This vegetation type don't have enough soil moisture to grow correctly when the floodplains are not activated. The increase of the soil moisture allows them to be more developed. Therefore, the floodplains scheme is important for a more realistic simulation of the vegetation. The remote sensing products provide a realistic description of the potential vegetation cover for the model (maxvegetfrac) which is used

as a limit for the realised vegetation fraction in the model (*vegetfrac*) which is related, along with the Leaf Area Index, to the development of the vegetation. Thus, the realised vegetation fraction depends on the soil moisture available and, if the floodplains are not considered, some vegetation types requiring larger quantity of water than other may not be able to develop in the simulation.

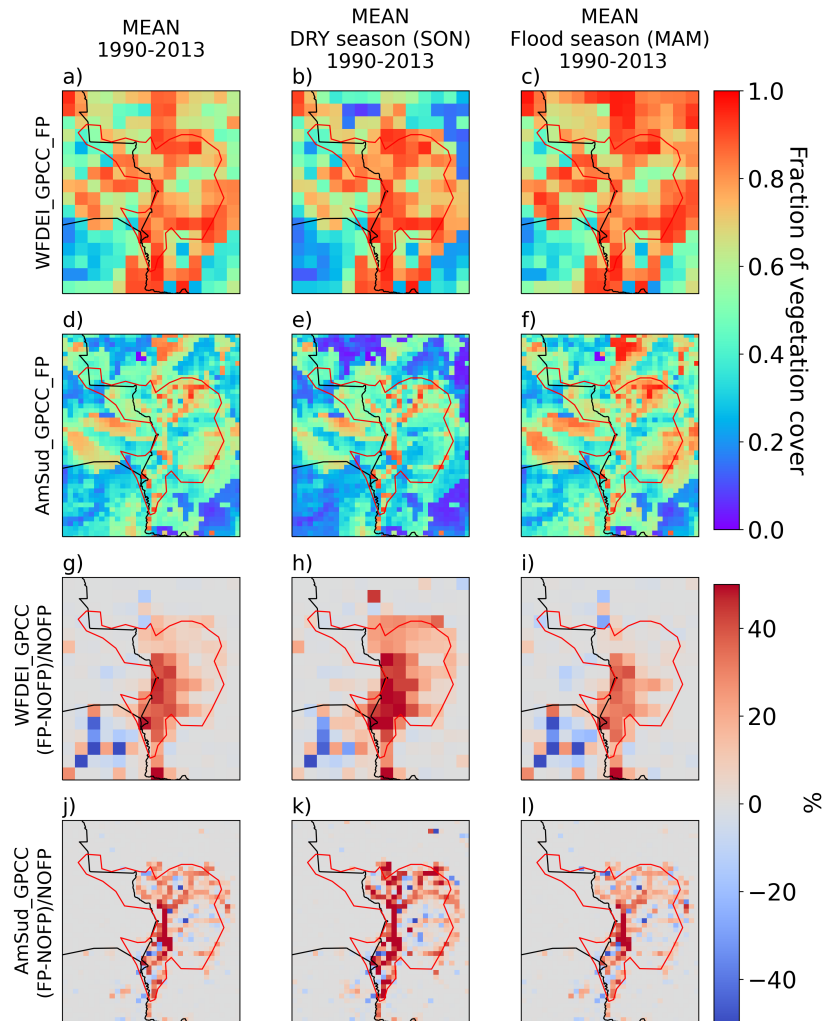


Figure 6.7. Fraction of each grid point covered by vegetation ($\sum_{j \in PFT} \text{vegetfrac}_j$ without considering the bare soil fraction) in WFDEI_GPCC_FP (a,b,c) and AmSud_GPCC_FP (d,e,f) and the relative difference between FP and NOFP for WFDEI_GPCC (g,h,i) and AmSud_GPCC (j,k,l) for the period 1990-2013 considering the full year (a,d,g,j), the dry season - SON (b,e,h,k) and the flood season - MAM (c,f,i,l).

The total fraction of vegetation cover (all the PFT types except bare soil) is represented for the FP simulation in Figure 6.7. This Figure also shows the relative difference between the FP and NOFP simulation. Similar pattern to the Figure 6.3 can be observed with an increase of the vegetation up to 30/40% in the WFDEI_GPCC_FP compared to the WFDEI_GPCC_NOFP and with an increase by more than 50% over the main rivers in AmSud_GPCC. The increase of the vegetation in the FP simulation compared to the NOFP occurs over the areas in which

the soil moisture has increased and more importantly over the central region of the Pantanal. The northern region in which the tropical broadleaf raingreen are much more developed in the FP simulation doesn't seem so affected compared to the central region.

Some regions over the Pantanal have a decrease of the vegetation. This can be explained by the reduction of the soil moisture related to the floodplains explained previously and observable in Figure 6.3.

Apart from the spatial extension of the vegetation, the density of the vegetation has also been considered through the Leaf Area Index (LAI). The changes of the LAI follow the same patterns as the changes of vegetation except that the differences in percentage between the FP and NOFP simulations are slightly higher for this variable (not shown). The higher development of the vegetation in FP (through higher vegetation fraction and LAI) also increases the roughness height for momentum (Z_{0m}) and the roughness height for heat (z_{0h}) in the ORCHIDEE model (not shown). These variables have an impact on the atmospheric boundary layer when coupled to an atmospheric model. The albedo decrease due to a higher soil moisture and the development of the vegetation over a large part of the Pantanal, but, over the most flooded part of the Pantanal, the albedo increase. This is related to the development of certain type of vegetation with a relatively high albedo which cover a dark color bare soil with a lower albedo.

6.3.2 Changes in Surface Energy Budget

The equation 6.1 shows that, over a large period of time, the net radiation is partitionned between the latent and sensible heat flux. To compare the relative distribution of latent heat flux and sensible heat flux, the evaporative fraction is shown in Figure 6.8 for the NOFP simulations and the FP simulations.

The evaporative fraction increases over all the Pantanal which means that the distribution of the surface heat fluxes changes. The latent heat fluxes increase while the sensible heat fluxes decrease and this is coherent with the decrease of the temperature over the Pantanal. The major differences follow the spatial structure of the flooded area.

In both simulations, the higher values of the mean evaporative fraction exceed 1 and this is accentuated in the AmSud_GPCC_FP simulation. This means that over the main floodplains, the sensible heat fluxes are negative for some grid points which corresponds to a surface cooler than the atmosphere over large period of time - i.e. on a 24 year average in this case (cf. equation 6.3). This behaviour is unrealistic in a tropical region and is related to the absence of feedback of the atmospheric forcings to the changes at the surface. The evaporative demand is high in the forcings because they don't consider the floodplains and, due to the lack of feedback, they are incoherent with the surface conditions. The floodplains scheme increases the evapotranspiration but it doesn't change the near surface specific humidity and, thus, don't lower the evaporative demand (cf. equation 6.2). This also explains the higher values in AmSud_GPCC_FP compared to WFDEI_GPCC_FP due to the higher evaporative demand of the forcing.

The increase of the evaporative fraction in the FP simulations has a larger spatial extension during the flood season which is related to the increase of the water availability for evapo-

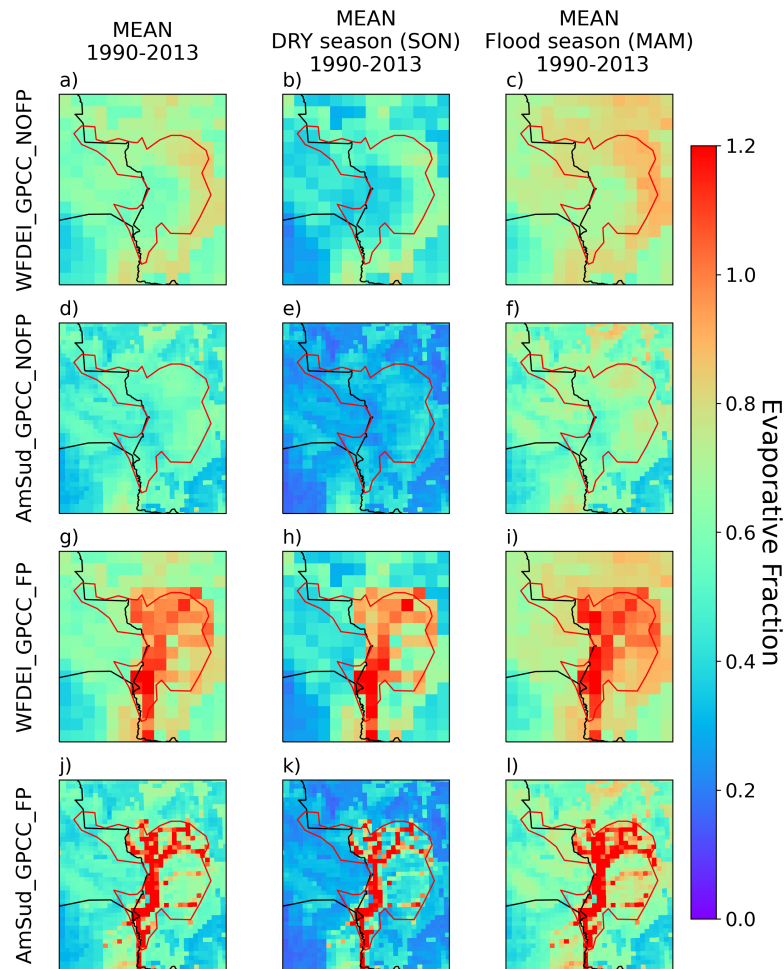


Figure 6.8. Mean Evaporative fraction for each grid point in WFDEI_GPCC_NOFP (a,b,c) and AmSud_GPCC_NOFP (d,e,f), the WFDEI_GPCC_FP (g,h,i) and the AmSud_GPCC_FP (j,k,l) for the period 1990-2013 considering the full year (a,d,g,j), the dry season - SON (b,e,h,k) and the flood season - MAM (c,f,i,l).

transpiration through the flooded area and soil moisture over a larger area (cf. Figure 6.3) compared to the dry season.

In equation 6.1, the sensible and latent heat flux are not the only variables which can be changed by the floodplains. The net radiation can also be affected and, in particular, through changes of the surface albedo. The albedo increase when the soil moisture increase and can change due to the development of the vegetation. In general, more vegetation leads to a lower albedo because it will absorb more radiation, however, this depends on the color of the bare soil and if there are changes of not of vegetation type. It can also decrease if the soil moisture increases over scarce vegetation regions. Figure 6.9 evaluates the averaged terms of the surface heat budget. The Ground Heat fluxes is not shown as it is negligible compared to the other fluxes.

The net shortwave radiation (SW_{net}) in the NOFP simulations has values close to the FP simulations. It is, as expected by the analysis of the forcings, higher in AmSud_GPCC. This

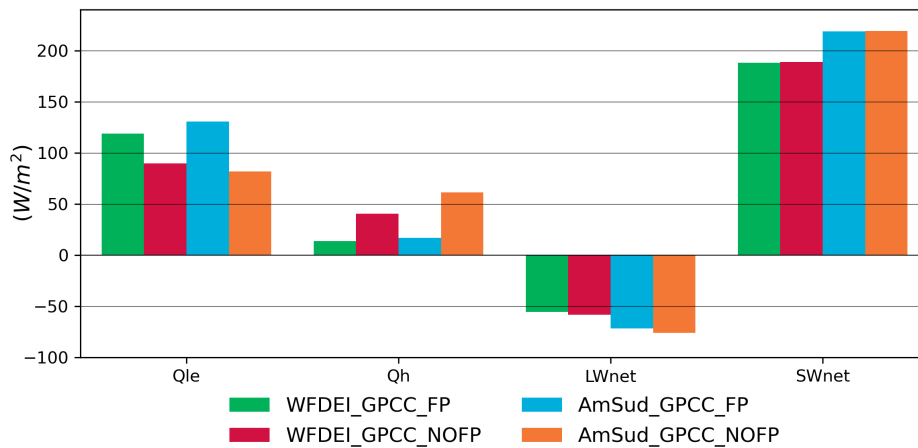


Figure 6.9. Average value over the Pantanal of the different terms of the equation 6.1 between 1990 and 2013.

means that although the albedo slightly change with the floodplains scheme, it doesn't have an important impact on the surface energy budget. The net longwave radiation (LW_{net}) slowly increase in the FP simulation compared to the NOFP and this is related to the decrease of the temperature.

On the contrary, the latent and sensible fluxes strongly changes between the NOFP and the FP simulations. The latent heat flux increases in the FP simulation compared to the NOFP by 30% (WFDEI_GPCC) and 60% (AmSud_GPCC) while the sensible heat flux decrease by 70% in both forcings.

Therefore, the changes of temperature and in the surface energy budget find their principal origin in the impact of the floodplains on the latent and sensible fluxes instead of the changes in net radiation.

6.3.3 Evapotranspiration

The changes in the surface energy budget are related to the evapotranspiration through the presence of open water surfaces, the increase of the soil moisture and the development of the vegetation. These impacts are reflected in the annual cycle of the evapotranspiration and its different components (bare soil evaporation, transpiration, evaporation from floodplains and interception loss) shown for both forcings in Figure 6.10.

The potential evaporation is lower through the year in the FP simulations compared to NOFP. This is a consequence of the decrease of the temperature over the floodplains which will decrease the $q_s(T_s)$ term in equation 6.2. This is confirmed by the fact that the potential evaporation changes between NOFP and FP follow the same spatial structure as the surface temperature (not shown). Despite this decrease of the potential evaporation, the evapotranspiration is higher in the FP simulations during all the year but this difference is increased between June and October which would correspond to the drier part of the year (even if it differs from the dry season definition in this chapter). This means that the evaporation over the floodplains is water-limited because, although there is a lower potential evaporation in FP, the potential

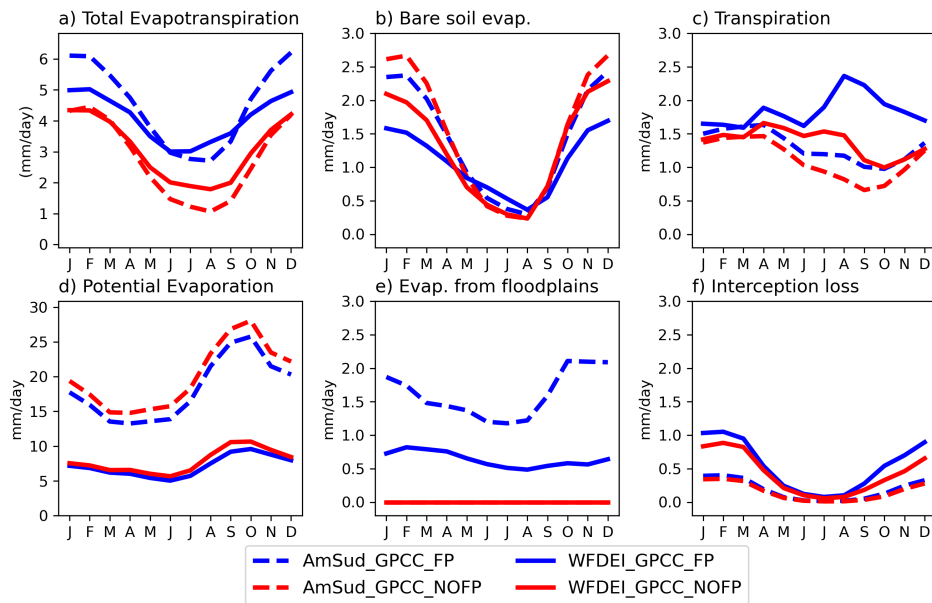


Figure 6.10. Annual cycle of the Evapotranspiration variables for WFDEI_GPCC: (a) Total evapotranspiration, (b) Bare soil evaporation, (c) Transpiration, (d) Potential Evaporation, (e) Evaporation from floodplains and (f) Interception loss.

evaporation remains sufficiently high so that the increased water availability increases the total evapotranspiration.

The changes in evapotranspiration should be affecting the potential evaporation by increasing the near surface air humidity. However, as the simulations considered are forced by atmospheric forcings, there is no feedback reducing the potential evaporation and, thus, being able to reduce the evapotranspiration. Therefore, all the evapotranspirative variables presented here are potentially overestimated by the lack of coupling.

The other variables give an overview of the processes involved in the increased evapotranspiration.

The bare soil evaporation is similar in the FP and NOFP simulation although it is higher in the NOFP simulation during the rainy season. This can be related to the fact that the bare soil evaporation is reduced in the FP simulation because the bare soil are flooded and thus, the precipitation goes to the floodplains reservoir instead of going on the bare soil.

The transpiration is higher in the FP simulation between June and November. This is related to: (1) the increase of the LAI and realised vegetation cover (*vegetfrac*) in the FP simulation and (2) to the increased soil moisture that remains into the ground until the driest period of the year allowing the transpiration to increase strongly during this period. The interception loss is higher in the FP simulation compared to the NOFP simulation during the rainy season since the canopy in the FP simulation can hold more water due to the higher LAI and the higher realised vegetation cover.

Comparing the transpiration between WFDEI_GPCC_FP and AmSud_GPCC_FP, we can observe higher values in WFDEI_GPCC_FP during the dry season. This is related to the more important increase of the soil moisture in WFDEI_GPCC_FP. The other main difference is that

the evaporation from the floodplains is much higher in AmSud_GPCC (around 1.5-2 mm/day) compared to WFDEI_GPCC (around 0.4-0.5 mm/day) which is related to the higher flooded area in AmSud_GPCC and to the difference of incoming radiation between both forcings.

Figure 6.11 shows the spatial representation of the evapotranspiration for the FP simulations over the period 1990-2013 considering the full period, only the dry period and only the flood period and also the difference of evapotranspiration between the FP and the NOFP simulations averaged over the same periods.

It can be observed that the spatial patterns of the differences in evapotranspiration are a combination between the spatial patterns of the soil moisture changes and of the flooded area. The difference between FP and NOFP has more extended changes in soil moisture with the low resolution forcing (WFDEI_GPCC) while the high resolution simulation (AmSud_GPCC) has a more extended and more marked flooded area over the Pantanal. If ignoring the higher values of evapotranspiration in AmSud_GPCC related to the differences between both forcings, the total evapotranspiration leads to similar changes in the FP simulation of both forcings.

Therefore, although the resolution of the forcing will have an impact on the relative importance of the different floodplains processes (soil moisture and flooded area), the floodplains scheme will have a similar impact on the evapotranspiration and the land-atmosphere fluxes at all resolutions.

6.3.4 Budyko Diagram

The Budyko diagram of the closed-catchment upstream of the Porto Murtinho stations (referred as UPRB) between 1990 and 2013 is presented in Figure 6.12. It allows exploring with more details the relationship between evaporation, potential evaporation and precipitation. Each point represents the average of the variables over the UPRB region for a year between 1990 and 2003. The star represent the mean value over the full period. The annual rainfall is the same for each forcing so the only variable that change is the actual evaporation and the potential evaporation.

Comparing the cloud of points and the mean value, the Budyko diagram confirms the previous results because it can be observed that the FP simulation has higher values of actual evaporation and lower values of potential evaporation. Despite the lower values of potential evaporation in the FP simulations, the points remain in the water limited part of the Budyko diagram. Considering that both forcings have the same average precipitation, the Budyko diagram also shows that the atmospheric conditions in the AmSud_GPCC forcing are more arid than WFDEI_GPCC which is attributable to the higher potential evaporation in AmSud_GPCC.

As it is also interesting to explore how the seasons affect these different aspects, a diagram inspired in the Budyko diagram framework is shown in Figure 6.13 for the Pantanal which is not a closed catchment. This diagram contains the hysteresis of the annual cycle with the mean value for each season as well as the annual mean within the Budyko framework.

Even if the Pantanal is not a closed catchment, the mean annual condition is always respecting the Budyko limits in the NOFP simulation. This is related to the fact that, in absence of floodplains scheme, no water from outside the Pantanal can evaporate over the Pantanal and,

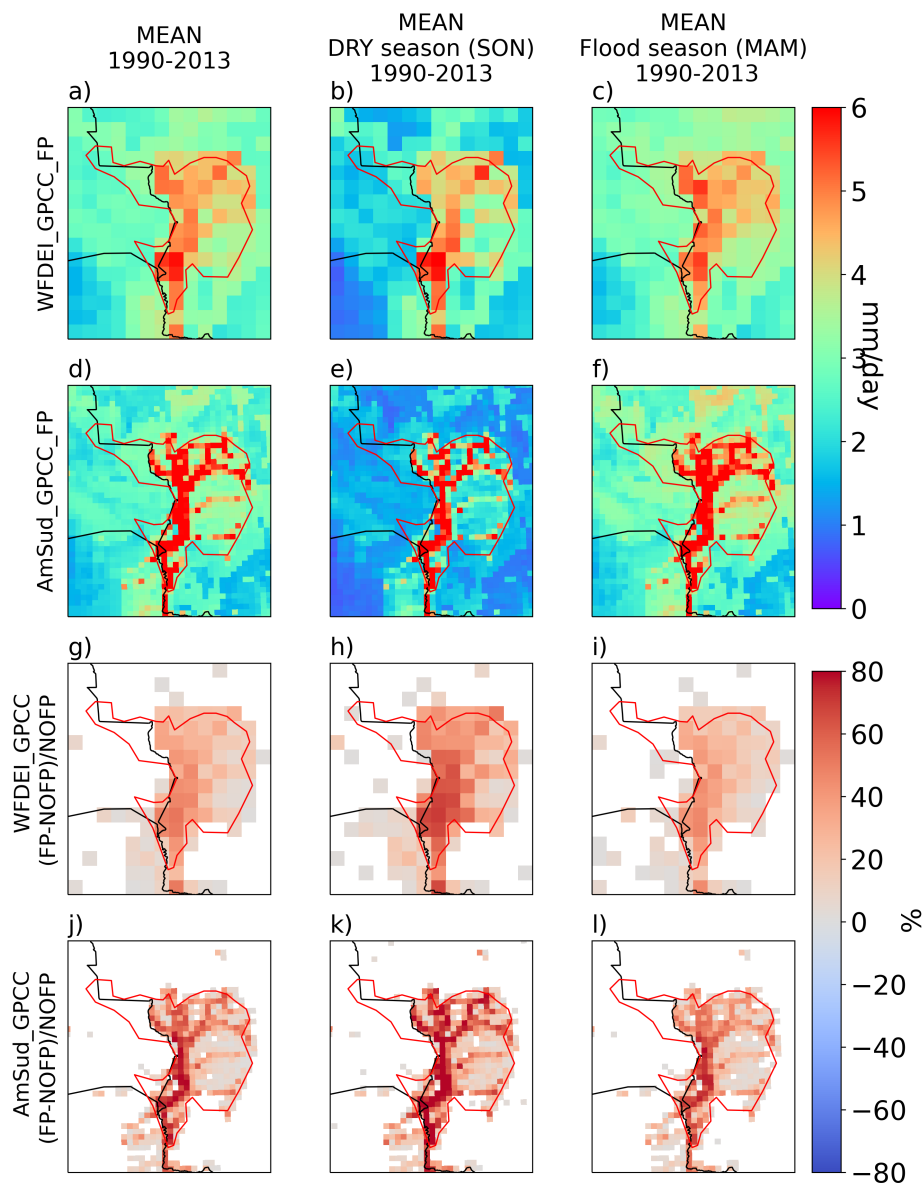


Figure 6.11. Evapotranspiration over each grid point in WFDEI_GPCC_FP (a,b,c) and AmSud_GPCC_FP (d,e,f) and the relative difference between FP and NOFP for WFDEI_GPCC (g,h,i) and AmSud_GPCC (j,k,l) for the period 1990-2013 considering the full year (a,d,g,j), the dry season - SON (b,e,h,k) and the flood season - MAM (c,f,i,l).

thus, the evaporation cannot be higher than the local precipitation. On the contrary, the mean annual condition of the Pantanal in the FP simulations is always exceeding the Budyko limits. This is explained by the fact that the FP simulation can evaporate non-local water from the upstream rainfall. In AmSud_GPCC_FP, all the seasons are exceeding the Budyko limits which means that there is a very high evapotranspiration over the region in this simulation which may confirm the fact that AmSud_GPCC may overestimate the evapotranspiration.

The seasons during which there are more precipitation over the Pantanal (DJF, MAM, SON) have lower values of AET/P. These values are close or lower than 1. On the contrary, the austral

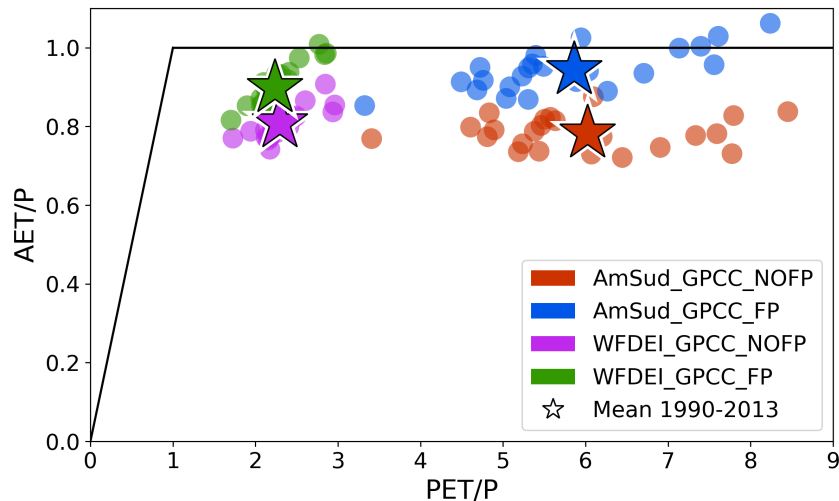


Figure 6.12. Budyko diagram for the FP and NOFP simulations forced by AmSud_GPCC and WFDEI_GPCC between 1990 and 2013. Each points represent the mean of the different variable over the Upper Paraguay River Basin (UPRB) averaged over a year of simulation. The stars represents the mean value over the 24 years of simulation.

winter has values of AET/P much higher than 1 because its precipitation is close to 0 although the potential evaporation remains relatively high which allows the evapotranspiration of the water remaining over the floodplains (cf. Figure 6.10). The major changes in the hysteresis between FP and NOFP in Figure 6.13 are noted in JJA and SON. This is because the Pantanal remains dry during these seasons and, therefore, the evapotranspiration relies more on the non local rainfall from the floodplains during these seasons.

The mean annual values over the x-axis are relatively high and principally for AmSud_GPCC where the potential evaporation is 6 times higher than the local precipitation. This is also related to the lack of feedback of the forcings in the offline simulations mentioned previously that inhibits the decrease of the potential evaporation.

6.4 Conclusion

After validating the floodplains scheme for the high resolution river routing, the simulations with and without floodplains forced by WFDEI_GPCC at a 0.5° resolution and AmSud_GPCC at a 20 km resolution have been analyzed with more details in the current chapter. At first, it focuses on the essentials aspects of the surface state variables: the soil moisture, the temperature and the vegetation. Then, the changes in the surface energy budget and then the evapotranspirative processes are analyzed more in details. These diagnostics have been performed considering different seasons over the period that both forcings have in common (1990-2013). These seasons were the dry season (SON) and the flood season (MAM that occurs just after the rainy season - DJF).

The floodplains infiltration increases the soil moisture over the whole grid cells which contains HTUs with flooded floodplains. The resolution play a role on the extension of the area affected

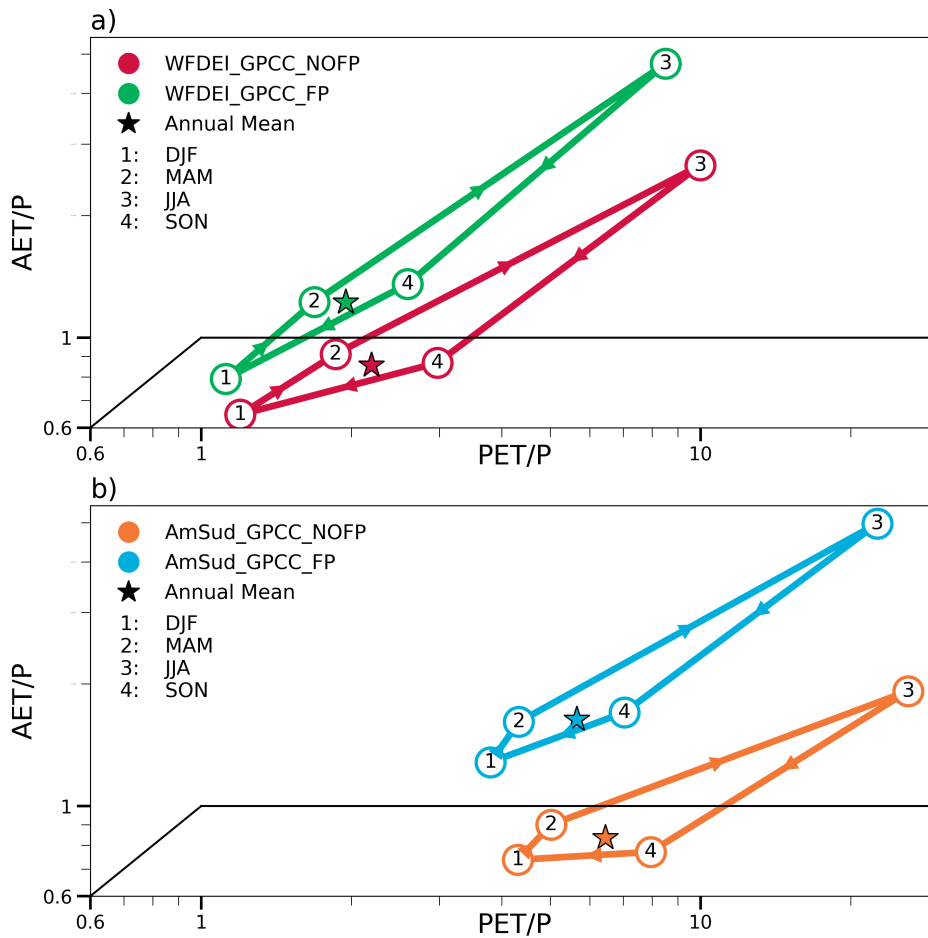


Figure 6.13. Budyko Inspired diagram for the evolution for the different season and the mean state of the most flooded grid points, i.e. with a mean flooded fraction higher than 5% for the different pair of simulations. The results for WFDEI_GPCC are shown in a) and for AmSud_GPCC in b).

by the soil moisture increase. The grid points at low resolution have a larger area, thus, the soil moisture is increasing over a larger area. Globally, the soil moisture increases over the most flooded part but in AmSud_GPCC, the soil moisture decreases over some of the less flooded grid points. This is related to balance of water between the floodplains reservoir and the soil moisture through (1) the infiltration from the floodplains and (2) the precipitation that falls on the floodplains instead of falling on the soil.

The vegetation dynamic is strongly influenced by the soil moisture. The infiltration of water from the floodplains into the soil increases the fraction of the Pantanal covered by vegetation and the density of the vegetation. The increased development of the vegetation in the FP simulation compared to the NOFP simulation is even higher during the dry season because in the NOFP simulation the water availability is very low during the dry season while on the FP simulation the vegetation can use the extra-water available from the floodplains and the increased soil moisture. These changes in vegetation will increase other variables such as the roughness height for momentum and the roughness height for heat. The albedo decreases over almost all the Pantanal but increases over the most flooded part due to the covering of the dark

soil by a vegetation type with a higher albedo. The potential vegetation cover in ORCHIDEE is constructed from a satellite product but these vegetation types requires a realistic water availability to grow as in the reality. Without floodplains, some PFTs predicted by the satellite database did not thrive. The improved coherence between the potential vegetation cover over the Pantanal and the development of the vegetation in the model is a good indicator of the fact that the floodplains scheme improves the land surface simulations over the Pantanal.

The dynamic of the land-atmosphere fluxes over the Pantanal are also affected by the activation of the floodplains scheme with the sensible heat fluxes diminishing while the latent heat fluxes are increasing. This is coherent with the surface temperature decrease over the floodplains. The changes between the FP and NOFP simulations showed that the net radiation change is low compared to the sensible and latent heat fluxes, thus, these two fluxes are the main cause of the changes in the surface energy budget.

The evapotranspiration allows to observe the different origins of the changes in the latent heat fluxes. The principal contributions to the increase of the evapotranspiration are the transpiration and the evaporation from the floodplains. The potential evaporation is lower in the FP simulation due to the decrease of the temperature. However this doesn't have an impact on the evapotranspiration increase. The changes in evapotranspiration are coherent with the influence of the resolution on the dynamic of the floodplains scheme: the transpiration is a more important contribution to the increase of the evapotranspiration in the low resolution while the floodplains evaporation is higher in the simulation forced by the high resolution forcing.

The examination of the evaporative fraction as well as the potential evaporation have shown that there is an overestimation of the evapotranspiration. This has been observed more clearly in the forcing AmSud_GPCC which represent an atmosphere with a higher evaporative demand compared to WFDEI_GPCC. This is caused by the absence of coupling with the atmosphere. The forcing used doesn't consider the floodplains and are not reacting to the surface conditions. This issue is enhanced in AmSud_GPCC because the precipitation is bias corrected but the other variables are not. This means that the atmospheric conditions remains as dry as with the original precipitation. Thus, despite the higher evapotranspiration the near surface humidity remains low and enhances, more than it should be, the evapotranspiration. The coupling between ORCHIDEE and an atmospheric model may help to analysis the impact of the floodplains in realistic conditions (with a feedback from the atmosphere) and gives the opportunity to analyze the land-atmosphere interaction.

The floodplains scheme has a major impact on the ORCHIDEE model through two factors: (1) the soil moisture and (2) the flooded area. The floodplains scheme have different dynamics depending on the resolution of the forcing. The low resolution forcing underestimates the flooded area but achieve to represent the impact of the floodplains on the soil moisture over a more extended area. The high resolution floodplains describe a realistic flooded area which follows the river network closely but its impact on the soil moisture is limited. It is difficult to improve the representation of the flooded area in the low resolution forcing but the representation of the soil moisture in the high resolution forcing can be improved by integrating an horizontal transfer of soil moisture between the grid points to represents the aquifer. Nevertheless, when considering the impact of the soil moisture and the flooded area, both forcings have a coherent

representation of the evapotranspiration even if this is caused by different dynamics.

To conclude, the different impacts of the floodplains scheme are coherent to what can be expected by the presence of open water surfaces and by the infiltration of water from the floodplains. Although the evapotranspiration is certainly overestimated, the simulation with floodplains brings a more realistic representation of the land surface over the Pantanal. Figure 6.14 resumes the different impacts of the presence of the floodplains in the land surface variables in a Land Surface model.

Through this chapter, the impacts of the high resolution floodplains in the ORCHIDEE model over the different surface variables have been better understood. These variables are expected to have an effect on the atmospheric boundary layer which has, at its turn, an impact over the regional circulation and, thus, on the precipitation. The evaluation of these feedbacks between the floodplains and the atmosphere will be assessed by comparing a coupled simulation with floodplains and without floodplains in the following chapter.

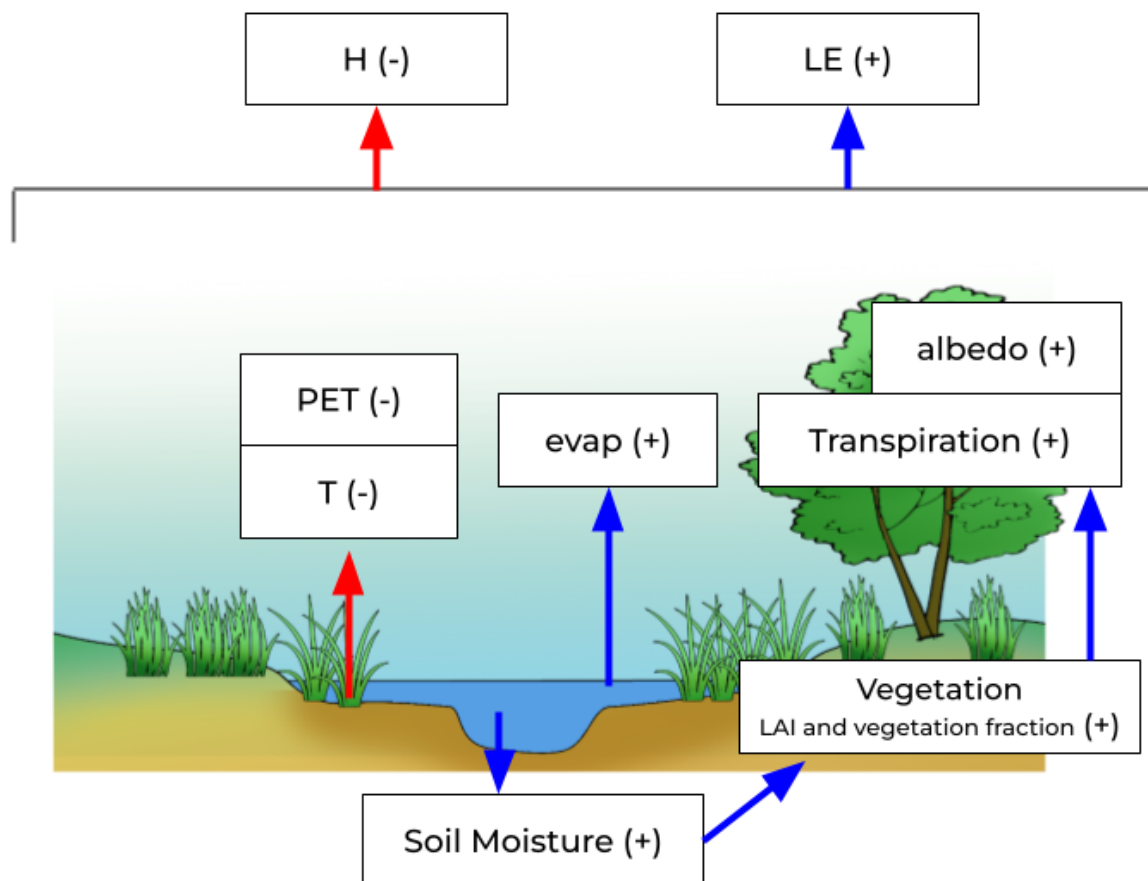


Figure 6.14. Summary of the different impact of the floodplains over the land surface variables in a Land Surface Model.

6.5 Acronyms

AmSud	RegIPSL simulation at 20 km over the South American domain
AmSud_GPCC	Atmospheric forcing based on a RegIPSL simulation at 20 km over the South American domain which precipitation is bias-corrected by GPCC
ESA	European Spatial Agency
ESA-CCI	European Spatial Agency Climate Change Initiative
FP	Offline simulations with the floodplains activated
GPCC	Global Precipitation Climatology Centre
HTU	Hydrological Transfer Unit
LAI	Leaf Area Index
LSM	Land Surface Model
NOFP	Offline simulations with the floodplains deactivated
ORCHIDEE	ORganizing Carbon and Hydrology in Dynamic EcosystEms
PFT	Plant Functional Type
UPRB	Upper Paraguay River Basin
WFDEI	WATCH forcing data bias corrected by ERAI

Feedback between the floodplains and the atmosphere

Contents

7.1	Introduction	165
7.2	Model description and Methodology	170
7.2.1	RegIPSL : Model description	170
7.2.2	Subdivision of the Pantanal region	172
7.2.3	Methodology	172
7.3	Results	174
7.3.1	Impact of the coupling	174
7.3.2	Impact of the floodplains on the coupled simulations	175
7.3.3	Changes in Precipitation over the Pantanal	183
7.3.4	Impact on the regional circulation	188
7.4	Discussion and Conclusion	192
7.5	Acronyms	195

7.1 Introduction

The previous chapter has shown that the annual flood dynamic of the Pantanal floodplains has an impact on the local surface conditions by increasing the evapotranspiration and the soil moisture, by reducing the temperature over the flooded area and by developing regionally both the LAI and the surface covered by the vegetation. However, the absence of land-atmosphere coupling causes an excessive evapotranspiration. This chapter aims to (1) understand how the floodplains influence the land-atmosphere coupling and (2) evaluate the impact of the floodplains on the atmosphere. A pair of land-atmosphere coupled simulations, one with the floodplains scheme activated and the other not, have been used to perform this study as well as an offline simulation of the floodplains to evaluate the impact of the coupling.

The evaluation of the impact of soil moisture on land-atmosphere has received a strong interest in the past decades (Delworth and Manabe, 1989; Koster et al, 2004; Dirmeyer, 2011; Seneviratne et al, 2013; Kumar et al, 2020) and, in particular, over the La Plata Basin which has been studied using climate models as well as satellite data (Ruscica et al, 2016, 2015, 2014; Sörensson and Menéndez, 2011; Spennemann et al, 2017; Menéndez et al, 2019; Coronato et al, 2020; Carril et al, 2016). Fewer studies have focused on the land-atmosphere feedbacks over specific features such as the lakes and wetlands. Concerning the lakes, several studies have focused on the impact of the Great Lakes in North America on the precipitation, and principally on the lake-effect snowfall (Gula and Richard Peltier, 2012; Notaro et al, 2015; Wright et al, 2013; Lucas-Picher et al, 2017) while some other studies have focused on the land-atmosphere coupling over tropical lakes such as the Lake Victoria in East Africa (Finney et al, 2019). Vanderkelen et al (2021) has evaluated the global impact of the open-water reservoirs on the atmosphere through global coupled simulations. Concerning the wetlands, Taylor (2010) has explored the remote feedback between the floodplains, rainfall and MSC over the Niger Inland Delta floodplains. This study has further been extended over all the sub-saharan Africa wetlands (Taylor et al, 2018).

Previous studies on land-atmosphere interactions gives reasons to believe that the floodplains might affect the atmosphere through complex land-atmosphere feedbacks affecting the Planetary Boundary Layer (PBL) vertical profile (Bonan, 1995; Koster et al, 2004; Krinner, 2003) through higher values of equivalent potential temperature and of Convective Available Potential Energy (Kohler et al, 2010; Adler et al, 2011). The tropical floodplains will have a more important impact if they are in a drier region such as a savannah as they will create strong temperature and heat fluxes horizontal gradient discontinuities at the surface. Moreover, these changes may affect the advection of the mass of air over the region (Kumar et al, 2020; Koster et al, 2016; Schubert et al, 2008).

Taylor (2010) shows that the Mesoscale Convective Systems (MCS) are more likely to trigger / re-intensify in the area surrounding the flooded wetlands and this occurs principally during the afternoon / evening. Taylor et al (2018) confirmed that the convection is enhanced around the wetlands and finds that it is suppressed over the flooded area. This phenomenon is related to strong surface heterogeneities which are related to the sensible and latent heat fluxes gradients which creates a "wetland breeze". This wetland breeze is coherent with previous studies which have connected a reduction of the precipitation over the large rivers of the Amazon with a "river breeze" (Silva Dias et al, 2004; Paiva et al, 2011). Taylor et al (2018) confirmed the conclusion that the rainfall is lower over the wetlands compared to the surrounding areas over other African wetlands. Therefore, wetlands have an impact on the local precipitation and can have an impact over the regional precipitation if the local climate involves long-lived MCS such as in the Sahel.

The precipitation changes detailed in Taylor (2010) and Taylor et al (2018) can be partly explained by the contrast between the wet soil of the floodplains and the surrounding drier soils and this has been explored by Adler et al (2011) which studied the impact of a wet soil band anomaly in Western Africa. In the absence of strong horizontal advection in the region, the presence of a wet anomaly contrasting with the surrounding drier soils results in (1) an higher

equivalent potential temperature (θ_e) in the PBL over the wet soil which increases the Convective Available Potential Energy (CAPE) and in (2) a lower actual temperature in the PBL which increases the Convective Inhibition (CIN). Although the CAPE value is higher over the wet feature, the increase of the CIN inhibits the precipitation from the Mesoscale Convective Systems over the wet soil by limiting the upward motion over the moist band. The horizontal advection of the air in the lower level of the atmosphere from the wet soil to the surrounding areas increases θ_e and the CAPE in the area surrounding the moist anomaly. This generates a vertical warm air advection which decreases the CIN. Therefore, the increase of the CAPE and decrease of the CIN in the area surrounding the wet anomaly will increase the precipitation.

The increased moisture supply from the tropical floodplains to the atmosphere may affect a much larger region by increasing the precipitation and changing the local land-atmosphere interactions through a positive feedbacks between precipitation and soil moisture. This positive feedback has largely been studied (Eltahir, 1998; Zheng and Eltahir, 1998; Small and Kurc, 2003). Eltahir (1998) proposed a simple mechanism to explain this positive feedback in the case of an increased soil moisture. This mechanism could explain how the land atmosphere interactions changes in the case of a regional increase of the precipitation over a much larger area than the floodplains themselves. It considers two main factors related to the increase of the soil moisture: (1) the decrease of the albedo and (2) the diminution of the Bowen ratio (Bowen ratio = H/LE with H the sensible heat and LE the latent heat). The second point is related to the increase of the latent heat fluxes compared to the sensible heat fluxes resulting in a decrease of the surface temperature. The net radiation at the surface (cf. equation 7.1) increases when the Longwave and Shortwave downward radiation increases (LW_{\downarrow} and SW_{\downarrow}) and when the Longwave and Shortwave upward radiation decreases (LW_{\uparrow} and SW_{\uparrow}). Both mechanisms will increase the net surface radiation, the first one by reducing directly the upward shortwave radiation (cf. equation 7.2) and the second one by reducing the upward longwave radiation through the reduction of the surface temperature (cf. equation 7.3).

$$R_n = LW_{\downarrow} - LW_{\uparrow} - SW_{\downarrow} - SW_{\uparrow} \quad (7.1)$$

$$LW_{\uparrow} = \epsilon\sigma T_S^4 + (1 - \epsilon)LW_{\downarrow} \quad (7.2)$$

$$SW_{\uparrow} = \alpha SW_{\downarrow} \quad (7.3)$$

where R_n is the net radiation at the surface, LW and SW are the shortwave and longwave radiation at the surface with the arrow indicating whether the fluxes are upward or downward, α is the albedo, ϵ is the longwave emittance, T_S the surface temperature and σ the Stefan-Boltzmann constant.

Assuming that the ground heat flux is negligible, the increased net surface radiation leads to an increase of total turbulent fluxes from the surface to the atmosphere. As said previously, there is an increase of total heat fluxes transfer and an important increase of the latent heat fluxes compared to the sensible heat fluxes (cf. lower Bowen ratio). This reduces the depth of the PBL. The Moist Static Energy (MSE) is a thermodynamic variable that describes the

total energy (geopotential energy, sensible and latent heat) in a layer of the atmosphere. The PBL MSE is useful to describe moist convection. Over a large area, the advection of MSE is negligible and, under this assumption, [Eltahir \(1998\)](#) describes the PBL MSE changes (cf. equation 7.4) as being supplied by the heat fluxes from the surface into the atmosphere (F) while it is reduced by the entrainment at the top of the PBL (EN), by the radiative cooling fluxes (R) and by the convective downdraft during precipitation events (C_o). The increased of the soil moisture is supposed to have a negligible direct impact on R and C while EN is supposed to remains small over a region with reduced sensible heat fluxes. Therefore, an increase of F due to a higher soil moisture over a large region will increase the local MSE of the PBL. The reduction of the PBL depth reinforces the increase of the PBL MSE. These conditions increase the vertical gradient of MSE and, therefore, create more unstable conditions that enhances the probability of convective event over the region.

$$\frac{\partial MSE}{\partial t} = F - EN - R - C \quad (7.4)$$

[Small and Kurc \(2003\)](#) resume the positive feedback between soil moisture and precipitation from the previous studies of [Betts and Ball \(1998\)](#); [Eltahir \(1998\)](#); [Zheng and Eltahir \(1998\)](#) by the following four steps mechanism:

1. the wet soils have a lower Bowen ratio which means they have higher latent heat fluxes compared to the sensible heat fluxes.
2. the lower Bowen ratio reduces the Planetary Boundary Layer Height (PBLH)
3. the shallower PBL induces the Moist Static Energy (MSE) to be more concentrated because of the low entrainment across the top of the Boundary Layer.
4. the higher MSE in the PBL increases the convective precipitation

The precipitation on the La Plata Basin is strongly related to the moisture transport from the South American Low Level Jet (SALLJ) ([Zanin and Satyamurty, 2020](#); [Martinez and Dominguez, 2014](#); [Su and Lettenmaier, 2009](#)). During the austral summer, the precipitation is mostly related to the moisture transport from the tropical Atlantic, the subtropical southwestern Atlantic, the tropical North Atlantic and the recycling of the precipitation over the Amazon and LPB ([Zanin and Satyamurty, 2020](#)). In austral winter, the precipitation in the LPB is more related to the recycling of the precipitation from the Southern Amazon and Upper Paraguay River Basin. Therefore, the Pantanal is an important source of moisture for the LPB precipitation during the austral winter. This is confirmed by ([Su and Lettenmaier, 2009](#)) which showed that the Pantanal is the only region of the LPB which has a high recycling of the evapotranspiration into precipitation over the basin throughout the year. The Pantanal is located over the SALLJ ([Zanin and Satyamurty, 2020](#); [Martins et al, 2013](#)) therefore the impact of the floodplains on the atmosphere and, in particular, on the PBL can affect the SALLJ by enhancing/reducing the moisture transport and/or by deflecting it. Moreover, the extra evapotranspiration related to the presence of the floodplains brings an extra moisture to the SALLJ ([Zanin and Satyamurty, 2020](#)). This explains why the Pantanal can affect a larger area downstream of the SALLJ.

This chapter aims to capture and estimate the impact of the floodplains over the climate using the high resolution floodplains scheme within RegIPSL, a regional coupled model. The RegIPSL simulations used in this Chapter are performed over the South American domain at a 20 km resolution. The description of the floodplains over the tropical and subtropical part of this domain is shown in Figure 7.1. In the Amazon, the floodplains represented are the main Amazon river and the Llanos de Moxos. There are other large flooded areas (flooded forest, swamps, lake) over the Amazon but their dynamics are not covered by the proposed parameterization of the floodplains (see Chapter 5). The region of interest is the Pantanal because it is a large tropical floodplain in a semi-arid climate region and, therefore, is supposed to have a the strong impact on the land-atmosphere interactions. The absence of important flooded areas over the Amazon will make more visible the effect of the Pantanal on the regional circulation.

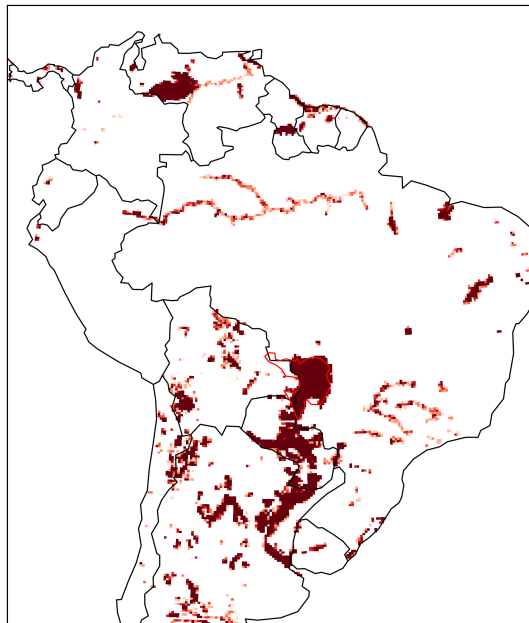


Figure 7.1. *Floodplains in the river routing file for the AmSud domain.*

RegIPSL is the regional model of the Institut Pierre Simon Laplace (IPSL; <https://gitlab.in2p3.fr/-/ipsl/lmd/intro/regipsi/regipsi/wikis/home>) which predecessor is the MORCE-MED plateforme. This model couples the ORCHIDEE LSM, the WRF atmospheric model, and the NEMO ocean model. This chapter focuses on the land atmosphere interactions, thus the ocean component of RegIPSL has not been activated for the simulations. The impact of the floodplains on the land-atmosphere interactions is assessed by comparing two coupled simulations : one with the floodplains activated (AmSud_Flood) and the other deactivated (AmSud_NoFlood) over a 22 year period (1998 - 2019). Additionally, the AmSud_Flood simulation is compared to an offline simulation without floodplains forced by the AmSud_NoFlood atmospheric conditions to study the impact of the coupling on the representation of the floodplains.

The present chapter tries to determine : (1) what is the impact of coupling on the representa-

tion of floodplains; (2) what is the impact of the Pantanal floodplains floodplains on the land-atmosphere interactions; (3) what are the impact on precipitation and (4) why including floodplains in Earth System Models and Regional Climate Models might improve the realism of the simulations. The methodology, models and data used in this chapter are presented in the second section. The third section evaluates the coupled simulation, assesses the impact of the floodplains scheme on the atmospheric variables and compares it to the absence of coupling. Section 4 presents the land-atmosphere interactions. The results are discussed and a conclusion is drawn in Section 4.

7.2 Model description and Methodology

7.2.1 RegIPSL : Model description

The Regional Climate Model of the Institut Pierre Simon Laplace (IPSL) is the RegIPSL coupled model which follows the development of the MORCE-MED platforme (Drobinski et al, 2012). RegIPSL couples 3 models representing different components of the Earth System : the Land Surface with the ORCHIDEE model (Organizing Carbon and Hydrology in Dynamic Ecosystems; Krinner et al., 2005), the atmosphere with the WRF model (Weather Research and Forecasting; Skamarock et al, 2008) and the ocean with the NEMO model (Nucleus for European Modelling of the Ocean; Madec and the NEMO Team, 2016). These different models are connected through the OASIS3-MCT coupler (Craig et al, 2017). The simulations performed in this chapter do not include the NEMO model. The management of the Input and Output is performed by XIOS (XML-IO-Server), an asynchronous parallel I/O server. ORCHIDEE uses the same grid as WRF and the WRF-ORCHIDEE coupling follows the method from Polcher et al (1998).

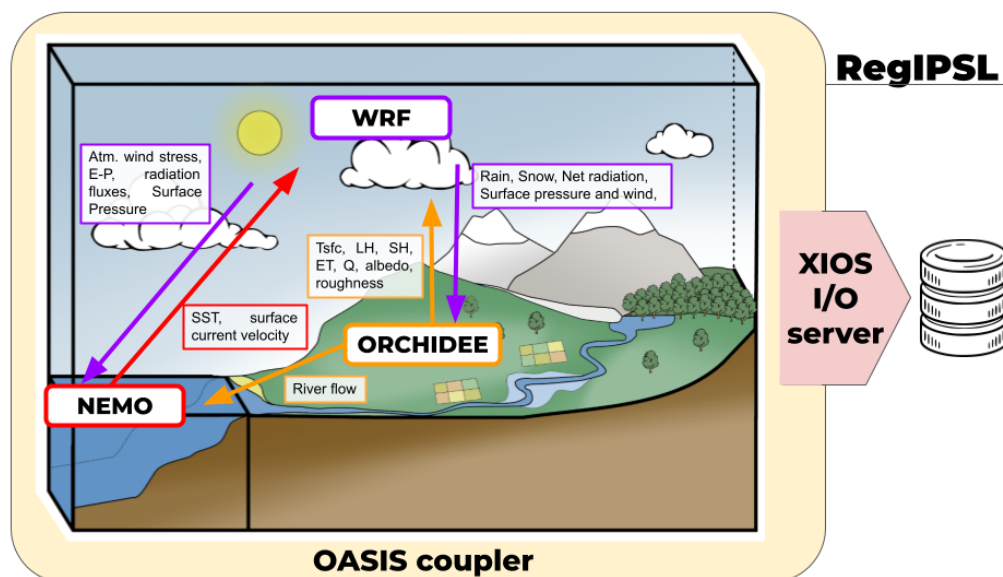


Figure 7.2. Scheme of RegIPSL coupled model.

The WRF model is commonly used in a large variety of climatological studies and for opera-

tional uses within a large range of spatial and temporal scales (Powers et al, 2017). The version of WRF used in the RegIPSL simulations is the version 3.7.1. The domain is a 20 km resolution Lambert Conformal projection covering the integrality of South America (cf. Figure 7.2). The simulations considered 50 vertical levels with a top atmospheric pressure set at 10 hPa. The microphysic scheme used is the Morrison 2-moment scheme (Morrison et al, 2009). The simulation of the PBL is implemented with the Mellor-Yamada-Nakanishi-Niino (MYNN) 2.5 boundary layer scheme (Nakanishi and Niino, 2009). The Rapid Radiative Transfer Model for General Circulation (RRTMG; Clough et al, 2005) is used to represent the radiation. The deep and shallow convection is represented by the Grell-Devenyi ensemble cumulus scheme (Grell and Freitas, 2014). A spectral nudging is used to avoid undesirable effects due to the prescribed boundary conditions thereby improving the simulation's performance (Omrani et al, 2015). The interaction with the surface is performed through the PBL. This configuration is a standard configuration for the WRF model and has been selected through a sensibility test of the different WRF configurations in the ORCHIDEE-WRF coupled simulation over the domain.

Subject	Option	Reference
Microphysics	Morrison 2-moment scheme (M2M)	Morrison et al (2009)
Planetary boundary layer	Mellor-Yamada-Nakanishi-Niino 2.5 scheme (MYNN)	Nakanishi and Niino (2009)
Radiation	Rapid Radiative Transfer Model for General Circulation (RRTMG)	Clough et al (2005)
Land surface model	ORCHIDEE	Krinner (2003)
Deep and shallow convection	Grell-Freitas ensemble cumulus scheme	Grell and Freitas (2014)

Table 7.1. *Parameterization of the WRF simulations.*

The ORCHIDEE model includes two main components : (1) SECHIBA, a component for the water and energy processes and fluxes and (2) STOMATE for the carbon processes and fluxes and for the vegetation dynamic. The soil hydrology is simulated through a 11-layer soil description (De Rosnay et al, 2000; de Rosnay et al, 2002; Campoy et al, 2013). The dynamical vegetation is simulated using 13 Plant Functional Types (PFTs) considered as a fraction of each grid cell which all have a different underlying parameterization. The PFT description used in the simulation has been constructed from the ESA-CCI database (European Space Agency-Climate Change Initiative; ESA, 2017). The river dynamic is simulated by the high resolution river routing scheme based on the Hydrological Transfer Unit concept (Nguyen-Quang et al, 2018b) constructed with RoutingPP (see Chapter 4 for more details) using the 2 km resolution version of MERIT-Hydro (Yamazaki et al, 2019) using a maximum of 55 sub-basins per grid cell. The maximal floodplains fraction over the HTUs are estimated using the interpolation of the GLWD dataset (WWF, 2004) to the MERIT-Hydro grid.

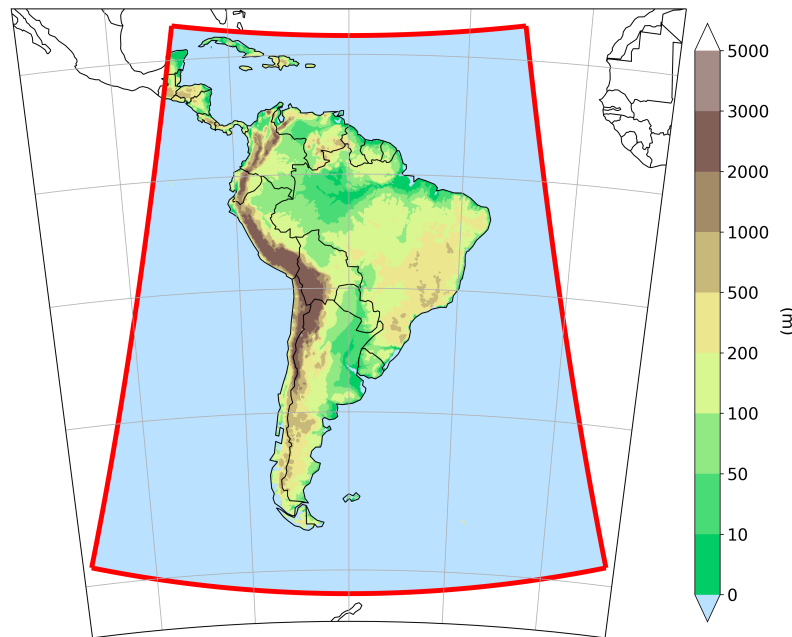


Figure 7.3. CORDEX-SA domain used for the simulations.

7.2.2 Subdivision of the Pantanal region

The study of the impact of the activation of the floodplains scheme in a coupled simulation must include the surroundings of the Pantanal because these regions can be affected by the floodplains through the land-atmosphere coupling. For this reason, 5 different regions have been considered among which 4 are represented in Figure 7.4 and are describe at continuation :

- **Pantanal (P)**: region of floodplains which will be directly affected by them
- **South (S)**: region south of the Pantanal, may include some floodplains too in its central part (see Figure 7.1)
- **West (W)**: region at the west of the Pantanal corresponding the the Gran Chaco
- **North-Northeast (NNE)**: region at the North and Northeast of the Pantanal which corresponds to the Cerrado
- **Most flooded part of the Pantanal (F)**: this subdomain is not shown in Figure 7.4. It is included in the Pantanal subregion but only considered the most flooded grid point of the Pantanal (with a mean flooded fraction for the 1998-2019 period that is higher than 0.7).

7.2.3 Methodology

Two simulations have been performed over the period 1998-2019 with the exact same configuration except that one simulation includes the floodplains scheme (AmSud_Flood)and the

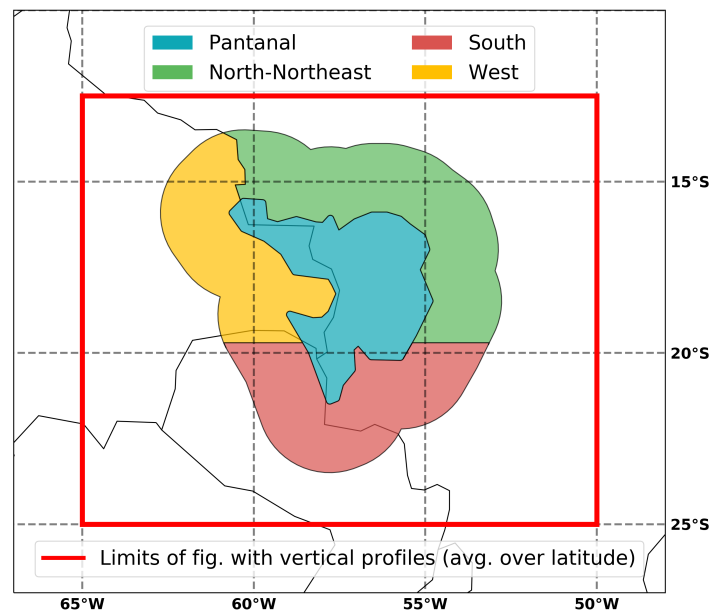


Figure 7.4. Regions considered to subdivide the Pantanal and its surroundings.

other doesn't (AmSud.NoFlood). The lateral conditions of these simulations are driven by the ERA5 reanalysis with a light spectral nudging above the PBL (Omrani et al, 2015). The initial conditions of these simulations are based on a 10 years offline spin-up of the land surface variables and a 2 year spin up of the atmospheric variables to ensure that the models are at equilibrium at the initialization of the simulations.

This set of simulation has been completed by an offline ORCHIDEE simulation with the floodplains scheme activated but forced by the atmospheric conditions of AmSud.NoFlood (AmSud_offline_FP).

Name	Description
AmSud_Flood	Coupled simulation with the floodplains scheme activated
AmSud_NoFlood	Coupled simulation with the floodplains scheme deactivated
AmSudNOF_offline_FP	Offline simulation of ORCHIDEE forced by the atmospheric simulation from AmSud.NoFlood simulation

Table 7.2. Description of the simulations.

The 4 main objectives of this chapter are the following :

1. **Evaluate the impact of the coupling** : by comparing the AmSud_Flood with the AmSud_offline_FP over the Pantanal,
2. **Evaluate the regional impact over the surface variables** : by comparing AmSud_Flood and AmSud_NoFlood
3. **Evaluate the precipitation changes** : by comparing AmSud_Flood and AmSud_NoFlood

4. **Evaluate the impact over the atmospheric circulation** : by comparing AmSud_Flood and AmSud_NoFlood

7.3 Results

7.3.1 Impact of the coupling

The previous chapter has shown that the absence of coupling may enhance the evapotranspiration of over the floodplains to unrealistic levels due to the fact that near-surface air humidity remains low. This error can be evaluated more in details through the comparison of AmSud_Flood and AmSudNOF_offline_FP which has the floodplains scheme activated but with the atmospheric conditions of the AmSud_NoFlood simulation (without floodplains). Both simulations are comparable because the AmSud_NoFlood has the same configuration (except for the floodplains) as AmSud_Flood.

Figure 7.5 shows the output from the different simulations with the Precipitation over the UPRB, the discharge, the mean flooded area for AmSud_Flood and AmSud_offline_FP and the annual cycle of the flooded area. The precipitation over the catchment is higher during the wet season in AmSud_Flood compared to AmSud_NoFlood. The discharge is better correlated with the observations when activating the floodplains scheme (AmSud_Flood and AmSud_offline_FP). The temporal and spatial evolution of the flooded area is similar in both AmSud_Flood and AmSud_offline_FP simulations. Despite the higher precipitation in AmSud_Flood over the entire basin and the higher evapotranspiration in AmSud_offline_FP over the Pantanal, the discharge is higher in AmSud_offline_FP. This is related to the changes of the P-E flux over the area upstream of the Pantanal in AmSud_Flood while the floodplains scheme doesn't affect these areas in the offline simulation.

Figure 7.6 shows the impact of the floodplains scheme on the different evapotranspiration variables and how it affects the uncoupled simulation. The simulations with floodplains have a higher total evapotranspiration and transpiration compared to AmSud_NoFlood. The main difference between the coupled and the uncoupled simulations with the floodplains activated is that the uncoupled simulation has a much higher potential evaporation than AmSud_Flood which increases strongly the evaporation from the floodplains and the transpiration. The atmosphere in the uncoupled simulation is unrealistically dry due to the absence of feedback from the atmosphere which promotes an increased potential evapotranspiration and, therefore, increases the different evaporative fluxes. The interception, the evaporation of the water that remains on the vegetation, depends on the state of the vegetation and on the precipitation. Although the difference of interception between the simulation is small, during the austral summer AmSud_Flood has a higher interception loss compared to AmSud_NoFlood which can be related to the increased precipitation. On the contrary, AmSud_offline_FP has a lower interception loss compared to AmSud_NoFlood. However, the transpiration in AmSud_offline_FP is higher signaling a more developed vegetation. Therefore, the lower interception in AmSud_offline_FP can be related to the different vegetation types covering the Pantanal in both simulations.

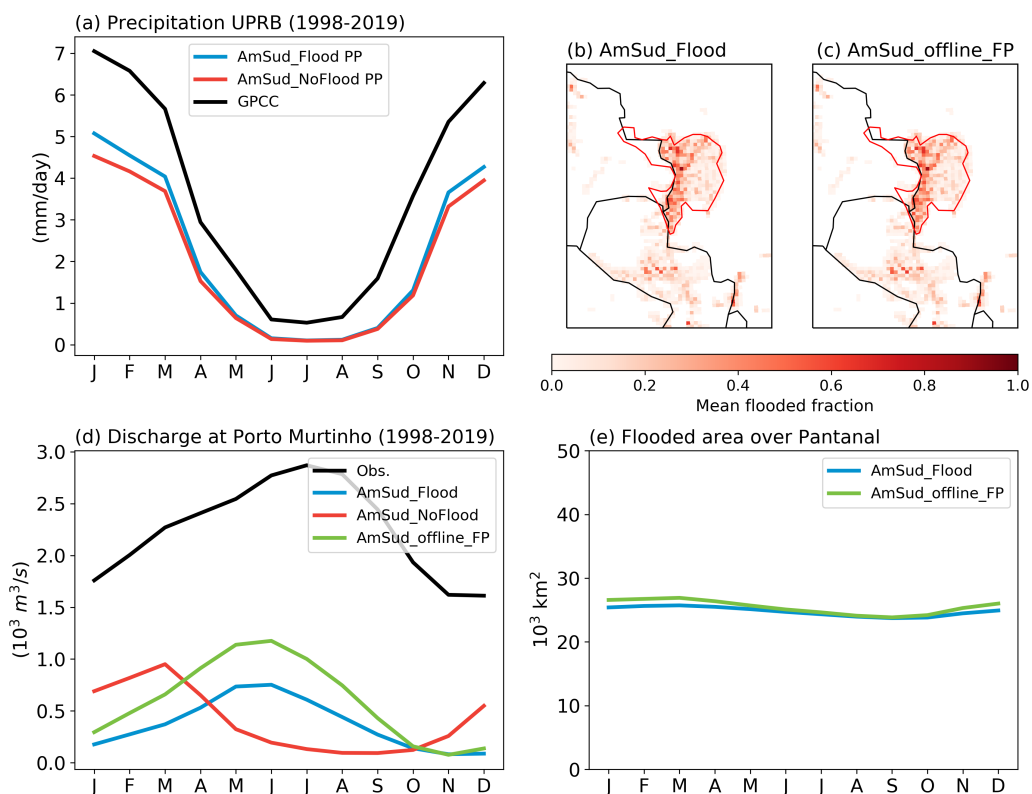


Figure 7.5. (a) shows the annual cycle between 1998 and 2019 of the precipitation over the Upper Paraguay River Basin for both coupled simulations, (b) and (c) represents respectively the mean flooded area in AmSud_Flood and AmSud_offline_FP while (e) represents the annual cycle of the flooded area for these two simulations. (d) shows the discharge at Porto Murtinho in the three simulations.

These results are coherent with the previous chapters and demonstrates that, although the representation of floodplains promotes more realistic surface conditions, the absence of coupling leads to an overestimation of the evaporative fluxes over the floodplains.

7.3.2 Impact of the floodplains on the coupled simulations

The local land-atmosphere interactions related to the Pantanal are shown in this subsection. Figure 7.7 shows the annual cycles of the precipitation over the five subregions defined previously for both simulations and compares them to the GPCC dataset. The precipitation increases during the wet season over all the regions except for the most flooded areas. It also increases during the austral autumn in the West region. Although these simulations are strongly underestimating the precipitation on the region, this precipitation increase in the AmSud_Flood simulation reduces this underestimation. Over the most flooded area, the precipitation is lower in the AmSud_Flood simulation which means that the underestimation of the precipitation in the simulation would be more important. However, over such a reduced region with a particular local feature (open water surface), the construction of the precipitation in the GPCC dataset may be biased because : (1) it is constructed from the rain gauge stations and central South

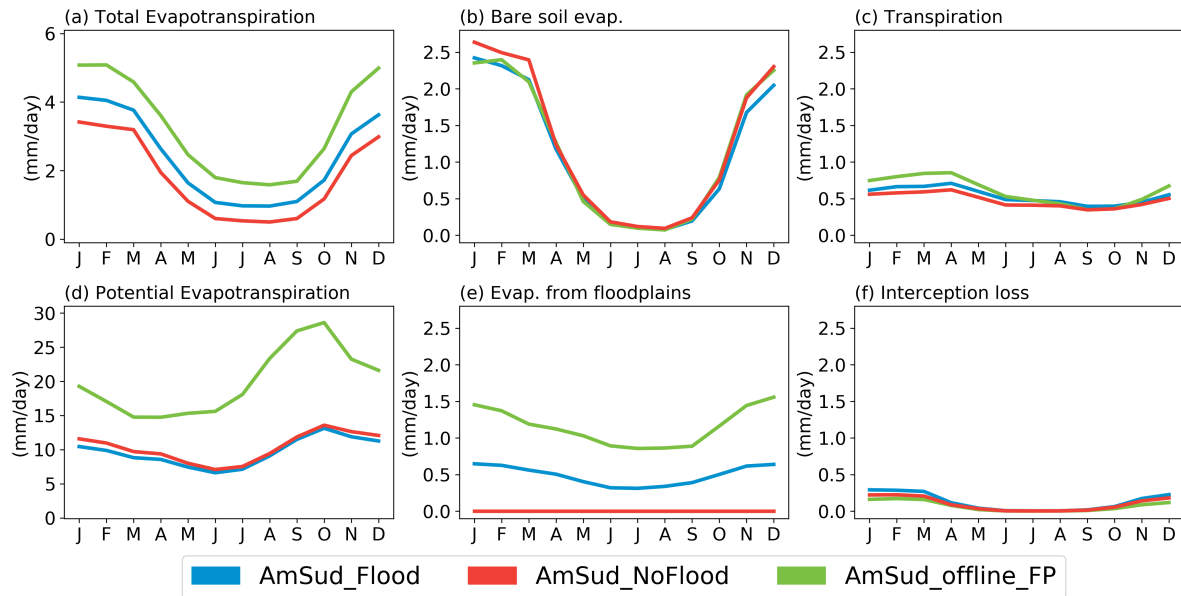


Figure 7.6. Changes of (a) Evapotranspiration, (b) bare soil evaporation, (c) transpiration, (d) Potential evapotranspiration, (e) Evaporation from floodplains and (f) Interception loss over the Pantanal between AmSud_Flood, AmSud_NoFlood AmSud_NoFlood_offline_FP.

America is a region with scarce rain gauge (Marengo et al, 2012) and (2) the interpolation of the precipitation doesn't consider local effect of the surface such as the effect of the open water surfaces (Paiva et al, 2011; Silva Dias et al, 2004).

The analysis of the precipitation changes can be completed by analyzing the P-E fluxes presented in Figure 7.8. The flooded areas are marked by strong negative P-E fluxes throughout over the year (less than -0.8). The changes compared to AmSud_NoFlood over these areas are significant for all the seasons. During the dry season (JJA), P-E is negative in both simulations but with lower values in AmSud_Flood. This decrease of P-E in JJA is significant over all the region except at the South/Southeast of the Pantanal. The lower values of P-E during the austral autumn (MAM) and winter (JJA) are related to the fact that the increase of evapotranspiration during these seasons is related to the increase of the precipitation in SON and DJF and therefore is more important than the increase of precipitation occurring in MAM and JJA. During the austral spring and even more during the austral summer, there are higher values of P-E in the AmSud_Flood simulation which is related to the increase of the precipitation in this simulation. In conclusion, the activation of the floodplains scheme turns the Pantanal from being a moisture sink ($P - E > 0$) to a moisture source ($P - E < 0$) because it is able to evaporate the water transported to the region by the hydrological network.

Figure 7.9 shows the mean vertical profile of the temperature average between 25°S and 12.5° which corresponds to the location of the Pantanal. The activation of the floodplains scheme leads to a significant decrease of the temperature between 1000 hPa and 800 hPa with differences of almost 1 K above the main Paraguay river around 57°W (the most flooded region). The area of significance extends over a larger longitudinal extent in DJF (between -60°W and -55°W) and extends vertically. The decrease of the temperature extends over a larger region

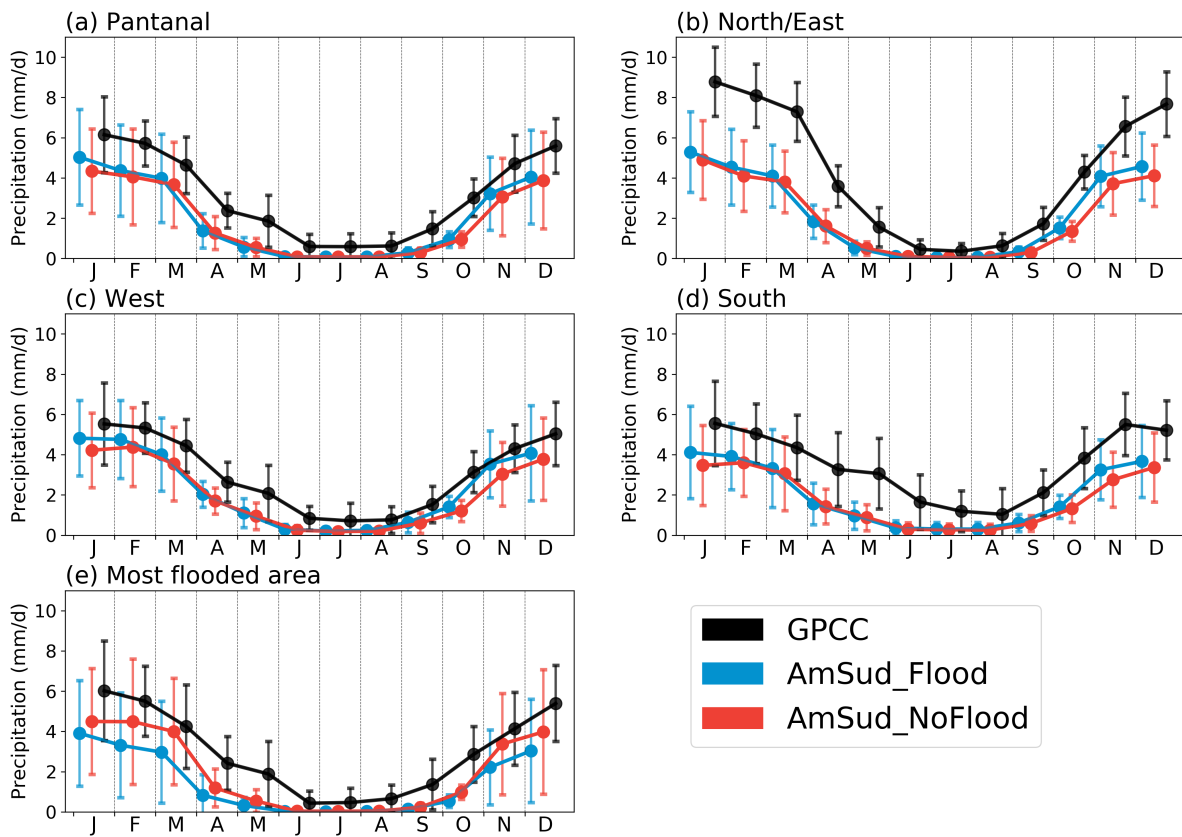


Figure 7.7. Annual cycle of the precipitation for AmSud.Flood, AmSud.NoFlood and the GPCP dataset over the five subregions defined between 1998 and 2019.

and vertically during the most rainy seasons (SON and DJF). This shows that the difference of temperature at the surface shown in the previous chapter can affect the atmosphere up to the height of 800 hPa and more importantly during the wet season. The decrease of the temperature is more important over the longitude with the most flooded areas (cf. Figure 7.9.i-l).

Another important aspect to analyze is the air humidity, this is why Figure 7.10 shows the mean vertical profile of the specific humidity average over the same latitude band. The floodplains scheme has different impact on the specific humidity. In general, in AmSud.Flood compared to AmSud.NoFlood, the specific humidity is higher over the lower level of the atmosphere (between 1000 hPa and 800 hPa) and is lower over the middle level of the atmosphere (between 800 and 400 hPa) and it has higher values over the higher level (between 400 hPa and 200 hPa). The increase over the lower level is significant during all the year but it is more important during the dry seasons (JJA) and partly during SON as it increases by 8% over the western region of the Pantanal. These differences related to the higher evapotranspiration have a more important impact on the atmosphere specific humidity during the drier period of the year. On the contrary, the negative difference of specific humidity over the middle level occurs principally in DJF and MAM with a significant decreases that can reach almost 6%. The increase over the higher level is only significant in DJF and MAM. The decrease of the specific humidity in AmSud.Flood around 700hPa is related with the lower PBL. Therefore, at this pressure level in the AmSud.Flood simulation, the drier free tropospheric air will replace the moist air from

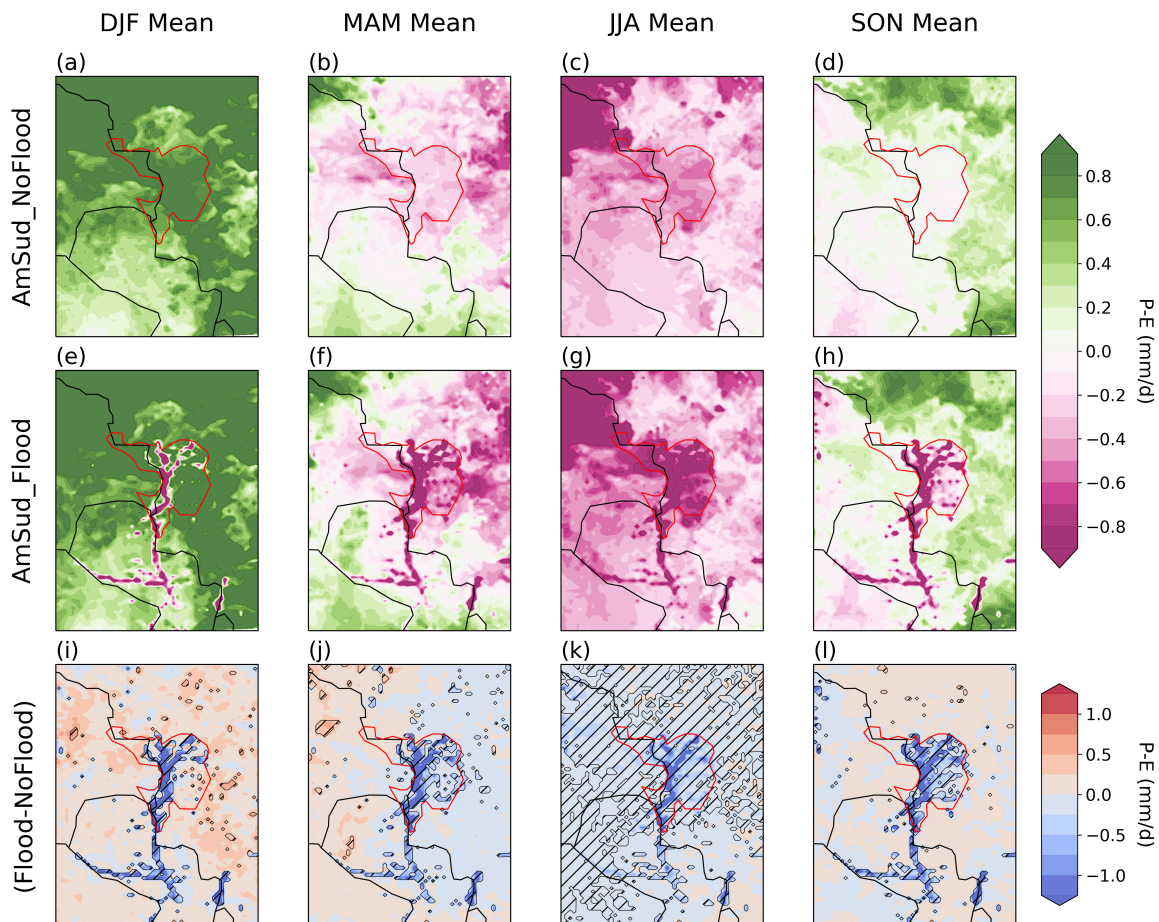


Figure 7.8. Presentation of the mean value of Precipitation minus Evapotranspiration for AmSud_NoFlood (a-d), AmSud_Flood (e-h) and the difference between both (i-l) average over the different season : DJF (a,e,i), MAM (b,f,j), JJA (c,g,k), SON (d,h,l). The differences between AmSud_Flood and AmSud_NoFlood, which have a significance level higher than 95% using a Student's t-test are hatched.

the well mixed PBL. The longitudinal profile of specific humidity increase when activating the floodplains corresponds well with the longitudinal profile of evapotranspiration. Therefore, this allows us to assume that the increase of the specific humidity over the lower layer is directly related with the increase of the evapotranspiration over the floodplains

The height of the PBL is shown in Figure 7.11. The activation of the floodplains scheme decreases significantly the PBL height over the Pantanal over all the year, over the South in DJF and over the West between March and November. This decrease is more important over the flooded areas where the height of the PBL is at least 20% lower. These relative changes are more important during the DJF and MAM season.

The MSE mentioned in the introduction can be analyzed through θ_e . Figure 7.12 shows the vertical profile along the longitude of the Pantanal averaged between 25°S and 12.5°S. There is a significant increase of θ_e in the lower layer of the atmosphere and decrease over the middle layer over all the longitudinal extent of the Pantanal in DJF. The significant increase over the

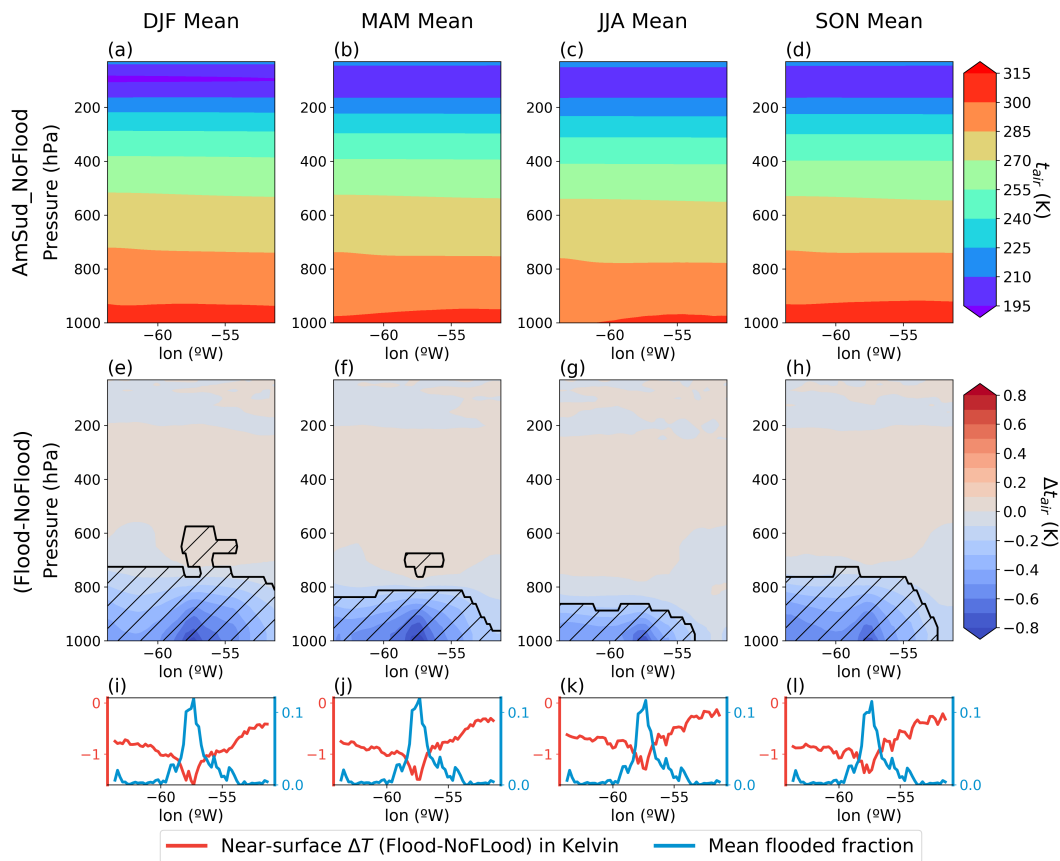


Figure 7.9. Mean vertical profile of actual temperature between 25°S and 12.5°S for *AmSud.NoFlood* (a-d) and the difference between *AmSud.Flood* and *AmSud.NoFlood* (e-h) for the different season: DJF (a,e), MAM (b,f), JJA (c,g) and SON (d,h). The differences between *AmSud.Flood* and *AmSud.NoFlood*, which have a significance level higher than 95% using a Student's *t*-test are hatched. The average of the difference of near-surface temperature between *AmSud.Flood* and *AmSud.NoFlood* as well as the average of the flooded fraction in *AmSud.Flood* between 25°S and 12.5°S is shown for DJF (i), MAM (j), JJA (k) and SON (l).

lower layer moves toward the West from March to August while the decrease move toward the East. In JJA, the decrease at 700hPa is smaller and not significant. In SON, in increase on the lower level moves back to the East and the decrease on the middle levels moves back to the West and is significant again.

Considering the Pantanal and its surrounding and if ignoring the particular local effect of the most flooded areas on the precipitation, these results are coherent with the mechanism described by [Eltahir \(1998\)](#) and presented in the introduction because, additionally to the decrease of the Bowen ratio due to the higher soil moisture, the MSE is higher in the lower layer and, in particular, in the PBL. In the meanwhile, the MSE decreases in the middle level, therefore, there is an higher gradient of MSE between the lower and middle level of the atmosphere what will increases the probability of convection over the region. This produces higher precipitation over the Pantanal and its surrounding (except for the most flooded areas).

The longitudinal profile of the difference of θ_e at the surface (Figure 7.12 from i to l) corresponds well with the precipitation changes West of 60°W in DJF, MAM and SON and East of

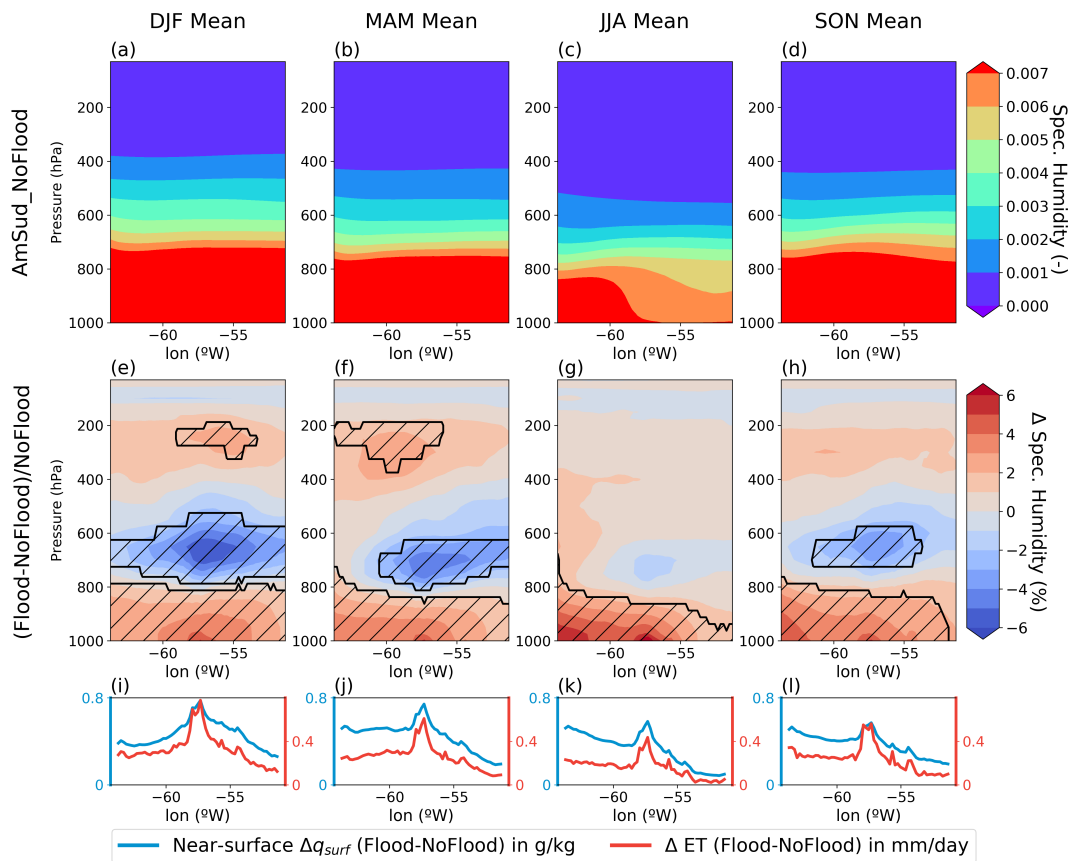


Figure 7.10. Mean vertical profile of specific humidity between 25°S and 12.5°S for AmSud_NoFlood (a-d) and the relative difference between AmSud_Flood and AmSud_NoFlood (e-h) for the different season: DJF (a,e), MAM (b,f), JJA (c,g) and SON (d,h). The differences between AmSud_Flood and AmSud_NoFlood, which have a significance level higher than 95% using a Student's t-test are hatched. The average of the difference of near-surface specific humidity and evapotranspiration between AmSud_Flood and AmSud_NoFlood between 25°S and 12.5°S is shown for DJF (i), MAM (j), JJA (k) and SON (l).

56°W in DJF and SON. Over the most flooded longitude (around $57/58^{\circ}\text{W}$) there is an increase of θ_e but a decrease of the precipitation. This is related to the processes described by Adler et al (2011). The surrounding of the Paraguay river, flowing from North to South, are the most flooded area which forms a moist band and, locally, there is an increase of the CAPE but, due to the dry/wet contrast, the CIN decreases locally over this moist band inhibiting the precipitation which explains the reduction of the precipitation around this longitude despite the increase θ_e . During JJA, the θ_e changes don't have a particular impact on the precipitation because the atmosphere is dry.

The cloud cover brings information to understand the precipitation and radiation fluxes changes. Figure 7.13 show the changes of the cloud cover over the different subregions. Apart the calculation of the total cloud cover, this figure also integrates the low level cloud cover (c_{ll} , from the surface and 680 hPa), the middle level cloud cover (c_{lm} , from 680 hPa to 440 hPa) and the high level cloud cover (c_{lh} from 440hPa to the top of the atmosphere). The total cloud cover is

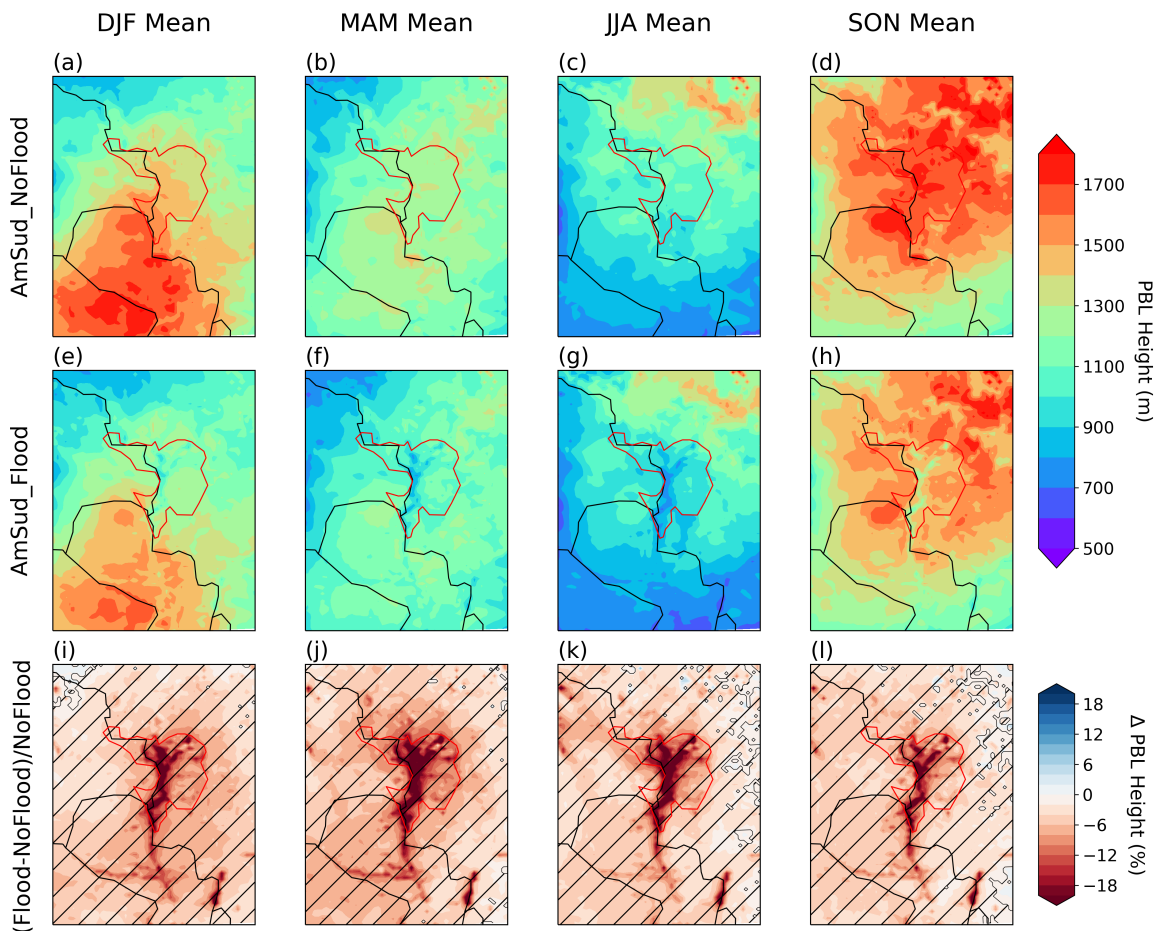


Figure 7.11. Mean value of the Planetary Boundary Layer height for AmSud_NoFlood (a-d), AmSud_Flood (e-h) and the relative difference between both (i-l) average over the different season : DJF (a,e,i), MAM (b,f,j), JJA (c,g,k), SON (d,h,l). The differences between AmSud_Flood and AmSud_NoFlood, which have a significance level higher than 95% using a Student's t-test are hatched.

similar in both simulations although it is slightly lower in AmSud_Flood over the most flooded and slightly higher between November and June in AmSud_Flood over the other regions. The high level cloud cover is not affected by the activation of the floodplains scheme and, as it represents the most important contribution to the cloud cover, it is better to analyze the low and middle level cloud cover.

The middle level cloud cover decreases between October and March in AmSud_Flood compared to AmSud_NoFlood over the Pantanal, North/East, and South while the low level cloud cover increases all over the year in the West and the South and between November and April in the North/East. This is related to what have been seen previously with the specific humidity where the lower PBL in AmSud_Flood turns the middle level of pressure into drier air. Both the middle and low level cloud cover decreases over the most flooded area what is related to the reduction of the precipitation over this region.

The annual cycle of the radiative fluxes at the surface are analyzed in Figure 7.14. This Figure shows that the downward longwave radiation ($rlds$) is similar over the different regions except

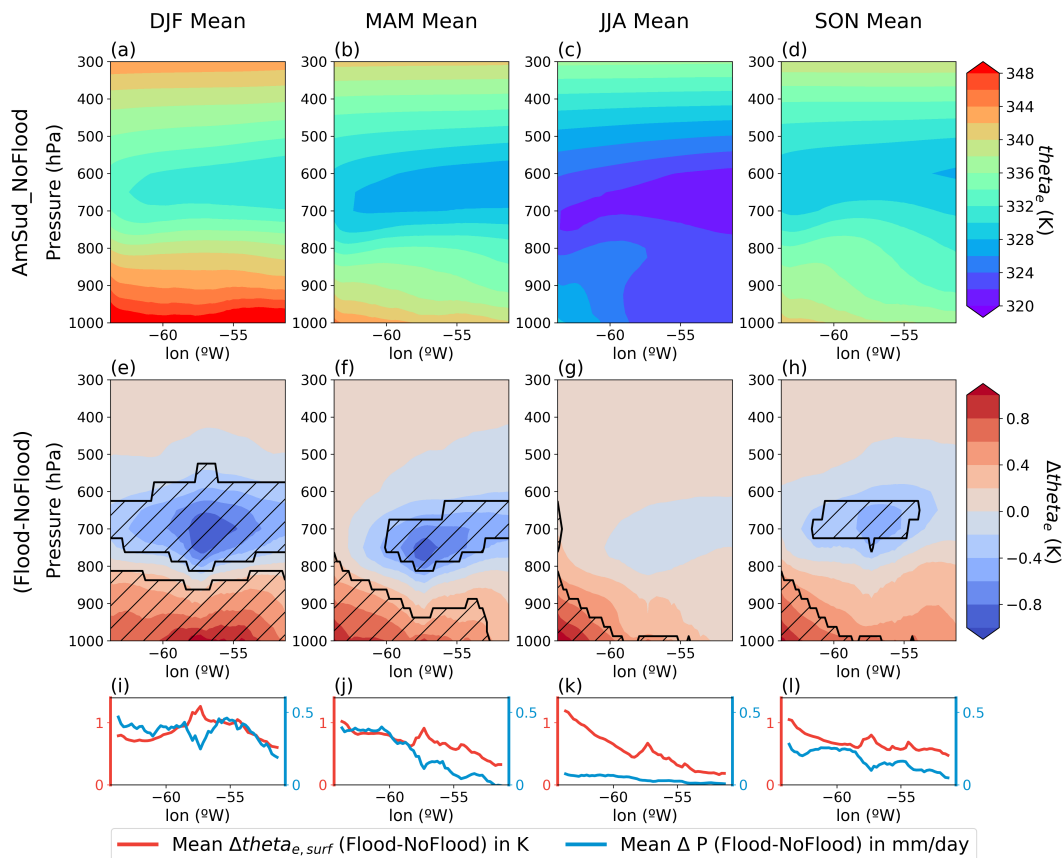


Figure 7.12. Mean vertical profile of equivalent potential temperature between 25°S and 12.5°S for AmSud_NoFlood (a-d) and the relative difference between AmSud_Flood and AmSud_NoFlood (e-h) for the different season: DJF (a,e), MAM (b,f), JJA (c,g) and SON (d,h). The differences between AmSud_Flood and AmSud_NoFlood, which have a significance level higher than 95% using a Student's t-test are hatched. The average of the difference of near-surface equivalent potential temperature and precipitation between AmSud_Flood and AmSud_NoFlood between 25°S and 12.5°S is shown for DJF (i), MAM (j), JJA (k) and SON (l).

over the most flooded area where it is lower in AmSud_Flood compared to AmSud_NoFlood. This can be related to the reduced cloud cover over this region.

The upward longwave radiation (r_{lus}) is lower in AmSud_Flood compared to AmSud_NoFlood and more importantly over the most flooded area which is related to the decrease of the surface temperature seen previously.

The downward shortwave radiation (r_{lds}) is similar in both simulations but is slightly higher over the most flooded area which is related to the lower presence of clouds over this regions.

The upward shortwave radiation (r_{lus}) is lower in AmSud_Flood compared to AmSud_NoFlood over the North/East and the West between November and April but more importantly, and during all the year, over the most flooded area. This can be related to the decrease of the albedo due to the vegetation changes and to the soil moisture increase.

Comparing the differences, the flux which is the most affected by the floodplains is the upward

longwave radiation. Therefore, the temperature change related to the activation of the floodplains scheme is the major source of difference in the radiation budget at the surface between AmSud_Flood and AmSud_NoFlood which leads to an increase net radiation at the surface over the different subregions studied. The period of the simulation is long enough to consider that the ground heat fluxes are negligible, therefore, this means that the increase of the net radiation increase the turbulent fluxes from the surface to the atmosphere.

7.3.3 Changes in Precipitation over the Pantanal

This subsection aims to define more precisely the origin of the precipitation changes over the Pantanal between AmSud_Flood and AmSud_NoFlood. From Taylor et al (2018) and Adler et al (2011), the PBL is supposed to be less turbulent over the most flooded part of the Pantanal inhibiting locally the convection and resulting in a lower precipitation while the precipitation is supposed to increase around these areas. Figure 7.15 shows the differences between both simulations by observing separately the convective and the non convective precipitation. The

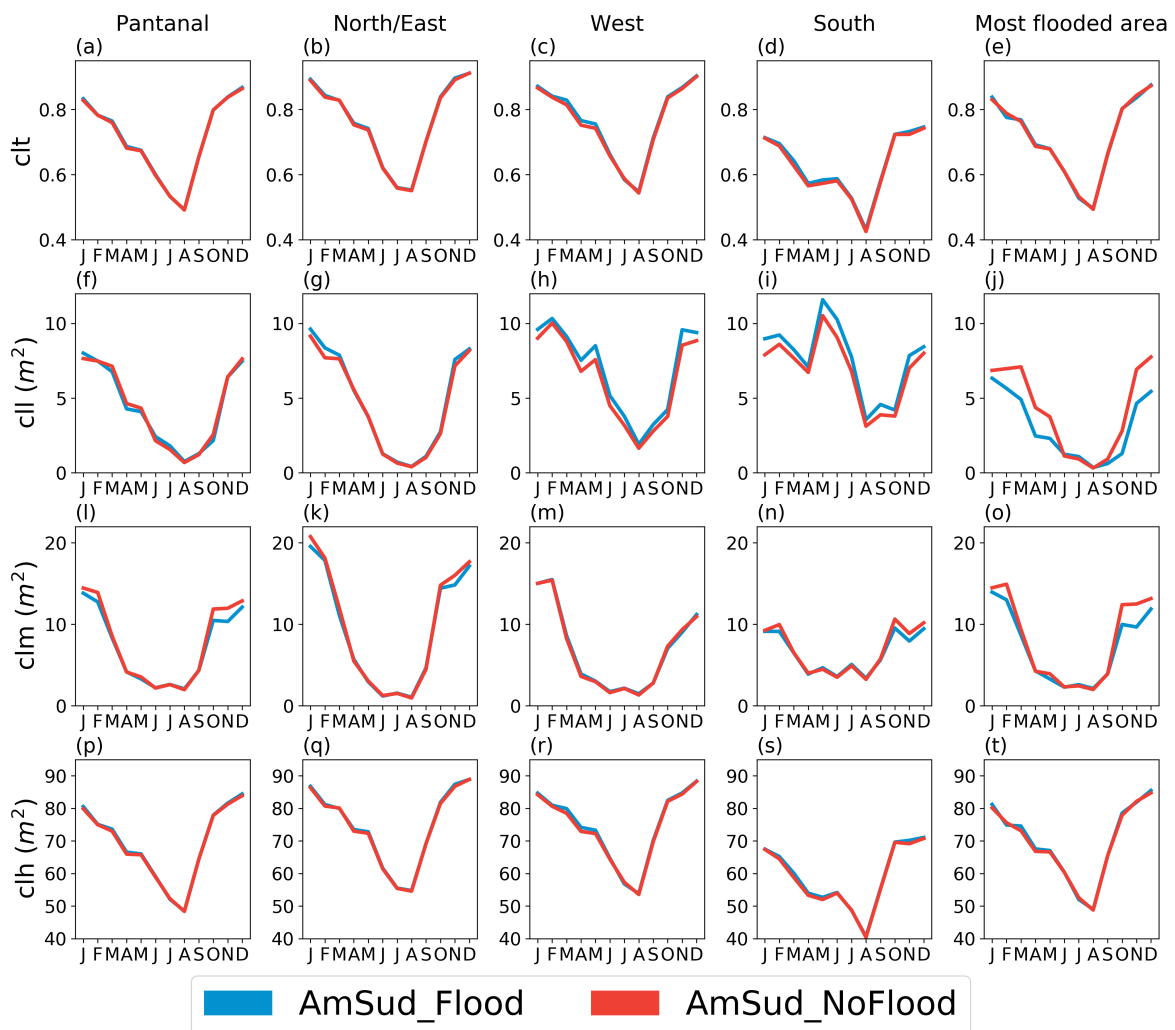


Figure 7.13. Annual cycle between 1998 and 2019 of the cloud cover fraction (*clt*, a-e), the low (*cll*, f-j), medium (*clm*, h-o) and high (*clh*, k-t) cloud cover over the different subregions: P (a,f,l,p), NNE (b,g,k,q), W (c,h,m,r), S (d,i,n,s) and F (e,j,o,t).

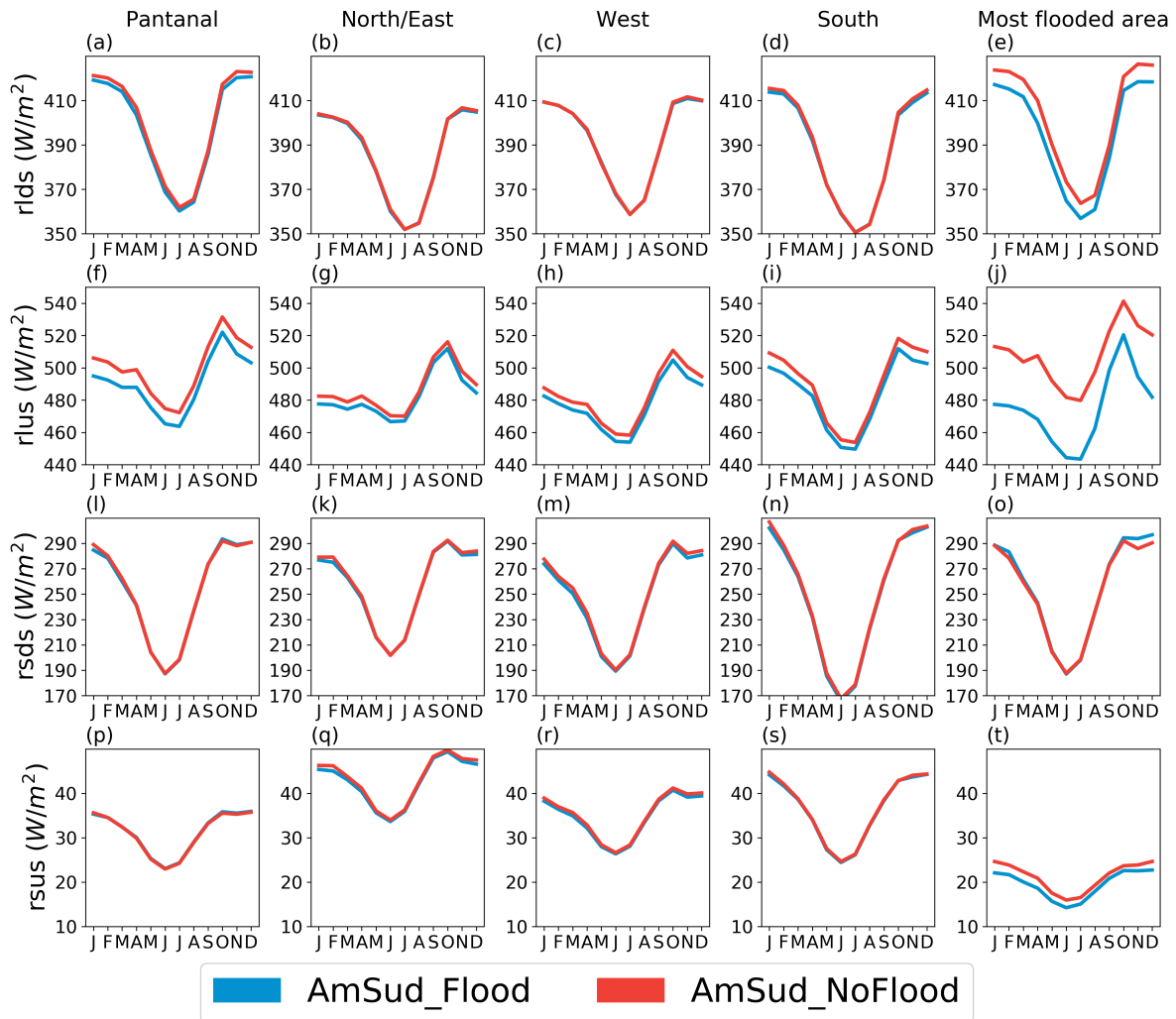


Figure 7.14. Annual cycle between 1998 and 2019 of the different radiative fluxes at the surface: downward (a-e) and upward (f-j) longwave radiation, downward (h-o) and upward (o-t) shortwave radiation over the different subregions: P (a,f,l,p), NNE (b,g,k,q), W (c,h,m,r), S (d,i,n,s) and F (e,j,o,t).

convective precipitation is the dominant origin of the precipitation over the region and has higher values to the North and East of the Pantanal between September and February. The non convective precipitation occurs principally in the South of the Pantanal between March and November and extends around the Pantanal in DJF.

The differences of non convective precipitation between AmSud_Flood and AmSud_NoFlood are significant on small and isolated patches. There is generally an increase of the non convective precipitation west of the Pantanal and a decrease at the Southeast of the Pantanal. The differences of convective precipitation are more important. There is a significant reduction of the precipitation in AmSud_Flood over the main Paraguay river between September and May. The precipitation increases significantly over the west of the Pantanal in MAM and SON while it increases significantly over the entire region except the main Paraguay in DJF.

The differences of precipitation in AmSud_Flood and AmSud_NoFlood may have 2 different origins: (1) a different number of days with precipitation and (2) higher values of daily precipitation

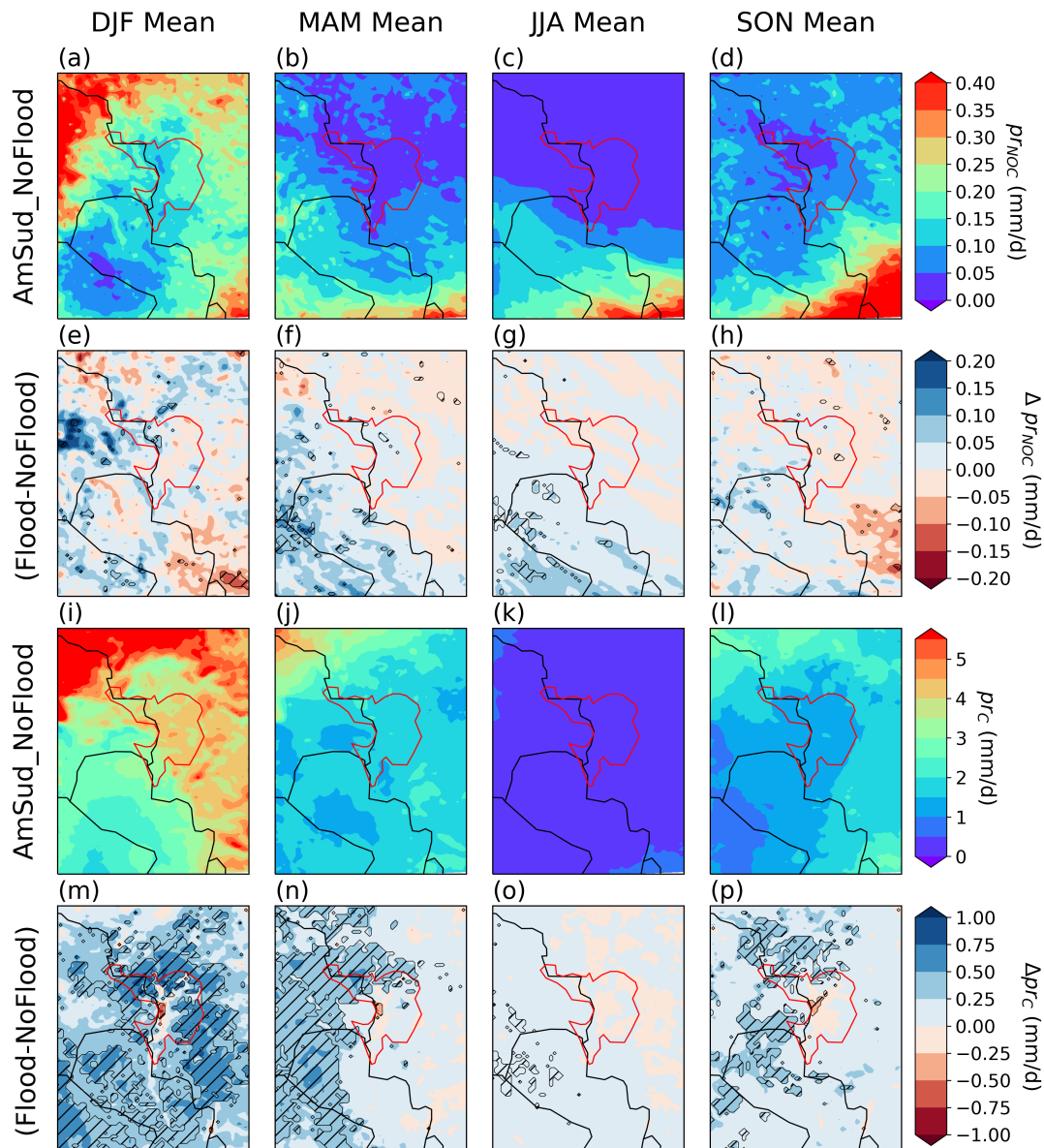


Figure 7.15. Non-convective (pr_{NOC} , a-d) and convective (pr_C , i-l) precipitation for AmSud_NoFlood and the respective difference between AmSud_Flood and AmSud_NoFlood (d-h for pr_{NOC} and m-p for pr_C). The results are averages between 1998 and 2019 over the different seasons: DJF (a,e,i,m), MAM (b,f,j,n), JJA (c,g,k,o) and SON (d,h,l,p). The differences between AmSud_Flood and AmSud_NoFlood, which have a significance level higher than 95% using a Student's *t*-test are hatched.

during the rain days. These aspects are explored in the following figures. A rainless day (rainy day) is defined as a day with a precipitation lower (higher) than 1 mm.

Figure 7.16 shows the frequency of rainless days during the different seasons. Comparing to GPCC, both simulations have a much higher number of rainless days. The difference is more important in DJF, MAM and SON but it should be noticed that, in JJA (dry season), the number of rainless days is almost 100% in the simulations while it remains below 80% for most seasons

in GPCC which will cause large differences. Comparing AmSud_Flood and AmSud_NoFlood, AmSud_NoFlood has a larger number of rainless days in DJF, MAM and SON over all the region except the most flooded region where the opposite happens.

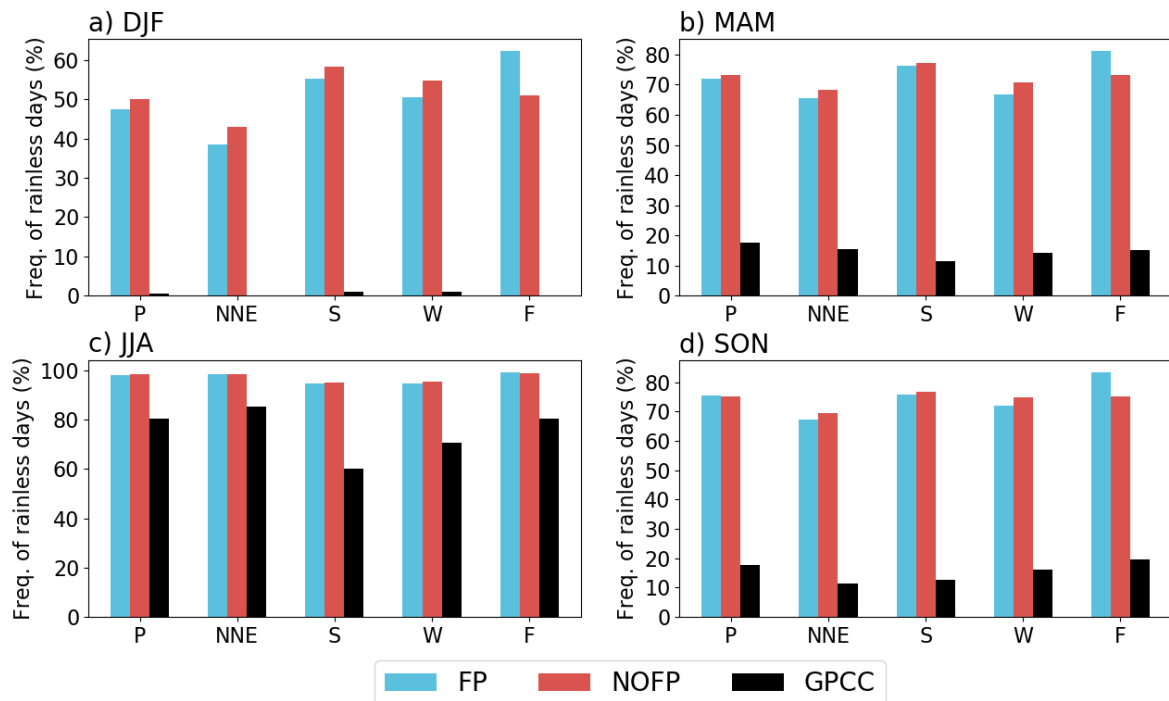


Figure 7.16. Frequency of rainless days ($PP < 1\text{mm}$) over the different regions: the Pantanal (P), North/East (NNE), South (S), West (W) and the most flooded area (F) between 1998 and 2019 for AmSud_Flood, AmSud_NoFlood and GPCC for the different seasons: DJF (a), MAM (b), JJA (c) and SON (d).

Figure 7.17 shows the boxplot of the precipitation in the simulations and in GPCC for the different seasons and periods considering only the rainy days. AmSud_Flood and AmSud_NoFlood have similar distributions, however the AmSud_Flood distribution tends to have slightly higher values of rainfall. On the contrary, the boxplot of GPCC is quite different as it has a much lower variability than the simulations but the median is usually at the same level as the simulations except in DJF over the North/East where it is higher and during JJA when it is lower.

The distribution of the daily precipitation over the different regions and seasons is similar in both simulations. This indicates that the difference of the precipitation between AmSud_Flood and AmSud_NoFlood is principally due to the number of rainy days. The quantity of rainy days is also the major difference between the simulations and GPCC because, during the dry season, GPCC shows lower values of precipitation but has a much higher number of rainy days. On the contrary for the North/East of the Pantanal during DJF, the daily precipitation is higher compared to the simulation and this is another factor enhancing the differences between GPCC and the simulations.

Finally, the differences between both simulations in the diurnal cycle of precipitation during the rainy season (DJF) is shown in Figure 7.18 using the local time reference (UTC-3). The period of major precipitation is the afternoon (12h-18h). During this period there is a signifi-

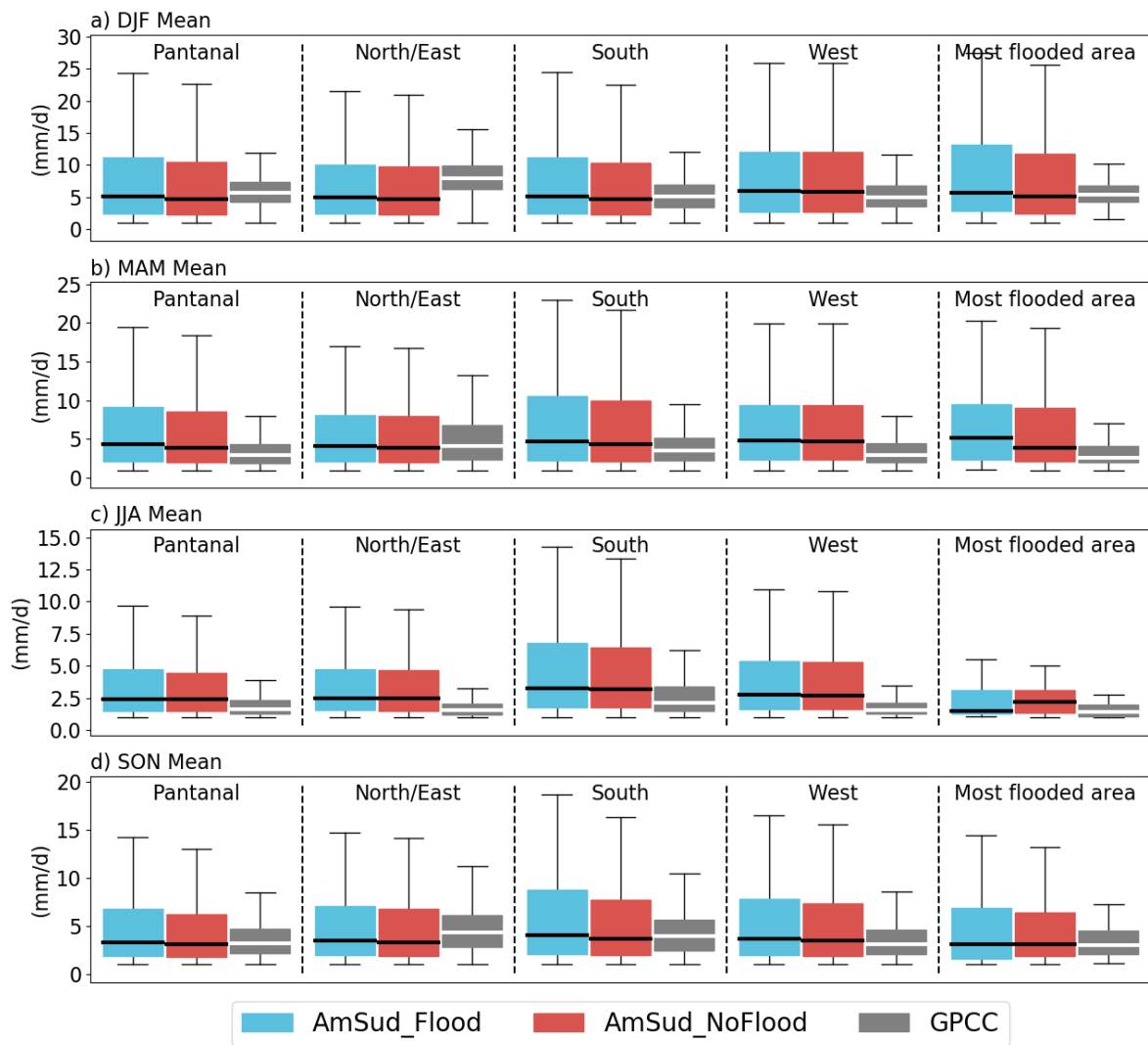


Figure 7.17. Boxplot of the distribution of the precipitation considering the rainy days ($PP > 1\text{mm}$) over the 5 subregions (P,NNE,W,S,F) for AmSud_Flood, AmSud_NoFlood and GPCP for the different seasons: DJF (a), MAM (b), JJA (c) and SON (d) during the 1998-2019 period.

cant increase of the precipitation in AmSud.Flood over all the Pantanal and the surrounding regions except over the most flooded area where the difference remains close to zero. There is a significant increase of the precipitation in the evening (18h-24h) around the Pantanal but principally over the North/East and there are significant increase in more reduced region at the North/NorthWest of the Pantanal and at the Southeast between 0h and 12h. These results are coherent with the mechanisms detailed by both Adler et al (2011) and Eltahir (1998) because the afternoon and the evening are the moment where the MSE in the PBL will be higher over the floodplains due to the evapotranspiration occurring during the day. However, it should be reminded that Adler et al (2011) explains the precipitation changes over the most flooded areas of the Pantanal and its close surroundings while Eltahir (1998) explains the processes involved with the precipitation increase over a larger are. The decrease of the precipitation over the main Paraguay in AmSud.Flood is visible and significant between 18h and 24h.

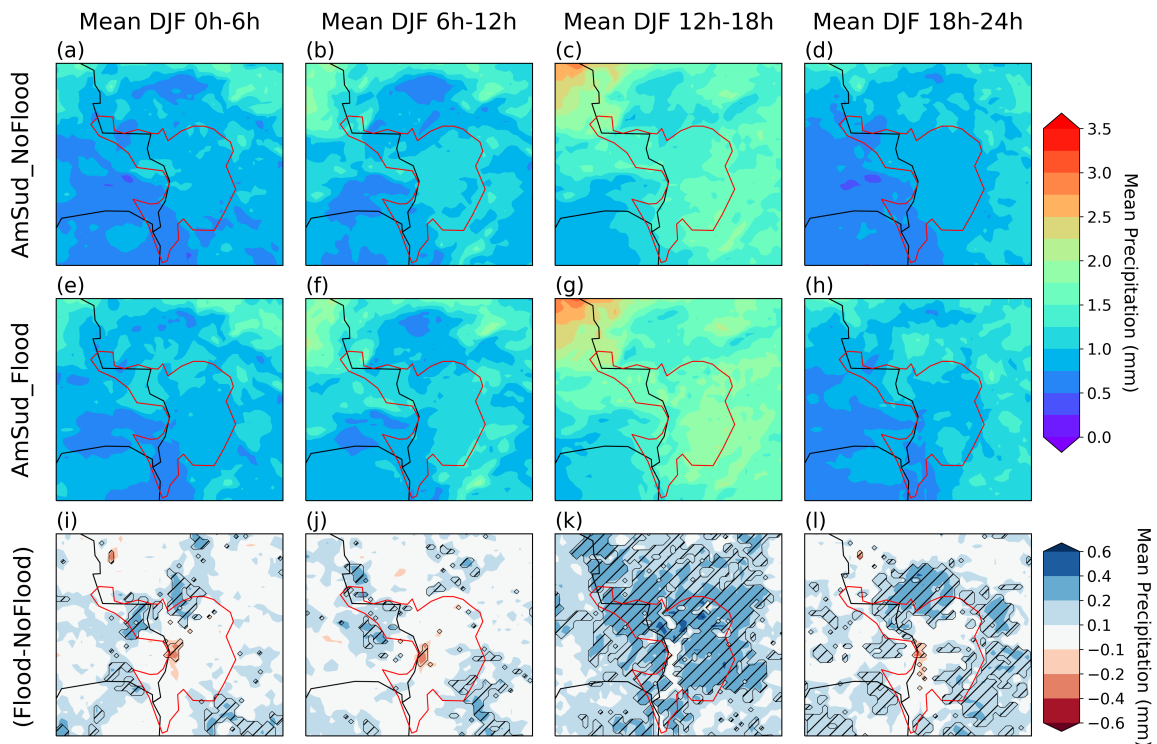


Figure 7.18. Average diurnal cycle of precipitation for *AmSud_NoFlood* (a-d), *AmSud_Flood* (e,h) and the difference between *AmSud_Flood* and *AmSud_NoFlood* (i-l) for the different 6 hours interval of a day considered in the local time (UTC-3): 0h-6h (a,e,i), 6h-12h (b,f,j), 12h-18h (c,g,k) and 18h-24h (d,h,l) averaged between 1998 and 2019. The differences between *AmSud_Flood* and *AmSud_NoFlood*, which have a significance level higher than 95% using a Student's t-test are hatched.

7.3.4 Impact on the regional circulation

The activation of the floodplains scheme on the atmosphere principally affects the lower atmosphere through the PBL. Therefore, it is interesting to observe the different circulation variables at a lower level such as the wind at 850 hPa (cf. Figure 7.19). The wind arrives to the southern Amazon from North/Northeast in summer and from the East/Northeast during the rest of the year. It is then deflected toward the South by the Andes mountain and flows along the higher orography. Due to the shape of the Andes that extend to the East at the latitude of the Pantanal, the wind flow at 850 hPa is more concentrated West of the Pantanal with much higher speeds (reaching wind speed of more than 10 m/s). This phenomenon is strongest during the dry season (JJA).

The wind flows to the La Plata Basin, southwest and southeast of the Pantanal. Comparing *AmSud_Flood* and *AmSud_NoFlood*, the floodplains have a significant impact on the wind flow at the West of the Pantanal in DJF where the vector of the difference goes in the opposite direction which indicates that the wind speed decreases. During MAM and JJA, there are significant changes over the most flooded area where the wind flow is increased toward the South. In JJA, the wind West of the Pantanal is deflected toward the main Paraguay (Eastern direction) in *AmSud_Flood* producing a mass convergence over the Pantanal. This traps the evaporated moisture over the Pantanal and contributes to the moistening of the PBL. During

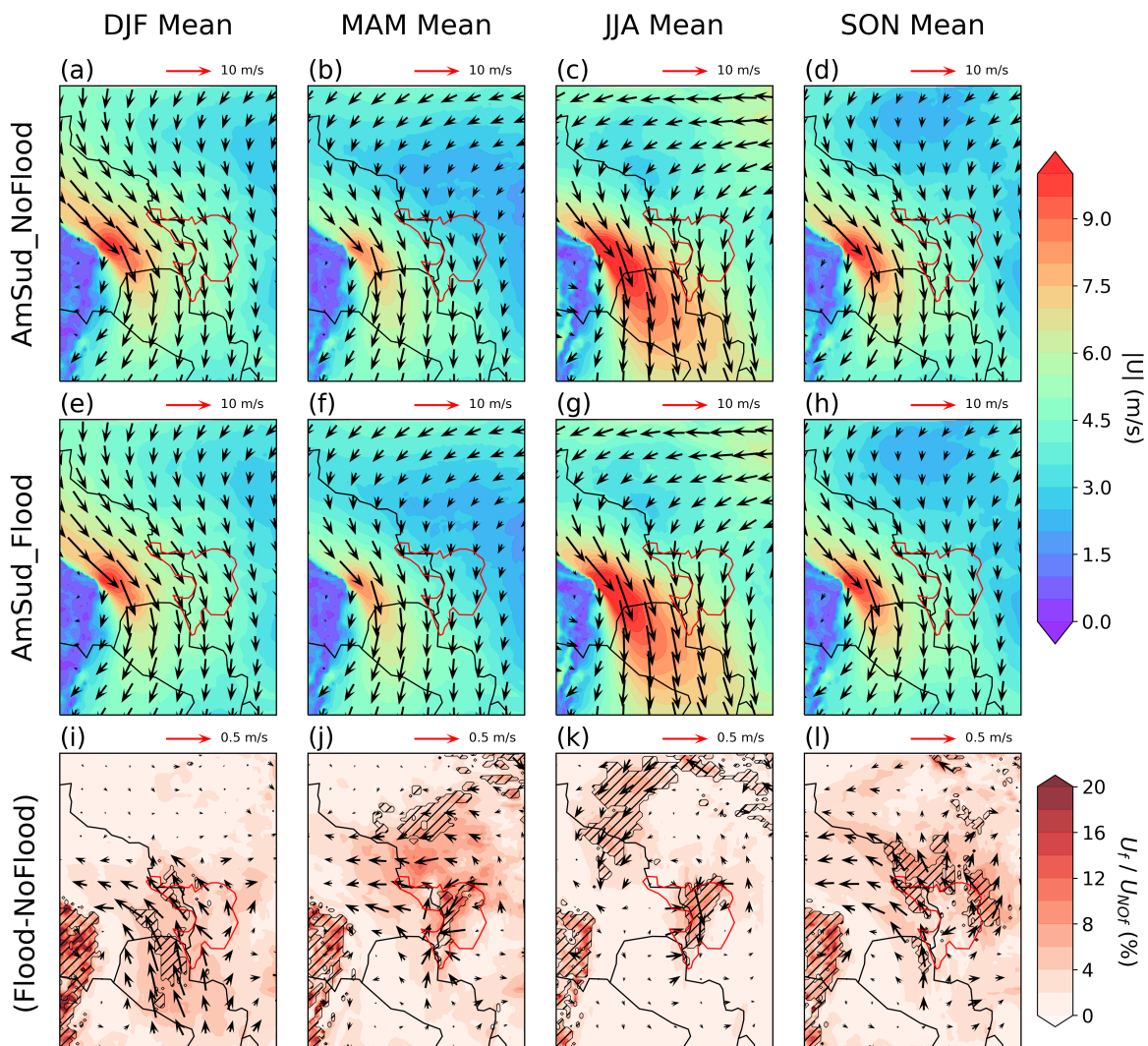


Figure 7.19. Wind at 850 hPa for AmSud_NoFlood (a-d), AmSud_Flood (e-h) and the difference between both between 1998 and 2019. The average for the different seasons is shown: DJF (a,e,i), MAM (b,f,j), JJA (c,g,k) and SON (d,h,l). The filled contour on the subplots indicates the windspeed.

this season, the air is too dry to have an impact on the precipitation, however, it has an impact on the increase of the lower level clouds cover South of the Pantanal. During MAM, we also observe strong changes for the wind flow West of the Pantanal which, although it is not significant, shows that the wind is deflected toward the West in AmSud_Flood. There are significant changes in the North/East and West regions of the Pantanal with differences of wind in the opposite direction of the main flow which mean that the wind speed is reduced.

To conclude, the floodplains scheme has an impact on the wind speed over the region which is part the SALLJ. In AmSud_Flood, the wind flow at 850 hPa is reduced in SON and DJF West of the Pantanal while it increases over the Paraguay river in MAM and JJA. It should also be noted that there is a significative increase of the wind flow toward the South over the Andes throughout the year.

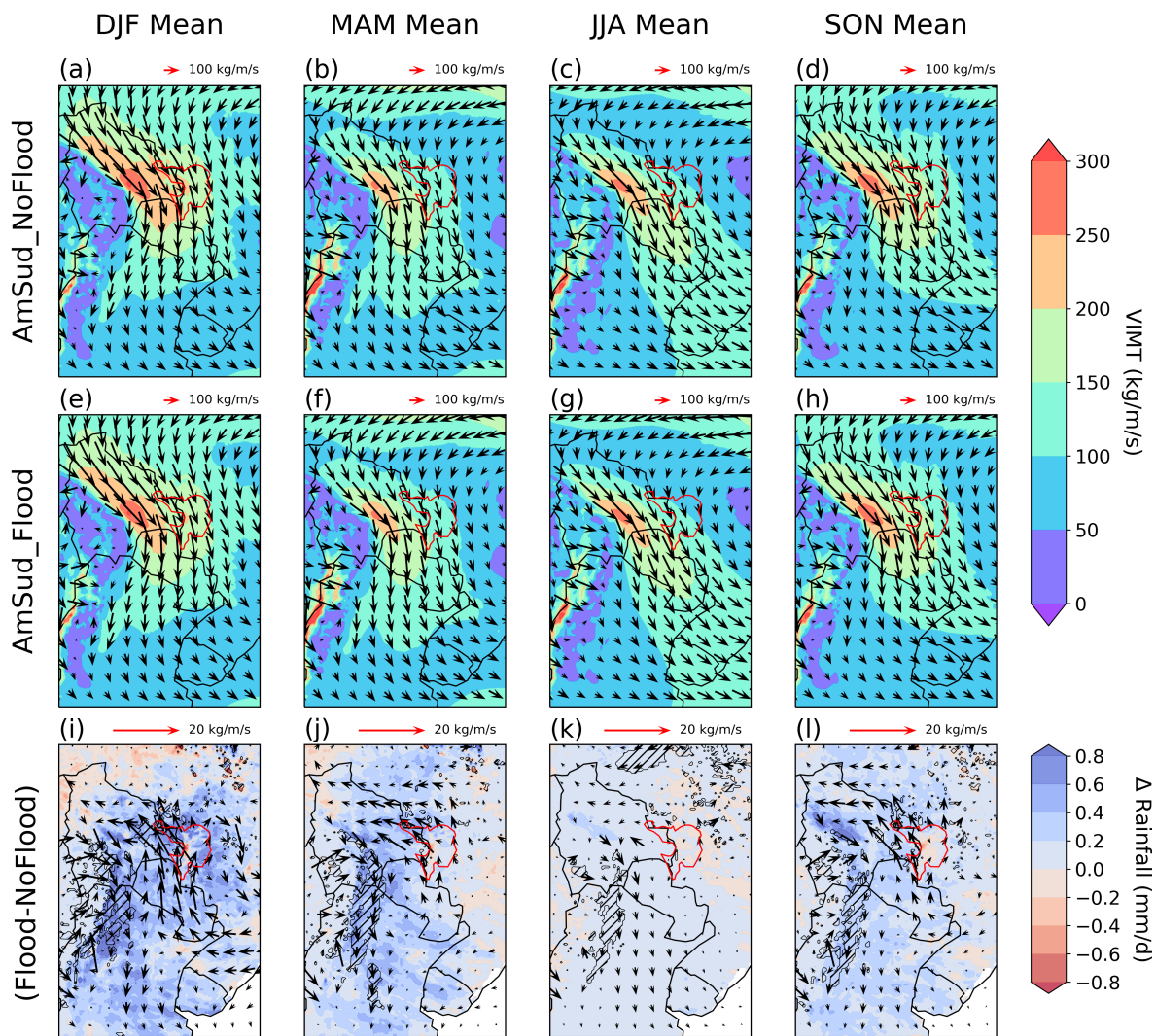


Figure 7.20. Vertically integrated moisture transport from the surface to 300 hPa for AmSud_NoFlood (a-d), AmSud_Flood (e-h) and the difference between both between 1998 and 2019. The average for the different season is shown: DJF (a,e,i), MAM (b,f,j), JJA (c,g,k) and SON (d,h,l). The filled contours on the subplots indicates the norm of the flux the AmSud_NoFlood (a-d) and AmSud_Flood (e-h) and the difference of precipitation between AmSud_Flood and AmSud_NoFlood in (i-l). The differences between vimt in AmSud_Flood and AmSud_NoFlood, which have a significance level higher than 90% using a Student's t-test are hatched.

The analysis of the wind changes can be completed by an analysis of the transport of humidity in the atmosphere. Figure 7.20 shows the vertically integrated moisture transport from the surface to 300 hPa such as it has been used in Montini et al (2019) to analyze the transport of humidity of the SALLJ. Figure 7.20 (i to l) provides in color shading the precipitation changes between AmSud_Flood and AmSud_NoFlood. The activation of the floodplains scheme weaken the transport of humidity at the West of the Pantanal in DJF and at its West/Northwest in MAM and SON. These changes are significant at the Northwest of the Pantanal in SON and DJF. It can be noticed that the places of major changes are coherent with the wind changes, therefore, the transport of humidity changes could be more related to the weakening of the wind than

to the reduction of the humidity. As discussed previously, the mass convergence over the Pantanal in JJA observed in Figure 7.19 doesn't impact significantly the moisture transport because it is the dry season and, thus, there is little moisture transported. On the contrary, the vertically integrated moisture transport increases significantly along the Andes and along the central longitude of Argentina throughout the year. This increases strongly the precipitation over this region. The flow of the SALLJ that goes from the Pantanal to Southeast Brazil is also reduced from the Pantanal in SON and DJF. The integration of the floodplains turned the Pantanal into a moisture source region which supply humidity to the regions downstream the SALLJ, principally along the Andes, increasing the regional precipitation.

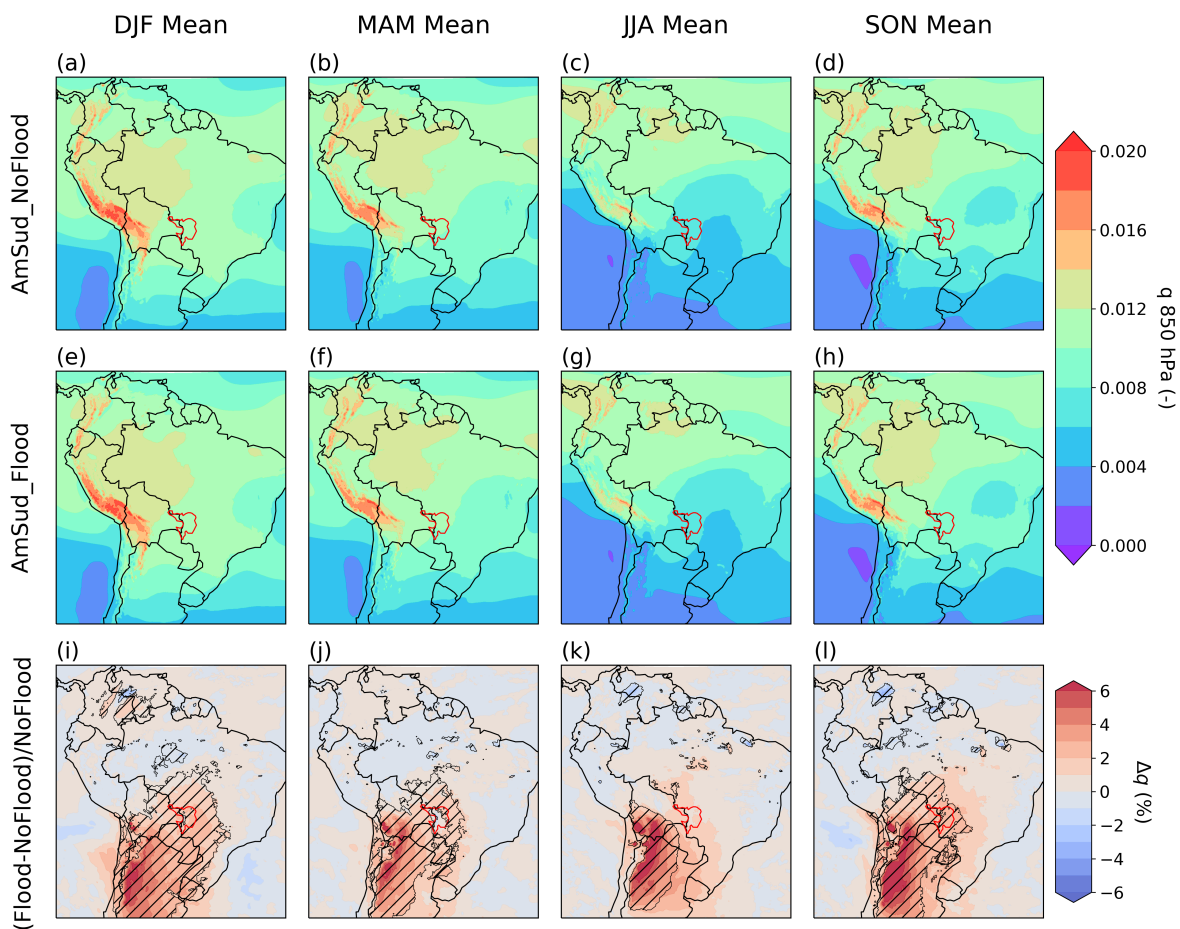


Figure 7.21. Specific humidity at 850 hPa for AmSud_NoFlood (a-d), AmSud_Flood (e-h) and the difference between both between 1998 and 2019. The average for the different season is shown: DJF (a,e,i), MAM (b,f,j), JJA (c,g,k) and SON (d,h,l). The differences between v_{imt} in AmSud_Flood and AmSud_NoFlood, which have a significance level higher than 95% using a Student's t-test are hatched.

Figure 7.21 shows the mean specific humidity at 850 hPa over tropical and subtropical South America and the difference between both simulations. There is a significant increase over the region around the Pantanal in between September and May while it is not the case for the Pantanal in MAM. The increase of specific humidity at 850hPa in AmSud_Flood is much higher over Southern Bolivia and Northwestern Argentina during all the year with increase

higher than 6%. This increase of the specific humidity increase over all Paraguay and Northern Argentina in DJF. It should be noted that, although there are some floodplains features along the Andes (cf. Figure 7.1), they do not contribute to an important change in evapotranspiration through the direct evaporation from the floodplains (not shown). On the contrary, the increased evapotranspiration along the Paraná related to the direct evaporation from the flooded area is higher but not as much as the direct evaporation from the Pantanal floodplains due to their subtropical location. Therefore, these changes of specific humidity are principally related to the tropical floodplains and, in particular, to the Pantanal.

A combination of two phenomena can explain the increase of the precipitation in Northern Argentina and in the Córdoba region. First, the changes in the SALLJ circulation may increase the precipitation such as what happens with the significant increase of the moisture transport along the Andes. Secondly, the extra moisture supply from the floodplains (Pantanal and Paraná) significantly increases the atmospheric moisture in Northern Argentina and, more generally, in the La Plata Basin what may enhance the precipitation.

7.4 Discussion and Conclusion

The impact of the floodplains on the atmosphere has been evaluated by comparing two coupled simulations between 1998-2019 with the same configuration except that one has the floodplains scheme activated (AmSud_Flood) and the other deactivated (AmSud_NoFlood). An offline simulation with the floodplains scheme activated forced by AmSud_NoFlood (AmSudNOF_offline_FP) has also been performed to evaluate the impact of the land-atmosphere coupling over the floodplains.

The comparison of AmSudNOF_offline_FP and AmSud_Flood confirmed that the potential evaporation is largely overestimated in the offline simulations over the floodplains what increases excessively the evapotranspirative fluxes over the floodplains leading to an overestimation of the evapotranspiration and latent heat fluxes.

The temperature decreases due to the higher evapotranspiration related to the soil moisture changes. This decrease of the temperature at the surface decreases the upward longwave radiation over the region. On the contrary, the changes of upward shortwave radiation linked are not coherent with what was expected by [Eltahir \(1998\)](#) in relation with an higher soil moisture. This is related to (1) the albedo changes in the model that don't depend only on the soil moisture but also on the vegetation changes and also on the vegetation type involved, therefore, the albedo doesn't necessarily decreases when the soil moisture increases. This is principally the case over the Pantanal because there are strong changes of vegetation related to the activation the floodplains scheme. Over the region surrounding the Pantanal the albedo decreases (not shown). It is also related to (2) the cloud cover changes, and in particular, in how the combination of a decrease of middle-level cloud cover and an increase of low-level cloud cover impact on the surface radiation budget. However, the lower upward longwave radiation is the predominant effect of the flooded areas on the radiative balance and, therefore, there is an increase of the net radiation over the floodplains and, as the ground heat fluxes can be neglected over such a long period, there is also an increase of total turbulent fluxes from

the surface to the atmosphere.

The activation of the floodplains scheme in the coupled simulations has an impacts on the precipitation with different mechanism involved depending on the spatial scale considered.

The precipitation changes over the Pantanal floodplains confirms the observations from [Taylor \(2010\)](#) and [Taylor et al \(2018\)](#) because the increase of the rainfall during the rainy season is mostly related to the afternoon precipitation and there is a decrease of the precipitation over the most flooded part of the Pantanal. This decrease is following the mechanism described by [Adler et al \(2011\)](#) because it occurs despite of the increase of the CAPE over the most flooded area and is related to the local wetland breeze that increases locally the CIN and, thus, inhibits the convection. The negative bias of precipitation over the most flooded area is related to a decrease of the cloud cover and a decrease of the rainy days. On the contrary, the increase of precipitation over the Pantanal is related to an increase of the rainy days.

On a larger scale, the activation of the floodplains scheme converts the Pantanal in a source of moisture for the atmosphere and affects the Planetary Boundary Layer (PBL) over the La Plata Basin by increasing the specific humidity, increasing the precipitation, increasing the Soil Moisture, reducing the temperature in the PBL and decreasing the height of the PBL. Although there is no significant reduction of the mid-level temperature, there is a significant decrease of the specific humidity. This leads to equivalent potential temperature higher in the lower level and lower over the middle level. The mechanisms explained in [Eltahir \(1998\)](#) are simplistic as they don't consider some more complex atmospheric variables such as the CIN. However, it seems to be able to explain the changes in the land-atmosphere interactions related to the increase of the precipitation over the La Plata Basin in the simulation with floodplains. The results are indeed coherent with this theory as we have a lower Bowen ratio, a lower PBL, a higher MSE in the PBL and an increased gradient of MSE between the PBL and the higher level of the atmosphere which increase the convection in the region. The presence of the Pantanal increase the regional precipitation and impact the land-atmosphere interactions through a positive feedback between soil moisture and precipitation.

The regional circulation is marked by the South American Low Level Jet (SALLJ) that brings moisture from the Amazon and the North of the La Plata Basin to the subtropical latitude and is the principal source of humidity for the precipitation over the LPB. The presence of the floodplains affects the SALLJ by reducing the strength of the moisture flux at the West of the Pantanal, principally through a wind speed reduction, and increases it along the Eastern Andes. The mechanism behind the impact of the Pantanal on the SALLJ are not clear and should be further investigated.

These changes in the circulation and the extra moisture supply from from the floodplains direct evaporation and from the evaporation related to the increased precipitation around the Pantanal increase the humidity transport the North and Northwest Argentina during all the year and in the whole LPB during the austral summer. These changes in the moisture transport and in the circulation increase the precipitation over the Northern Argentina but most importantly along the Andes which is related to significant changes of the SALLJ. However, it is not clear if the increase of the precipitation further to the east of the Andes, in Central North Argentina, is related to (1) the changes of the SALLJ and / or (2) a soil moisture-precipitation positive

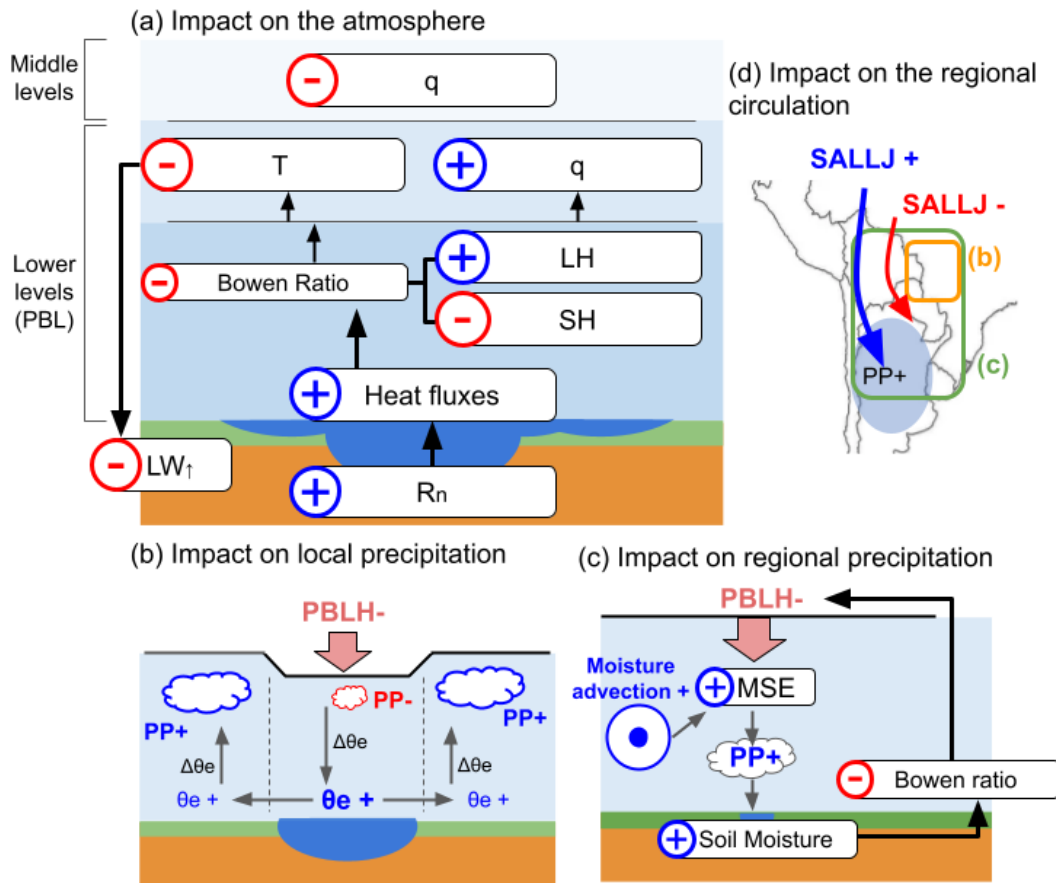


Figure 7.22. Summary of the local impacts of the floodplains (a) on the atmosphere, (b) on the local precipitation, (c) on the regional precipitation and (d) on the regional circulation as demonstrated with the comparison of a coupled simulation integrating the floodplains with a coupled simulations without floodplains.

feedback due to the increased rainfall along the Andes.

The local impacts of the Pantanal tropical floodplains on the atmosphere and their influence on the regional climate are summarized in Figure 7.22 with the impact of the floodplains on the atmospheric conditions (Fig. 7.22.a), the mechanisms behind precipitation changes over the floodplains (Fig. 7.22.b) and, on a larger scale, over the region (Fig. 7.22.c) and the impact of the Pantanal on the regional circulations.

The Pantanal shows how a large tropical floodplains in a semi-arid region affects the atmosphere locally and regionally through the regional circulation and, in particular, through a low-level jet feature. The Pantanal is a region which is very sensitive to local changes such as vegetation changes related to wildfire, human activities affecting the land cover and the rivers hydrology and regional precipitation changes. All these elements are threats for the wetlands such as the Pantanal that may affects its hydrology and degrade its rich ecosystem. As shown in this chapter, the regional climate is strongly affected by the Pantanal floodplains and can be impacted by the potential drying of the Pantanal.

7.5 Acronyms

AMMA	African Monsoon Multidisciplinary Analysis
AmSud	RegIPSL simulation at 20 km over the South American domain
AmSud_Flood	RegIPSL simulation at 20 km over the South American domain with the floodplains activated
AmSud_NoFlood	RegIPSL simulation at 20 km over the South American domain with the floodplains deactivated
ERA	ECMWF Re-Analysis
ERA5	ECMWF Re-Analysis fifth generation
ESA	European Spatial Agency
ESA-CCI	European Spatial Agency Climate Change Initiative
GLWD	Global Lake and Wetlands Dataset
GPCC	Global Precipitation Climatology Centre
HRU	Hydrological Response Unit
HTU	Hydrological Transfer Unit
IPSL	Institut Pierre Simon Laplace
JULES	Joint UK Land Environment Simulator
LAI	Leaf Area Index
LPB	La Plata Basin
LSM	Land Surface Model
M2M	Morrison 2-moment scheme
MORCE-MED	Model Of the Regional Coupled Earth system platform over the Mediterranean area
MYNN	Mellor-Yamada-Nakanishi-Niino 2.5 boundary layer scheme
NEMO	Nucleus for European Modelling of the Ocean
ORCHIDEE	ORganizing Carbon and Hydrology in Dynamic EcosystEms

PBL	Planetary Boundary Layer
PFT	Plant Functional Type
RRTMG	Radiation and Rapid Radiative Transfer Model for General Circulation
RegIPSL	Institut Pierre Simon Laplace's Regional Earth System Model
RoutingPP	Pre-Processor of the routing input for ORCHIDEE high resolution routing scheme
SACZ	South Atlantic Convergence Zone
SALLJ	South American Low Level Jet
SAMS	South American Monsoon System
SECHIBA	Schématisation des EChanges Hydriques à l'Interface Biosphère-Atmosphère
STOMATE	Saclay Toulouse Orsay Modèle pour l'Analyse des Ecosystèmes Terrestres
UPRB	Upper Paraguay River Basin
WRF	Weather Research and Forecasting
XIOS	XML-IO-Server

Discussion, conclusion and perspectives

Contents

8.1	Synthesis	197
8.1.1	What brings the necessity to represent the tropical floodplains in a LSM?	198
8.1.2	Highlight the difficulties of flooded area detection / representation . . .	198
8.1.3	Importance to facilitate the development and integration of new processes in LSM	199
8.1.4	Implementation of a high resolution floodplains scheme	200
8.1.5	Assess the impact of the tropical floodplains on the surface conditions	200
8.1.6	Evaluate the impact of the tropical floodplains on the atmosphere . . .	201
8.1.7	Analyze the impact of the Pantanal on the regional climate	201
8.2	Perspectives	202
8.2.1	Improve the floodplains representation	202
8.2.2	Going further on the floodplains study	203
8.2.3	Include more wetland type	203
8.2.4	Going further in the River Modelling	205
8.2.5	Toward more Coupled simulation with RegIPSL	205
8.3	Acronyms	206

This chapter summarizes the results and conclusions drawn along the thesis. It also provides perspectives for future research in relation with findings from the present thesis work.

8.1 Synthesis

Large tropical floodplains, such as the Pantanal in the heart of Central South America, are important features of the hydrological cycle and are among the world's richest ecosystems.

Therefore, they are regions whose natural processes deserves to be studied whether it is with the purpose of (1) better understanding the different natural processes occurring there or of (2) emphasizing the ecological services they provide and their impact on the local climate and hydrology.

The study of the natural processes over such large regions can be performed through remote sensing and numerical modelling. In the second case, it requires a hydrological model representing large floodplains coupled to a routing scheme which contains all the information needed to constrain it with atmospheric, hydrological and remote sensing information.

The aim of this thesis is to study the complex land-atmosphere-river-floodplains interactions over the Pantanal region. This has been accomplished with the development and use of a high resolution floodplains scheme for the ORCHIDEE model. The scheme developed can be used with the last version of the model and, therefore, can be activated in a regional model coupling the land and the atmosphere.

In order to facilitate the development of the high resolution floodplains scheme, a pre-processing tool has been developed to construct the river routing of ORCHIDEE from high resolution hydrological dataset. This underlies the importance to create tools which are easy to use, flexible to be adapted to different circumstances and that can be easily modified by the community.

8.1.1 What brings the necessity to represent the tropical floodplains in a LSM?

The original version of the floodplains scheme developed for the 0.5° resolution river routing scheme of ORCHIDEE has been used, in a first approach, to evaluate the impact of representing floodplains in a Land Surface Model over a large period of 40 years. The integration of the floodplains scheme in ORCHIDEE improved the representation of the water cycle over the Upper Paraguay River Basin which contains the Pantanal. The use of different atmospheric forcings allowed to conclude that the impact of the floodplains is larger than the uncertainty inherent in the atmospheric information available. The integration of the floodplains leads to an increase of the evapotranspiration over the region and a decrease of the latent heat fluxes respect to the sensible heat fluxes.

These simulations allowed to develop a more robust method to estimate the evapotranspiration over the Pantanal combining the simulations with observations (a model-guided water balance). Although the conclusion is affected by an uncertainty, the result shows that the Pantanal evapotranspiration can exceed local precipitation. It is estimated that, in the absence of floodplains representation in the model, the evapotranspiration over the Pantanal is underestimated by between 6% and 12%.

8.1.2 Highlight the difficulties of flooded area detection / representation

The main feature to describe the floodplains is the flooded area. The knowledge of the flooded area is crucial to study the large floodplains and, in particular, to correctly estimate the evapotranspiration over these regions. The description of the river network and of the orography have a high uncertainty due to the low slope in these regions. Therefore, the flooded area is

also important as it gives informations on how these two variables interact.

Chapter 3 exemplifies the development and evaluation of a flooded area detection method using the spectral indexes from optical satellite data. Although their estimates seem coherent, Chapter 5 shows that there may exist large discrepancies among the satellite estimates because, depending on the satellite sensor and on the method used, some regions can be erroneously considered as flooded due to the saturated soil while others, actually flooded, can remain undetected as hidden below lush vegetation. The model will have a different representations of the flooded area based on the orography and the river network that can coincide with the satellite estimate over certain regions. However, it can miss some floods because of the absence of some processes such as, for instance, the case of divergent flows over the Taquari river in the Pantanal or due to the uncertainty of ancillary data. On the contrary, it may detect some flooded areas undetectable by the satellite due to other issues such as the clouds or the vegetation.

However, comparing the model outputs with the satellite estimates helps to highlight issues which needs to be adressed in the vision of floodplains provided by remote sensing and modelling. Therefore, in a certain sense, the development in floodplains modelling and satellite estimate of the flooded area are complementary.

8.1.3 Importance to facilitate the development and integration of new processes in LSM

Land Surface Models aim to realistically represent the water cycle. On the one hand, there has been an increase interest in integrating / improving processes linked with the land hydrological cycle whether it concerns natural or human-related processes. On the other hand, the representation of the horizontal water transport in Land Surface Models tends to be performed at higher resolution through the use of sub-grid parameterization of the river routing scheme or through hydrological model coupling.

Climate research aims to study the uncertainty of the climate system through the combined used of a large variety of models. The models should be able to adapt to the different framework of comparison and, therefore, require to be flexible in term of grid structure, resolution and ancillary data used. It is also of interest for the scientific community that the models remains easily manipulable, understandable and their improvement or the integration of new functionalities should remain accessible to the community.

A major difficulty for the development of the floodplains scheme has been the construction of the high resolution river routing tool which was directly present in the ORCHIDEE model. This difficulty resulted as an opportunity to create a separate pre-processing tool (RoutingPP) to construct the routing file. It has been the adequate occasion to improve the methodology of HTUs construction and to optimize the whole process through the use of parallelization. RoutingPP has made the HTUs construction easily understandable, flexible, adapted to other uses and providing a solid basis to further development. It is also completely accessible for the scientific community in a GIT repository (<https://gitlab.in2p3.fr/ips1/lmd/intro/routingpp>).

8.1.4 Implementation of a high resolution floodplains scheme

The original version of the floodplains scheme in ORCHIDEE was available for the 0.5° routing scheme. The floodplains scheme has been adapted to the higher resolution river routing scheme. It is based on the HTU structure and had to integrate some new behaviours such as the overflow of the floodplains because the lower extent of the hydrological units brings the necessity to include the horizontal transport of the water in the floodplains between the hydrological units. The conversion of the volume in the floodplains reservoir into an estimate of the flooded area has been improved with the higher resolution data used to construct the HTUs.

The high resolution floodplains scheme is flexible as it has been adapted to work with the HTUs-based version of the river routing scheme and, thus, can be used with different of atmospheric grid at different resolutions and can use different dataset to describe the areas potentially affected by the floodplains.

8.1.5 Assess the impact of the tropical floodplains on the surface conditions

The validation of the model has been performed by analyzing the river discharge at the outflow of the Pantanal and the flooded area using several atmospheric forcings at different resolutions. After this validation, the comparison of simulations with and without floodplains allowed to evaluate the impact of the floodplains on surface conditions. There are two main processes induced by the floodplains which drive the other land surface processes: the soil moisture and the flooded area. The representation of these processes is affected by the resolution and by the atmospheric forcing used.

However, in all cases, the flooded area increases the evaporation through direct evaporation and the soil moisture is increased due to floodplains infiltration. The soil moisture changes increase the vegetation cover and the density of the vegetation and, therefore, its transpiration. As a consequence, the heat fluxes at the surface are also affected. The net radiation and the latent heat fluxes increases while the sensible heat fluxes decreases. This comes along with a lower surface temperature over the floodplains.

The water that remains in the floodplains has a strong impact during the dry season due to the lack of water availability. Thus, despite the smaller area of the floodplains during the dry season, they have a higher impact on the surface conditions.

The increase of potential evaporation and of evapotranspiration are quite important in the offline simulations with floodplains. The order of magnitude of these changes is unrealistic for a tropical region. This overestimation of the evaporative fluxes is related to the lack of coupling with the atmospheric conditions. The atmospheric forcings available do not take into account the extra humidity provided by the Pantanal and, therefore, the atmosphere remains dry even in the presence of the floodplains in the simulation which increase excessively the evapotranspiration.

8.1.6 Evaluate the impact of the tropical floodplains on the atmosphere

Such large changes on the surface fluxes have an impact on the atmosphere, this impact has been assessed through a pair of coupled simulation, one with floodplains and another without. These coupled simulations allow, for the first time, to assess the impact of the coupling by comparing the coupled simulation with floodplains with an offline simulation including floodplains but forced by the atmospheric conditions of the coupled simulations without floodplains. The potential evaporation doubles when there is no coupling which confirms the overestimation of the evaporative fluxes in the absence of coupling.

The presence of floodplains has a strong impact on the lowest level of the atmosphere with a decrease of the temperature and an increase of the specific humidity close to the surface. The Planetary Boundary Layer Height decrease while the Moist Static Energy in the Boundary Layer increase. As explained in [Eltahir \(1998\)](#), these conditions increase the regional precipitation which in turn creates a positive feedback between soil moisture and precipitation. In conclusion, the presence of the Pantanal floodplains wettens a region much larger than the Pantanal.

The increase of the precipitation principally occurs during the wet season and is mainly related to the increase of the afternoon / evening precipitation such as described in [Taylor \(2010\)](#). There is also a decrease of the precipitation over the most flooded area which is related to a wetland breeze phenomena and is coherent with previous studies ([Taylor et al, 2018](#); [Paiva et al, 2011](#)). This decrease of the precipitation is explained with more details in [Adler et al \(2011\)](#): although the CAPE increases over the floodplains due to the extra-evaporation, the contrast with the dry area surrounding the floodplains creates a downdraft over the floodplains that reduces the CIN and, therefore, inhibits the circulation. This also creates an horizontal advection of the air over the floodplains which will increase the CAPE around the floodplains and create an updraft in the surrounding of the floodplains explaining part of the precipitation increase in the close surrounding of the Pantanal floodplains.

8.1.7 Analyze the impact of the Pantanal on the regional climate

One of the most important insight of this thesis is that the presence of floodplains over the Pantanal is affecting the regional circulation and, therefore, an area which is much larger than the direct surrounding of the Pantanal.

The integration of floodplains in the simulation decreases the South American Low Level Jet at the West of the Pantanal and increases it near the East Andes at the level of the Pantanal. The extra precipitation over the region also provides an extra supply of moisture for the Low Level Jet that increases the specific humidity over the lower layer of the atmosphere all over the Eastern Andes in the extratropical latitude and over the Paraguay and Northern and Central Argentina. As a consequence, there is an increase of the precipitation over this whole region.

8.2 Perspectives

This study focused on (1) the development of a floodplains scheme compatible with the high resolution river routing in ORCHIDEE and (2) the evaluation of the impact of the integration of the floodplains in the model by studying the Pantanal region in Central South America.

The region of interest chosen, the Pantanal, was particularly pertinent to show the impact of the tropical floodplains on the surface conditions, on the atmosphere and on the regional climate. However, it should be interesting to expand this study to the other tropical floodplains which can be present under other climatic conditions. Moreover, as in any model development, the processes represented can always be improved or completed by extra processes.

In order to progress in the development of the land hydrological processes in Land Surface Models and in the study of the large tropical floodplains, possible future topics for research are presented as following:

8.2.1 Improve the floodplains representation

The representation of the tropical floodplains in ORCHIDEE can be improved by the following points:

■ Handle partial floodplains (e.g. main Amazon river)

The floodplains scheme developed in this thesis was oriented toward the correct representation of the Pantanal. It works perfectly over other floodplains, however, it could be improved to better fit with the specificity of other floodplains such as over the main Amazon river whose floodplains are very important for the local hydrology (Guimberteau et al, 2013). Over the Pantanal, most of the HTUs have a fraction potentially flooded equal to 1, i.e. they can be fully flooded. On the contrary, the HTUs over the main Amazon river have a fraction potentially flooded lower than 1.

The floodplains scheme should be adapted to consider the case of the HTUs partially defined as floodplains. This can be done by reducing the amount of water transferred to the floodplains reservoir when the maximal floodplains fraction of the HTU is lower than 1. The difference in the inflow of water can flow directly to the main reservoir. This would allow to represent correctly the floodplains and the river discharge.

■ Improve the volume/surface relationship

There are different solutions to estimate the flooded area in a HTU from the volume/surface relationship. In this thesis, the methodology used focuses on diminishing the memory consumed by the model to simulate the floodplains by considering them as channels whose shape and height is defined from the distribution of the orography within the pixels composing a HTU.

A more memory consumptive method would consist in using more directly the distribution of the orography within a HTU and perform a progressive flooding of the pixels from the high resolution hydrological network that compose each HTU. However, this method would be very

memory consumptive what make it unusable over large domain. Moreover it is possible that the improvement of the flooded area using this method won't worth the memory use issues it brings.

More efficient methods would use the distinction within each HTU of the main river such as the use of a floodplain elevation profile such as in CAMA-Flood (Yamazaki et al, 2011, 2014) or using the information from the Height Above the Nearest Drainage (HANDS, Nobre et al, 2011) such as in MGB-IPH (Collischonn et al, 2007; Pontes et al, 2017; Fleischmann et al, 2021b).

A possible adaptation for ORCHIDEE would be to define different threshold for the HANDS variable, in each HTU there is a corresponding area calculated for each threshold. The difficulty is to estimate the river height to be able to flood progressively these different areas.

■ Integrate a subsurface runoff

One of the major limit identified for the floodplains scheme in ORCHIDEE is the impossibility of the water within the floodplains and the soil moisture to affect the soil moisture of the neighbour grid cells.

The representation of these horizontal transport of groundwater could be represented by a sub-surface Darcian diffusion scheme or by a large scale aquifer transport based on a ground-water routing scheme. This would allow for the floodplains to extend horizontally through an horizontal diffusion of the water in the soil.

8.2.2 Going further on the floodplains study

The floodplains scheme in ORCHIDEE allows to represent the processes related to the floodplains. This scheme can serve as a basis for the integration of other floodplains related processes such as:

- the **dissolved organic carbon** to integrate this inflow of nutrient into the fluvial system and the ocean,
- the **carbon cycle** over the flooded area, principally through the flooded vegetation and the methane production,
- the interaction between floodplains and **wildfire**,
- the study of the impact of **climate change** and **land use** changes on the floodplains.

8.2.3 Include more wetland type

The features modeled by the floodplains scheme in the ORCHIDEE model represent only a certain type of wetland which floods due to the overflow of large rivers. There are others types of wetlands that could be implemented in ORCHIDEE to be able to (1) determine the impact of these complex ecosystems on the hydrological cycle and the land atmosphere-interactions and (2) to improve the representation of the hydrological cycle.

The different types of wetlands that could be represented additionally in ORCHIDEE are detailed below and are accompanied with example in South America that could have a relatively important impact in the Land Surface Models:

- **the swamps and flooded forest:** this type of wetland can be represented by considering the infiltration of part of the water in the river routing reservoirs into the soil without considering a flooded area. This would be important for the Amazon basin for the regions surrounding the main Amazon river but also for the Llanos de Moxos in the Madeira basin.
- **the lakes:** they can be considered as open water surface that will be fed by the river flow. However, these flooded areas will also need to be converted from a volume. The major issue is that, as they can represent large areas and have an important depth, ORCHIDEE will require to model the internal dynamic of the lake and to take into account their surface temperature.

The lakes are fed by one or various inflows and they can have one or various outflow if they are in the middle of a catchment. However, if the lakes are located at the outflow of an endorheic basin, they don't have any outflow. Some notable large South American lakes are the Titicaca lake, Mar Chiquita, some lakes over the Pantanal and the Amazon but also the higher latitude lakes in Patagonia such as the Argentino Lake and the Viedma lake.

- **the wetlands surrounding the lakes:** there can exist large wetlands around the lakes such as it is the case with the marshes of the Rio Dulce in the North of Mar Chiquita. These wetlands are the water to land transition between the lake and the dry lands. These wetlands may be difficult to represent because they are strongly related to the representation of the lake area but with a dense vegetation which allows for strong evapotranspiration.
- **the coastal wetland:** these wetlands are located on the coast and depends on both rivers and ocean. Therefore, they require the presence of an ocean model to be represented. Another difficulty lies in the necessity to model the water salinity in these regions.
- **the deltas:** the deltas are regions where the river network bifurcates and, therefore, are places which are difficult to model. Representing the deltas would require to add an extra layer to the purely convergent river routing scheme in ORCHIDEE. This extra layer would allow the transfer of water to multiple HTUs over the deltas such as it is done in [Yamazaki et al \(2014\)](#). In South America, this would benefit to the simulation of the Amazon Delta, the Paraná river between Posadas and Timbues, the Paraná Delta and the Orinoco Delta.
- **the ponds:** in the Argentinian Pampas, there are relatively small open water features that are too small to be considered as deep lakes. These features are isolated and principally created by the local precipitation and aquifer. They could be parameterized in ORCHIDEE as some kind of ponds which are alimented by the aquifer transport and the precipitation.

8.2.4 Going further in the River Modelling

Aside from the representation of the wetlands, some other processes related of the river modelling could be implemented taking advantage of the preprocessing tool of the river routing.

These processes are principally related to the human activities:

- **Dams:** which can be handled such as the lakes except that their outflow is managed by a human criteria and their water can be used for other human processes such as irrigation. This also helps determines the electrical production in the case of hydropower plants.
- **Irrigation:** the irrigation make the link between the representation of the vegetation related to agricultural activities in the model and the water in the river network system (and in particular the water in the dams).
- **Water withdrawals:** for industrial activities or human consumption.

Apart from allowing to represent the impact of these activities on the hydrological cycle, these features would also help to make forecast and determine how the human activities can be affected by climate change. A dam irrigation supply/demand scheme has already been implemented in ORCHIDEE and validated over the Yellow River Basin in China (Zhou et al, 2021b). The irrigation from the dams water storage is crucial in certain regions such as in the semi-arid Mendoza region in Argentina.

The water withdrawals are particularly important in South America where the population tends to be concentrated in very large cities. There is a strong dependence on the hydropower, principally in Brazil, with the presence of very large dams such as Itaipu or Yacyretá on the Paraná river.

8.2.5 Toward more Coupled simulation with RegIPSL

Finally, the RegIPSL regional model has proven to be an adequate tool to evaluate the impact of the features implemented in the ORCHIDEE model. The floodplains scheme has proven to have a significant impact on the atmospheric simulation in the model.

On the one hand, RegIPSL is worthwhile as it supports the study of the land-atmosphere interactions related to the development of new features in ORCHIDEE. On the other hand, these new features allows to encourage the evaluation of the RegIPSL model with different configurations and new features and, therefore, encourage the development and improvement of the coupled model simulations.



Anthony Schrapffer

8.3 Acronyms

HTU	Hydrological Transfer Unit
IPSL	Institut Pierre Simon Laplace
LSM	Land Surface Model
MGB-IPH	Modelo de Grandes Bacias do Instituto de Pesquisas Hidráulicas
ORCHIDEE	ORganizing Carbon and Hydrology in Dynamic EcosystEms
RegIPSL	Institut Pierre Simon Laplace's Regional Earth System Model
RoutingPP	Pre-Processor of the routing input for ORCHIDEE high resolution routing scheme

Appendices

APPENDIX **A**

Acronyms

AMMA	African Monsoon Multidisciplinary Analysis
ANA	Agencia Nacional de Aguas
ATTZ	Aquatic-Terrestrial Transition Zone
AmSud	RegIPSL simulation at 20 km over the South American domain
AmSud_Flood	RegIPSL simulation at 20 km over the South American domain with the floodplains activated
AmSud_GPCC	Atmospheric forcing based on a RegIPSL simulation at 20 km over the South American domain which precipitation is bias-corrected by GPCC
AmSud_NoFlood	RegIPSL simulation at 20 km over the South American domain with the floodplains deactivated
CAMA-FLOOD	Catchment-based Macro-scale Floodplain model
CH4	Methane
CLARIS-Ipb	Change Assessment and Impact Studies in La Plata Basin
CMIP6	Coupled Model Intercomparison Project
CO2	Carbon Dioxide
CRMSE	Centered Root Mean Square Error
CRU	Climatic Research Unit
DEM	Digital Elevation Model
DOM	Dissolved organic Matter
DYNAMICO	Icosahedral Dynamical Core atmospheric model of the Institut Pierre Simon Laplace

ERA	ECMWF Re-Analysis
ERA-40	ECMWF Re-Analysis second generation
ERA5	ECMWF Re-Analysis fifth generation
ERA1	ECMWF Interim Re-Analysis
ESA	European Spatial Agency
ESA-CCI	European Spatial Agency Climate Change Initiative
ESM	Earth System Model
ETOPO5	Earth topography five minute grid
FP	Offline simulations with the floodplains activated
GEWEX	Global Energy and Water Exchanges
GFPLAIN250m	Gridded dataset of Earth's floodplains at 250-m resolution
GIEMS	Global Inundation Extent from Multi-Satellites
GIEMS-2	Global Inundation Extent from Multi-Satellites version 2
GIEMS-D15	Global Inundation Extent from Multi-Satellites downscaled 15 arcseconds
GLWD	Global Lake and Wetlands Dataset
GPCC	Global Precipitation Climatology Centre
GRACE	Gravity Recovery and Climate Experiment
GSWP3	Global Soil Wetness Project Phase 3
HEC-RAS 1D	Hydrologic Engineering Center's River Analysis System
HR	Offline simulations with the high resolution river routing scheme in ORCHIDEE
HRU	Hydrological Response Unit
HTU	Hydrological Transfer Unit
HyMAP	Hyperspectral Mapper sensor
HydroDEM	Hydrologically coherent Digital Elevation Model
HydroSHEDS	Hydrological data and maps based on SHuttle Elevation
IPCC	Intergovernmental Panel on Climate Change
IPSL	Institut Pierre Simon Laplace

ISBA-CTRIP	Interaction Sol-Biosphère-Atmosphère CNRM's Total Runoff and Integrating Pathways
ITCZ	Intertropical Convergence Zone
JULES	Joint UK Land Environment Simulator
LAI	Leaf Area Index
LPB	La Plata Basin
LR	Offline simulations with the low resolution river routing scheme in ORCHIDEE (cf. routing scheme at °)
LSM	Land Surface Model
M2M	Morrison 2-moment scheme
MERIT DEM	Multi-Error-Removed Improved-Terrain Digital Elevation Model
MERIT Hydro	Multi-Error-Removed Improved-Terrain Hydrologically coherent Digital Elevation Model
MGB-IPH	Modelo de Grandes Bacias do Instituto de Pesquisas Hidráulicas
mNDWI	Modified Normalized Difference Water Index
MODIS	Moderate Resolution Imaging Spectroradiometer
MORCE-MED	Model Of the Regional Coupled Earth system platform over the Mediterranean area
MYNN	Mellor-Yamada-Nakanishi-Niino 2.5 boundary layer scheme
NASA	National Aeronautics and Space Administration
NCEP	National Centers for Environmental Prediction
NDMI	Normalized Difference Moisture Index
NDVI	Normalized Difference Vegetation Index
NEMO	Nucleus for European Modelling of the Ocean
NIR	Near-infrared spectral band
NOAH-MP	Noah-Multiparameterization Land Surface Model
NOFP	Offline simulations with the floodplains deactivated
NSE	Nash-Sutcliffe Efficiency
ORCHIDEE	ORganizing Carbon and Hydrology in Dynamic EcosystEms
PBIAS	Percent Bias Index

PBL	Planetary Boundary Layer
PCA	Principal Component Analysis
PFT	Plant Functional Type
RAMSAR	Ramsar Convention on Wetlands of International Importance Especially as Waterfowl Habitat
RCM	Regional Coupled Model
RMSE	Root Mean Square Error
RRTMG	Radiation and Rapid Radiative Transfer Model for General Circulation
RegIPSL	Institut Pierre Simon Laplace's Regional Earth System Model
RoutingPP	Pre-Processor of the routing input for ORCHIDEE high resolution routing scheme
SACZ	South Atlantic Convergence Zone
SALLJ	South American Low Level Jet
SAMS	South American Monsoon System
SAR	Synthetic Aperture Radar sensor
SECHIBA	Schématisation des EChanges Hydriques à l'Interface Biosphère-Atmosphère
SESA	Southeastern South America
SRTM3	Shuttle Radar Topography Mission 3 arcseconds
SST	Sea Surface Temperature
STN-30	Simulated Topological Network 30 arcseconds
STOMATE	Saclay Toulouse Orsay Modèle pour l'Analyse des Ecosystèmes Terrestres
SWIR	Shortwave Infrared spectral band
TWS	Total Water Storage
UPRB	Upper Paraguay River Basin
USDA	United States Department of Agriculture
WFD	WATCH forcing data
WFDEI	WATCH forcing data bias corrected by ERAI
WRF	Weather Research and Forecasting

WRF-HYDRO	Weather Research and Forecasting Hydro Modeling System
WWF	World Wide Fund for Nature
WaterMAP	Surface Water Mapping Product
XIOS	XML-IO-Server

APPENDIX B

List of Variables

AET	Actual Evapotranspiration
C	Reduction factor for floodplains infiltration
Co	Convective downdraft during precipitation events
CAPE	Convective Available Potential Energy
CIN	Convective Inhibition
c_p	Specific heat
d	distance of the river within an HTU
E	Evapotranspiration
$E_{f,i}$	Evaporation over the floodplains of the HTU i
EN	Entrainment at the top of the PBL
E_{pot}	Potential evaporation
F	Heat fluxes from the surface into the atmosphere
$f_{max,i}$	Maximal fraction of the HTU i that can be flooded
$F_{out,j}$	
G	Ground Heat Flux
$h_{0,i}$	Height at which the floodplains of the HTU i are fully covered
H	Sensible Heat Flux
$I_{f,i}$	Infiltration from the floodplain into the soil moisture reservoir
k_{litt}	Averaged conductivity for saturated infiltration in the litter layer

LE	Latent Heat Flux
LT	Latent Heat Flux from Transpiration
maxvegetfrac	Maximal fraction of a grid point occupied by vegetation
M_t	Model value at time t
OF	Overflow time constant
OF_{repeat}	Number of repetition of the overflow water transfer within a single time step
$O_{i,j}$	Overflow from HTU i to HTU j
O_t	Observation value at time t
P	Precipitation
Q	River Discharge
q_a	Specific humidity of the air at the surface
$Q_{f,i}$	River discharge from the floodplains reservoir to the stream reservoir within the HTU i
$Q_{j,i}$	Discharge from the reservoir j of the HTU i into the downstream HTU
q_s	Specific humidity of the air when it is saturated
r_a	Aerodynamic resistance
R	Radiative cooling fluxes
R_{limit}	Limiter for the floodplains reduction of the discharge
R_n	Net Radiation
$S_{B,i}$	Surface of the grid point that contains the HTU i
$S_{f,i}$	Flooded surface of the HTU i
$S_{fmax,i}$	Maximal flooded surface of the HTU i
S_i	Surface of the HTU i
T_a	Air temperature
T_s	Surface temperature
vegetfrac	Fraction of a grid point occupied by vegetation
$V_{j,i}$	Volume of water in the reservoir j of the HTU i
W	Water storage
β	β parameter for the evapotranspiration

β_i	Shape factor of the HTU i
Δz	Difference of height
$\Delta h_{i,j \in \{i-1\}}$	Difference of flood height between the HTU i and one of its upstream HTU j
$\delta_{\hat{\tau},i}$	Fraction of the grid point $\hat{\tau}$ occupied by the HTU i
λ	Unique topindex for a grid point used in the 0.5° resolution river routing
$\Lambda_{S,i}$	Topindex over the main river of the HTU i , used for the stream and floodplains reservoirs
$\bar{\Lambda}_i$	Topindex average over the HTU i , used for the fast and slow reservoirs
ρ	Air density
τ_i	Time constant of the reservoir
θ_e	Equivalent Potential Energy

Bibliography

- Acharya TD, Subedi A, Lee DH (2018) Evaluation of water indices for surface water extraction in a landsat 8 scene of Nepal. *Sensors (Switzerland)* DOI 10.3390/s18082580
- Adam L, Döll P, Prigent C, Papa F (2010) Global-scale analysis of satellite-derived time series of naturally inundated areas as a basis for floodplain modeling. *Advances in Geosciences* DOI 10.5194/adgeo-27-45-2010
- Adler B, Kalthoff N, Gantner L (2011) The impact of soil moisture inhomogeneities on the modification of a mesoscale convective system: An idealised model study. *Atmospheric Research* DOI 10.1016/j.atmosres.2011.03.013
- Ahmad SK, Hossain F (2020) Forecast-informed hydropower optimization at long and short-time scales for a multiple dam network. *Journal of Renewable and Sustainable Energy* DOI 10.1063/1.5124097
- Aires F, Prigent C, Fluet-Chouinard E, Yamazaki D, Papa F, Lehner B (2018) Comparison of visible and multi-satellite global inundation datasets at high-spatial resolution. *Remote Sensing of Environment* DOI 10.1016/j.rse.2018.06.015
- Alfieri L, Salamon P, Pappenberger F, Wetterhall F, Thielen J (2012) Operational early warning systems for water-related hazards in Europe. DOI 10.1016/j.envsci.2012.01.008
- Alho C, Sabino J (2011) A conservation agenda for the Pantanal's biodiversity. *Brazilian Journal of Biology* 71(1 suppl 1):327–335, DOI 10.1590/s1519-69842011000200012
- Alho CJ, Silva JS (2012) Effects of severe floods and droughts on wildlife of the pantanal wetland (Brazil)-a review. DOI 10.3390/ani2040591
- Alho CJ, Vieira LM (1997) Fish and wildlife resources in the Pantanal wetlands of Brazil and potential disturbances from the release of environmental contaminants. DOI 10.1897/1551-5028(1997)016<0071:FAWRIT>2.3.CO;2
- Alho CJR (2005) *The World's Largest Wetlands. The World's Largest Wetlands: Ecology and Conservation* DOI 10.1017/CBO9780511542091

- Alho CJR, Lacher TE, Gonçalves HC (1988) Environmental Degradation in the Pantanal Ecosystem. *BioScience* DOI 10.2307/1310449
- Alkama R, Decharme B, Douville H, Becker M, Cazenave A, Sheffield J, Voldoire A, Tyteca S, Le Moigne P (2010) Global evaluation of the ISBA-TRIP continental hydrological system. Part I: Comparison to GRACE terrestrial water storage estimates and in situ river discharges. *Journal of Hydrometeorology* DOI 10.1175/2010JHM1211.1
- de Almeida TIR, Penatti NC, Ferreira LG, Arantes AE, do Amaral CH (2015) Principal component analysis applied to a time series of MODIS images: the spatio-temporal variability of the Pantanal wetland, Brazil. *Wetlands Ecology and Management* DOI 10.1007/s11273-015-9416-4
- Aldorf D, Han SC, Bates P, Melack J (2010) Seasonal water storage on the Amazon floodplain measured from satellites. *Remote Sensing of Environment* DOI 10.1016/j.rse.2010.05.020
- Araujo AGdJ, Obregón GO, Sampaio G, Monteiro AMV, da Silva LT, Soriano B, Padovani C, Rodriguez DA, Maksic J, Farias JFS (2018) Relationships between variability in precipitation, river levels, and beef cattle production in the Brazilian Pantanal. *Wetlands Ecology and Management* DOI 10.1007/s11273-018-9612-0
- Arcand S, Luo L, Zhong S, Pei L, Bian X, Winkler JA (2019) Modeled changes to the Great Plains low-level jet under a realistic irrigation application. *Atmospheric Science Letters* DOI 10.1002/asl.888
- Arora VK, Chiew FH, Grayson RB (1999) A river flow routing scheme for general circulation models. *Journal of Geophysical Research Atmospheres* DOI 10.1029/1999JD900200
- Assine ML (2005) River avulsions on the Taquari megafan, Pantanal wetland, Brazil. *Geomorphology* DOI 10.1016/j.geomorph.2005.02.013
- Baik J, Zohaib M, Kim U, Aadil M, Choi M (2019) Agricultural drought assessment based on multiple soil moisture products. *Journal of Arid Environments* DOI 10.1016/j.jaridenv.2019.04.007
- Balsamo G, Pappenberger F, Dutra E, Viterbo P, van den Hurk B (2011) A revised land hydrology in the ECMWF model: A step towards daily water flux prediction in a fully-closed water cycle. *Hydrological Processes* DOI 10.1002/hyp.7808
- Barros V, Chamorro L, Coronel G, Baez J (2005) The Major Discharge Events in the Paraguay River: Magnitudes, Source Regions, and Climate Forcings. *Journal of Hydrometeorology* DOI 10.1175/jhm-378.1
- Barros V, Clarke R, Silva Dias P (2006) El cambio climático en la cuenca Del Plata. Consejo Nacional de Investigaciones Científicas y Técnicas - CONICET
- Beck HE, Van Dijk AI, De Roo A, Dutra E, Fink G, Orth R, Schellekens J (2017) Global evaluation of runoff from 10 state-of-the-art hydrological models. *Hydrology and Earth System Sciences* DOI 10.5194/hess-21-2881-2017

- Bell VA, Kay AL, Jones RG, Moore RJ (2007) Use of a grid-based hydrological model and regional climate model outputs to assess changing flood risk. *International Journal of Climatology* DOI 10.1002/joc.1539
- Berbery EH, Barros VR (2002) The Hydrologic Cycle of the La Plata Basin in South America. *Journal of Hydrometeorology* DOI 10.1175/1525-7541(2002)003<0630:thcotl>2.0.co;2
- Bergier I (2010) River level sensitivity to SOI and NAO in Pantanal and Amazonia. In: Conference: 3o. Simpósio de Geotecnologias do Pantanal at Caceres
- Bergier I (2013) Effects of highland land-use over lowlands of the Brazilian Pantanal. *Science of the Total Environment* 463-464:1060–1066, DOI 10.1016/j.scitotenv.2013.06.036
- Betts AK, Ball JH (1998) FIFE surface climate and site-average dataset 1987-89. *Journal of the Atmospheric Sciences* DOI 10.1175/1520-0469(1998)055<1091:FSCASA>2.0.CO;2
- Betts AK, Silva Dias MAF (2010) Progress in understanding land-surface-atmosphere coupling from LBA research. *Journal of Advances in Modeling Earth Systems* DOI 10.3894/james.2010.2.6
- Beven K, Cloke H, Pappenberger F, Lamb R, Hunter N (2015) Hyperresolution information and hyperresolution ignorance in modelling the hydrology of the land surface. *Science China Earth Sciences* 58(1):25–35, DOI 10.1007/s11430-014-5003-4
- Bhuiyan MAE, Nikolopoulos EI, Anagnostou EN, Polcher J, Albergel C, Dutra E, Fink G, Martínez-De La Torre A, Munier S (2019) Assessment of precipitation error propagation in multi-model global water resource reanalysis. *Hydrology and Earth System Sciences* DOI 10.5194/hess-23-1973-2019
- Bierkens MF (2015) Global hydrology 2015: State, trends, and directions. *Water Resources Research* DOI 10.1002/2015WR017173
- Blaschke T, Hay GJ, Kelly M, Lang S, Hofmann P, Addink E, Queiroz Feitosa R, van der Meer F, van der Werff H, van Coillie F, Tiede D (2014) Geographic Object-Based Image Analysis - Towards a new paradigm. *ISPRS Journal of Photogrammetry and Remote Sensing* 87:180–191, DOI 10.1016/j.isprsjprs.2013.09.014
- Bonan GB (1995) Sensitivity of a GCM simulation to inclusion of inland water surfaces. *Journal of Climate* DOI 10.1175/1520-0442(1995)008<2691:SOAGST>2.0.CO;2
- Bonetto AA (1975) Hydrologic regime of the Paraná River and its influence on ecosystems. Springer-Verlag, New York
- Borges AV, Gypens N (2010) Carbonate chemistry in the coastal zone responds more strongly to eutrophication than to ocean acidification. *Limnology and Oceanography* 55(1):346–353, DOI 10.4319/lo.2010.55.1.0346

- Borma LS, Da Rocha HR, Cabral OM, Von Randow C, Collicchio E, Kurzatkowski D, Brugger PJ, Freitas H, Tannus R, Oliveira L, Rennó CD, Artaxo P (2009) Atmosphere and hydrological controls of the evapotranspiration over a floodplain forest in the Bananal Island region, Amazonia. *Journal of Geophysical Research: Biogeosciences* DOI 10.1029/2007JG000641
- Boschetti M, Nutini F, Manfron G, Brivio PA, Nelson A (2014) Comparative analysis of normalised difference spectral indices derived from MODIS for detecting surface water in flooded rice cropping systems. *PLoS ONE* DOI 10.1371/journal.pone.0088741
- Bradford JB, Schlaepfer DR, Lauenroth WK, Yackulic CB, Duniway M, Hall S, Jia G, Jamiyan-sharav K, Munson SM, Wilson SD, Tietjen B (2017) Future soil moisture and temperature extremes imply expanding suitability for rainfed agriculture in temperate drylands. *Scientific Reports* DOI 10.1038/s41598-017-13165-x
- Brauman KA, Daily GC, de Duarte TK, Mooney HA (2007) The nature and value of ecosystem services: An overview highlighting hydrologic services. *Annual Review of Environment and Resources* DOI 10.1146/annurev.energy.32.031306.102758
- Bravo JM, Allasia D, Paz AR, Collischonn W, Tucci CE (2012) Coupled Hydrologic-Hydraulic Modeling of the Upper Paraguay River Basin. *Journal of Hydrologic Engineering* DOI 10.1061/(ASCE)HE.1943-5584.0000494
- Bravo JM, Collischonn W, da Paz AR, Allasia D, Domecq F (2014) Impact of projected climate change on hydrologic regime of the Upper Paraguay River basin. *Climatic Change* 127(1):27–41, DOI 10.1007/s10584-013-0816-2
- Brunner GW (2010) HEC-RAS River Analysis System. DOI CPD-68
- Budyko M (1974) *Climate and Life*. Academic P, New York, NY, USA
- Campbell MA, Ferguson CR, Burrows DA, Beauharnois M, Xia G, Bosart LF (2019) Diurnal effects of regional soil moisture anomalies on the great plains low-level jet. *Monthly Weather Review* DOI 10.1175/MWR-D-19-0135.1
- Campoy A, Ducharne A, Cheruy F, Hourdin F, Polcher J, Dupont JC (2013) Response of land surface fluxes and precipitation to different soil bottom hydrological conditions in a general circulation model. *Journal of Geophysical Research Atmospheres* DOI 10.1002/jgrd.50627
- Carril AF, Menéndez CG, Remedio AR, Robledo F, Sörensson A, Tencer B, Boulanger JP, de Castro M, Jacob D, Le Treut H, Li LZ, Penalba O, Pfeifer S, Rusticucci M, Salio P, Samuelsson P, Sanchez E, Zaninelli P (2012) Performance of a multi-RCM ensemble for South Eastern South America. *Climate Dynamics* 39(12):2747–2768, DOI 10.1007/s00382-012-1573-z
- Carril AF, Cavalcanti IF, Menéndez CG, Sörensson A, López-Franca N, Rivera JA, Robledo F, Zaninelli PG, Ambrizzi T, Penalba OC, Da Rocha RP, Sánchez E, Bettolli ML, Pessacq N, Renom M, Ruscica R, Solman S, Tencer B, Grimm AM, Rusticucci M, Cherchi A, Tedeschi R, Zamboni L (2016) Extreme events in the la Plata basin: A retrospective analysis of what we have learned during CLARIS-LPB project. *Climate Research* DOI 10.3354/cr01374

- Carton JA (1991) Effect of seasonal surface freshwater flux on sea surface temperature in the tropical Atlantic Ocean. *Journal of Geophysical Research* 96(C7):12,593, DOI 10.1029/91jc01256
- Carvalho LM, Jones C, Liebmann B (2004) The South Atlantic convergence zone: Intensity, form, persistence, and relationships with intraseasonal to interannual activity and extreme rainfall. *Journal of Climate* DOI 10.1175/1520-0442(2004)017<0088:TSACZI>2.0.CO;2
- Chaney N, Torres-Rojas L, Vergopolan N, Fisher C (2020) Two-way coupling between the sub-grid land surface and river networks in Earth system models. *Geoscientific Model Development Discussions* pp 1–31, DOI 10.5194/GMD-2020-291
- Chaney NW, Metcalfe P, Wood EF (2016) HydroBlocks: a field-scale resolving land surface model for application over continental extents. *Hydrological Processes* DOI 10.1002/hyp.10891
- Charney J, Stone PH, Quirk WJ (1975) Drought in the Sahara: A biogeophysical feedback mechanism. *Science* DOI 10.1126/science.187.4175.434
- Chen F, Manning KW, Lemone MA, Trier SB, Alfieri JG, Roberts R, Tewari M, Niyogi D, Horst TW, Oncley SP, Basara JB, Blanken PD (2007) Description and evaluation of the characteristics of the NCAR high-resolution land data assimilation system. *Journal of Applied Meteorology and Climatology* DOI 10.1175/JAM2463.1
- Clarke RT (2005) The relation between interannual storage and frequency of droughts, with particular reference to the Pantanal Wetland of South America. *Geophysical Research Letters* DOI 10.1029/2004GL021742
- Clough SA, Shephard MW, Mlawer EJ, Delamere JS, Iacono MJ, Cady-Pereira K, Boukabara S, Brown PD (2005) Atmospheric radiative transfer modeling: A summary of the AER codes. *Journal of Quantitative Spectroscopy and Radiative Transfer* DOI 10.1016/j.jqsrt.2004.05.058
- Collischonn W, Allasia D, da Silva BC, Tucci CE (2007) The MGB-IPH model for large-scale rainfall-runoff modelling. *Hydrological Sciences Journal* DOI 10.1623/hysj.52.5.878
- Compo GP, Whitaker JS, Sardeshmukh PD, Matsui N, Allan RJ, Yin X, Gleason BE, Vose RS, Rutledge G, Bessemoulin P, BroNnimann S, Brunet M, Crouthamel RI, Grant AN, Groisman PY, Jones PD, Kruk MC, Kruger AC, Marshall GJ, Maugeri M, Mok HY, Nordli O, Ross TF, Trigo RM, Wang XL, Woodruff SD, Worley SJ (2011) The Twentieth Century Reanalysis Project. DOI 10.1002/qj.776
- Coronato T, Carril AF, Zaninelli PG, Giles J, Ruscica R, Falco M, Sörensson AA, Fita L, Li LZ, Menéndez CG (2020) The impact of soil moisture–atmosphere coupling on daily maximum surface temperatures in Southeastern South America. *Climate Dynamics* DOI 10.1007/s00382-020-05399-9
- Craig A, Valcke S, Coquart L (2017) Development and performance of a new version of the OASIS coupler, OASIS3-MCT-3.0. *Geoscientific Model Development* DOI 10.5194/gmd-10-3297-2017

- Dadson SJ, Ashpole I, Harris P, Davies HN, Clark DB, Blyth E, Taylor CM (2010) Wetland inundation dynamics in a model of land surface climate: Evaluation in the Niger inland delta region. *Journal of Geophysical Research Atmospheres* DOI 10.1029/2010JD014474
- Dadson SJ, Bell VA, Jones RG (2011) Evaluation of a grid-based river flow model configured for use in a regional climate model. *Journal of Hydrology* DOI 10.1016/j.jhydrol.2011.10.002
- Davis J, O'Grady AP, Dale A, Arthington AH, Gell PA, Driver PD, Bond N, Casanova M, Finlayson M, Watts RJ, Capon SJ, Nagelkerken I, Tingley R, Fry B, Page TJ, Specht A (2015) When trends intersect: The challenge of protecting freshwater ecosystems under multiple land use and hydrological intensification scenarios. *Science of the Total Environment* DOI 10.1016/j.scitotenv.2015.03.127
- de Almeida Pereira GH, Júnior CC, Fronza G, Deppe FAC (2019) Multitemporal analysis of sar images for detection of flooded areas in Pantanal. *RA'E GA - O Espaço Geografico em Analise* DOI 10.5380/raega.v46i3.66988
- De Rosnay P, Bruen M, Polcher J (2000) Sensitivity of surface fluxes to the number of layers in the soil model used in GCMs. *Geophysical Research Letters* DOI 10.1029/2000GL011574
- Decharme B, Douville H, Prigent C, Papa F, Aires F (2008) A new river flooding scheme for global climate applications : Off-line evaluation over South America. *Journal of Geophysical Research Atmospheres* DOI 10.1029/2007JD009376
- Decharme B, Alkama R, Douville H, Becker M, Cazenave A (2010) Global evaluation of the ISBA-TRIP continental hydrological system. Part II: Uncertainties in river routing simulation related to flow velocity and groundwater storage. *Journal of Hydrometeorology* DOI 10.1175/2010JHM1212.1
- Decharme B, Delire C, Minvielle M, Colin J, Vergnes JP, Alias A, Saint-Martin D, Séférian R, Sénési S, Voldoire A (2019) Recent Changes in the ISBA-CTRIP Land Surface System for Use in the CNRM-CM6 Climate Model and in Global Off-Line Hydrological Applications. *Journal of Advances in Modeling Earth Systems* DOI 10.1029/2018MS001545
- Dee DP, Uppala SM, Simmons AJ, Berrisford P, Poli P, Kobayashi S, Andrae U, Balmaseda MA, Balsamo G, Bauer P, Bechtold P, Beljaars AC, van de Berg L, Bidlot J, Bormann N, Delsol C, Dragani R, Fuentes M, Geer AJ, Haimberger L, Healy SB, Hersbach H, Hólm EV, Isaksen L, Kållberg P, Köhler M, Matricardi M, McNally AP, Monge-Sanz BM, Morcrette JJ, Park BK, Peubey C, de Rosnay P, Tavolato C, Thépaut JN, Vitart F (2011) The ERA-Interim reanalysis: Configuration and performance of the data assimilation system. *Quarterly Journal of the Royal Meteorological Society* DOI 10.1002/qj.828
- Delworth T, Manabe S (1989) The Influence of Soil Wetness on Near-Surface Atmospheric Variability. *Journal of Climate* DOI 10.1175/1520-0442(1989)002<1447:tioswo>2.0.co;2
- Dirmeyer PA (2003) The role of the land surface background state in climate predictability. *Journal of Hydrometeorology* DOI 10.1175/1525-7541(2003)004<0599:TROTLS>2.0.CO;2

- Dirmeyer PA (2011) The terrestrial segment of soil moisture-climate coupling. *Geophysical Research Letters* DOI 10.1029/2011GL048268
- Dirmeyer PA (2013) Characteristics of the water cycle and land-atmosphere interactions from a comprehensive reforecast and reanalysis data set: CFSv2. *Climate Dynamics* DOI 10.1007/s00382-013-1866-x
- Dirmeyer PA, Schlosser CA, Brubaker KL (2009) Precipitation, recycling, and land memory: An integrated analysis. *Journal of Hydrometeorology* DOI 10.1175/2008JHM1016.1
- Dogliotti AI, Gossn JI, Vanhellemont Q, Ruddick KG (2018) Detecting and quantifying a massive invasion of floating aquatic plants in the Río de la Plata turbid waters using high spatial resolution ocean color imagery. *Remote Sensing* DOI 10.3390/rs10071140
- Döll P, Lehner B (2002) Validation of a new global 30-min drainage direction map. *Journal of Hydrology* DOI 10.1016/S0022-1694(01)00565-0
- D'Orgeval T (2006) Impact du changement climatique sur le cycle de l'eau en Afrique de l'Ouest: modélisation et incertitudes. PhD thesis, Université Paris VI
- D'Orgeval T, Polcher J, De Rosnay P (2008) Sensitivity of the West African hydrological cycle in ORCHIDEE to infiltration processes. *Hydrology and Earth System Sciences* DOI 10.5194/hess-12-1387-2008
- Douville H, Chauvin F (2000) Relevance of soil moisture for seasonal climate predictions: A preliminary study. *Climate Dynamics* DOI 10.1007/s003820000080
- Drobinski P, Anav A, Lebeaupin Brossier C, Samson G, Stéfanon M, Bastin S, Baklouti M, Béranger K, Beuvier J, Bourdallé-Badie R, Coquart L, D'Andrea F, de Noblet-Ducoudré N, Diaz F, Dutay JC, Ethe C, Foujols MA, Khvorostyanov D, Madec G, Mancip M, Masson S, Menut L, Palmieri J, Polcher J, Turquety S, Valcke S, Viovy N (2012) Model of the Regional Coupled Earth system (MORCE): Application to process and climate studies in vulnerable regions. *Environmental Modelling and Software* DOI 10.1016/j.envsoft.2012.01.017
- Dubos T, Dubey S, Tort M, Mittal R, Meurdesoif Y, Hourdin F (2015) DYNAMICO-1.0, an icosahedral hydrostatic dynamical core designed for consistency and versatility. *Geoscientific Model Development* DOI 10.5194/gmd-8-3131-2015
- Ducharne A, Golaz C, Leblois E, Laval K, Polcher J, Ledoux E, de Marsily G (2003) Development of a high resolution runoff routing model, calibration and application to assess runoff from the LMD GCM. *Journal of Hydrology* 280(1-4):207–228, DOI 10.1016/S0022-1694(03)00230-0
- Edwards M (1989) Global gridded elevation and bathymetry on 5-minute geographic grid (etopo5). NOAA, National Geophysical Data Center, Boulder, Colorado, USA
- Ek MB, Holtslag AA (2004) Influence of soil moisture on boundary layer cloud development. *Journal of Hydrometeorology* DOI 10.1175/1525-7541(2004)005(0086:IOSMOB)2.0.CO;2

- Eltahir EA (1998) A soil moisture-rainfall feedback mechanism 1. Theory and observations. *Water Resources Research* DOI 10.1029/97WR03499
- ESA (2017) Esa cci land cover time-series v2.0.7 (1992-2015). Tech. rep., European Space Agency-Climate Change Initiative
- Fan FM, Siqueira VA, Fleischmann AS, Brêda JPF, de Paiva RCD, Pontes PRM, Collischonn W (2021) On the discretization of river networks for large scale hydrologic-hydrodynamic models. *Revista Brasileira de Recursos Hídricos* DOI 10.1590/2318-0331.262120200070
- Fan Y, Clark M, Lawrence DM, Swenson S, Band LE, Brantley SL, Brooks PD, Dietrich WE, Flores A, Grant G, Kirchner JW, Mackay DS, McDonnell JJ, Milly PC, Sullivan PL, Tague C, Ajami H, Chaney N, Hartmann A, Hazenberg P, McNamara J, Pelletier J, Perket J, Rouholahnejad-Freund E, Wagener T, Zeng X, Beighley E, Buzan J, Huang M, Livneh B, Mohanty BP, Nijssen B, Safeeq M, Shen C, van Verseveld W, Volk J, Yamazaki D (2019) Hill-slope Hydrology in Global Change Research and Earth System Modeling. *Water Resources Research* 55(2):1737–1772, DOI 10.1029/2018WR023903
- Farr TG, Rosen PA, Caro E, Crippen R, Duren R, Hensley S, Kobrick M, Paller M, Rodriguez E, Roth L, Seal D, Shaffer S, Shimada J, Umland J, Werner M, Oskin M, Burbank D, Alsdorf DE (2007) The shuttle radar topography mission. *Reviews of Geophysics* DOI 10.1029/2005RG000183
- Fassoni-Andrade AC, Fleischmann AS, Papa F, de Paiva RCD, Wongchuig S, Melack JM, Moreira AA, Paris A, Ruhoff A, Barbosa C, Maciel DA, Novo E, Durand F, Frappart F, Aires F, Abrahão GM, Ferreira-Ferreira J, Espinoza JC, Laipelt L, Costa MH, Espinoza-Villar R, Calmant S, Pellet V (2021) Amazon Hydrology From Space: Scientific Advances and Future Challenges. *Reviews of Geophysics* DOI 10.1029/2020rg000728
- Fatras C, Parrens M, Peña Luque S, Al Bitar A (2021) Hydrological Dynamics of the Congo Basin From Water Surfaces Based on L-Band Microwave. *Water Resources Research* DOI 10.1029/2020WR027259
- Fekete BM, Looser U, Pietroniro A, Robarts RD (2012) Rationale for monitoring discharge on the ground. *Journal of Hydrometeorology* DOI 10.1175/JHM-D-11-0126.1
- Finney DL, Marsham JH, Jackson LS, Kendon EJ, Rowell DP, Boorman PM, Keane RJ, Stratton RA, Senior CA (2019) Implications of improved representation of convection for the East Africa water budget using a convection-permitting model. *Journal of Climate* DOI 10.1175/JCLI-D-18-0387.1
- Fleischmann A, Siqueira V, Paris A, Collischonn W, Paiva R, Pontes P, Crétaux JF, Bergé-Nguyen M, Biancamaria S, Gosset M, Calmant S, Tanimoun B (2018) Modelling hydrologic and hydrodynamic processes in basins with large semi-arid wetlands. *Journal of Hydrology* 561:943–959, DOI 10.1016/J.JHYDROL.2018.04.041
- Fleischmann A, Papa F, Fassoni-Andrade A, Melack JM, Wongchuig S, Paiva RCDD, Hamilton SK, Fluet-Chouinard E, Barbedo R, Aires F, Bitar AA, Bonnet MP, Coe M, Ferreira-Ferreira J,

- Hess L, Jensen K, McDonald K, Ovando A, Park E, Parrens M, Pinel S, Prigent C, Resende AF, Revel M, Rosenqvist A, Rosenqvist J, Rudorff C, Silva TSF, Yamazaki D, Collischonn W (2021a) How much inundation occurs in the Amazon River basin ? Remote Sensing of Environment DOI 10.1002/ESSOAR.10508718.1
- Fleischmann AS, Brêda JP, Passaia OA, Wongchuig SC, Fan FM, Paiva RC, Marques GF, Collischonn W (2021b) Regional scale hydrodynamic modeling of the river-floodplain-reservoir continuum. Journal of Hydrology DOI 10.1016/j.jhydrol.2021.126114
- Fluet-Chouinard E, Lehner B, Rebelo LM, Papa F, Hamilton SK (2015) Development of a global inundation map at high spatial resolution from topographic downscaling of coarse-scale remote sensing data. Remote Sensing of Environment DOI 10.1016/j.rse.2014.10.015
- Foulds L (1992) Graph theory applications / L. R. Foulds, 2nd edn. Universitext, Springer-Verlag, New York Berlin Heidelberg
- Fraser LH, Keddy PA (2005) The world's largest wetlands: Ecology and conservation. Cambridge University Press, DOI 10.1017/CBO9780511542091
- Garvine RW, Whitney MM (2006) An estuarine box model of freshwater delivery to the coastal ocean for use in climate models. Journal of Marine Research DOI 10.1357/002224006777606506
- Gentine P, Massmann A, Lintner BR, Hamed Alemohammad S, Fu R, Green JK, Kennedy D, Vilà-Guerau De Arellano J (2019) Land-atmosphere interactions in the tropics - A review. Hydrology and Earth System Sciences DOI 10.5194/hess-23-4171-2019
- Gerrits AM, Savenije HH, Veling EJ, Pfister L (2009) Analytical derivation of the Budyko curve based on rainfall characteristics and a simple evaporation model. Water Resources Research DOI 10.1029/2008WR007308
- Getirana A, Jung HC, Van Den Hoek J, Ndehedehe CE (2020) Hydropower dam operation strongly controls Lake Victoria's freshwater storage variability. Science of the Total Environment DOI 10.1016/j.scitotenv.2020.138343
- Getirana A, Kumar SV, Konapala G, Ndehedehe CE (2021) Impacts of Fully Coupling Land Surface and Flood Models on the Simulation of Large Wetlands' Water Dynamics: The Case of the Inner Niger Delta. Journal of Advances in Modeling Earth Systems DOI 10.1029/2021ms002463
- Gonçalves H, Mercante M, Santos E (2011) Hydrological cycle. Brazilian Journal of Biology 71(1 suppl 1):241–253, DOI 10.1590/S1519-69842011000200003
- Gond V, Bartholomé E, Ouattara F, Nonguierma A, Bado L (2004) Surveillance et cartographie des plans d'eau et des zones humides et inondables en régions arides avec l'instrument VEGETATION embarqué sur SPOT-4. International Journal of Remote Sensing DOI 10.1080/0143116031000139908

- Gong L, Halldin S, Xu CY (2011) Global-scale river routing-an efficient time-delay algorithm based on HydroSHEDS high-resolution hydrography. *Hydrological Processes* 25(7):1114–1128, DOI 10.1002/hyp.7795
- Gottgens JF, Perry JE, Fortney RH, Meyer JE, Benedict M, Rood BE (2001) The Paraguay-paraná Hidrovía: Protecting the pantanal with lessons from the past. DOI 10.1641/0006-3568(2001)051[0301:TPPHAP]2.0.CO;2
- Graham ST, Famiglietti JS, Maidment DR (1999) Five-minute, 1/2 °, and 1 ° data sets of continental watersheds and river networks for use in regional and global hydrologic and climate system modeling studies. *Water Resources Research* DOI 10.1029/1998WR900068
- Grell GA, Freitas SR (2014) A scale and aerosol aware stochastic convective parameterization for weather and air quality modeling. *Atmospheric Chemistry and Physics* DOI 10.5194/acp-14-5233-2014
- Greve P, Gudmundsson L, Orlowsky B, Seneviratne SI (2016) A two-parameter Budyko function to represent conditions under which evapotranspiration exceeds precipitation. *Hydrology and Earth System Sciences* DOI 10.5194/hess-20-2195-2016
- Guimberteau M, Drapeau G, Ronchail J, Sultan B, Polcher J, Martinez JM, Prigent C, Guyot JL, Cochonneau G, Espinoza JC, Filizola N, Fraizy P, Lavado W, De Oliveira E, Pombosa R, Noriega L, Vauchel P (2012a) Discharge simulation in the sub-basins of the Amazon using ORCHIDEE forced by new datasets. *Hydrology and Earth System Sciences* DOI 10.5194/hess-16-911-2012
- Guimberteau M, Drapeau G, Ronchail J, Sultan B, Polcher J, Martinez JM, Prigent C, Guyot JL, Cochonneau G, Espinoza JC, Filizola N, Fraizy P, Lavado W, De Oliveira E, Pombosa R, Noriega L, Vauchel P (2012b) Discharge simulation in the sub-basins of the Amazon using ORCHIDEE forced by new datasets. *Hydrology and Earth System Sciences* DOI 10.5194/hess-16-911-2012
- Guimberteau M, Ronchail J, Espinoza JC, Lengaigne M, Sultan B, Polcher J, Drapeau G, Guyot JL, Ducharne A, Ciais P (2013) Future changes in precipitation and impacts on extreme streamflow over Amazonian sub-basins. *Environmental Research Letters* DOI 10.1088/1748-9326/8/1/014035
- Gula J, Richard Peltier W (2012) Dynamical downscaling over the Great Lakes Basin of North America using the WRF regional climate model: The impact of the great lakes system on regional greenhouse warming. *Journal of Climate* DOI 10.1175/JCLI-D-11-00388.1
- Haddeland I, Clark DB, Franssen W, Ludwig F, Voß F, Arnell NW, Bertrand N, Best M, Folwell S, Gerten D, Gomes S, Gosling SN, Hagemann S, Hanasaki N, Harding R, Heinke J, Kabat P, Koirala S, Oki T, Polcher J, Stacke T, Viterbo P, Weedon GP, Yeh P (2011) Multimodel estimate of the global terrestrial water balance: Setup and first results. *Journal of Hydrometeorology* 12(5):869–884, DOI 10.1175/2011JHM1324.1

- Hamilton SK (1999) Potential effects of a major navigation project (Paraguay–Paraná Hidrovía) on inundation in the Pantanal floodplains. *Regulated Rivers: Research and Management* 15(4):289–299, DOI 10.1002/(SICI)1099-1646(199907/08)15:4<289::AID-RRR520>3.0.CO;2-I
- Hamilton SK (2002) HYDROLOGICAL CONTROLS OF ECOLOGICAL STRUCTURE AND FUNCTION IN THE PANTANAL WETLAND (BRAZIL). IAHS Special Publication The Ecohydrology of South American Rivers and Wetlands
- Hamilton SK, Sippel SJ, Melack J (1996) Inundation patterns in the Pantanal Wetland of South America determined from passive microwave remote sensing. *Archiv für Hydrobiologie*
- Hamilton SK, Sippel SJ, Melack JM (2002) Comparison of inundation patterns among major South American floodplains. *Journal of Geophysical Research Atmospheres* DOI 10.1029/2000JD000306
- Hamilton SK, Sippel SJ, Melack JM (2004) Seasonal inundation patterns in two large savanna floodplains of South America: The Llanos de Moxos (Bolivia) and the Llanos del Orinoco (Venezuela and Colombia). *Hydrological Processes* DOI 10.1002/hyp.5559
- Hannah DM, Demuth S, van Lanen HA, Looser U, Prudhomme C, Rees G, Stahl K, Tallaksen LM (2011) Large-scale river flow archives: Importance, current status and future needs. *Hydrological Processes* DOI 10.1002/hyp.7794
- Hao Z, Yuan X, Xia Y, Hao F, Singh VP (2017) An overview of drought monitoring and prediction systems at regional and global scales. *Bulletin of the American Meteorological Society* DOI 10.1175/BAMS-D-15-00149.1
- Harding R, Best M, Blyth E, Hagemann S, Kabat P, Tallaksen LM, Warnaars T, Wiberg D, Weedon GP, van Lanen H, Ludwig F, Haddeland I (2011) WATCH: Current Knowledge of the Terrestrial Global Water Cycle. *Journal of Hydrometeorology* DOI 10.1175/jhm-d-11-024.1
- Harris I, Jones PD, Osborn TJ, Lister DH (2014) Updated high-resolution grids of monthly climatic observations - the CRU TS3.10 Dataset. *International Journal of Climatology* DOI 10.1002/joc.3711
- Harrison JA, Caraco N, Seitzinger SP (2005) Global patterns and sources of dissolved organic matter export to the coastal zone: Results from a spatially explicit, global model. *Global Biogeochemical Cycles* DOI 10.1029/2005GB002480
- Haylock MR, Peterson TC, Alves LM, Ambrizzi T, Anunciação YM, Baez J, Barros VR, Berlato MA, Bidegain M, Coronel G, Corradi V, Garcia VJ, Grimm AM, Karoly D, Marengo JA, Marino MB, Moncunill DF, Nechet D, Quintana J, Rebello E, Rusticucci M, Santos JL, Trebejo I, Vincent LA (2006) Trends in total and extreme South American rainfall in 1960–2000 and links with sea surface temperature. *Journal of Climate* DOI 10.1175/JCLI3695.1
- Haylock MR, Hofstra N, Klein Tank AMG, Klok EJ, Jones PD, New M (2008) A European daily high-resolution gridded data set of surface temperature and precipitation for 1950–2006. *Journal of Geophysical Research* 113(D20):D20,119, DOI 10.1029/2008JD010201

- Hordoir R, Polcher J, Brun-Cottan JC, Madec G (2008) Towards a parametrization of river discharges into ocean general circulation models: A closure through energy conservation. *Climate Dynamics* 31(7-8):891–908, DOI 10.1007/S00382-008-0416-4/TABLES/2
- Huang B, Mehta VM (2010) Influences of freshwater from major rivers on global ocean circulation and temperatures in the MIT ocean general circulation model. *Advances in Atmospheric Sciences* 27(3):455–468, DOI 10.1007/s00376-009-9022-6
- Inglada J, Vincent A, Arias M, Marais-Sicre C (2016) Improved early crop type identification by joint use of high temporal resolution sar and optical image time series. *Remote Sensing* DOI 10.3390/rs8050362
- IPCC (2019) IPCC SR: Climate Change and Land. An IPCC Special Report on climate change, desertification, land degradation, sustainable land management, food security, and greenhouse gas fluxes in terrestrial ecosystems
- IPCC AR6 WGI (2021) Chp. 12: Climate change information for regional impact and for risk assessment. In: *Climate Change 2021: The Physical Science Basis. Contribution of Working Group I to the Sixth Assessment Report of the Intergovernmental Panel on Climate Change*, Cambridge University Press, chap Chapter 12
- Johnson RH, Mapes BE (2001) *Mesoscale Processes and Severe Convective Weather*. Meteorological Monographs DOI 10.1175/0065-9401-28.50.71
- Jolliffe IT, Cadima J (2016) Principal component analysis: A review and recent developments. DOI 10.1098/rsta.2015.0202
- Jones PD, Lister DH, Harpham C, Rusticucci M, Penalba O (2013) Construction of a daily precipitation grid for southeastern South America for the period 1961-2000. *International Journal of Climatology* DOI 10.1002/joc.3605
- Jönsson P, Eklundh L (2004) TIMESAT - A program for analyzing time-series of satellite sensor data. *Computers and Geosciences* DOI 10.1016/j.cageo.2004.05.006
- Jung HC, Hamski J, Durand M, Alsdorf D, Hossain F, Lee H, Azad Hossain AK, Hasan K, Khan AS, Zeaul Hoque AK (2010) Characterization of complex fluvial systems using remote sensing of spatial and temporal water level variations in the Amazon, Congo, and Brahmaputra rivers. *Earth Surface Processes and Landforms* DOI 10.1002/esp.1914
- Junk WJ, Furch K (1993) A general review of tropical South American floodplains. *Wetlands Ecology and Management* DOI 10.1007/BF00188157
- Junk WJ, Piedade MTF (2005) The Amazon River basin. *The World's Largest Wetlands: Ecology and Conservation* pp 63–117, DOI 10.1017/CBO9780511542091.004
- Junk WJ, Bayley PB, Sparks RE (1989) The flood pulse concept in river-floodplain systems. D P Dodge [ed] *Proceedings of the International Large River Symposium Can Spec Publ Fish Aquat Sci* 106(Proceedings of the International Large River Symposium.):p. 110–127

- Junk WJ, Da Cunha CN, Wantzen KM, Petermann P, Strüssmann C, Marques MI, Adis J (2006) Biodiversity and its conservation in the Pantanal of Mato Grosso, Brazil. In: *Aquatic Sciences*, DOI 10.1007/s00027-006-0851-4
- Junk WJ, Piedade MTF, Schöngart J, Cohn-Haft M, Adeney JM, Wittmann F (2011) A classification of major naturally-occurring amazonian lowland wetlands. *Wetlands* DOI 10.1007/s13157-011-0190-7
- Kauffeldt A, Wetterhall F, Pappenberger F, Salamon P, Thielen J (2016) Technical review of large-scale hydrological models for implementation in operational flood forecasting schemes on continental level. DOI 10.1016/j.envsoft.2015.09.009
- Kayranli B, Scholz M, Mustafa A, Hedmark Å (2010) Carbon storage and fluxes within freshwater wetlands: A critical review. *Wetlands* DOI 10.1007/s13157-009-0003-4
- Kim H (2017) Global Soil Wetness Project Phase 3 Atmospheric Boundary Conditions (Experiment 1) [Data set]. Data Integration and Analysis System (DIAS) DOI <https://doi.org/10.20783/DIAS.501>
- Kirschke S, Bousquet P, Ciais P, Saunois M, Canadell JG, Dlugokencky EJ, Bergamaschi P, Bergmann D, Blake DR, Bruhwiler L, Cameron-Smith P, Castaldi S, Chevallier F, Feng L, Fraser A, Heimann M, Hodson EL, Houweling S, Josse B, Fraser PJ, Krummel PB, Lamarque JF, Langenfelds RL, Le Quéré C, Naik V, O'doherty S, Palmer PI, Pison I, Plummer D, Poulter B, Prinn RG, Rigby M, Ringeval B, Santini M, Schmidt M, Shindell DT, Simpson IJ, Spahni R, Steele LP, Strode SA, Sudo K, Szopa S, Van Der Werf GR, Voulgarakis A, Van Weele M, Weiss RF, Williams JE, Zeng G (2013) Three decades of global methane sources and sinks. DOI 10.1038/ngeo1955
- Knist S, Goergen K, Buonomo E, Christensen OB, Colette A, Cardoso RM, Fealy R, Fernández J, García-Díez M, Jacob D, Kartsios S, Katragkou E, Keuler K, Mayer S, Van Meijgaard E, Nikulin G, Soares PM, Sobolowski S, Szepszo G, Teichmann C, Vautard R, Warrach-Sagi K, Wulfmeyer V, Simmer C (2017) Land-atmosphere coupling in EURO-CORDEX evaluation experiments. *Journal of Geophysical Research* DOI 10.1002/2016JD025476
- Kohler M, Kalthoff N, Kottmeier C (2010) The impact of soil moisture modifications on CBL characteristics in West Africa: A case-study from the AMMA campaign. *Quarterly Journal of the Royal Meteorological Society* DOI 10.1002/qj.430
- Koster RD, Dirmeyer PA, Guo Z, Bonan G, Chan E, Cox P, Gordon CT, Kanae S, Kowalczyk E, Lawrence D, Liu P, Lu CH, Malyshev S, McAvaney B, Mitchell K, Mocko D, Oki T, Oleson K, Pitman A, Sud YC, Taylor CM, Verseghy D, Vasic R, Xue Y, Yamada T (2004) Regions of strong coupling between soil moisture and precipitation. *Science* DOI 10.1126/science.1100217
- Koster RD, Guo Z, Dirmeyer PA, Bonan G, Chan E, Cox P, Davies H, Gordon CT, Kanae S, Kowalczyk E, Lawrence D, Liu P, Lu CH, Malyshev S, McAvaney B, Mitchell K, Mocko D, Oki T, Oleson KW, Pitman A, Sud YC, Taylor CM, Verseghy D, Vasic R, Xue Y, Yamada T

- (2006) GLACE: The Global Land-Atmosphere Coupling Experiment. Part I: Overview. DOI 10.1175/JHM510.1
- Koster RD, Chang Y, Wang H, Schubert SD (2016) Impacts of local soil moisture anomalies on the atmospheric circulation and on remote surface meteorological fields during boreal summer: A comprehensive analysis over North America. *Journal of Climate* DOI 10.1175/JCLI-D-16-0192.1
- Krinner G (2003) Impact of lakes and wetlands on boreal climate. *Journal of Geophysical Research: Atmospheres* DOI 10.1029/2002jd002597
- Krinner G, Viovy N, de Noblet-Ducoudré N, Ogée J, Polcher J, Friedlingstein P, Ciais P, Sitch S, Prentice IC (2005) A dynamic global vegetation model for studies of the coupled atmosphere-biosphere system. DOI 10.1029/2003GB002199
- Kumar S, Newman M, Lawrence DM, Lo MH, Akula S, Lan CW, Livneh B, Lombardozzi D (2020) The GLACE-Hydrology Experiment: Effects of Land-Atmosphere Coupling on Soil Moisture Variability and Predictability. *Journal of Climate* DOI 10.1175/JCLI-D-19-0598.1
- Kumar SV, Peters-Lidard CD, Tian Y, Houser PR, Geiger J, Olden S, Lighty L, Eastman JL, Doty B, Dirmeyer P, Adams J, Mitchell K, Wood EF, Sheffield J (2006) Land information system: An interoperable framework for high resolution land surface modeling. *Environmental Modelling and Software* DOI 10.1016/j.envsoft.2005.07.004
- Kuppel S, Houspanossian J, Noretto MD, Jobbágy EG (2015) What does it take to flood the Pampas?: Lessons from a decade of strong hydrological fluctuations. *Water Resources Research* DOI 10.1002/2015WR016966
- Lauerwald R, Regnier P, Camino-Serrano M, Guenet B, Guimberteau M, Ducharne A, Polcher J, Ciais P (2017) ORCHILEAK (revision 3875): a new model branch to simulate carbon transfers along the terrestrial-aquatic continuum of the Amazon basin. *Geoscientific Model Development* 10(10):3821–3859, DOI 10.5194/gmd-10-3821-2017
- Lauwaet D, van Lipzig NPM, Van Weverberg K, De Ridder K, Goyens C (2012) The precipitation response to the desiccation of Lake Chad. *Quarterly Journal of the Royal Meteorological Society* DOI 10.1002/qj.942
- Le Quéré C, Peters GP, Andres RJ, Andrew RM, Boden TA, Ciais P, Friedlingstein P, Houghton RA, Marland G, Moriarty R, Sitch S, Tans P, Arneeth A, Arvanitis A, Bakker DC, Bopp L, Canadell JG, Chini LP, Doney SC, Harper A, Harris I, House JI, Jain AK, Jones SD, Kato E, Keeling RF, Klein Goldewijk K, Körtzinger A, Koven C, Lefèvre N, Maignan F, Omar A, Ono T, Park GH, Pfiel B, Poulter B, Raupach MR, Regnier P, Rödenbeck C, Saito S, Schwinger J, Segschneider J, Stocker BD, Takahashi T, Tilbrook B, Van Heuven S, Viovy N, Wanninkhof R, Wiltshire A, Zaehle S (2014) Global carbon budget 2013. *Earth System Science Data* DOI 10.5194/essd-6-235-2014
- Leady BS, Gottgens JF (2001) Mercury accumulation in sediment cores and along food chains in two regions of the Brazilian Pantanal. *Wetlands Ecology and Management* DOI 10.1023/A:1011856517552

- Lebel T, Cappelaere B, Galle S, Hanan N, Kergoat L, Levis S, Vieux B, Descroix L, Gosset M, Mougin E, Peugeot C, Seguis L (2009) AMMA-CATCH studies in the Sahelian region of West-Africa: An overview. *Journal of Hydrology* DOI 10.1016/j.jhydrol.2009.03.020
- Lee H, Beighley RE, Alsdorf D, Jung HC, Shum CK, Duan J, Guo J, Yamazaki D, Andreadis K (2011) Characterization of terrestrial water dynamics in the Congo Basin using GRACE and satellite radar altimetry. *Remote Sensing of Environment* DOI 10.1016/j.rse.2011.08.015
- Lehner B, Verdin K, Jarvis A (2008) New global hydrography derived from spaceborne elevation data. *Eos* DOI 10.1029/2008EO100001
- Li L, Hao ZC, Wang JH, Wang ZH, Yu ZB (2008) Impact of Future Climate Change on Runoff in the Head Region of the Yellow River. *Journal of Hydrologic Engineering* DOI 10.1061/(asce)1084-0699(2008)13:5(347)
- Li X, Jiang F, Li L, Wang G (2011) Spatial and temporal variability of precipitation concentration index, concentration degree and concentration period Xinjiang, China. *International Journal of Climatology* DOI 10.1002/joc.2181
- Liebmann B, Allured D (2005) Daily precipitation grids for South America. *Bulletin of the American Meteorological Society* 86(11):1567–1570, DOI 10.1175/BAMS-86-11-1567
- Lin P, Pan M, Beck HE, Yang Y, Yamazaki D, Frasson R, David CH, Durand M, Pavel-sky TM, Allen GH, Gleason CJ, Wood EF (2019) Global Reconstruction of Naturalized River Flows at 2.94 Million Reaches. *Water Resources Research* 55(8):6499–6516, DOI 10.1029/2019WR025287
- Lloyd SP (1982) Least Squares Quantization in PCM. *IEEE Transactions on Information Theory* DOI 10.1109/TIT.1982.1056489
- Louzada RO, Bergier I, Assine ML (2020) Landscape changes in avulsive river systems: Case study of Taquari River on Brazilian Pantanal wetlands. *Science of the Total Environment* DOI 10.1016/j.scitotenv.2020.138067
- Lucas-Picher P, Laprise R, Winger K (2017) Evidence of added value in North American regional climate model hindcast simulations using ever-increasing horizontal resolutions. *Climate Dynamics* DOI 10.1007/s00382-016-3227-z
- Madec G, the NEMO Team (2016) NEMO ocean engine. Note du Pôle de modélisation
- Marengo JA, Liebmann B, Grimm AM, Misra V, Silva Dias PL, Cavalcanti IF, Carvalho LM, Berbery EH, Ambrizzi T, Vera CS, Saulo AC, Nogues-Paegle J, Zipser E, Seth A, Alves LM (2012) Recent developments on the South American monsoon system. DOI 10.1002/joc.2254
- Marengo JA, Oliveira GS, Alves LM (2016) Climate change scenarios in the Pantanal. In: *Dynamics of the Pantanal Wetland in South America*, Springer, DOI 10.1007/698_2015_357

- Marthews TR, Dadson S, Clark D, Blyth E, Hayman G, Yamazaki D, Becher O, Martínez-de la Torre A, Prigent C, Jiménez C (2021) Inundation prediction in tropical wetlands from JULES-CaMa-Flood global land surface simulations. *Hydrology and Earth System Sciences Discussions* pp 1–31, DOI 10.5194/hess-2021-109
- Martinez JA, Dominguez F (2014) Sources of Atmospheric Moisture for the La Plata River Basin*. *Journal of Climate* DOI 10.1175/JCLI-D-14-00022.s1
- Martínez-Espinosa C, Sauvage S, Al Bitar A, Green PA, Vörösmarty CJ, Sánchez-Pérez JM (2021) Denitrification in wetlands: A review towards a quantification at global scale. DOI 10.1016/j.scitotenv.2020.142398
- Martins R, Sá L, Moraes O (2013) Low Level Jets in the Pantanal Wetland Nocturnal Boundary Layer – Case Studies. *American Journal of Environmental Engineering* DOI 10.5923/j.ajee.20130301.06
- Masson S, Delecluse P (2001) Influence of the Amazon river runoff on the tropical atlantic. *Physics and Chemistry of the Earth, Part B: Hydrology, Oceans and Atmosphere* 26(2):137–142, DOI 10.1016/S1464-1909(00)00230-6
- Melton JR, Wania R, Hodson EL, Poulter B, Ringeval B, Spahni R, Bohn T, Avis CA, Beerling DJ, Chen G, Eliseev AV, Denisov SN, Hopcroft PO, Lettenmaier DP, Riley WJ, Singarayer JS, Subin ZM, Tian H, Zürcher S, Brovkin V, Van Bodegom PM, Kleinen T, Yu ZC, Kaplan JO (2013) Present state of global wetland extent and wetland methane modelling: Conclusions from a model inter-comparison project (WETCHIMP). *Biogeosciences* DOI 10.5194/bg-10-753-2013
- Menéndez CG, Giles J, Ruscica R, Zaninelli P, Coronato T, Falco M, Sörensson A, Fita L, Carril A, Li L (2019) Temperature variability and soil–atmosphere interaction in South America simulated by two regional climate models. *Climate Dynamics* DOI 10.1007/s00382-019-04668-6
- Mianabadi A, Coenders-Gerrits M, Shirazi P, Ghahraman B, Alizadeh A (2019) A global Budyko model to partition evaporation into interception and transpiration. *Hydrology and Earth System Sciences* DOI 10.5194/hess-23-4983-2019
- Minotti PG (2018) The parana-paraguay fluvial corridor (Argentina). In: *The Wetland Book II: Distribution, Description, and Conservation*, Springer, DOI 10.1007/978-94-007-4001-3_242
- Mishra V, Cherkauer KA, Bowling LC (2010) Parameterization of lakes and wetlands for energy and water balance studies in the great lakes region. *Journal of Hydrometeorology* DOI 10.1175/2010JHM1207.1
- Mitchell TD, Jones PD (2005) An improved method of constructing a database of monthly climate observations and associated high-resolution grids. *International Journal of Climatology* DOI 10.1002/joc.1181
- Mitsch WJ, Nahlik A, Wolski P, Bernal B, Zhang L, Ramberg L (2010) Tropical wetlands: Seasonal hydrologic pulsing, carbon sequestration, and methane emissions. *Wetlands Ecology and Management* DOI 10.1007/s11273-009-9164-4

- Mitsch WJ, Bernal B, Nahlik AM, Mander Ü, Zhang L, Anderson CJ, Jørgensen SE, Brix H (2013) Wetlands, carbon, and climate change. *Landscape Ecology* DOI 10.1007/s10980-012-9758-8
- Mitsch, William J, Gosselink JG (2015) *Wetlands Fifth Edition*. Wiley, [arXiv:1011.1669v3](https://arxiv.org/abs/1011.1669v3)
- Montini TL, Jones C, Carvalho LMV (2019) The South American Low-Level Jet: A New Climatology, Variability, and Changes. *Journal of Geophysical Research: Atmospheres* 124(3):1200–1218, DOI 10.1029/2018JD029634
- Moriasi DN, Arnold JG, Van Liew MW, Bingner RL, Harmel RD, Veith TL (2007) Model Evaluation Guidelines for Systematic Quantification of Accuracy in Watershed Simulations. *Transactions of the ASABE* 50(3):885–900, DOI 10.13031/2013.23153
- Morrison H, Thompson G, Tatarskii V (2009) Impact of cloud microphysics on the development of trailing stratiform precipitation in a simulated squall line: Comparison of one- and two-moment schemes. *Monthly Weather Review* DOI 10.1175/2008MWR2556.1
- Nakanishi M, Niino H (2009) Development of an improved turbulence closure model for the atmospheric boundary layer. *Journal of the Meteorological Society of Japan* DOI 10.2151/jmsj.87.895
- Nakhavali M, Friedlingstein P, Lauerwald R, Tang J, Chadburn S, Camino-Serrano M, Guenet B, Harper A, Walmsley D, Peichl M, Gielen B (2018) Representation of dissolved organic carbon in the JULES land surface model (vn4.4-JULES-DOCM). *Geoscientific Model Development* 11(2):593–609, DOI 10.5194/gmd-11-593-2018
- Nardi F, Annis A, Baldassarre GD, Vivoni ER, Grimaldi S (2019) GFPLAIN250m, a global high-resolution dataset of earth's floodplains. *Scientific Data* DOI 10.1038/sdata.2018.309
- Neiff J (1996) Large rivers of South America: toward the new approach. *SIL Proceedings, 1922-2010* DOI 10.1080/03680770.1995.11900701
- Neiff JJ, Poi de Neiff ASG, Casco SL (2005) Importancia ecológica del Corredor Fluvial Paraguay-Paraná como contexto del manejo sostenible. *Humedales fluviales de América del Sur*
- Neiff J (1999) El régimen de pulsos en ríos y grandes humedales de Sudamérica. *Centro de ecología aplicada del litoral (CECOAI)*
- New M, Hulme M, Jones P (1999) Representing twentieth-century space-time climate variability. Part I: Development of a 1961-90 mean monthly terrestrial climatology. *Journal of Climate*
- New M, Hulme M, Jones P (2000) Representing twentieth-century space-time climate variability. Part II: Development of 1901-96 monthly grids of terrestrial surface climate. *Journal of Climate* DOI 10.1175/1520-0442(2000)013<2217:RTCSTC>2.0.CO;2
- Ngo-Duc T, Polcher J, Laval K (2005) A 53-year forcing data set for land surface models. *Journal of Geophysical Research: Atmospheres* 110(D6):1–13, DOI 10.1029/2004JD005434

- Ngo-Duc T, Oki T, Kanae S (2007) A variable streamflow velocity method for global river routing model: model description and preliminary results. *Hydrology and Earth System Sciences Discussions* DOI 10.5194/hessd-4-4389-2007
- Nguyen-Quang T, Polcher J, Ducharne A, Arsouze T, Zhou X, Schneider A, Fita L (2018a) ORCHIDEE-ROUTING: revising the river routing scheme using a high-resolution hydrological database. *Geoscientific Model Development* 11(12):4965–4985, DOI 10.5194/gmd-11-4965-2018
- Nguyen-Quang T, Polcher J, Ducharne A, Arsouze T, Zhou X, Schneider A, Fita L (2018b) ORCHIDEE-ROUTING: revising the river routing scheme using a high-resolution hydrological database. *Geoscientific Model Development* 11(12):4965–4985, DOI 10.5194/gmd-11-4965-2018
- Nguyen-Quang T, Polcher J, Ducharne A, Arsouze T, Zhou X, Schneider A, Fita L (2018c) ORCHIDEE-ROUTING: Revising the river routing scheme using a high-resolution hydrological database. *Geoscientific Model Development* DOI 10.5194/gmd-11-4965-2018
- Niedermeier A, Hoja D, Lehner S (2005) Topography and morphodynamics in the German Bight using SAR and optical remote sensing data. *Ocean Dynamics* DOI 10.1007/s10236-005-0114-2
- Nobre AD, Cuartas LA, Hodnett M, Rennó CD, Rodrigues G, Silveira A, Waterloo M, Saleska S (2011) Height Above the Nearest Drainage - a hydrologically relevant new terrain model. *Journal of Hydrology* DOI 10.1016/j.jhydrol.2011.03.051
- Notaro M, Bennington V, Vavrus S (2015) Dynamically downscaled projections of lake-effect snow in the Great Lakes basin. *Journal of Climate* DOI 10.1175/JCLI-D-14-00467.1
- Ogilvie A, Belaud G, Delenne C, Bailly JS, Bader JC, Oleksiak A, Ferry L, Martin D (2015a) Decadal monitoring of the Niger Inner Delta flood dynamics using MODIS optical data. *Journal of Hydrology* DOI 10.1016/j.jhydrol.2015.01.036
- Ogilvie A, Belaud G, Delenne C, Bailly JS, Bader JC, Oleksiak A, Ferry L, Martin D (2015b) Decadal monitoring of the Niger Inner Delta flood dynamics using MODIS optical data. *Journal of Hydrology* DOI 10.1016/j.jhydrol.2015.01.036
- Oki T, Kanae S (2006) Global hydrological cycles and world water resources. DOI 10.1126/science.1128845
- Oki T, Sud YC (1998) Design of Total Runoff Integrating Pathways (TRIP)—A Global River Channel Network. *Earth Interactions* DOI 10.1175/1087-3562(1998)002<0001:dotrip>2.0.co;2
- Olson J, Watts J, Allison L (1985) Major world ecosystem complexes ranked by carbon in live vegetation: A database. *Sciences*-New York
- Omrani H, Drobinski P, Dubos T (2015) Using nudging to improve global-regional dynamic consistency in limited-area climate modeling: What should we nudge? *Climate Dynamics* DOI 10.1007/s00382-014-2453-5

- Padovani (2010) Dinâmica Espaço-Temporal das Inundações do Pantanal. PhD thesis, Piracicaba: Escola Superior de Agricultura Luiz de Queiroz, Centro de Energia Nuclear na Agricultura, Universidade de São Paulo, URL <http://www.teses.usp.br/teses/disponiveis/91/91131/tde-14022011-170515/pt-br.php>
- Paiva RC, Collischonn W, Tucci CE (2011) Large scale hydrologic and hydrodynamic modeling using limited data and a GIS based approach. *Journal of Hydrology* DOI 10.1016/j.jhydrol.2011.06.007
- Pappenberger F, Cloke HL, Balsamo G, Ngo-Duc T, Oki T (2010) Global runoff routing with the hydrological component of the ECMWF NWP system. *International Journal of Climatology* DOI 10.1002/joc.2028
- da Paz AR, Bravo JM, Allasia D, Collischonn W, Tucci CEM (2010) Large-scale hydrodynamic modeling of a complex river network and floodplains. *Journal of Hydrologic Engineering* DOI 10.1061/(ASCE)HE.1943-5584.0000162
- da Paz AR, Collischonn W, Tucci CEM, Padovani CR (2011) Large-scale modelling of channel flow and floodplain inundation dynamics and its application to the Pantanal (Brazil). *Hydrological Processes* DOI 10.1002/hyp.7926
- da Paz AR, Collischonn W, Bravo JM, Bates PD, Baugh C (2014) The influence of vertical water balance on modelling Pantanal (Brazil) spatio-temporal inundation dynamics. *Hydrological Processes* DOI 10.1002/hyp.9897
- Peel MC, Finlayson BL, McMahon TA (2007) Updated world map of the Köppen-Geiger climate classification. *Hydrology and Earth System Sciences* DOI 10.5194/hess-11-1633-2007
- Pekel JF, Cottam A, Gorelick N, Belward AS (2016) High-resolution mapping of global surface water and its long-term changes. *Nature* DOI 10.1038/nature20584
- Penatti NC, de Almeida TIR, Ferreira LG, Arantes AE, Coe MT (2015) Satellite-based hydrological dynamics of the world's largest continuous wetland. *Remote Sensing of Environment* DOI 10.1016/j.rse.2015.08.031
- Peng Y, Xiao Y, Fu Z, Dong Y, Zheng Y, Yan H, Li X (2019) Precision irrigation perspectives on the sustainable water-saving of field crop production in China: Water demand prediction and irrigation scheme optimization. *Journal of Cleaner Production* DOI 10.1016/j.jclepro.2019.04.347
- Polcher J (2003) Les processus de surface à l'échelle globale et leurs interactions avec l'atmosphère. PhD thesis, Habilitation à diriger des recherches. Université Paris VI
- Polcher J, McAvaney B, Viterbo P, Gaertner MA, Hahmann A, Mahfouf JF, Noilhan J, Phillips T, Pitman A, Schlosser CA, Schulz JP, Timbal B, Verseghy D, Xue Y (1998) A proposal for a general interface between land surface schemes and general circulation models. *Global and Planetary Change* DOI 10.1016/S0921-8181(98)00052-6

- Pontes PRM, Fan FM, Fleischmann AS, de Paiva RCD, Buarque DC, Siqueira VA, Jardim PF, Sorribas MV, Collischonn W (2017) MGB-IPH model for hydrological and hydraulic simulation of large floodplain river systems coupled with open source GIS. *Environmental Modelling and Software* 94:1–20, DOI 10.1016/j.envsoft.2017.03.029
- Powers JG, Klemp JB, Skamarock WC, Davis CA, Dudhia J, Gill DO, Coen JL, Gochis DJ, Ahmadov R, Peckham SE, Grell GA, Michalakes J, Trahan S, Benjamin SG, Alexander CR, Dimego GJ, Wang W, Schwartz CS, Romine GS, Liu Z, Snyder C, Chen F, Barlage MJ, Yu W, Duda MG (2017) The weather research and forecasting model: Overview, system efforts, and future directions. *Bulletin of the American Meteorological Society* DOI 10.1175/BAMS-D-15-00308.1
- Prigent C, Jimenez C, Bousquet P (2020) Satellite-Derived Global Surface Water Extent and Dynamics Over the Last 25 Years (GIEMS-2). *Journal of Geophysical Research: Atmospheres* DOI 10.1029/2019JD030711
- Redelsperger JL, Thorncroft CD, Diedhiou A, Lebel T, Parker DJ, Polcher J (2006) African Monsoon Multidisciplinary Analysis: An international research project and field campaign. *Bulletin of the American Meteorological Society* DOI 10.1175/BAMS-87-12-1739
- Regnier P, Friedlingstein P, Ciais P, Mackenzie FT, Gruber N, Janssens IA, Laruelle GG, Lauerwald R, Luysaert S, Andersson AJ, Arndt S, Arnosti C, Borges AV, Dale AW, Gallego-Sala A, Godd eris Y, Goossens N, Hartmann J, Heinze C, Ilyina T, Joos F, Larowe DE, Leifeld J, Meysman FJ, Munhoven G, Raymond PA, Spahni R, Suntharalingam P, Thullner M (2013) Anthropogenic perturbation of the carbon fluxes from land to ocean. *Nature Geoscience* 6(8):597–607, DOI 10.1038/ngeo1830
- Reynolds CA, Jackson TJ, Rawls WJ (2000) Estimating soil water-holding capacities by linking the Food and Agriculture Organization soil map of the world with global pedon databases and continuous pedotransfer functions. *Water Resources Research* DOI 10.1029/2000WR900130
- Ringeval B, De Noblet-Ducoudr e N, Ciais P, Bousquet P, Prigent C, Papa F, Rossow WB (2010) An attempt to quantify the impact of changes in wetland extent on methane emissions on the seasonal and interannual time scales. *Global Biogeochemical Cycles* DOI 10.1029/2008GB003354
- Rochetin N, Couvreur F, Guichard F (2017) Morphology of breeze circulations induced by surface flux heterogeneities and their impact on convection initiation. *Quarterly Journal of the Royal Meteorological Society* DOI 10.1002/qj.2935
- Rodell M, Beaudoin HK, L'Ecuyer TS, Olson WS, Famiglietti JS, Houser PR, Adler R, Bosilovich MG, Clayson CA, Chambers D, Clark E, Fetzer EJ, Gao X, Gu G, Hilburn K, Huffman GJ, Lettenmaier DP, Liu WT, Robertson FR, Schlosser CA, Sheffield J, Wood EF (2015a) The observed state of the water cycle in the early twenty-first century. *Journal of Climate* DOI 10.1175/JCLI-D-14-00555.1
- Rodell M, Beaudoin HK, L'Ecuyer TS, Olson WS, Famiglietti JS, Houser PR, Adler R, Bosilovich MG, Clayson CA, Chambers D, Clark E, Fetzer EJ, Gao X, Gu G, Hilburn K,

- Huffman GJ, Lettenmaier DP, Liu WT, Robertson FR, Schlosser CA, Sheffield J, Wood EF (2015b) The observed state of the water cycle in the early twenty-first century. *Journal of Climate* DOI 10.1175/JCLI-D-14-00555.1
- de Rosnay P, Polcher J, Bruen M, Laval K (2002) Impact of a physically based soil water flow and soil-plant interaction representation for modeling large-scale land surface processes. *Journal of Geophysical Research: Atmospheres* DOI 10.1029/2001jd000634
- Rouse W, Haas RH, Deering DW (1974) Monitoring vegetation systems in the Great Plains with ERTS, NASA SP-351. Third ERTS-1 Symposium, Vol 1
- Ruscica RC, Sörensson AA, Menéndez CG (2014) Hydrological links in Southeastern South America: soil moisture memory and coupling within a hot spot. *International Journal of Climatology* 34(14):3641–3653, DOI 10.1002/JOC.3930
- Ruscica RC, Sörensson AA, Menéndez CG (2015) Pathways between soil moisture and precipitation in southeastern South America. *Atmospheric Science Letters* DOI 10.1002/asl2.552
- Ruscica RC, Menéndez CG, Sörensson AA (2016) Land surface-atmosphere interaction in future South American climate using a multi-model ensemble. *Atmospheric Science Letters* DOI 10.1002/asl.635
- Salio P, Nicolini M, Zipser EJ (2007) Mesoscale Convective Systems over Southeastern South America and Their Relationship with the South American Low-Level Jet. *Monthly Weather Review* DOI 10.1175/mwr3305.1
- Schamm K, Ziese M, Becker A, Finger P, Meyer-Christoffer A, Schneider U, Schröder M, Stender P (2014) Global gridded precipitation over land: a description of the new GPCP First Guess Daily product. *Earth System Science Data* 6(1):49–60, DOI 10.5194/essd-6-49-2014
- Schlenker W, Hanemann WM, Fisher AC (2007) Water availability, degree days, and the potential impact of climate change on irrigated agriculture in California. *Climatic Change* DOI 10.1007/s10584-005-9008-z
- Schlesinger WH, Bernhardt ES (2013) *Biogeochemistry: An Analysis of Global Change*, Third Edition. *Biogeochemistry: An Analysis of Global Change*, Third Edition pp 1–672
- Schmidt R, Flechtner F, Meyer U, Neumayer KH, Dahle C, König R, Kusche J (2008) Hydrological signals observed by the GRACE satellites. DOI 10.1007/s10712-008-9033-3
- Schneider U, Finger P, Meyer-Christoffer A, Rustemeier E, Ziese M, Becker A (2017) Evaluating the Hydrological Cycle over Land Using the Newly-Corrected Precipitation Climatology from the Global Precipitation Climatology Centre (GPCP). *Atmosphere* 8(12):52, DOI 10.3390/atmos8030052
- Schrapfner A, Sörensson A, Polcher J, Fita L (2020) Benefits of representing floodplains in a Land Surface Model: Pantanal simulated with ORCHIDEE CMIP6 version. *Climate Dynamics* DOI 10.1007/s00382-020-05324-0

- Schubert SD, Suarez MJ, Pegion PJ, Koster RD, Bacmeister JT (2008) Potential predictability of long-term drought and pluvial conditions in the U.S. Great Plains. *Journal of Climate* DOI 10.1175/2007JCLI1741.1
- Seneviratne SI, Stöckli R (2008) "The Role of Land–Atmosphere Interactions for Climate Variability in Europe" *Climate Variability and Extremes during the Past 100 years*. Springer
- Seneviratne SI, Corti T, Davin EL, Hirschi M, Jaeger EB, Lehner I, Orlowsky B, Teuling AJ (2010a) Investigating soil moisture-climate interactions in a changing climate: A review. DOI 10.1016/j.earscirev.2010.02.004
- Seneviratne SI, Corti T, Davin EL, Hirschi M, Jaeger EB, Lehner I, Orlowsky B, Teuling AJ (2010b) Investigating soil moisture-climate interactions in a changing climate: A review. DOI 10.1016/j.earscirev.2010.02.004
- Seneviratne SI, Wilhelm M, Stanelle T, Van Den Hurk B, Hagemann S, Berg A, Cheruy F, Higgins ME, Meier A, Brovkin V, Claussen M, Ducharne A, Dufresne JL, Findell KL, Ghattas J, Lawrence DM, Malyshev S, Rummukainen M, Smith B (2013) Impact of soil moisture-climate feedbacks on CMIP5 projections: First results from the GLACE-CMIP5 experiment. *Geophysical Research Letters* DOI 10.1002/grl.50956
- Shaffer GP, Gosselink JG, Hoepfner SS (2005) The Mississippi River alluvial plain. *The World's Largest Wetlands: Ecology and Conservation* pp 272–315, DOI 10.1017/CBO9780511542091.009
- Sheng M, Lei H, Jiao Y, Yang D (2017) Evaluation of the Runoff and River Routing Schemes in the Community Land Model of the Yellow River Basin. *Journal of Advances in Modeling Earth Systems* 9(8):2993–3018, DOI 10.1002/2017MS001026
- Shukla J, Mintz Y (1982) Influence of land-surface evapotranspiration on the earth's climate. *Science* DOI 10.1126/science.215.4539.1498
- Silva CB, Silva MES, Ambrizzi T (2017) Climatic variability of river outflow in the Pantanal region and the influence of sea surface temperature. *Theoretical and Applied Climatology* DOI 10.1007/s00704-016-1760-7
- Silva Dias MA, Silva Dias PL, Longo M, Fitzjarrald DR, Denning AS (2004) River breeze circulation in eastern Amazonia: Observations and modelling results. *Theoretical and Applied Climatology* DOI 10.1007/s00704-004-0047-6
- Skamarock WC, Klemp JB, Dudhia J, Gill DO, Barker D, Duda MG, . . . , Powers JG (2008) A description of the advanced research WRF version 3, NCAR Tech. Note, NCAR/TN-468+STR. Natl Cent for Atmos Res Boulder, Colorado
- Small EE, Kurc SA (2003) Tight coupling between soil moisture and the surface radiation budget in semiarid environments: Implications for land-atmosphere interactions. *Water Resources Research* DOI 10.1029/2002WR001297

- Sörensson AA, Menéndez CG (2011) Summer soil-precipitation coupling in South America. *Tellus, Series A: Dynamic Meteorology and Oceanography* DOI 10.1111/j.1600-0870.2010.00468.x
- Sorooshian S, Lawford R, Try P, Rossow W, Roads J, Polcher J, Sommeria G, Schiffer R (2005) Water and energy cycles: Investigating the links. *World Meteorological Organization Bulletin* 54(2):58–64
- Spennemann PC, Saulo AC (2015) An estimation of the land-atmosphere coupling strength in South America using the Global Land Data Assimilation System. *International Journal of Climatology* DOI 10.1002/joc.4274
- Spennemann PC, Rivera JA, Osman M, Celeste Saulo A, Penalba OC (2017) Assessment of seasonal soil moisture forecasts over Southern South America with emphasis on dry and wet events. *Journal of Hydrometeorology* DOI 10.1175/JHM-D-17-0015.1
- Su F, Lettenmaier DD (2009) Estimation of the surface water budget of the La Plata Basin. *Journal of Hydrometeorology* DOI 10.1175/2009JHM1100.1
- Subin ZM, Riley WJ, Mironov D (2012) An improved lake model for climate simulations: Model structure, evaluation, and sensitivity analyses in CESM1. *Journal of Advances in Modeling Earth Systems* DOI 10.1029/2011MS000072
- Sutanudjaja EH, Van Beek R, Wanders N, Wada Y, Bosmans JH, Drost N, Van Der Ent RJ, De Graaf IE, Hoch JM, De Jong K, Karssenberg D, López López P, Peßenteiner S, Schmitz O, Straatsma MW, Vannamettee E, Wisser D, Bierkens MF (2018) PCR-GLOBWB 2: A 5 arcmin global hydrological and water resources model. *Geoscientific Model Development* DOI 10.5194/gmd-11-2429-2018
- Sutcliffe J, Brown E (2018) Water losses from the Sudd. *Hydrological Sciences Journal* 63(4):527–541, DOI 10.1080/02626667.2018.1438612
- Taylor CM (2010) Feedbacks on convection from an African wetland. *Geophysical Research Letters* DOI 10.1029/2009GL041652
- Taylor CM, Prigent C, Dadson SJ (2018) Mesoscale rainfall patterns observed around wetlands in sub-Saharan Africa. *Quarterly Journal of the Royal Meteorological Society* DOI 10.1002/qj.3311
- Taylor KE (2001) Summarizing multiple aspects of model performance in a single diagram. *Journal of Geophysical Research Atmospheres* DOI 10.1029/2000JD900719
- Thielen D, Schuchmann KL, Ramoni-Perazzi P, Marquez M, Rojas W, Quintero JI, Marques MI (2020) Quo vadis Pantanal? Expected precipitation extremes and drought dynamics from changing sea surface temperature. *PLoS ONE* DOI 10.1371/journal.pone.0227437
- Urakawa LS, Kurogi M, Yoshimura K, Hasumi H (2015) Modeling low salinity waters along the coast around Japan using a high-resolution river discharge dataset. *Journal of Oceanography* 71(6):715–739, DOI 10.1007/s10872-015-0314-4

- Van Beek LP, Wada Y, Bierkens MF (2011) Global monthly water stress: 1. Water balance and water availability. *Water Resources Research* DOI 10.1029/2010WR009791
- Vanderkelen I, van Lipzig NP, Lawrence DM, Droppers B, Golub M, Gosling SN, Janssen AB, Marcé R, Schmied HM, Perroud M, Pierson D, Pokhrel Y, Satoh Y, Schewe J, Seneviratne SI, Stepanenko VM, Tan Z, Woolway RI, Thiery W (2020) Global Heat Uptake by Inland Waters. *Geophysical Research Letters* DOI 10.1029/2020GL087867
- Vanderkelen I, van Lipzig NPM, Sacks WJ, Lawrence DM, Clark MP, Mizukami N, Pokhrel Y, Thiery W (2021) Simulating the Impact of Global Reservoir Expansion on the Present-Day Climate. *Journal of Geophysical Research: Atmospheres* 126(16):e2020JD034485, DOI 10.1029/2020JD034485
- Vera C, Baez J, Douglas M, Emmanuel CB, Marengo J, Meitin J, Nicolini M, Nogues-Paegle J, Paegle J, Penalba O, Salio P, Saulo C, Silva Dias MA, Silva Dias P, Zipser E (2006) The South American low-level jet experiment. *Bulletin of the American Meteorological Society* 87(1):63–77, DOI 10.1175/BAMS-87-1-63
- Verdin KL, Verdin JP (1999) A topological system for delineation and codification of the Earth's river basins. *Journal of Hydrology* 218(1-2):1–12, DOI 10.1016/S0022-1694(99)00011-6
- Vermote EF, Saleous NZ (2006) Operational atmospheric correction of modis visible to middle infrared land surface data in the case of an infinite lambertian target. In: *Earth Science Satellite Remote Sensing: Science and Instruments*, DOI 10.1007/978-3-540-37293-6_8
- Verri G, Pinardi N, Oddo P, Ciliberti SA, Coppini G (2018) River runoff influences on the Central Mediterranean overturning circulation. *Climate Dynamics* 50(5-6):1675–1703, DOI 10.1007/s00382-017-3715-9
- Verstraete MM, Pinty B (1996) Designing optimal spectral indexes for remote sensing applications. *IEEE Transactions on Geoscience and Remote Sensing* DOI 10.1109/36.536541
- Vincendon B, Ducrocq V, Saulnier GM, Bouilloud L, Chancibault K, Habets F, Noilhan J (2010) Benefit of coupling the ISBA land surface model with a TOPMODEL hydrological model version dedicated to Mediterranean flash-floods. *Journal of Hydrology* DOI 10.1016/j.jhydrol.2010.04.012
- Viovy N (2018) CRUNCEP Version 7 - Atmospheric Forcing Data for the Community Land Model
- Vishwakarma BD, Zhang J, Sneeuw N (2021) Downscaling GRACE total water storage change using partial least squares regression. *Scientific Data* DOI 10.1038/s41597-021-00862-6
- Vorosmarty CJ, Sahagian D (2000) Anthropogenic disturbance of the terrestrial water cycle. DOI 10.1641/0006-3568(2000)050[0753:ADOTTW]2.0.CO;2
- Vörösmarty CJ, Fekete BM, Meybeck M, Lammers RB (2000) Global system of rivers: Its role in organizing continental land mass and defining land-to-ocean linkages. *Global Biogeochemical Cycles* 14(2):599–621, DOI 10.1029/1999GB900092

- Vorosmarty CJ, Fekete BM, Meybeck M, Lammers RB (2000) Global system of rivers: Its role in organizing continental land mass and defining land-To-Ocean linkages. *Global Biogeochemical Cycles* DOI 10.1029/1999GB900092
- Wada Y, Van Beek LP, Wanders N, Bierkens MF (2013) Human water consumption intensifies hydrological drought worldwide. *Environmental Research Letters* DOI 10.1088/1748-9326/8/3/034036
- Wakode HB, Baier K, Jha R, Azzam R (2018) Impact of urbanization on groundwater recharge and urban water balance for the city of Hyderabad, India. *International Soil and Water Conservation Research* DOI 10.1016/j.iswcr.2017.10.003
- Wang F, Polcher J, Peylin P, Bastrikov V (2018) Assimilation of river discharge in a land surface model to improve estimates of the continental water cycles. *Hydrology and Earth System Sciences* 22(7):3863–3882, DOI 10.5194/hess-22-3863-2018
- Watanabe MD, Ortega E (2014) Dynamic emergy accounting of water and carbon ecosystem services: A model to simulate the impacts of land-use change. *Ecological Modelling* DOI 10.1016/j.ecolmodel.2013.03.006
- Weedon GP, Balsamo G, Bellouin N, Gomes S, Best MJ, Viterbo P (2014) The WFDEI meteorological forcing data set: WATCH Forcing data methodology applied to ERA-Interim reanalysis data. *Water Resources Research* DOI 10.1002/2014WR015638
- Wei J, Dirmeyer PA (2012) Dissecting soil moisture-precipitation coupling. *Geophysical Research Letters* DOI 10.1029/2012GL053038
- van der Wiel K, Kapnick SB, Vecchi GA, Smith JA, Milly PC, Jia L (2018) 100-year lower mississippi floods in a global climate model: Characteristics and future changes. *Journal of Hydrometeorology* DOI 10.1175/JHM-D-18-0018.1
- Wood EF, Roundy JK, Troy TJ, van Beek LPH, Bierkens MFP, Blyth E, de Roo A, Döll P, Ek M, Famiglietti J, Gochis D, van de Giesen N, Houser P, Jaffé PR, Kollet S, Lehner B, Lettenmaier DP, Peters-Lidard C, Sivapalan M, Sheffield J, Wade A, Whitehead P (2011) Hyperresolution global land surface modeling: Meeting a grand challenge for monitoring Earth's terrestrial water. *Water Resources Research* 47(5), DOI 10.1029/2010WR010090
- Woodward C, Shulmeister J, Larsen J, Jacobsen GE, Zawadzki A (2014) The hydrological legacy of deforestation on global wetlands. *Science* DOI 10.1126/science.1260510
- Wright DM, Posselt DJ, Steiner AL (2013) Sensitivity of lake-effect snowfall to lake ice cover and temperature in the great lakes region. *Monthly Weather Review* DOI 10.1175/MWR-D-12-00038.1
- WWF (2004) Global Lakes and Wetlands Database GLWD. GLWD Documentation pp 1–7, URL <http://www.worldwildlife.org/pages/global-lakes-and-wetlands-database>
- Xie X, Jiang X, Zhang T, Huang Z (2019) Regional water footprints assessment for hydroelectricity generation in China. *Renewable Energy* DOI 10.1016/j.renene.2019.01.089

- Xu H (2006) Modification of normalised difference water index (NDWI) to enhance open water features in remotely sensed imagery. *International Journal of Remote Sensing* DOI 10.1080/01431160600589179
- Xue J, Su B (2017) Significant remote sensing vegetation indices: A review of developments and applications. DOI 10.1155/2017/1353691
- Yamazaki D, Oki T, Kanae S (2009) Deriving a global river network map and its sub-grid topographic characteristics from a fine-resolution flow direction map. *Hydrology and Earth System Sciences* DOI 10.5194/hess-13-2241-2009
- Yamazaki D, Kanae S, Kim H, Oki T (2011) A physically based description of floodplain inundation dynamics in a global river routing model. *Water Resources Research* DOI 10.1029/2010WR009726
- Yamazaki D, De Almeida GA, Bates PD (2013) Improving computational efficiency in global river models by implementing the local inertial flow equation and a vector-based river network map. *Water Resources Research* DOI 10.1002/wrcr.20552
- Yamazaki D, Sato T, Kanae S, Hirabayashi Y, Bates PD (2014) Regional flood dynamics in a bifurcating mega delta simulated in a global river model. *Geophysical Research Letters* DOI 10.1002/2014GL059744
- Yamazaki D, Ikeshima D, Tawatari R, Yamaguchi T, O'Loughlin F, Neal JC, Sampson CC, Kanae S, Bates PD (2017) A high-accuracy map of global terrain elevations. *Geophysical Research Letters* DOI 10.1002/2017GL072874
- Yamazaki D, Ikeshima D, Sosa J, Bates PD, Allen G, Pavelsky T (2019) MERIT Hydro: A high-resolution global hydrography map based on latest topography datasets. *Water Resources Research* p 2019WR024873, DOI 10.1029/2019WR024873
- Yang Z, Qian Y, Liu Y, Berg LK, Gustafson WI, Feng Z, Sakaguchi K, Fast JD, Tai SL, Yang B, Huang M, Xiao H (2020) Understanding irrigation impacts on low-level jets over the Great Plains. *Climate Dynamics* DOI 10.1007/s00382-020-05301-7
- Yin Z, Ottlé C, Ciais P, Zhou F, Wang X, Jan P, Dumas P, Peng S, Li L, Zhou X, Piao S (2020) Irrigation, damming, and streamflow fluctuations of the Yellow River. *Hydrology and Earth System Sciences Discussions* DOI 10.5194/hess-2020-7
- Zanin PR, Satyamurty P (2020) Hydrological processes interconnecting the two largest watersheds of South America from seasonal to intra-monthly time scales: A critical review. *International Journal of Climatology* DOI 10.1002/joc.6443
- Zaninelli PG, Menéndez CG, Falco M, López-Franca N, Carril AF (2019) Future hydroclimological changes in South America based on an ensemble of regional climate models. *Climate Dynamics* DOI 10.1007/s00382-018-4225-0
- Zheng X, Eltahir EA (1998) A soil moisture-rainfall feedback mechanism 2. Numerical experiments. *Water Resources Research* DOI 10.1029/97WR03497

- Zhou J, Lau KM, Zhou J, Lau KM (1998) Does a Monsoon Climate Exist over South America? *Journal of Climate* 11(5):1020–1040, DOI 10.1175/1520-0442(1998)011<1020:DAMCEO>2.0.CO;2
- Zhou X, Polcher J, Dumas P (2021a) Representing Human Water Management in a Land Surface Model Using a Supply/Demand Approach. *Water Resources Research* DOI 10.1029/2020WR028133
- Zhou X, Polcher J, Dumas P (2021b) Representing Human Water Management in a Land Surface Model Using a Supply/Demand Approach. *Water Resources Research* DOI 10.1029/2020WR028133
- Zhou X, Prigent C, Yamazaki D (2021c) Toward improved comparisons between land-surface-water-area estimates from a global river model and satellite observations. *Water Resources Research* 57(5):e2020WR029,256, DOI 10.1029/2020WR029256
- Zhuang Q, Melack JM, Zimov S, Walter KM, Butenhoff CL, Aslam K Khalil M (2009) Global methane emissions from wetlands, rice paddies, and lakes. *Eos* DOI 10.1029/2009EO050001

Titre: Analyse numérique à haute résolution de l'interaction surface-rivière-plaine d'inondation-atmosphère dans le bassin de La Plata Basin

Mots clés: Modélisation, Plaines d'Inondation, Pantanal, Hydrologie, Interaction Sol-Atmosphère

Résumé: Les plaines d'inondation tropicales sont des régions inondées temporairement ou en permanence dû au débordement des rivières sur des zones de faible relief. Les plaines d'inondation peuvent avoir un régime annuel d'inondation prévisible ce qui en fait d'importants écosystèmes avec une riche biodiversité qui fournissent de nombreux services écologiques. Le Pantanal, l'une des plus grandes plaines d'inondation au monde, est la région d'étude de cette thèse. L'objectif est de développer un schéma de plaines d'inondation pour le modèle de surface ORCHIDEE compatible avec des modèles atmosphériques à haute résolution pour les raisons suivantes : (1) pour améliorer la représentation de l'impact des plaines d'inondation sur les cycles de l'eau et de l'énergie dans ORCHIDEE, (2) étudier la dynamique des plaines d'inondation du Pantanal et (3) évaluer l'impact des plaines d'inondation sur les interactions sol-atmosphère sur cette région. Dans un premier temps, la version originale à basse résolution des plaines d'inondation dans ORCHIDEE a été utilisée pour montrer l'importance d'inclure les plaines d'inondation dans les modèles de surface parce que cela améliore la représentation du cycle de l'eau et permet de représenter des flux plus réalistes entre la surface et l'atmosphère. Le schéma de plaines d'inondation à haute résolution développé dans cette thèse est basé sur

la construction d'un graphe de routage des rivières sur une grille atmosphérique utilisant des modèles numériques de terrain conditionnés hydrologiquement à haute résolution via le concept d'Unité de Transfert Hydrologique (HTUs). Un outil de pré-traitement flexible et parallélisé a été développé pour faciliter et améliorer la construction du graphe de routage des rivières sur différents types de grilles atmosphériques ce qui facilite l'intégration de données additionnelles qui sont requises pour la représentation des plaines d'inondation. Ce schéma doit faire face à de nouvelles problématiques liées à la résolution tel que la possibilité pour un HTU d'inonder ses voisins. Ce schéma a été validé en comparaison avec des observations et avec la version précédente dans ORCHIDEE. La comparaison des simulations avec et sans plaines d'inondation forcées par des forçages atmosphériques à différentes résolutions a permis d'évaluer : (1) l'impact des plaines d'inondation sur les variables en surface et (2) comment la résolution affecte la simulation de la dynamique des plaines d'inondation. Le schéma des plaines d'inondation à haute résolution a été utilisé dans une simulation du modèle RegIPSL (modèle couplé entre ORCHIDEE et WRF) pour étudier comment celui-ci modifie les interactions surface-atmosphère sur la région du Pantanal et comment il impacte localement ou à distance sur le climat d'Amérique du Sud.

Title: High resolution numerical analysis of the land-river-floodplains-atmosphere interaction in the La Plata Basin

Keywords: Modelling, Floodplains, Pantanal, Hydrology, Land-Atmosphere Interaction

Abstract: Tropical floodplains are regions which are temporarily or permanently flooded due to the overflow of rivers over a lowland area. Floodplains over large rivers may have a predictable annual flood regime which is why they are important ecological places with a rich biodiversity providing important ecological services. The Pantanal which is one of the world's largest tropical floodplains is the region of study for this thesis. The aim is to develop a floodplains scheme for the ORCHIDEE Land Surface Model (LSM) compatible with high resolution atmospheric models for the following reasons : (1) improve the representation of the impact of floodplains on the water and energy cycle in ORCHIDEE, (2) study the dynamic of the Pantanal floodplains and (3) evaluate the impact of floodplains on the land-atmosphere interactions over this region. Initially, the original low resolution version of the floodplains in ORCHIDEE has been used to show the importance of including floodplains in a Land Surface Models as it improves the representation of the water cycle and allows to represent more realistic land-atmosphere fluxes. The high resolution floodplains scheme developed here is based on the construction of the river routing graph on an atmo-

spheric grid using high resolution Hydrologically-conditioned DEM via the Hydrological Transfer Units (HTUs) concept. A parallelized flexible pre-processing tool has been developed in order to facilitate and improve the construction of the river routing graph on different types of atmospheric grids which facilitates the integration of additional hydrological data required for the representation of floodplains. This scheme had to handle new issues related to the resolution such as the possibility of an HTU to flood its neighbours. This scheme has been validated in comparison to observations and to its previous version in ORCHIDEE. The comparison of simulations with and without floodplains forced by atmospheric forcings with different resolutions allowed us to evaluate : (1) the impact of floodplains on land surface variables and (2) how the resolution affects the simulation of the floodplain dynamics. The high resolution floodplains scheme has been used in a simulation of the RegIPSL model (coupled ORCHIDEE-WRF model) to study how it modifies land-atmosphere interactions over the Pantanal region and the local and remote impact on the climate of South America.